UNIVERSITY OF SOUTHAMPTON
FACULTY OF SCIENCE
DEPARTMENT OF GEOLOGY

THE RECORD OF DEPOSITION AND THE MIGRATION OF ELEMENTS IN SALT MARSHES

A THESIS PRESENTED FOR THE DEGREE OF DOCTOR OF PHILOSOPHY

BY

JAMES THOMAS LEWIS

SEPTEMBER 1997

UNIVERSITY OF SOUTHAMPTON

ABSTRACT

FACULTY OF SCIENCE
GEOLOGY

Doctor of Philosophy

THE RECORD OF DEPOSITION AND THE MIGRATION OF ELEMENTS IN SALT MARSHES

by James Thomas Lewis

Salt marshes (intertidal grasslands) accumulate relatively undisturbed sediment profiles in coastal zones. Chemical signatures of the conditions present during deposition (from both the atmospheric and marine environments) can be preserved in the sediment record, and it may therefore be possible to reconstruct the historical flux of certain elements to the marsh. This research project investigates the distribution of a suite of geochemical parameters within sediment cores from Hythe Marsh, Southampton Water. A variety of analytical techniques have been employed to provide detailed concentration profiles of major and trace elements. The salt marsh sediments are composed of a mixture of minerogenic particles, derived from the suspended estuarine load, and organic materials produced *in-situ* by the marsh vegetation. The abundance of lattice-bound elements (Si, Al, K, Ti and Cr) is controlled by the composition of the bulk sedimentary matrix, whereas redox-sensitive species (such as Fe, Mn and S) are concentrated within particular depth horizons, according to the prevalent redox climate. The vertical distributions of the latter three elements permit the identification of oxic, sub-oxic and sulphidic diagenetic zones within several decimetres of the sediment prism. The redistribution of different elements through diagenesis, as redox conditions change with depth in response to the microbial demand for electron acceptors, takes place through the diffusion of ions and complexes in solution. The construction and field-testing of a gel-based equilibration sampler during this research has led to the retrieval of high resolution pore water samples which were analysed for dissolved iron and manganese. These reveal that reduction of oxidised forms of both of these elements takes place within the upper section of the sediment prism.

Activities of two radionuclides, ^{137}Cs and ^{210}Pb, have been analysed throughout the cores and may be interpreted to determine average accretion rates for the marsh sediments. Distinct sub-surface activity peaks are observed for ^{137}Cs, which may be correlated with the known fallout history of the isotope, whereas ^{210}Pb profiles exhibit an approximately exponential decline with depth. The mean accumulation rates yielded by the two independent techniques are in good agreement for all cores studied and slightly lower than the estimated mean rate of sea-level rise across the region. Extrapolation of the sediment accretion rate allows a chronology to be established for the prism which may be used to attempt the reconstruction of pollution trends for trace metals. Inventories of these isotopes contained within the salt marsh sediments are compared to their predicted flux histories. This comparison is enhanced for ^{210}Pb through the continuous collection, over three years, of local rain water samples for ^{210}Pb activity measurements. The depositional flux of this isotope, determined here for the Southampton Water region, is in good agreement with previous measurements of the mean annual atmospheric ^{210}Pb flux within the U.K..

Differences arise in the behaviour of various trace elements to the changing conditions encountered upon burial. The resulting competition between the preservation of a depositional record and the removal of such by early diagenetic processes is considered. The historical introduction of anthropogenic copper to the marsh can be related to the operations of the Esso refinery at Fawley and the sediment record shows close correlation to the estimated discharge pattern. Other trace elements (As, P, Zn and Ni) exhibit considerable diagenetic lability and are often found in association with secondary phases (principally manganese oxides, iron oxyhydroxides and sulphides and organic substrates). Stable lead isotope analysis is effective in revealing the probable sources which have contributed to the accumulation of this element over time, although remobilisation of lead following burial is implied by its observed association with diagenetic features of the sediment core geochemistries. The mixing of natural lead in the study area with anthropogenic lead derived from a range of sources is demonstrated by isotope ratio plots, thereby enabling source apportionment. The influence of imported lead (such as that derived from Australian and Canadian Precambrian ores) is evident throughout the sediments analysed.

Contents

List of Figures

Acknowledgements

A considerable number of people have contributed in some fashion or other to the final completion of this thesis. Firstly, I would like to express my gratitude to N.E.R.C. for providing the funding required for the research, and to the I.O.S. Deacon Laboratory (now the Challenger Division, Southampton Oceanography Centre) for assisting with a C.A.S.E. award. I know that I owe both of my supervisors, Dr. Ian Croudace and Dr. John Thomson, an immense debt for the faultless manner in which they have guided and encouraged me throughout the entire period of our collaboration. Obligado muchas graçias, señores! Additional, but no less essential, technical expertise has been forthcoming from various members of the Geology Department staff as and when I have needed it, and I particularly appreciate the efforts made in this respect by Dr. Andy Cundy, Posy, Dr. Andy Milton, Wink, Sonia, Phil, Bob and John. For all of the people that give me cause to smile, whether you know it or not, there is a part of you in here, too. Thanks for friendships ought not be necessary; just please remember, all of you folk that make my head the way it is today, that you can call on me anytime for whatever you need. You know who you are if you know me at all. For Hilary, Gordon, Steve, Belinda, Lou, Tamsin and Linda - you are always in my heart and mind. One final recognition is in need of airing: for keeping my head reeling with cycle-logical hope and adventure, Besse, this thesis is dedicated to the future of your kind.

Chapter One

Introduction

1.1 Research aims

1.1.1 *Pollution trends*

This research project contributes to a wider investigation of the geochemical nature of marine sediments within the Solent region being conducted by members of the Southampton Oceanography Centre. Salt marshes in general have previously been used to reveal useful information concerning the geochemical nature of their surroundings through the reconstruction of historical trends in the deposition of certain elements, particularly metals, on account of their particle reactive nature (e.g. McCaffrey and Thomson 1980; Allen and Rae 1986). However, the application of such techniques has received limited attention within the U.K. and is therefore considered to represent a valid investigation for an estuary as commercially important as Southampton Water. Essentially, since salt marshes may accrete vertical sediment sequences over periods of decades to centuries the inclusion of chemically-labelled particles from the estuary into different layers of sediment at different times may result in the formation of a time-dependent variation in sediment chemistry over depth. The retrieval and sectioning of sediment cores from suitable regions may exploit this property of the accretionary prism to reveal local historical trends in metal discharges from anthropogenic activities. For any such reconstruction to be placed in a temporal framework it is essential to determine a chronology throughout the sediment profile. A number of methods are available to achieve this and the present study uses two independent radiometric methods based on detailed activity profiles of ^{210}Pb (a natural radionuclide) and ^{137}Cs (an anthropogenic radionuclide). Additional information on the local flux of atmospheric ^{210}Pb is obtained through the analysis of rain water samples collected continuously for the three year duration of the research project.

1.1.2 *Salt marsh chemistry*

In order for historical reconstructions to generate meaningful results it is essential that the movement of elements throughout the sediment profile following burial is relatively small compared to the solid phase concentrations present. However, a salt marsh sediment prism represents a system in which intense physico-chemical gradients and diagenetic changes exist, driven by the burial and decay of organic materials, which may bring about changes in the speciation of many elements. Diagenetic redistribution must involve the generation of dissolved species and therefore the composition of the pore water phase is an important indicator of the likely processes causing remobilisation. The behaviour of many elements within salt marshes is incompletely understood and any investigation of their distributions in the solid and dissolved

phases may make significant contributions to our knowledge of the underlying geochemistry. The competition which exists between the preservation of depositional flux trends and the redistribution of different elements within the sediment prism is assessed throughout this report.

1.2 The study region

1.2.1 *Southampton Water*

Southampton Water forms a north-westerly extension to the central Solent and may be considered as an approximately rectangular water body 10 km long and 2 km wide (Figure 1.1). The rivers Test and Itchen contribute most of the freshwater input to the estuary (along with a lesser amount from the River Hamble) although the total input from freshwater sources is relatively small compared to the tidal influence. Sediments within this system typically consist of mud or sandy mud derived from Tertiary deposits and are protected from the prevailing south-westerly winds by the NW-SE orientation of the estuary itself and the shelter afforded by the Isle of Wight against powerful waves. The tidal regime within the estuary is famous for its double high-water stand which, combined with the short duration of the ebb flow, occupying only 3¾ hours of the 12½ hour tidal cycle (MacMillan 1952), yields a long 'flood and stand' period favourable to shipping. The particular tidal characteristics of this area are attributable to a combination of its situation near to the nodal portion of the English Channel and the existence of two passages into the Solent.

1.2.2 *Salt marshes in the Solent*

A considerable area of the Solent system is taken up by intertidal sediments, chiefly mudflats but also comprising significant areas of salt marsh (Tubbs 1980). Many salt marshes within the region owe their development to colonisation by *Spartina* species, in particular the vigorous *S. anglica* which was able to colonise mudflat areas hostile to less halophytic plants. The origins of this invasive species of *Spartina* lie in the accidental introduction, during the second half of the nineteenth century, of an alien species from North America, *Spartina alterniflora*. Hybridisation of this and native *S. maritima* produced an infertile strain, *S. townsendii*, first recorded at Hythe in 1870 (Tubbs 1980). The formation of *S. anglica* appears to have resulted from genetic development of *S. townsendii* (through self-duplication of chromosomes).
Following initial colonisation of mudflats by *S. anglica* the subsequent increase in surface elevation may provide conditions in which other plant species may thrive. Achieving an

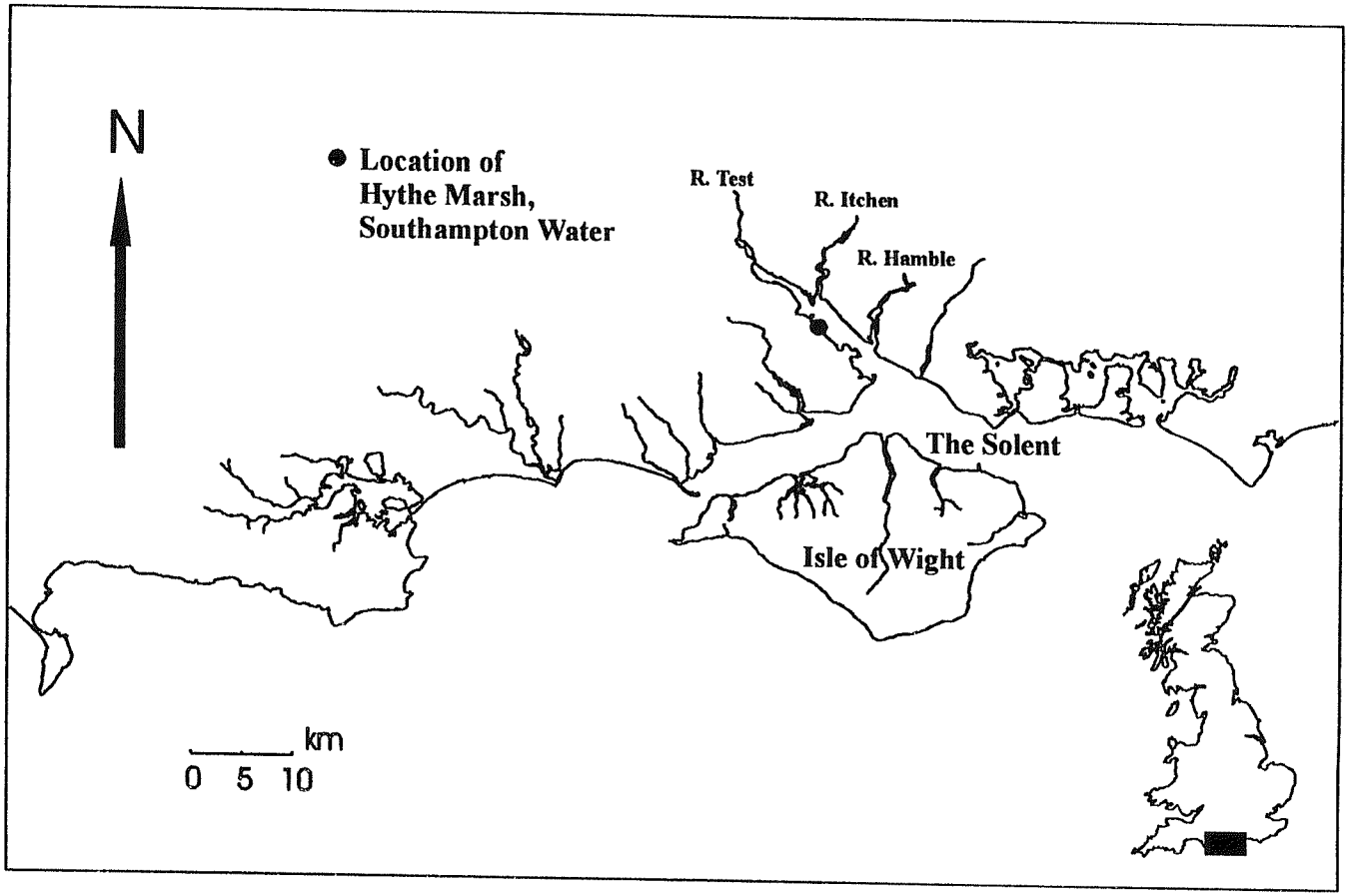

Figure 1.1:

Location of the Hythe Marsh study site, Southampton Water, within the Solent Estuarine System.

optimum surface height within the tidal range is an important requirement for the maturation and survival of a salt marsh. These ecosystems are therefore the subject of much interest regarding their future development on account of the predicted effects which anthropogenically-increased atmospheric CO_2 concentrations may have on global sea levels. Since marshes are highly effective at dissipating incident wave energy they may be a very important interface between terrestrial and marine environments which has so far been little understood and generally ignored as increasing areas of this type of habitat are reclaimed for purposes of human development.

1.2.3 *Hythe Marsh*

Local *Spartina* marshes typically date from the late nineteenth century, although marsh colonisation by alternative plant species has been occurring for several centuries in many locations (Tubbs 1980). In Southampton Water extensive salt marshes at the present time are confined to the western flank, and much of this area has been reclaimed for human industrial, residential and leisure purposes (Hooke and Riley 1987). The 1/10560 Ordnance Survey First Edition County Series maps, mostly dating from around 1870, confirm that a salt marsh has existed at Hythe for at least a century, although the intertidal zone has since narrowed considerably (Hooke and Riley 1987). The greater portion of the marsh now consists of a thriving mixed-plant community which has been responsible for the accretion of a prism of fine-grained sediments up to several hundred metres wide (Figure 1.2). The sediment surface at the study site is almost horizontal, gaining only 11 cm of height from the outer edge, at 4.44 ± 0.1 m O.D., to the landward limit, at 4.55 ± 0.1 m O.D. (Hubbard, 1994, *pers. com.*). This lies very close to the mean height of high water spring tides, at 4.5 m O.D. (Associated British Ports, Tide Tables), accounting for the dry nature of the sediment prism. The proximity of the site (Figures 1.3 and 1.4) to areas under major industrial use (an oil refinery, power stations and associated chemical industries all lie within a radius of several miles) and urban construction (opposite the waterfront and docks of the city of Southampton) implies that the sediment prism may contain distinguishable signals of materials discharged into the estuary from these developments over recent decades.

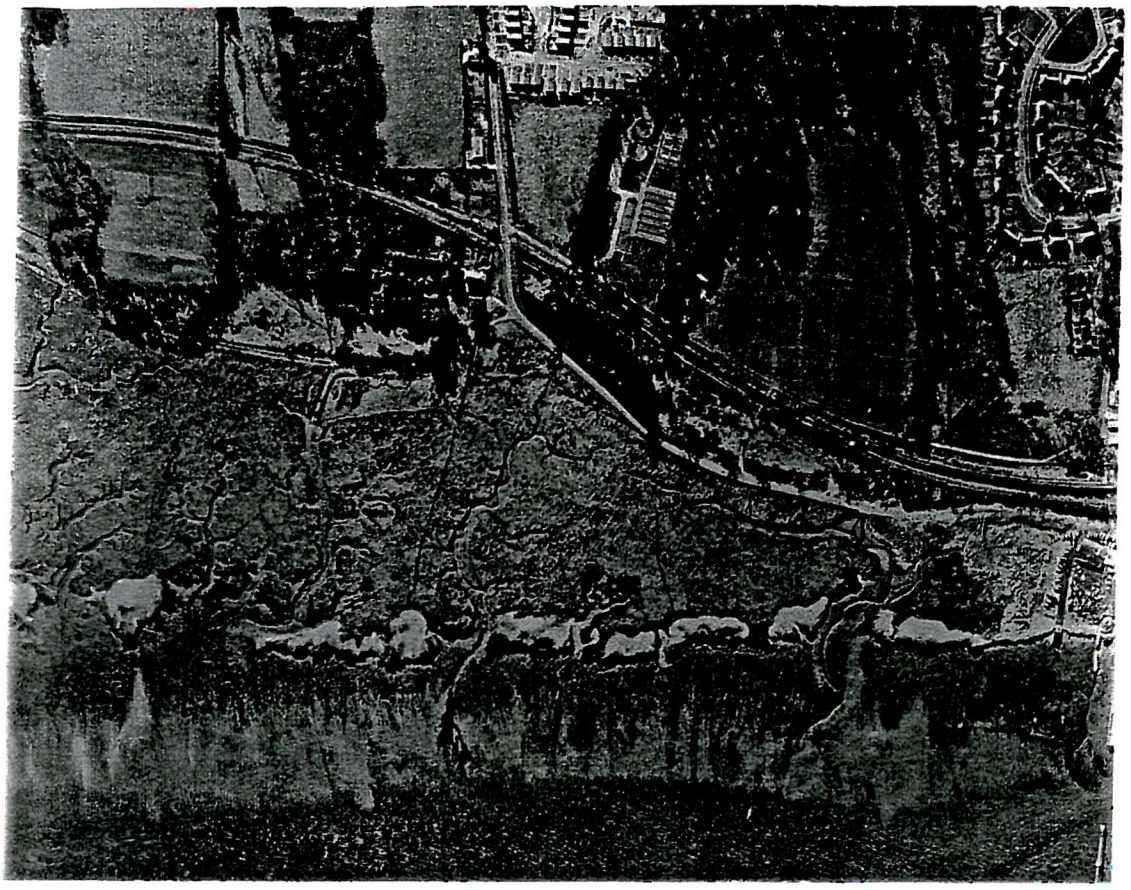

Figure 1.2:

Top: Hythe Marsh and mudflats from the 1963 aerial survey of Southampton Water.
Bottom: Wider view (from the 1940s) of the intertidal zone near Hythe.
Samples were retrieved from the narrow strip of salt marsh nearest to the observer.

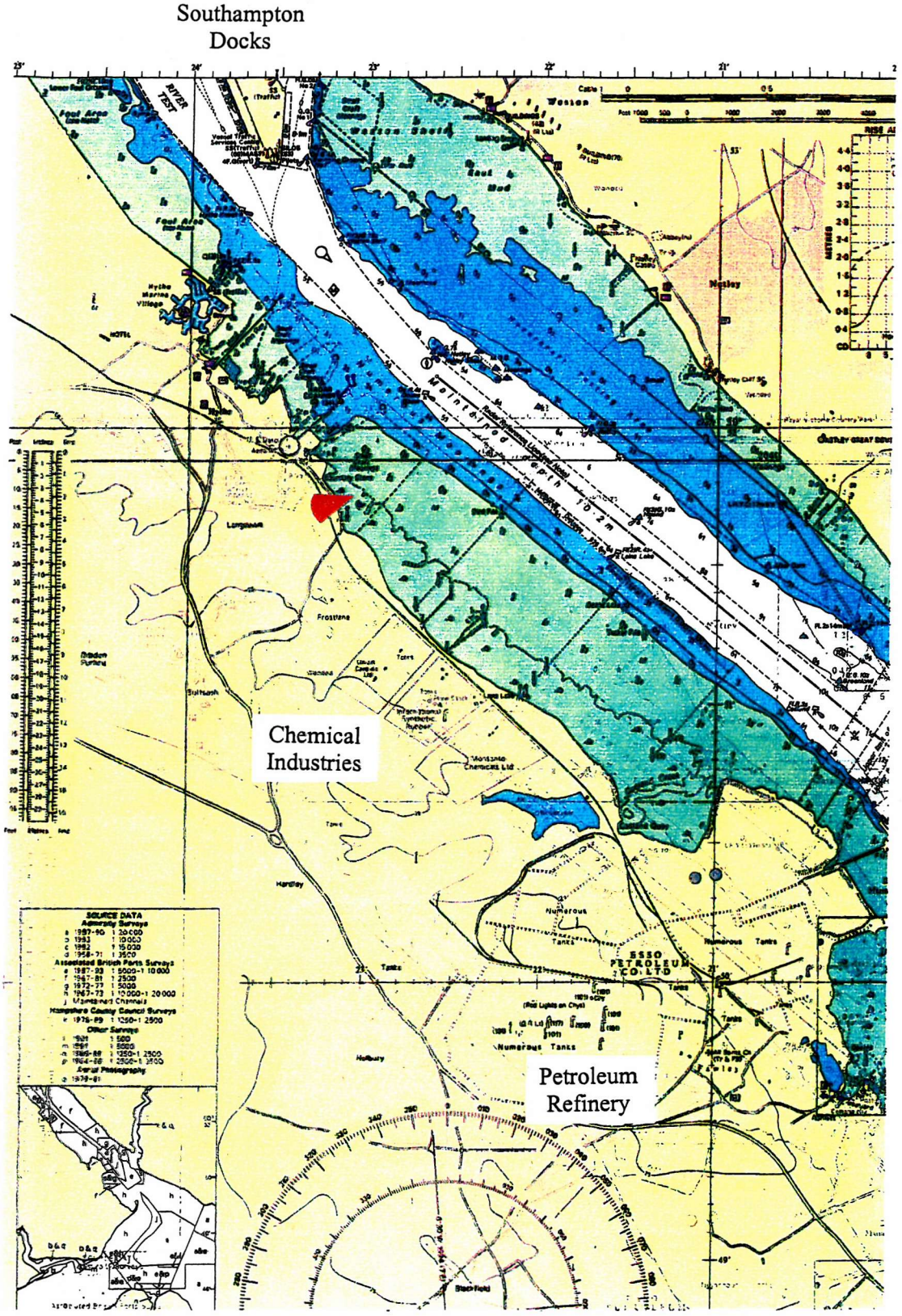

Figure 1.3:

Location of Hythe Marsh (red pointer) on the western shore of Southampton Water, revealing the proximity of the site to petroleum and chemical industries, as well as Southampton Docks (promontory at top left of figure).

Figure 1.4:

Land-use patterns within the study region.
Woodlands and fields are coloured green and brown, built-up areas are grey and white.
Note major urban developments of Southampton (top-left),
Portsmouth (centre-right) and industrial developments at Fawley (centre-left).

1.3 Thesis structure

- **Chapter Two** is a description of the methods used in the collection and analysis of sediment, rain water and pore water samples.

- **Chapter Three** describes the sedimentary characteristics of the salt marsh cores and the distribution of elements controlled by the composition of the sedimentary matrix (C_{org}, Si, Al, K, Ti, Cr, Na, Cl, Mg and Ca).

- **Chapter Four** considers the routing of ^{137}Cs and ^{210}Pb through the environment and the sediment accumulation rates determined at the study site using these techniques. The measured rainfall flux of $^{210}Pb_{xs}$ is discussed along with the salt marsh inventories.

- **Chapter Five** introduces the diagenetic environment likely to be prevalent in salt marshes and the distributions of iron, sulphur and manganese found within the sampled cores.

- **Chapter Six** discusses the profiles of trace elements (As, Br, Cu, I, P, Pb, Ni, and Zn) and analyses the apparent competition between the preservation of an historical flux and the participation of elements in early diagenetic reactions.

- **Chapter Seven** describes the stable isotope characteristics of lead present within two of the sediment cores in terms of the possible origin and temporal deposition of Pb within the prism.

- **Chapter Eight** summarises the results and conclusions of the project.

- **Appendix A** reviews the various methods which may be employed to collect pore water samples from sediment sequences.

- **Appendix B** is a compilation of the raw data obtained throughout this research.

- **Appendices C and D** are copies of two publications from Environmental Science and Technology to which the author has contributed. Further submissions to journals will be made in due course.

Chapter Two

Methodology

2.1 Sediment analyses

2.1.1 *Sampling procedure*

Sediment cores were retrieved from Hythe Marsh by the insertion of a 1m long plastic coring tube, with an internal diameter of 10 cm, down through the surface of the salt marsh (Figure 2.1). Following return to the laboratory, cores were split vertically and X-radiographed with a Hewlett Packard Faxitron X-ray machine. Core sections, placed in a sand-filled box to reduce "edge" effects, were typically exposed to X-rays at 56 kV for 24 minutes. Photography of example core sections and visual logging of the prominent sedimentary characteristics were performed prior to the cores being sectioned at depth intervals of 0.5 - 1.0 cm. Individual sediment samples were weighed wet, oven dried at ~90°C, weighed again and then ground to a powder, within tungsten-carbide pots, using a TEMA® gyratory swing mill.

2.1.2 *Radionuclide measurement*

2.1.2.1 ^{137}Cs

Homogenised sediment samples were analysed for caesium-137 activity using a Canberra 30% N-type HPGe gamma ray spectrometer. Approximately 20 g sediment powder was placed in the lead-shielded well detector and counted for a period of at least 30000 seconds, depending on the activity of the sample, in order to yield maximum counting errors of <5% for those samples exhibiting the prominent activity peak. The detector is routinely calibrated using a mixed-radionuclide source and all spectra were analysed by FITZPEAKS gamma analysis software. The accuracy of ^{137}Cs activities in sediments was verified through analysis of a standard Irish Sea sediment (from the International Atomic Energy Authority; IAEA 135). The effect of variable sample geometry (where insufficient material was available to completely fill the counting vial) was accounted for through repeated counting of a single homogeneous powder sample having different geometries. The lower limit of detection for ^{137}Cs is 0.5 Bq kg^{-1}.

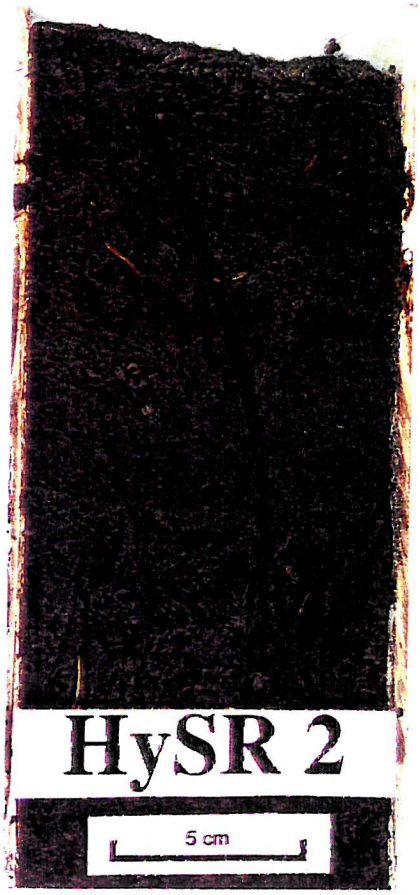

Figure 2.1:

Hythe Marsh sediment cores:
Top: core retrieval at the study site.
Bottom: sediment core following vertical splitting.

2.1.2.2 ^{210}Pb

Lead-210 determination was carried out using a proxy method similar to that of Flynn (1968) involving the measurement of ^{210}Po, grand-daughter of ^{210}Pb. Approximately 5 g of sediment powder was subjected to acid reflux under *aqua regia* followed by concentrated (~12N) HCl (Analar grade reagents). An internal standard of 0.5 ml ^{209}Po (4.86 dpm ml^{-1}) was added to the mixture during the initial stages of the acid treatment to compensate for possible variations in the recovery of ^{210}Po. The sediment suspension was centrifuged after each reflux stage and the leachates were then combined and evaporated to dryness. Following dissolution of the evaporated residue in hydrochloric acid polonium was autodeposited on to freshly polished silver discs (in 0.8M HCl solution with ~1 g ascorbic acid added to inhibit ferric oxide deposition) and counted on 450 mm^2 Passivated Implanted Planar Silicon detectors (Canberra SPD-450-25-100-AM) under vacuum. Count times were typically 80000 seconds, sufficient to reduce the counting error of each analysis to <7%. Due to the much longer half-life of the parent isotope creating a secular equilibrium between ^{210}Pb and ^{210}Po, the activity of each of these isotopes within sediment samples older than about two years (approximately five times the half-life of the daughter ^{210}Po) ought to be equal. Detection limits for ^{210}Po are 0.1 Bq kg^{-1}.

2.1.3 *Major and minor element analysis*

The major and trace element composition of the sediments was determined by X-ray fluorescence analysis using a Philips® PW1400 automatic sequential wavelength dispersive X-ray spectrometer.

- **Major element** measurements were made on fused beads using sediment subsamples (0.4 g ignited powder) dissolved, at 5:1 dilution, in a eutectic flux composed of 4 parts lithium metaborate : 1 part lithium tetraborate. Absorption and enhancement matrix effects were corrected for using the influence coefficients supplied by Philips. For elements well above their detection limit the precision is typically less than 1% r.s.d (relative standard deviation). During processing of the samples careful weighing prior to and after ignition at 970°C permitted determination of the loss on ignition (LOI).

- **Trace elements** were determined on 10 g non-ignited powder pellets (40 mm diameter) pressed to 12 tonnes per inch. Standard reference materials were included in the sample measurements to assess accuracy. The precision of the determinations is typically about 5% r.s.d. and the lower limit of detection is nominally 1-5 ppm for trace elements.

2.1.4 *Lead isotope determination*

Lead isotopic abundances were measured using a VG Elemental PQ2+ ICP-MS (inductively-coupled plasma mass spectrometer). In order to maximise the precision of this analytical technique for the determination of lead isotopes the abundance of solutes other than lead within the sample solutions should be reduced as much as possible. Furthermore, the possible contamination of samples with additional lead must be strictly avoided through the use of clean laboratory techniques and high purity reagents. Triple distilled, deionised water (Millipore MQ+ system; 18.2 MΩcm resistivity) was used at all times for rinsing labware and diluting solutions. Procedural blanks were included within each group of samples and treated in exactly the same manner as the samples themselves in order to control possible contamination resulting from reagents and laboratory practice.

The *aqua regia* and hydrochloric acid reflux digestions (as described above) effectively remove a wide range of elements (including lead) from the sediment surfaces. Following evaporation to dryness an aliquot of the leachate residue was converted to bromide salts, rather than chloride, through the twice-repeated addition and evaporation of 0.5 ml of concentrated HBr (Analar grade). The final residue was then dissolved in 3 ml 0.2M HBr. Anion exchange columns were prepared using 0.5 g Dowex 1X8 200-400 mesh chloride form resin in a standard laboratory Pastette® (providing a 1.5 cm column of resin). The resin was cleaned with 5 ml 50% HNO_3 and then preconditioned with 3 ml 50% HBr followed by 5 ml of 0.2M HBr (all reagents of Analar grade). An apparatus able to hold 48 small ion exchange columns, greatly increasing sample turnover, was specially constructed for these experiments and also incorporated an aluminium heat block suitable for performing the evaporations.

Samples (3 ml 0.2M HBr) were loaded on to the columns followed by two vial rinses and a column wash, each of 3 ml 0.2M HBr. Distribution coefficients (K_d) for lead in 0.2M HBr are approximately 3 x 10^3 (Korkisch 1989). Undesirable elements (such as iron and manganese) are flushed through the column during the rinsing stages and the effluent becomes clear. Elution of lead from the resin was effected with 9 ml of 0.5M HNO_3, the first millilitre of which was discarded in order to reduce the bromide content of the final solution. From the Pb concentration data derived from the XRF the probable lead content of the eluent was calculated and the solutions diluted accordingly (with Aristar grade HNO_3) to yield final solutions with ~10 ppb Pb. These were introduced into the ICP-MS, set to peak jumping mode across the mass range 204-208, and run along with a standard reference material (NIST 981) to calibrate the lead isotope ratios and correct for any temporal drift in sensitivity. Internal standards (^{203,205}Th

and ^{209}Bi) were added during analysis of the second sediment core to enable the application of a mass-dependent drift correction.

2.1.5 *Organic carbon measurement*

Sediments for carbon determination were divided into two subsamples, one of which was treated with hydrochloric acid to remove the calcium carbonate component and then neutralised by repeated flushing with distilled water. All samples were oven dried immediately prior to analysis and stored in a desiccator until ready for introduction into the analytical system. A Carbo Erba Instruments CHNS-O EA1108 Elemental Analyser was used to determine the carbon content of the powders. Both normal and decalcified samples were weighed (20 mg), sealed into tin capsules and oxidised at 1000°C by flash pyrolysis. Gas chromatography is used to separate the products and detection is achieved *via* flame ionisation. The percentage of carbon present within each powder is calculated by the software of the equipment (Carbo Erba EAGER) and may be interpreted as % total carbon (untreated samples), % organic carbon (decalcified samples) and % carbonate carbon (difference between untreated and decalcified samples).

2.1.6 *Scanning electron microscopy*

A sediment core was obtained during the latter part of the project for investigation by Scanning Electron Microscopy (SEM) to determine the crystalline nature of the iron sulphide present at depth. Fresh wet sediment samples from several depth intervals were initially dispersed in a cylinder of deoxygenated water to separate the heaviest fraction through gravitational settling. After about ten per cent of the initial material had settled to the bottom of the cylinder the fraction remaining in suspension was decanted and discarded. The slurry at the base of the tank was freeze-dried, mixed with resin in a mould, agitated to remove bubbles of air and then allowed to set. The surface of this resin block was polished and coated with graphite prior to loading into the sample chamber of a JEOL 6400 Scanning Electron Microscope. Backscattered electron imaging of the specimens was used to identify the most dense particles at relatively low magnification followed by quantitative and qualitative energy dispersive X-ray microanalysis (with a spatial resolution of ~5 μm) to identify iron sulphide minerals. Photographs were obtained of interesting features.

2.2 Rainfall sampling

2.2.1 *Collection*

The collection of rainfall samples on the roof of the Geology department, Building 44 at the Highfield Campus, was initiated in March 1993 by Dr. Andrew Cundy (PhD 1992) and used clean polypropylene funnels connected to HDPE flasks (2.5 litre capacity) *via* a short length of tube. Typically two to four of these collectors were in use at any given time and each flask was acidified with 50 ml 5M HNO_3 prior to deployment. The turnover period of the collection was arbitrarily determined to allow sufficient precipitation to collect in the flasks and yet not overfill them if avoidable. The collection period for individual samples ranged from 3 to 72 days, with a mean of 18 days. Sample volumes collected were typically of several litres (minimum ~0.5 l, maximum ~10 l). The acidified collectants were stored prior to analysis according to the procedure outlined below.

2.2.2 *Analysis*

In order to analyse the polonium and lead content of the samples it was first necessary to concentrate the isotopes of interest into a more suitable medium. This was effected through chemical scavenging of these elements from the rain water *via* the *in-situ* precipitation of manganese dioxide. A radiotracer (^{209}Po) and lead carrier were both added to the samples prior to scavenging to assess the experimental yield of each element. Two litres of collectant (acidified rain water) were measured into a clean HDPE flask along with 100 µl ^{209}Po solution (4.86 dpm ml^{-1}), 4 ml 0.2M $KMnO_4$ and 1.00 ml 0.122M $Pb(NO_3)_2$ carrier following which the flask was shaken peridically and allowed to equilibrate for at least six hours. Procedural blanks were prepared according to the same methods using two litres of MQ+ deionised water instead of rain water. With continuous monitoring, the pH of the solutions was then adjusted from its initial value (typically 0.5-1) to a pH of 8-9, under which conditions the precipitation of MnO_2 effectively scavenges both polonium and lead from solution (Eakins and Morrison 1975). This latter stage of the procedure is achieved by the careful addition of an excess of Mn^{2+} ions in the form of 4 ml 0.3M $MnCl_2$. The flasks were stirred throughout this addition, shaken and left overnight for the brown solid to settle. The mixture was passed through a 0.45 µm cellulose nitrate membrane filter, from which the precipitate was then dissolved with 10 ml of 1.5M HCl and 0.2 ml of 30% H_2O_2 solution. Two beaker rinses, each of 5 ml 1.5M HCl, were combined with the solution to yield a final volume of about 25 ml into which a freshly polished silver disc was placed along with ~0.5 g of ascorbic acid. Polonium was allowed to autodeposit onto the

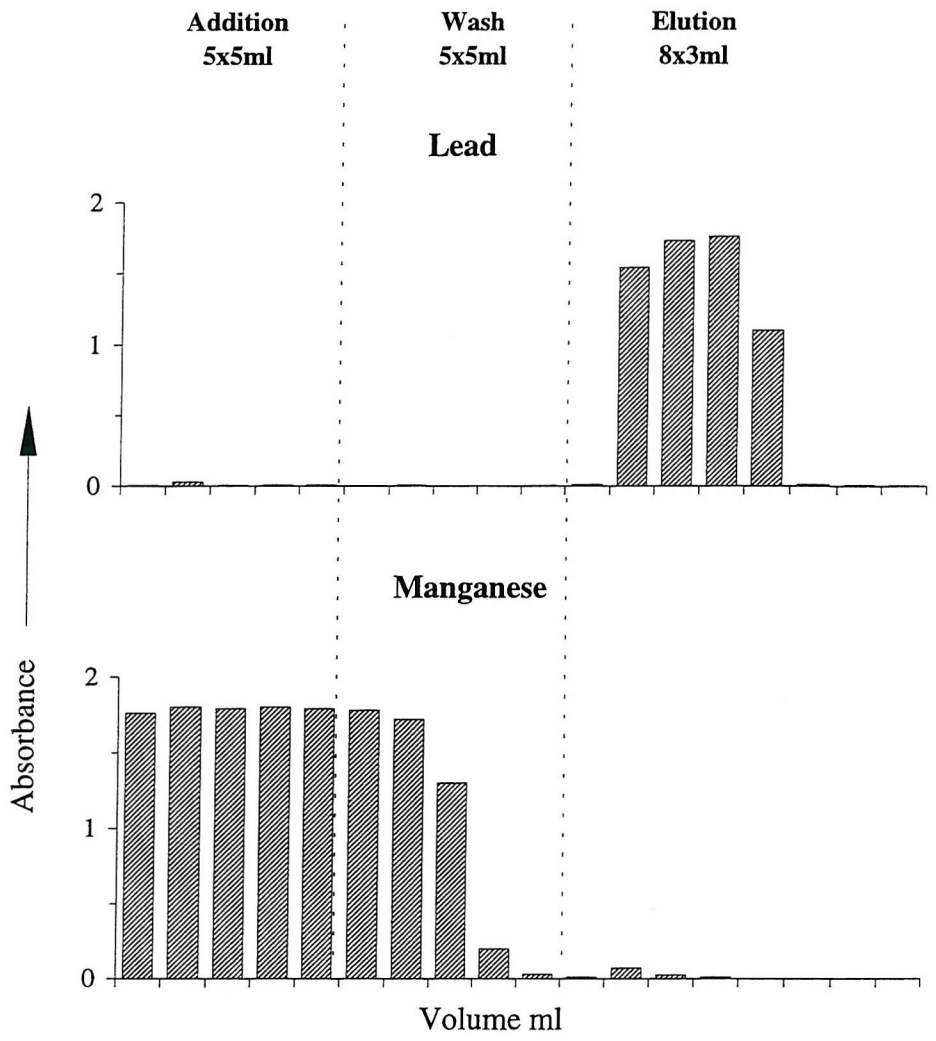

Figure 2.2:
Elution profiles of lead and manganese for the rainfall analyses, determined by Flame Atomic Absorption Spectroscopy.

2.3 Pore water sampling

2.3.1 *Thin-film gel sampler*

2.3.1.1 Method development

Having opted for the collection of samples *via* the equilibration of an artificially-introduced gel phase with salt marsh pore waters (see Appendix A) laboratory trials were initially conducted to establish the ability of an acrylamide gel to reproduce accurately the concentration of analytes from test solutions. The manufacture of these gels must be done with great care in a fume-extraction cupboard due to the toxicity of the acrylamide monomer. In addition, clean laboratory practice was maintained to avoid contamination of the sensitive samples handled. This involved the use of high purity reagents and MQ+ deionised water at all times. Details of the method followed to manufacture the polymer gel are given in Davison *et al* (1994). The monomer (acrylamide) and cross-linker (acrylaide) solution is well mixed with initiator and catalyst solutions (ammonium persulphate and TEMED, respectively), then pipetted carefully into a suitably shaped mould and allowed to set in warm (~40°C) conditions for 15 minutes. Hydration of the gel in water causes it to expand (complete after 24 hour immersion) after which it may be stored under water until required.

Trial pieces of this gel material were immersed in standard solutions containing a range of dissolved species for variable periods of time, then removed and weighed. Dissolved iron within the gel polymer was immobilised *via* immersion of gels in 10 mM NaOH for two hours and later extracted into solution once more with 3 ml 5% HNO_3 (Aristar grade). These solutions were analysed by graphite furnace atomic absorption spectroscopy (GFAAS), after dilution to the appropriate concentration range, along with suitable standards. In other experiments the fixing stage was omitted, in favour of equilibration followed by immediate back-extraction into dilute nitric acid, so that the equilibration of other elements (not fixed by the alkaline conditions) could be assessed.

2.3.1.2 Assembly

The field device initially constructed during this project was based on the similar, though smaller, apparatus described in Davison *et al* (1991). A Perspex block of dimensions 5 x 2 x 104 cm formed the backbone of the equipment and this was milled along one face to create a 1 mm high, 2 mm wide, raised border around the edges. The central recess held a full-length gel strip (4.6 x 0.08 x 100 cm) covered by a 0.45 μm pore size membrane filter. The filter and gel were then held in place by a Perspex cover plate, fixed with Nylon screws, which had a 3 cm wide window running the length of the apparatus to allow aqueous exchange between the gel and pore waters (Figure 2.3). Prior to deployment in the field the equipment required deoxygenation, effected through the 48 hour immersion of the fully-asssembled rig in MQ+ water being rigorously bubbled with nitrogen gas through a sintered glass diffuser.

2.3.1.3 Sampling

The first deployment of the sampling device at Hythe Marsh was conducted on August 2nd 1995. The deoxygenated apparatus was transported to the marsh without exposure to the atmosphere, rapidly removed from its containment tank and pushed down through the sediment surface. After 90 minutes the device was retrieved and rinsed with MQ+ water, then disassembled and the gel sheet sliced as quickly as possible at depth intervals of 1 cm. The individual gel pieces were placed into pre-weighed acid-washed vials and returned to the laboratory where, after weighing, they were acidified with 2.5M HNO_3. A second deployment was performed on August 15th 1995 and on this occasion the probe was left to equilibrate with the marsh pore waters for 48 hours before being removed. Upon retrieval the gel was not sliced in the field, as in the previous trial, but was immediately fully immersed in a solution of 10 mM NaOH to fix iron within the gel phase (Davison *et al* 1991). The rig was later dismantled in a clean-lab before extraction of the metal load, again from 1 cm wide gel pieces, with 1.00 ml 2.5M HNO_3 under centrifugation and overnight swirling on an automatic shaking table.

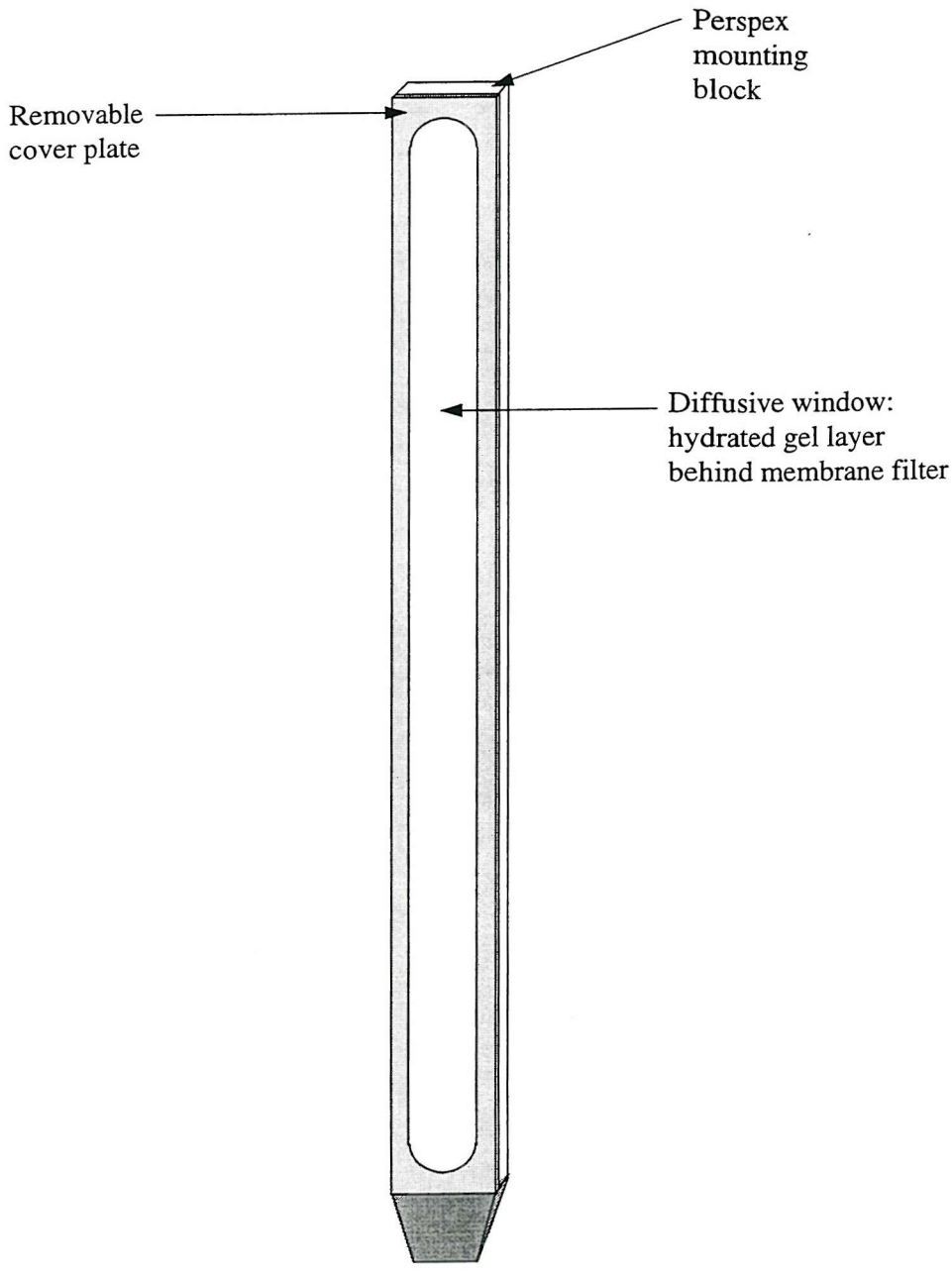

Figure 2.3:

Thin-film gel sampler constructed for pore water equilibration, full length of apparatus is one metre.

2.3.1.4 Analysis

The acid leach solutions obtained from the two deployments of the thin-film gel sampler were analysed using GFAAS to determine iron concentrations. Trial runs of leachate solutions led to their subsequent dilution by a factor of between 5 and 100 in order to bring them into the optimum analytical range of the spectroscope. Calibration and measurement (injecting 10 µl subsamples) over the range 0 - 200 ppb was conducted at 248.3 nm wavelength with matrix-matched standards. Ramp and flash times for the furnace were in accord with the manufacturer's recommendations. Analytical drift was monitored and corrected for through repeated runs of a standard with intermediate concentration. The preparation of all samples and standards during dilution and analysis was carried out in a filtered laminar flow hood.

2.3.2 *Chambered sampling device*

2.3.2.1 Assembly

A second gel-based sampler, consisting of segregated chambers to contain individual gel pieces rather than employing a continuous sheet, was fashioned from a Nylon block on the Geology department milling machine. Ninety-four cells, each with a horizontal length of 3.5 cm, a vertical height of 0.8 cm, and a depth of 1.3 cm, were milled from one side of the slab. The surface was then stripped away down the centre to leave three raised edges, two on the long sides and one across the base, approximately 3 mm high. These were cut with an angled milling tool, triangular in cross-section, which was also used to cut the outer edges of a covering plate (with a 2.5 cm wide diffusion window). The trapezoid cross-section of both the covering plate and the Nylon backbone allow the apparatus to be assembled simply by sliding the cover plate between the grooved walls (Figure 2.4).

2.3.2.2 Method development

Further method development became necessary when it was discovered that acrylamide gel pieces could not be cast (as had been intended) using the cells themselves as moulds, even if incompletely filled with the reactant mixture, due to the later expansion of the gel in three dimensions under complete hydration. A number of experiments, incorporating different proportions of monomer, cross-linker and water, failed to produce a gel with the required physical properties; absorption of more water appears inevitable following the polymerisation and setting of the fresh gel material. As an alternative to attempting the casting and transfer of

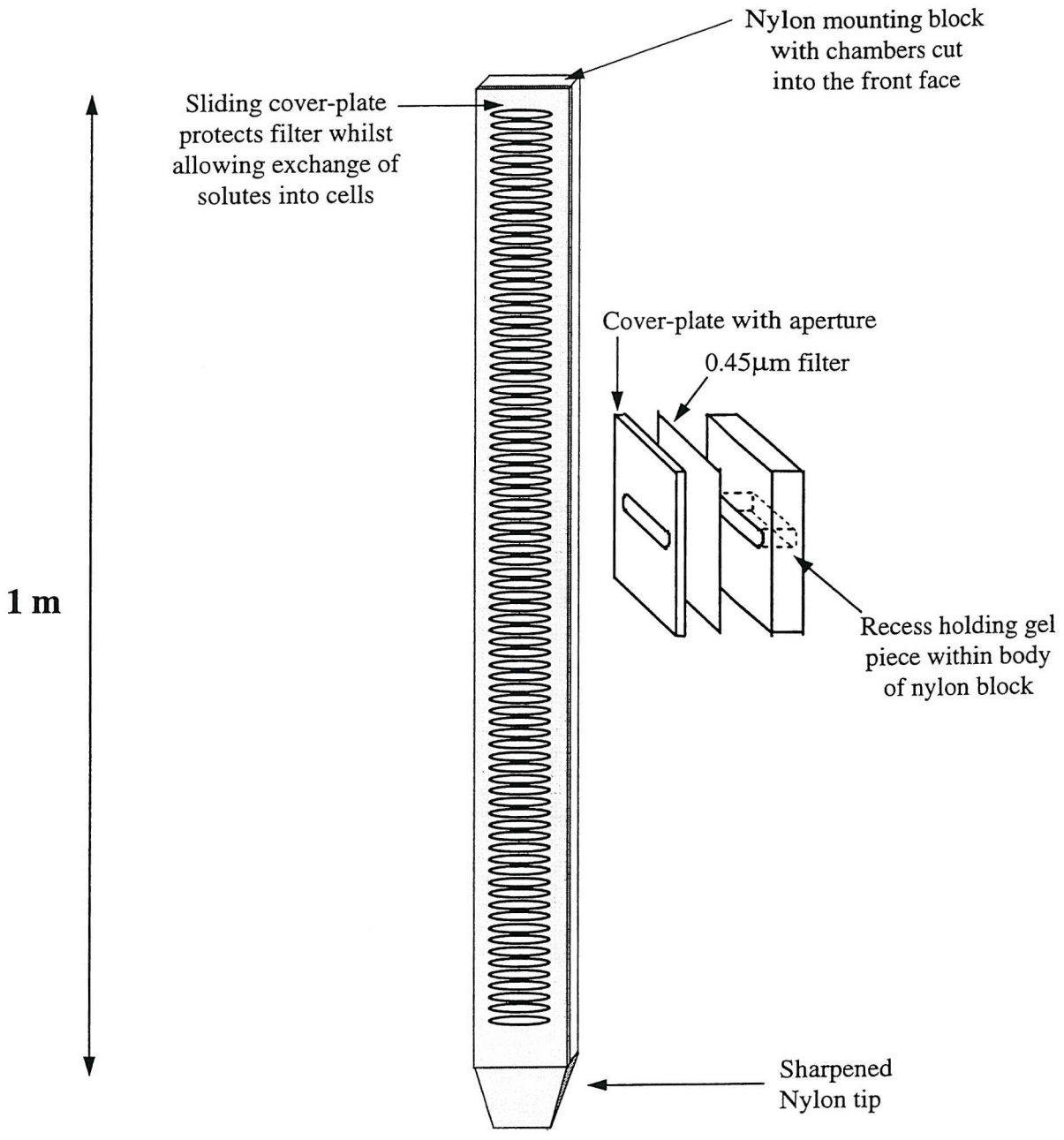

Figure 2.4:

Diagram of the chambered device constructed during this project to accomodate pieces of gel for pore water dialysis.

acrylamide gel pieces from separate moulds, *via* a hydration stage, into the chambers of the sampler an alternative gel, TreviGel™ 5000 (also commercially available for electrophoresis purposes), was given trial. Manufacture of this material is readily achieved through the simple microwave heating of a dispersion of the powder product in water. Initial tests soon verified that blocks of this material (cast as 1 part gel : 99 parts water) exhibit negligible physical expansion during later immersion in water and, although not as durable as the acrylamide gels, are of sufficient strength to survive the necessary handling procedures. An additional benefit of the gel is its non-toxic polysaccharide composition, as opposed to the neurotoxic acrylamide, making it safer and thus easier to employ. Later experiments yielded a method for effecting the almost complete dissolution of the gel. This involved heating the gel to about 70°C in loosely-sealed vials containing 50% nitric acid (Primar grade) in the ratio 2 parts gel : 1 part acid.

Following verification of the physical properties of TreviGel™ 5000 it was necessary to investigate whether the material could also reproduce solute concentrations accurately through equilibration. A radionuclide source solution (in 0.1M HNO_3), containing a mixture of gamma-emitting isotopes (^{241}Am, ^{133}Ba, ^{109}Cd, ^{139}Ce, ^{57}Co, ^{60}Co, ^{137}Cs, ^{155}Eu, ^{54}Mn, ^{22}Na, ^{88}Y and ^{65}Zn) at different specific activities, was mixed with filtered coastal seawater (1 ml source + 15 ml seawater) to provide a radiolabelled standard. Pieces of TreviGel™ material were immersed in this saline solution for an arbitrary 35 hours (Figure 2.5). Both the gel and the final solution were then counted in the gamma spectrometer described previously. In addition to this end-point determination a second experiment was designed to assess the time taken for the complete equilibration of gel units held within the chambered apparatus. Eighteen of the cells at one end of the device were filled with warm TreviGel™ solution and allowed to set (30 minutes refrigeration). The apparatus was then submerged in 750 ml 1M nitric acid labelled with ^{65}Zn radiotracer. Gel samples were removed from the rig over a period of 187 hours, placed into preweighed counting vials and analysed for ^{65}Zn activity (Figure 2.6).

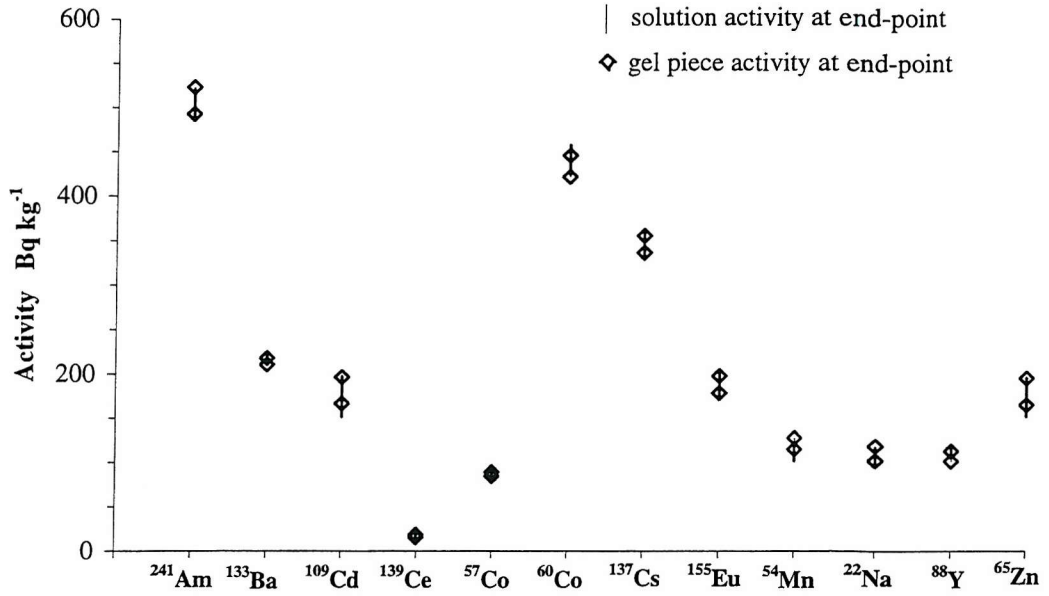

Figure 2.5:
Free gel end-point experiment after 35 hours.

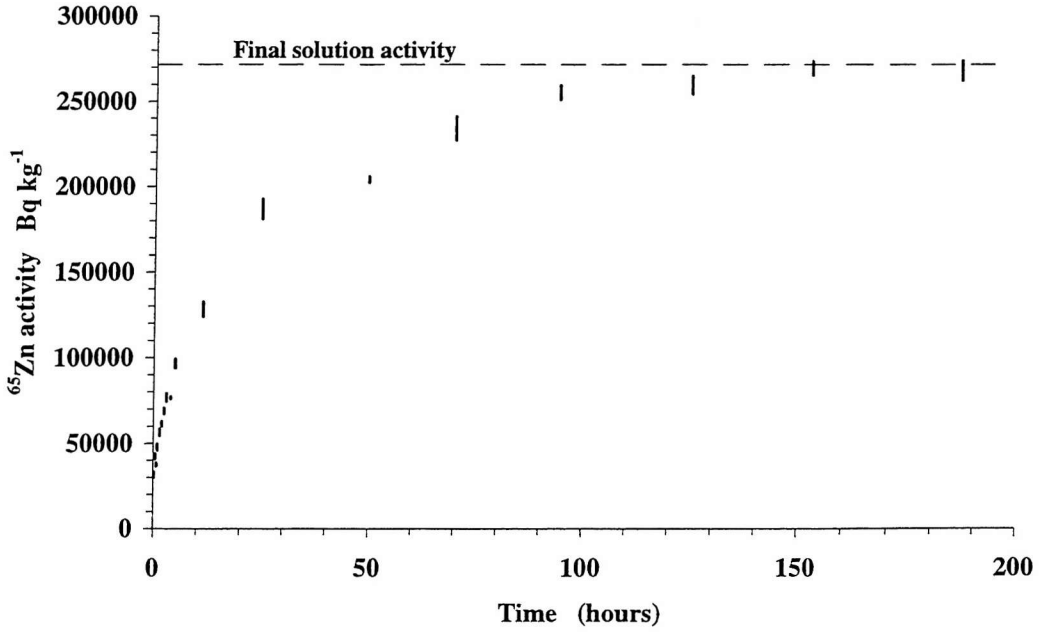

Figure 2.6:
Apparatus equilibration experiment.

2.3.2.3 Sampling

The fully assembled sampler consists of the gel-filled Nylon block, covered by a membrane filter and windowed Nylon plate, sealed around the edges against particle contamination with waterproof plastic tape. The unit was immersed in a tank of deoxygenated MQ+ water for at least six days immediately prior to field use. Deployment at Hythe Marsh was carried out on two occasions, with the probe being left to equilibrate for twelve days in each case. Upon withdrawal from the sediment prism the device was cleaned with MQ+, drained and then wrapped with plastic film during transportation. Once back in the laboratory, the pieces were removed from their cells with a clean Perspex spatula and placed into preweighed acid-washed vials. Gels were dissolved under heating with 1.75 ml 50% HNO_3 in loosely-capped vials and then diluted by the addition of 12.25 ml MQ+.

2.3.2.4 Analysis

2.3.2.4(a) ICP-AES

Dissolved gel solutions, diluted to one tenth the original pore water concentration, were analysed for iron and manganese using inductively-coupled plasma atomic emission spectroscopy (ICP-AES) within the Challenger Division, Southampton Oceanography Centre. Blanks and multi-element standards were prepared in a Class 100 laminar flow hood and matrix-matched to the composition of the samples, including the addition of a similar proportion of dissolved gel material.

2.3.2.4(b) GFAAS

GFAAS analysis attempted for Zn encountered high background signals, only removed by a long ashing stage which also caused unavoidable loss of Zn from the furnace (probably as volatile zinc-chloride). Matrix modification with Pd failed to yield meaningful spectra. Repetition of samples for Cu also yielded spurious results (standard absorbances not in same order as concentrations) attributed to similar interferences from the salt content. The attempted removal of the interfering solutes is described below (ICP-MS section) but unfortunately did not lead to the acquisition of meaningful results with either of these two techniques.

2.3.2.4(c) FAAS

Dissolved gel solutions (diluted ten times from pore water concentration) in a matrix of 5% HNO_3 were analysed using flame atomic absorption spectroscopy (FAAS) for iron only, as a independent check on the data obtained from the ICP-AES analyses. This involved injections of 0.5 ml volume subsamples into a mixed air-acetylene flame calibrated with matrix-matched standards and blanks (incorporating both dissolved gel material and an artificial saline component). For a limited number of samples further dilution was necessary to bring the iron concentration into the optimum analytical range.

2.3.2.4(d) ICP-MS

The introduction of samples containing relatively high levels of total dissolved solids (>0.2 %) into an ICP-MS instrument may result in the build-up of residual deposits and blockages within the apparatus. Furthermore, the diverse elemental composition of the samples creates interferences across a wide range of mass numbers, due to the presence of multiple ions such as ClO^-. Consequentially, the sensitivity of the detector to many analytes is reduced considerably (McLaren *et al* 1985). The dissolved gel samples from the second deployment of the chambered device were diluted by a factor of fifty from their pore water concentration to reduce the likely TDS concentration to <0.1%. These were analysed in the ICP-MS along with suitable multi-element standards, internal standards and blanks containing dissolved gel material and artificial sea water. Interferences were observed during these analyses, and a programme of laboratory work was consequently undertaken in an attempt to purify the sample solutions of the saline component.

The removal of unwanted dissolved solids from marine solutions prior to analysis by ICP-MS (and other techniques) is problematic but may be achieved with a number of different procedures (McLaren *et al* 1985). The method adopted to attempt separation during this study was through the use of ion exchange columns as these are well suited to the processing of a large number of small volume samples and suitable apparatus had already been constructed to contain 48 customised ion exchange columns. A dithiocarbamate resin was prepared by stirring the following reactants together in a conical flask at 20°C:

10 g flash silica (modified with trimethoxy-silyl-propyl-ethylene-diamine),

50 ml MQ+ H_2O,

25 ml 0.25M NaOH,

20 ml propanol,

25 ml carbon disulphide, CS_2.

Testing of the flash silica with $CuSO_4$ solution prior to reaction yielded a deep indigo colour, due to Cu-amine complexation, thus verifying the presence of amine groups on the modified resin. After filtering and washing with propanol the dithiocarbamate resin produced in the reaction vessel was tested, again with $CuSO_4$, and yielded a dark-brown colouration (due to Cu-sulphide complexation). At a pH of 8-9 there is strong complexation of a wide range of metals with the active groups of this resin (Taylor 1991). Trial experiments, using a mixed radionuclide source of gamma emitting isotopes, established the ability of the resin to retain many metals of interest whilst allowing sodium and chlorine to flush through the column. However, upon further experimentation with lower concentrations of analytes in the test solutions (5 ppb metal concentration in the nitric acid eluent) and analysis by ICP-MS a significant contamination of all eluents, including blanks, was discovered. This was likely to be due to contamination of the initial reactants (silica, propanol or CS_2) since all apparatus and later procedures were carried out under clean conditions. To counteract this problem the propanol and CS_2 reagents were purified by sub-boiling distillation prior to repeating the experiments. However, contamination of the solutions continued to be a problem throughout the remainder of the experimental period and due to time constraints on the duration of the project it unfortunately became necessary to abandon this avenue of research prior to obtaining the intended results.

Chapter Three

Sediment Facies

The chemical transformations investigated during this project take place within a system composed of sediments and pore waters. Minerogenic particles are incorporated into the sediment prism along with organic materials produced by the marsh plants, and saline waters regularly inundate the pore interstices. Those elements considered in this chapter are those whose abundance is primarily dictated by the detrital mineral phase (Si, Al, K, Ti and Cr) or the presence of saline pore fluids (Na, Cl, Mg and Ca). The distribution of organic material within the sediments is also considered.

3.1 Normalisation of data

Normalisation of certain data to the aluminium content throughout the cores is effective in revealing whether differences in bulk concentration are due to variations in the abundance of the detrital mineral phase. Aluminium is often used as a proxy parameter for mineralogical variation (Loring 1991) and has been shown to be representative of the clay mineral content of Southampton Water sediments by Cundy (1994). The normalisation of data must be carefully scrutinised since the results obtained may incorporate artifacts from the normalisation process.

Consider a sedimentary material which is composed only of organic carbon detritus and clay mineral grains. The mineral lattice may contain many elements which are absent from the surface of the organic materials and whose abundance is therefore strictly controlled by the proportion of clay minerals within the sediment. Peaks in the element concentration may be attributable to increased abundances of the carrier phase (in this case clay mineral particles) and therefore normalisation of the data to this phase will effectively remove variations in element concentration which are caused by the variable sediment composition. In a sample with twice as much organic material as a reference sample, implying that the element concentration and the abundance of mineral particles are therefore both halved, the ratio of element to aluminium remains constant (Figure 3.1). If, however, there is no valid reason for assuming that the element concentration profile is controlled solely by the abundance of minerogenic particles then such normalisation may produce misleading results. For example, a sediment sample incorporating a third sedimentary phase, such as a carbonate mineral, which also contributes some of the element under study, may not be suitable for normalisation to aluminium. In such cases, variations in the concentration of the desired element may not be proportional to the abundance of the normalising parameter (see Figure 3.1 for a diagrammatic representation). This is known as the 'closed sum' problem and needs to be considered prior to normalisation to avoid generating misleading results.

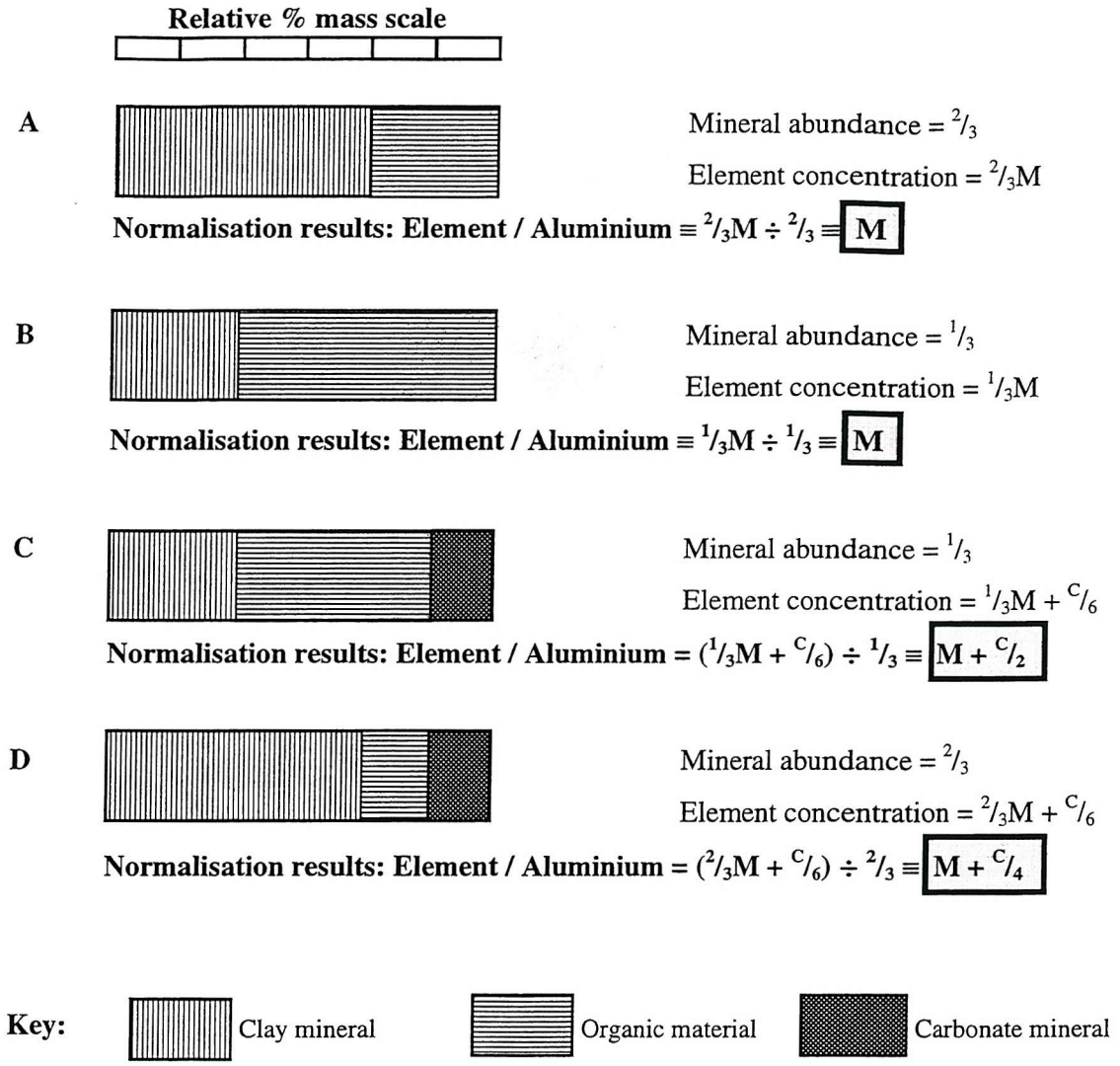

Figure 3.1:

Depiction of four theoretical normalisation scenarios to demonstrate the 'closed sum' problem. M is the % element within the clay mineral phase; C is that within the carbonate phase.

A and B: Despite having element concentrations which differ by a factor of two, samples A and B may be compared following normalisation and have equivalent elemental abundances.

C and D: For samples C and D, however, where a third phase (carbonate) contributes the same amount of element to each sample, the normalisation exaggerates the concentration in sample C relative to sample D, despite the higher actual elemental abundance within the latter sample.

Geochemical parameters were determined in detail throughout five cores, each removed from a different part of the salt marsh to provide materials from different sedimentary and diagenetic environments lying on a traversing line. A brief summary of the principal attributes of each core (name, length, date obtained, location on marsh, geochemical parameters measured) is given in order of increasing distance from the seaward edge of the marsh (Table 3.1 and Figure 3.2).

3.2 Sedimentary facies

The salt marsh prism at Hythe is composed of organic-rich mud. Visual logging of the four sediment cores discussed in detail in this report (reasons for excluding core HySR1 from detailed geochemical discussion can be found in Chapter 4) reveals that the distribution of different sediment facies is neither uniform with depth in any given core nor the same at different locations across the marsh (Figure 3.3). The sediment cores typically exhibit a brownish surficial decimetre beneath which the muds become progressively more grey with increasing depth. The abundance of root materials, both living and decaying, is highly non-uniform between cores and increases considerably in the two cores retrieved from the middle and rear zones of the marsh (cores HySR3 and HySR5, respectively). The facies distributions recorded in the sediment cores are of benefit when interpreting the geochemical behaviour of many elements within the prism.

3.3 Organic carbon distribution

Organic carbon may be sourced to a salt marsh sediment prism through two dominant processes: the deposition and burial of particulate organic carbon at the sediment surface and the *in-situ* growth of organic materials by the marsh plant community. Loss of carbon may occur through erosion and decomposition. Measurement of C_{org} was performed on 59 samples distributed throughout cores HySR1, HySR3 and HySR5, whereas loss on ignition was determined on all core samples during preparation (Figure 3.4). The strong correlation between these two parameters ($r^2 = 0.95$) permits extrapolation of the LOI data into C_{org} data with a high degree of confidence. In this fashion, organic carbon profiles have been empirically determined for unknown samples throughout the four main sediment cores, and display features characteristic of the superimposition of the processes which govern the distribution of this element (Figure 3.5).

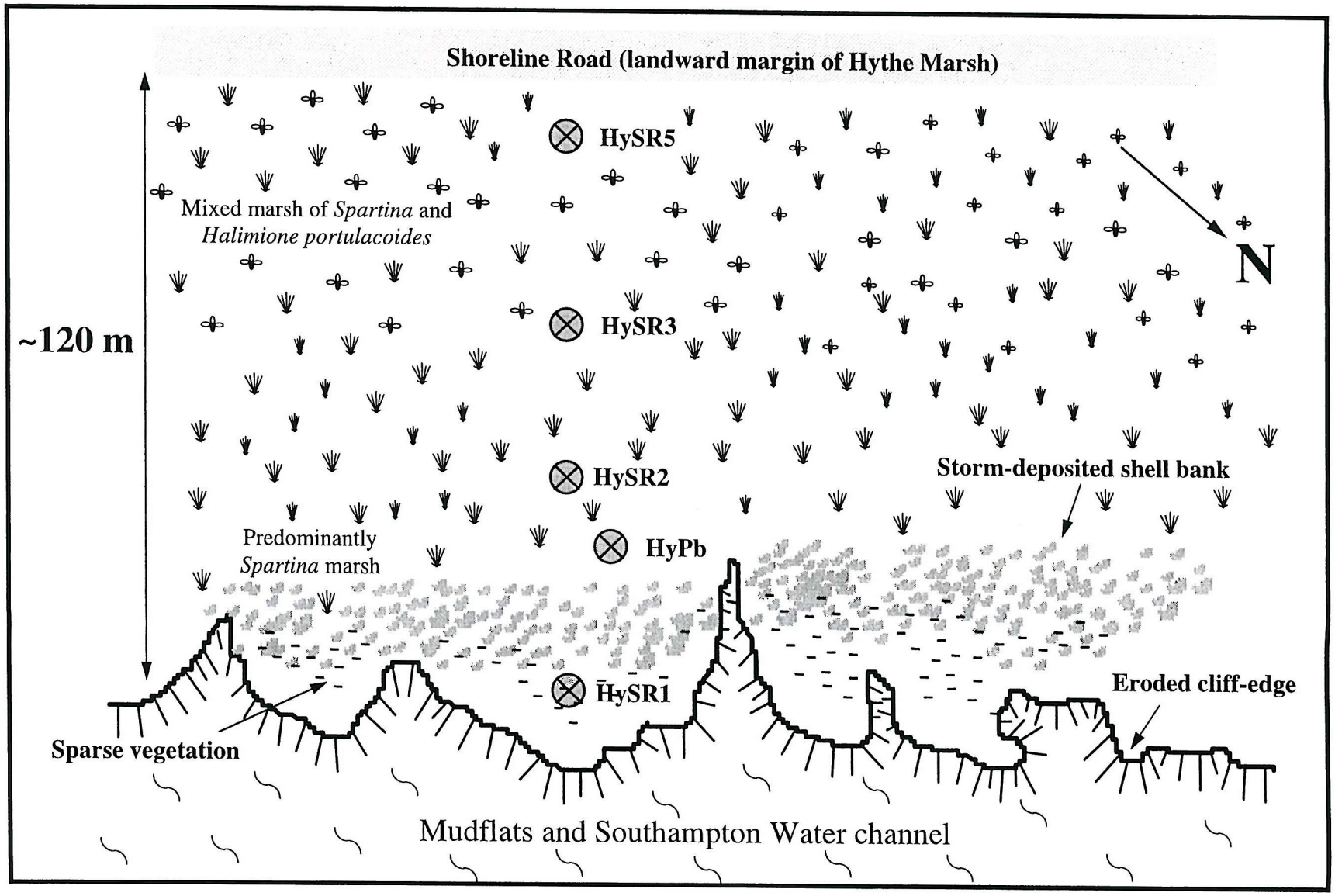

Figure 3.2:
Diagram of coring sites at the Hythe Marsh study site.

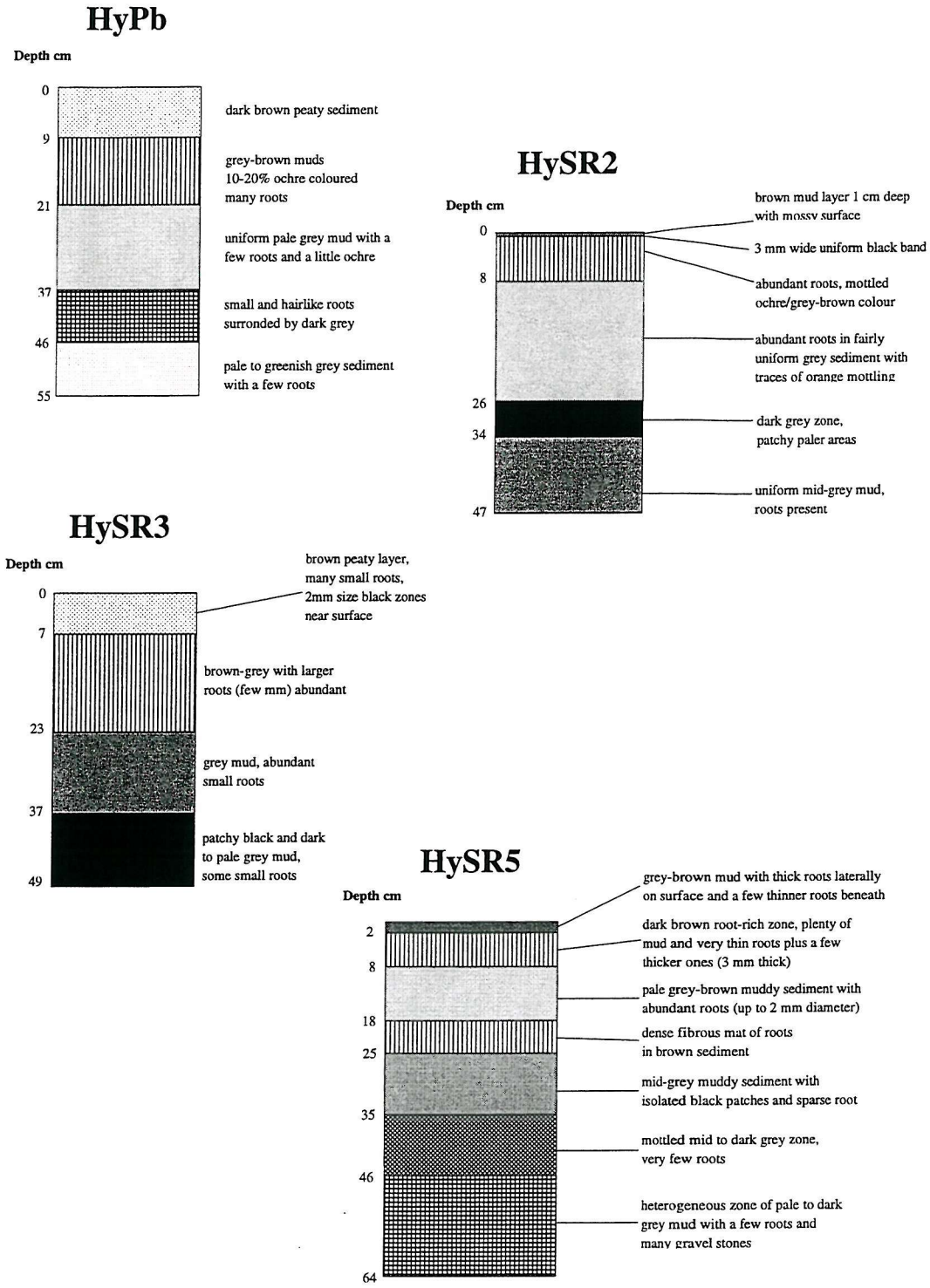

Figure 3.3:
Visual logs of dominant sedimentary facies in split salt marsh cores

Core HySR1:	80 cm long (1 cm samples); February 8th, 1994.
Location:	***Front cliff:*** Adjacent to eroded cliff-edge at seaward margin.
Analyses:	Majors, traces, carbon and ^{137}Cs.
Core HyPb:	50 cm long (0.5 cm samples); January 5th, 1995.
Location:	***Marsh front:*** 3 m landward of storm deposits (~20 m from mudflat).
Analyses:	Majors, traces, ^{210}Pb and stable lead isotopes.
Core HySR2:	45 cm long (1 cm samples); February 8th, 1994.
Location:	***Front of marsh:*** 8 m landward of storm deposits.
Analyses:	Majors, traces, ^{137}Cs and ^{210}Pb.
Core HySR3:	45 cm long (1 cm samples); February 8th, 1994.
Location:	***Middle of marsh:*** ~55 m each way to seaward and landward edges.
Analyses:	Majors, traces, carbon, ^{137}Cs and ^{210}Pb.
Core HySR5:	60 cm long (1 cm samples); January 5th, 1995.
Location:	***Rear of marsh:*** 10 m from landward edge
Analyses:	Majors, traces, carbon, ^{137}Cs, ^{210}Pb and stable lead isotopes.

Table 3.1:

Sediment core locations and parameters measured.

Evident in all profiles is the decrease in "C"$_{org}$ concentration at great depth due to a combination of microbial decomposition and the lack of a replenishing carbon source. Organic material is generally most abundant at intermediate depths where active root growth takes place, suggesting that the marsh vegetation constitutes the chief carbon source to the sub-surface communities. These depths are also the least dense core sections on account of their peaty nature (Figure 3.5). In the case of core HySR2, which exhibits a declining carbon load from the surface downcore, the main source appears to be due to deposition on the sediment surface and high-C_{org} root rich depth intervals are absent. The sediments in this core are also considerably denser than the other three cores on account of having a more minerogenic composition.

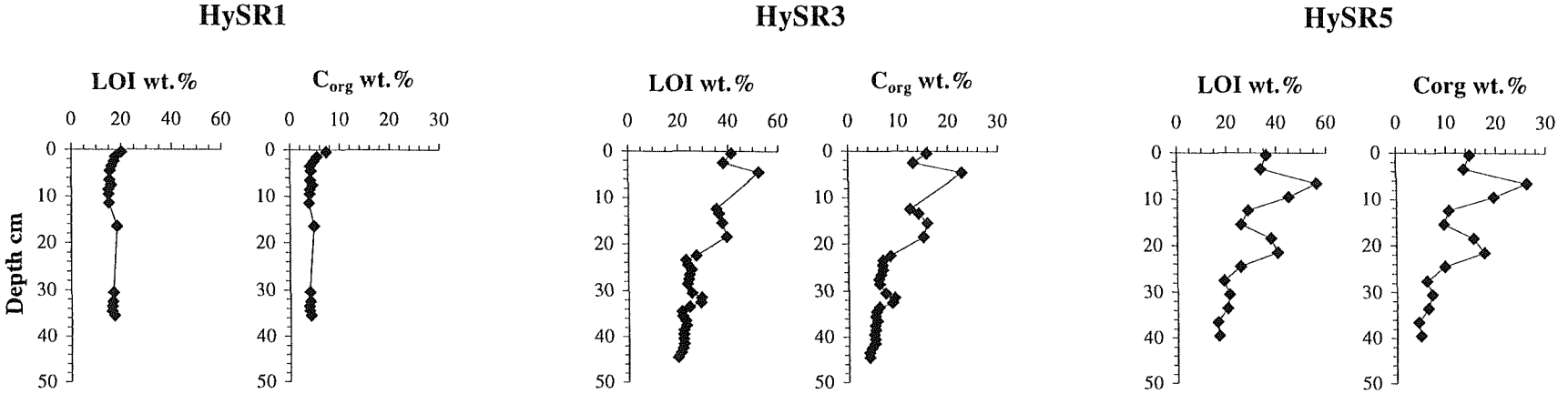

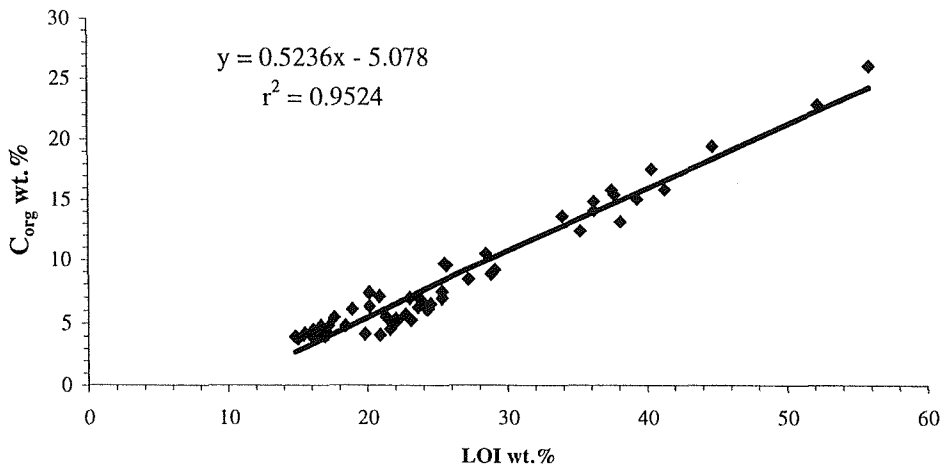

Regression results:

C_{org} = [(0.524+/-0.016) x LOI] - (5.078+/-1.130)

Examples of errors:

If LOI is 60 wt.%, C_{org} = 26.4 +/- 2.1

If LOI is 20 wt.%, C_{org} = 5.4 +/- 1.5

Figure 3.4:
Correlation between organic carbon and loss on ignition for all samples.

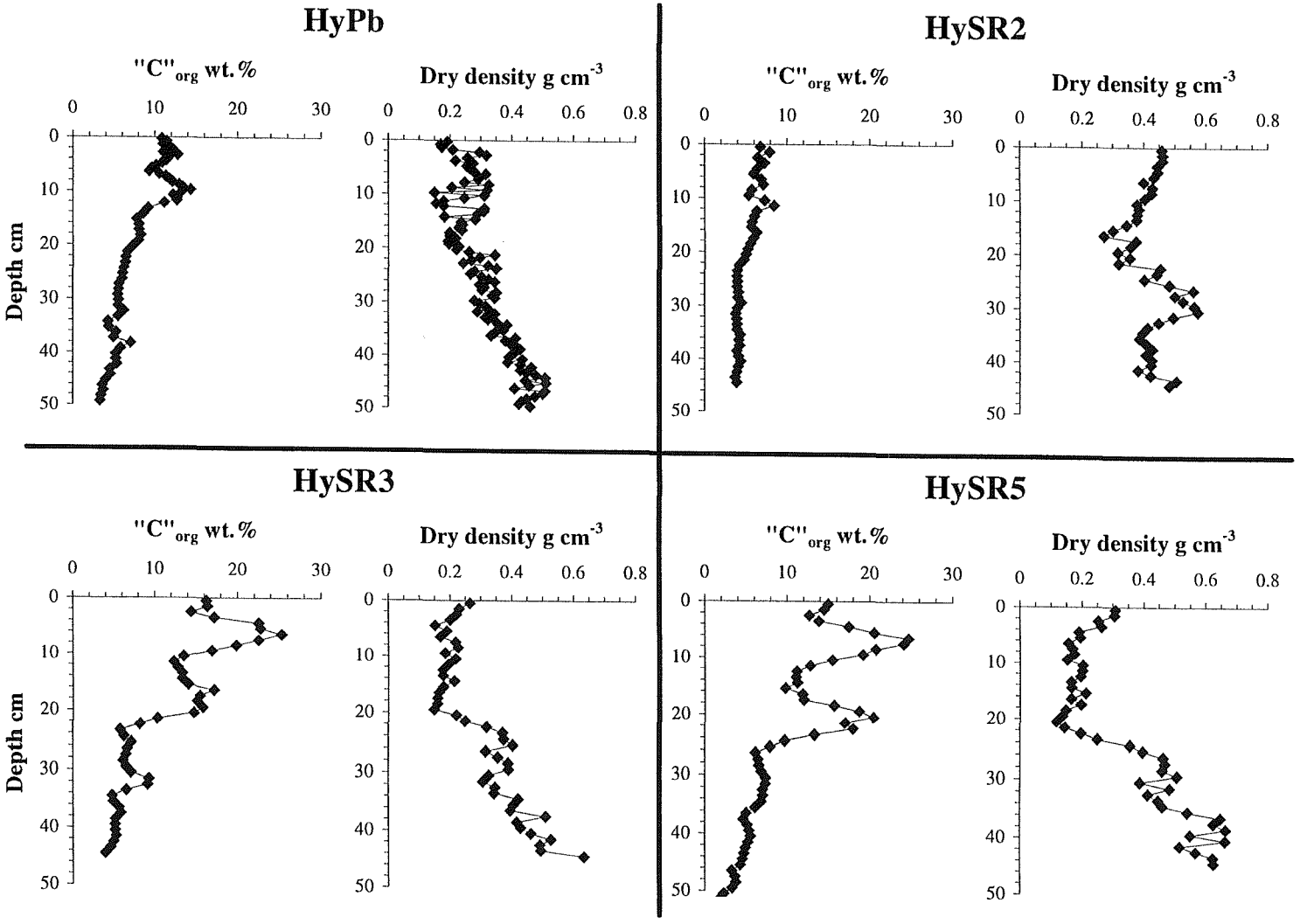

Figure 3.5:
Empirically determined organic carbon concentration profiles (from LOI correlation).

3.4 Core mineralogy and major solutes

3.4.1 *Si, Al, K, Ti and Cr*

A number of elements analysed during this study appear to exhibit negligible post-depositional redistribution within the sediment prism. The existence of silicon, aluminium, potassium, titanium and chromium in recent sediments is primarily due to their incorporation within the crystal structure of allogenic mineral particles (Shotyk *et al* 1990). In such lattice-bound sites the atoms exhibit inert geochemical behaviour and so variations determined in their concentration-depth profiles usually originate from changes in the composition of the sedimentary material (Figure 3.6). Such effects in Hythe Marsh are attributable either to variation in the predominance of the organic fraction (corresponding to the lattice-element minima present in the upper decimetres of cores HySR3 and HySR5) or the rare occurence of sand and flint gravels (core HySR5, basal quarter). Normalisation of the data to aluminium, which is also subjected to the effects of variable sedimentary composition, compensates for concentration variations of Si, Ti, K and Cr which are due to the abundance of the clay mineral carrier phase. The normalised profiles (Figure 3.6) reveal that these element distributions conform to one another very closely and exhibit negligible diagenetic activity.

Core	Si/Al	Ti/Al	K/Al	Cr/Al
HyPb	2.9 ± 0.1	0.056 ± 0.002	0.31 ± 0.02	11.6 ± 0.5
HySR2	3.0 ± 0.1	0.058 ± 0.001	0.28 ± 0.01	12.6 ± 0.5
HySR3	2.9 ± 0.1	0.059 ± 0.002	0.27 ± 0.01	12.9 ± 0.5
HySR5	2.9 ± 0.1	0.061 ± 0.002	0.29 ± 0.01	13.7 ± 0.3

Table 3.2:

Element to aluminium ratios for lattice-bound elements in Hythe sediment cores.

The constancy of the parameters Si/Al, K/Al, Ti/Al and Cr/Al throughout each core (Figure 3.6) additionally identify the composition of the mineral component as being consistent over time at each sample site, with the exception of core HySR5. In these latter samples the increased abundance of a siliceous phase at depth (flint stones) results in a different mineralogical composition of the sedimentary matrix. The mean ratios of each of these

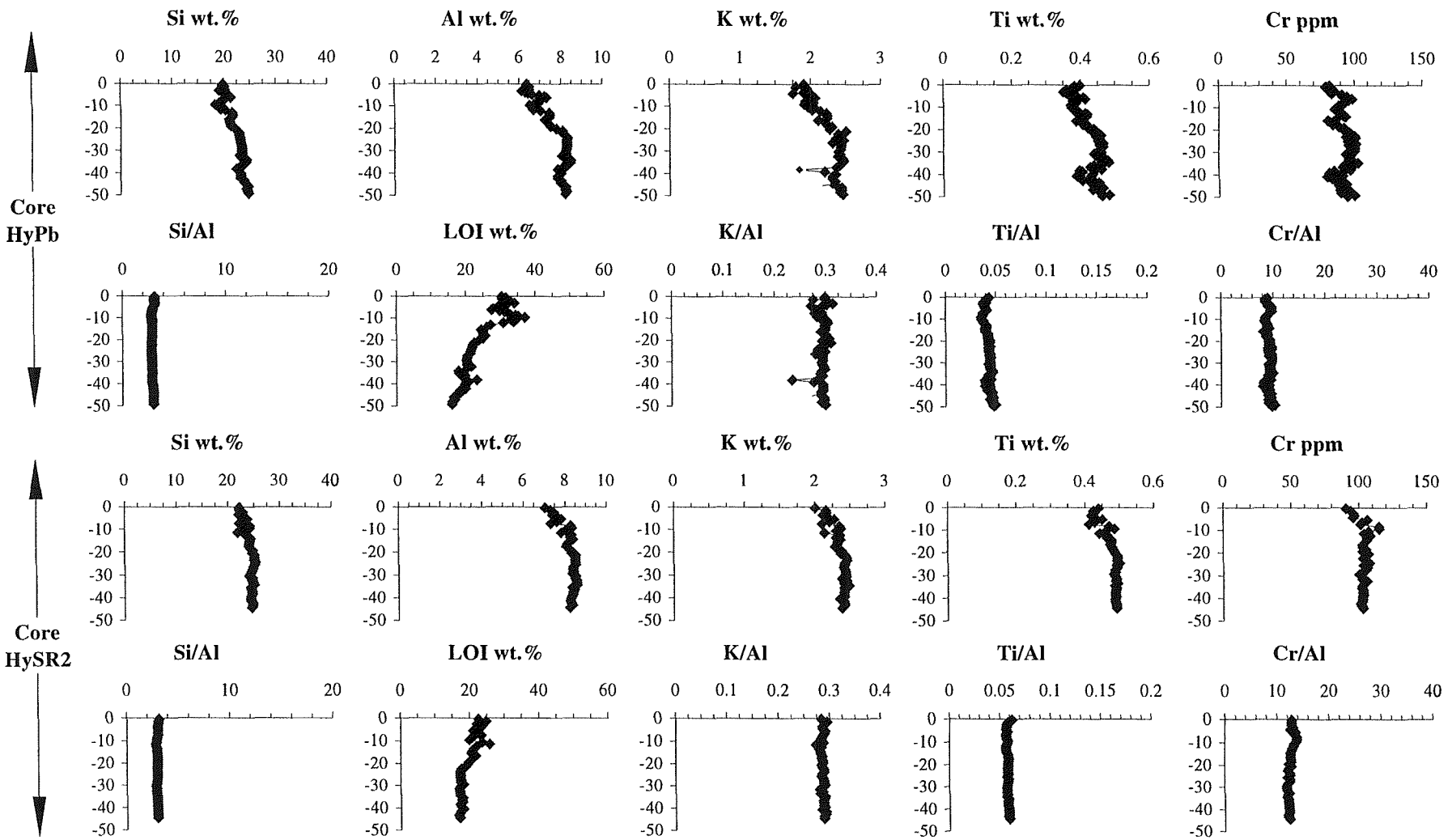

Figure 3.6 (a):
Concentration profiles and normalised ratios of elements controlled by mineralogical variations. Loss on ignition also shown.

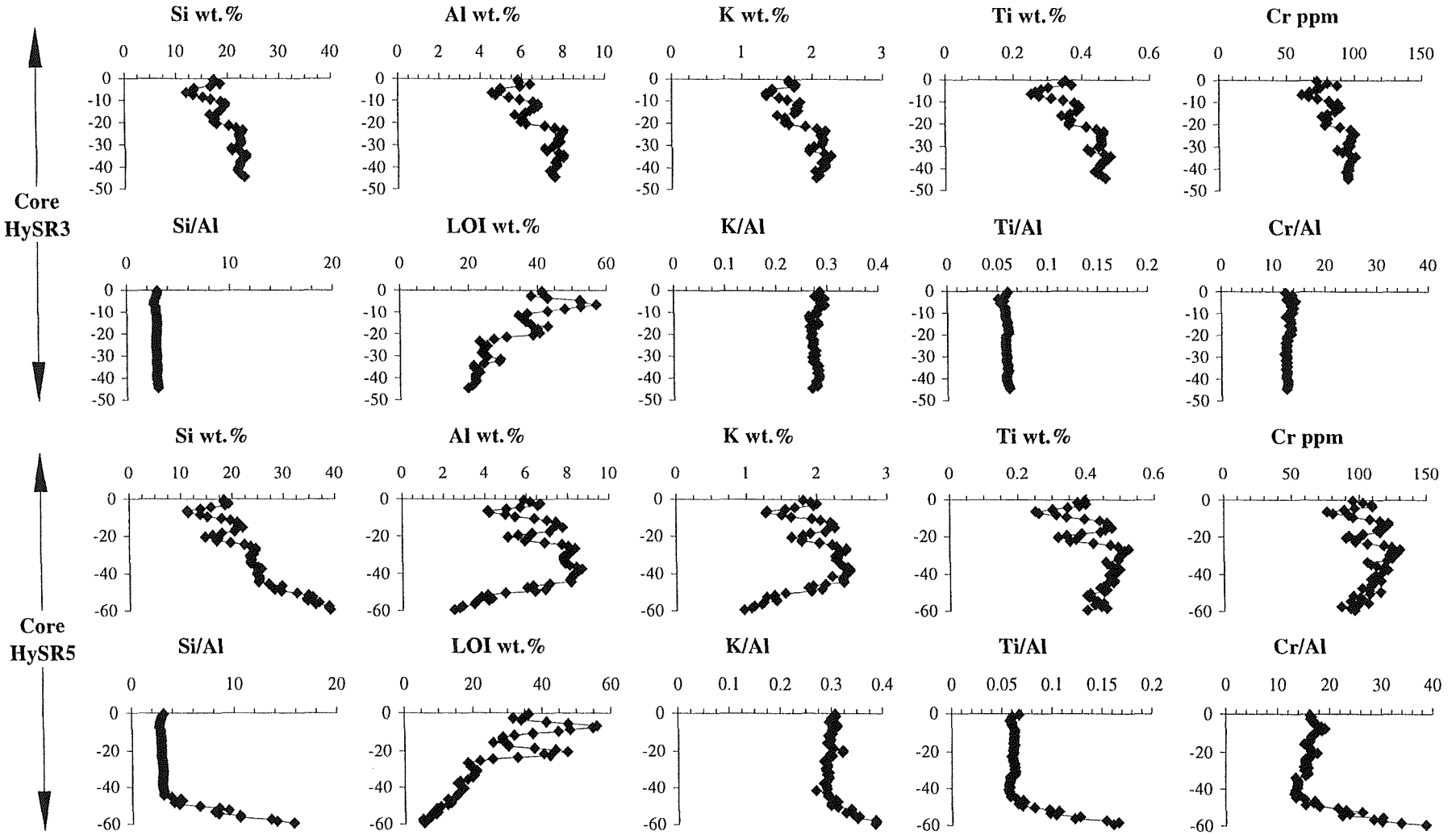

Figure 3.6 (b):
Concentration profiles and normalised ratios of elements controlled by mineralogical variations. Loss on ignition also shown.

elements to aluminium, within the muddy portion of each sediment core, may be compared to identify mineralogical variations between the cores. For the elements Si, K, Ti and Cr these values are in reasonable agreement (Table 3.2) and do not show significant alteration from one site to another. The bulk of the mineral fraction thus appears to be relatively uniform across the marsh.

3.4.2 *Manipulation of element data*

The distribution in Hythe Marsh sediments of those elements considered above is easily understood simply in terms of the abundance of detrital mineral particles. For many other elements, however, more complex processes interact to generate the overall solid phase distributions measured in the laboratory. Interpretation of the element data may therefore be facilitated by calculation of the contribution made to the total concentration by certain phases of the sediment matrix. The equations (Figure 3.7) used throughout this report to calculate more helpful data from the total concentration profiles are explained below:

3.4.2.1 Salinity correction

Certain of the elements considered in this chapter, along with iodine and bromine (discussed in Chapter 6), are major dissolved constituents of sea water and thus may be present in the saline pore waters of the marsh at a significant concentration. To account for this contribution the data for Na, Mg, Ca, Br, I and S may also be considered following correction for a sea water-derived component, determined from the amount of chlorine present and the known mean sea water composition (Equation 3.1). This manipulation of the data, assuming that all of the Cl originates from sea water, is effective in identifying certain features of the element profiles which derive from the presence of saline interstitial fluids. The symbol # is used to represent data which have been corrected for such a component (e.g. Ca# wt.%). For iodine the contribution from this phase is typically no more than a few per cent. The other elements, however, are present in significant part as dissolved constituents.

3.4.2.2 Excess element concentration

A wide range of elements may be found occupying the lattice sites of common sedimentary minerals and in unpolluted regions this may dictate the background concentration of the element in a sediment sequence (Williams *et al* 1994). It is useful to be able to distinguish between this component and any anthropogenic contribution present. This may be done by calculating the amount of each element present relative to aluminium (as a proxy of the mineralogical composition) and identifying the value of the detrital (chiefly lattice-bound) element to aluminium ratio in these sediments. The detrital element concentration within any sample may then be determined and enable calculation of the "excess" (non-lattice-bound) element concentration (Equation 3.2). This parameter is given the symbol * (e.g. Cu*) throughout this report.

Salinity correction

$$X\# = X_{tot} - (X/Cl_{sw} \times Cl_{sample})$$ **Equation 3.1**

where X# is the salinity-corrected element concentration ($\mu g\ g^{-1}$),

X_{tot} is the total element concentration ($\mu g\ g^{-1}$),

X/Cl_{sw} is the ratio of element to chlorine is normal seawater,

and Cl_{sample} is the chlorine concentration in the sample.

Excess element concentration

$$X^* = X_{tot} - (R_{det} \times C_{al})$$ **Equation 3.2**

where X^* is the excess element concentration ($\mu g\ g^{-1}$),

X_{tot} is the total element concentration ($\mu g\ g^{-1}$),

R_{det} is the detrital ratio of the element to aluminium,

and C_{Al} is the concentration of Al (wt.%).

Figure 3.7:

Calculations applied to selected element data throughout this report.

3.4.3 *Na, Cl, Mg and Ca*

Examination of both the total (Figure 3.8) and the salinity-corrected (Figure 3.9) data reveals that the presence of both chlorine and sodium within the marsh sediments is predominantly due to the inclusion of saline waters within the sample material. An excess of chlorine over sodium, relative to the assumed sea water composition, is evident in some core sections at depths where intense root growth occurs. This could be caused by the assimilation and upward transportation of sodium ions within the plant tissue, although the exact origin of this phenomenon has not been investigated here.

The distribution of calcium enrichment within the upper sediments conforms closely to that of excess manganese. Association of these two elements (Figure 3.10) may derive from the precipitation of $CaCO_3$ as a result of the generation of alkalinity, concomitant to the oxidation of organic matter by manganese (Froelich *et al* 1979; discussed in Chapter 5). Other peaks in Ca# are found, in similar fashion to magnesium, at depths abundant with organic material in cores HySR3 and HySR5 (Figure 3.9). These peaks are evident for both elements only after normalisation to aluminium and may therefore be an artifact of the data manipulation. The presence of a source phase for these elements other than sea water and clay mineral particles (calcium carbonate, for example), which is uniformly distributed throughout the core, could be responsible for generation of the elevated ratios simply due to the decreased abundance of the normalising element (see Figure 3.1). Furthermore, the adsorptive capacity of humic substances for dissolved Mg^{2+} and Ca^{2+} is able to immobilise these cationic species from flood waters and may result in their concentration into the solid phase at depths with abundant organic materials (Mantoura *et al* 1978). In such a case the normalisation procedure would certainly create erroneous data since the actual carrier phase (C_{org}) is present at an elevated concentration whilst the assumed normalising phase (Al) is diluted.

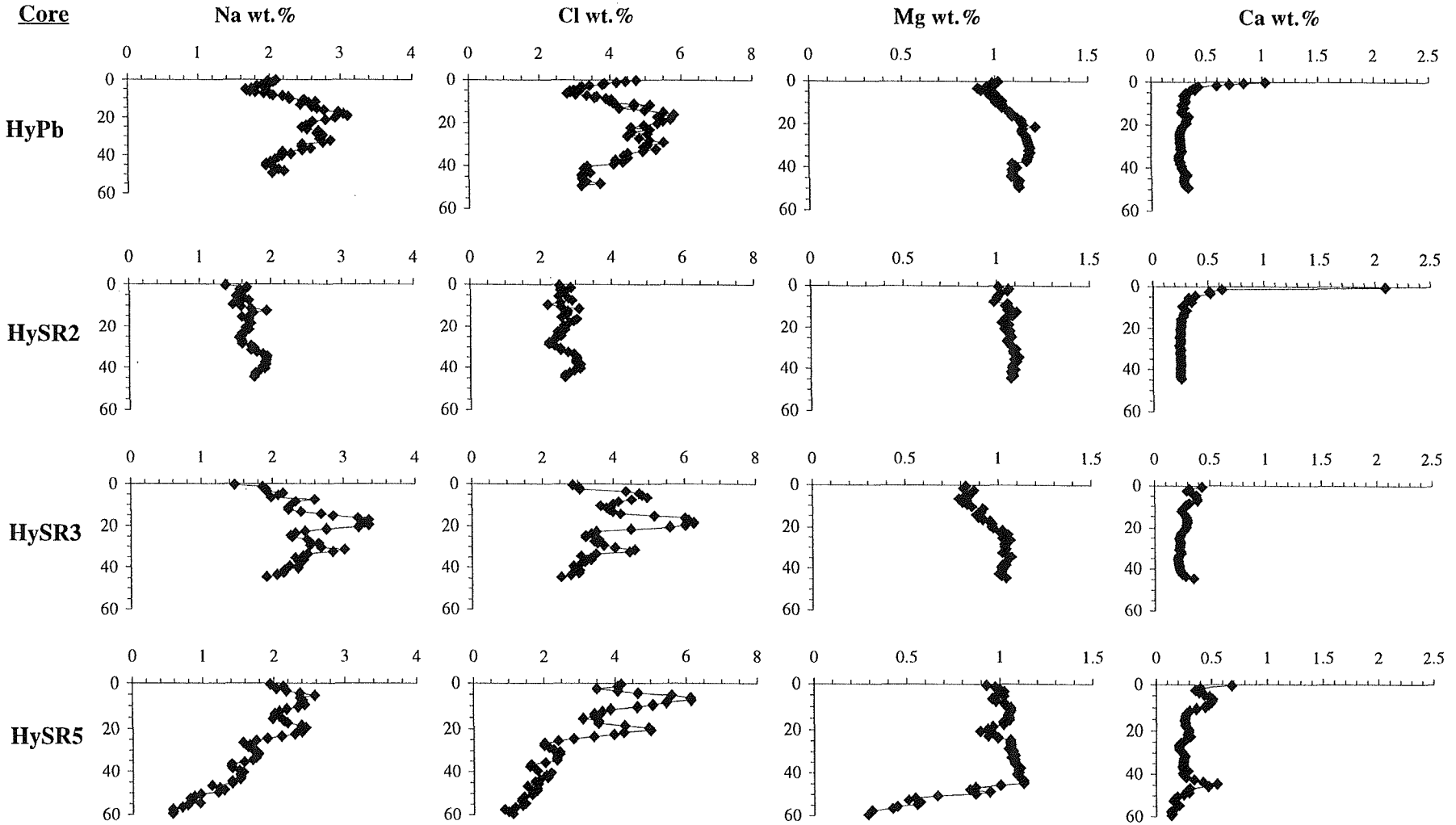

Figure 3.8:
Sediment core profiles of elements controlled by mineralogical variations (Mg and Ca) and/or saline pore fluids (all elements).

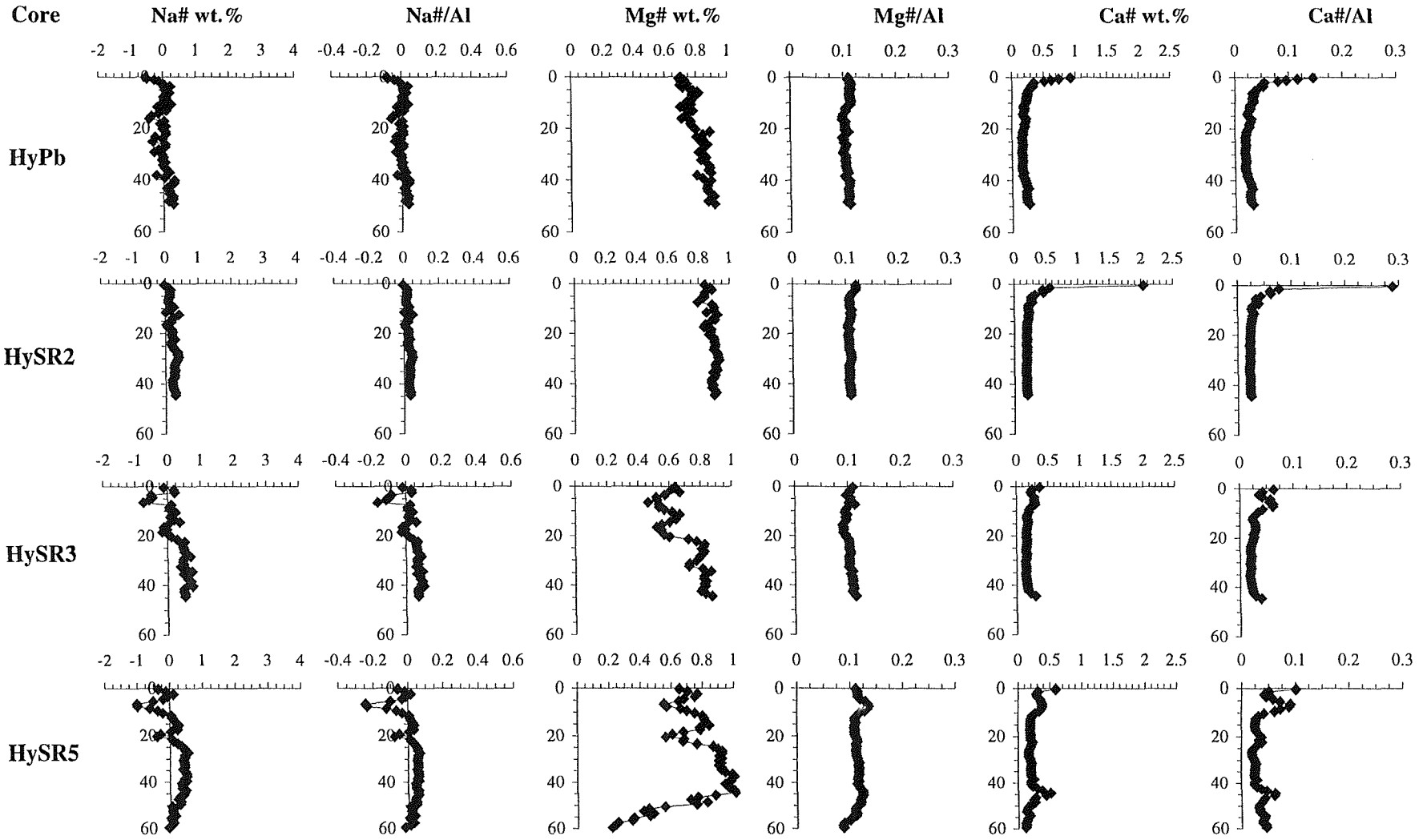

Figure 3.9:
Profiles of sodium, magnesium and calcium following removal of the salinity-derived component and normalised to aluminium.

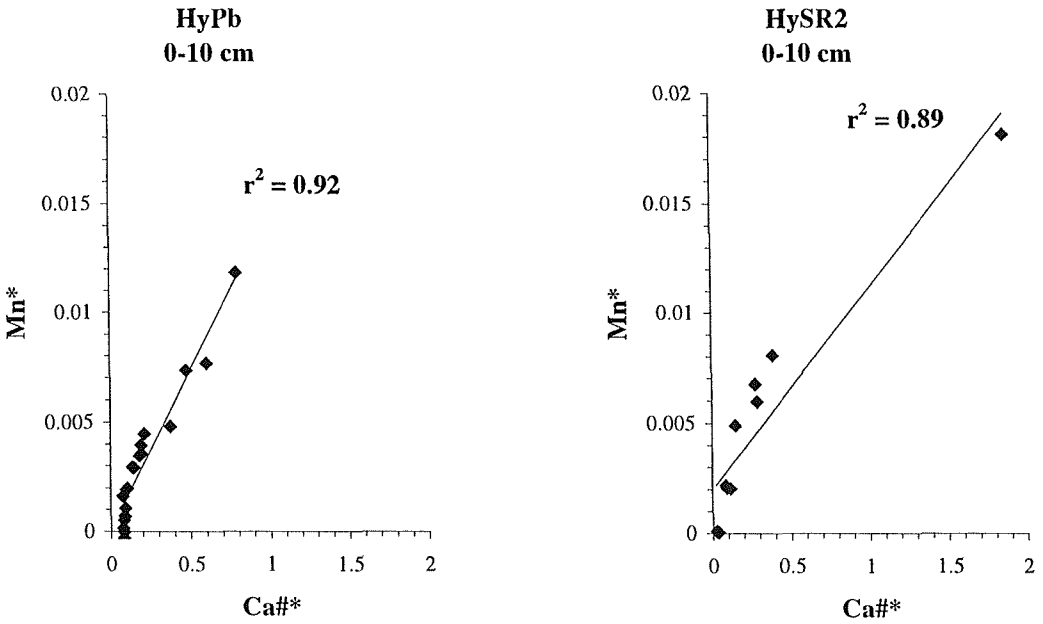

Figure 3.10:
Correlation between excess calcium and excess manganese concentrations over the depth of manganese enrichment within the two front-marsh cores.

3.5 Summary

The sediments of Hythe Marsh contain a range of identifiable facies but are essentially composed of mud, with an approximately constant mineralogical composition, and root materials. Core HySR2 is the most minerogenic whilst cores HySR3 and HySR5 each contain a double sub-surface organic carbon peak created by the lateral growth of roots within the peaty upper section. The distributions of Si, Al, K, Ti, Cr, Na, Cl, Mg and Ca can be accounted for (with minor exceptions in areas of root abundance) by the nature of the sedimentary matrix and the composition of the pore fluids. There is therefore little evidence of diagenetic activity within this suite of elements, a situation which contrasts markedly with the behaviour of many other elements to be considered (Chapters 5 and 6).

Chapter Four

Core Chronologies

4.1 Application of ^{137}Cs to studies of sediment accretion

The interpretation of ^{137}Cs activity profiles in contemporary soils and sediments to elucidate accumulation rates has received much attention in recent years (Ritchie and McHenry 1990). Numerous accounts exist of the successful application of this radiometric technique in a wide variety of sedimentary environments including lakes (Krishnaswamy *et al* 1971; Robbins and Edgington 1975), coastal basins (Chanton *et al* 1983) and salt marshes (DeLaune *et al* 1978; Milan *et al* 1995). However, some workers have reported incidences where there has been a failure in the method to yield reliable chronologies (Davis *et al* 1984; Longmore *et al* 1986) and it is therefore necessary to exercise caution when attempting to use ^{137}Cs profiles for dating purposes. The assumptions underlying the technique must be critically examined for each application to ensure that the rates of accumulation derived from the particular study are meaningful.

4.1.1 *Origin*

Caesium-137 is not a naturally-occurring isotope but is present in the environment as a result of human activities. It is a significant component, ~6% of the yield (Davis 1963), of the spectrum of nuclides produced following nuclear fission and is unstable. Decay occurs through beta emission with an associated gamma energy of 662 keV and a half-life of 30 years.

4.1.1.1 Weapons testing

Caesium-137 enters the environment via the detonation of thermonuclear weapons or other experimental devices, and releases from either civil or military nuclear installations, either intentionally or accidentally. The most significant contribution by far to the global ^{137}Cs budget has been from the nuclear weapons test programmes, comprising about 800 detonations over the past few decades (Carter and Moghissi 1977). The radioactivity derived from these explosions is not restricted to the area surrounding the test site, but instead may be injected into the stratosphere where it is able to circulate and become incorporated into global fallout (Davis 1963). Generation of ^{137}Cs began in July 1945 with the first US nuclear test, Trinity, in the desert near Alamogordo, New Mexico. Over the following decades the frequency and magnitude of nuclear detonations has not been constant, resulting in a temporal variability in the introduction of fission-derived radioisotopes into the environment. The ensuing characteristic radioactive fallout pattern has been described by several workers and has been shown to have latitudinal variation and to be linearly correlated with rainfall (Davis 1963). The

trend in the deposition of ^{137}Cs in the Northern Hemisphere (Playford *et al* 1992) is shown in Figure 4.1. This varies somewhat from that which is observed in the Southern Hemisphere as a consequence of the greater yield of nuclear detonations in the Northern Hemisphere and incomplete stratospheric mixing between the two hemisperes. The key features of the ^{137}Cs fallout pattern and their origins (Carter and Moghissi 1977) are:

- **onset of deposition**

  Detectable levels of ^{137}Cs in surface environments away from specific test sites are generally thought to have first been deposited in 1954 (Wise 1980), although the exact year used tends to vary between authors. Schaffner *et al* (1987) assumed the first appearance of the isotope in James River Estuary sediments to correspond to 1950, whereas Davis (1963) suggests that measurable stratospheric fallout began following the detonation of the first large thermonuclear device in 1952;
- **fallout peak 1958-59**

  The detonation of 96 nuclear devices during 1958 increased the cumulative yield (in equivalent tonnes of TNT) from ~47 Mtonne to ~75 Mtonne;
- **fallout peak 1963**

  Very few nuclear tests were conducted between November 1958 and September 1961 during the Moratorium on Nuclear Testing agreed between the US, UK and USSR. However, in 1961 and 1962 a large number of high yield devices were detonated increasing the cumulative yield from ~75 Mtonne at the end of 1960 to ~256 Mtonne by the end of 1962;
- **Limited Test Ban Treaty**

  This agreement, between the US, UK and USSR, entered into force in October 1963 and prevented these nations from carrying out nuclear weapons tests that would cause radioactive debris to be carried outside of their national boundaries.

4.1.1.2 Other sources of ^{137}Cs

Sources of ^{137}Cs other than from the weapons testing programmes tend to be considerably more localised and thus may vary in their significance relative to global fallout depending on the location under observation. The only such source of radioactivity of concern to the present study is that due to fallout derived from the nuclear reactor accident at Chernobyl, Ukraine, which occurred on 26th April 1986. This resulted in the deposition of ^{137}Cs and other isotopes across much of Europe (Anspaugh *et al* 1988) with a very high degree of regional variability related to proximity to the accident, wind direction and rainfall patterns. The plume of

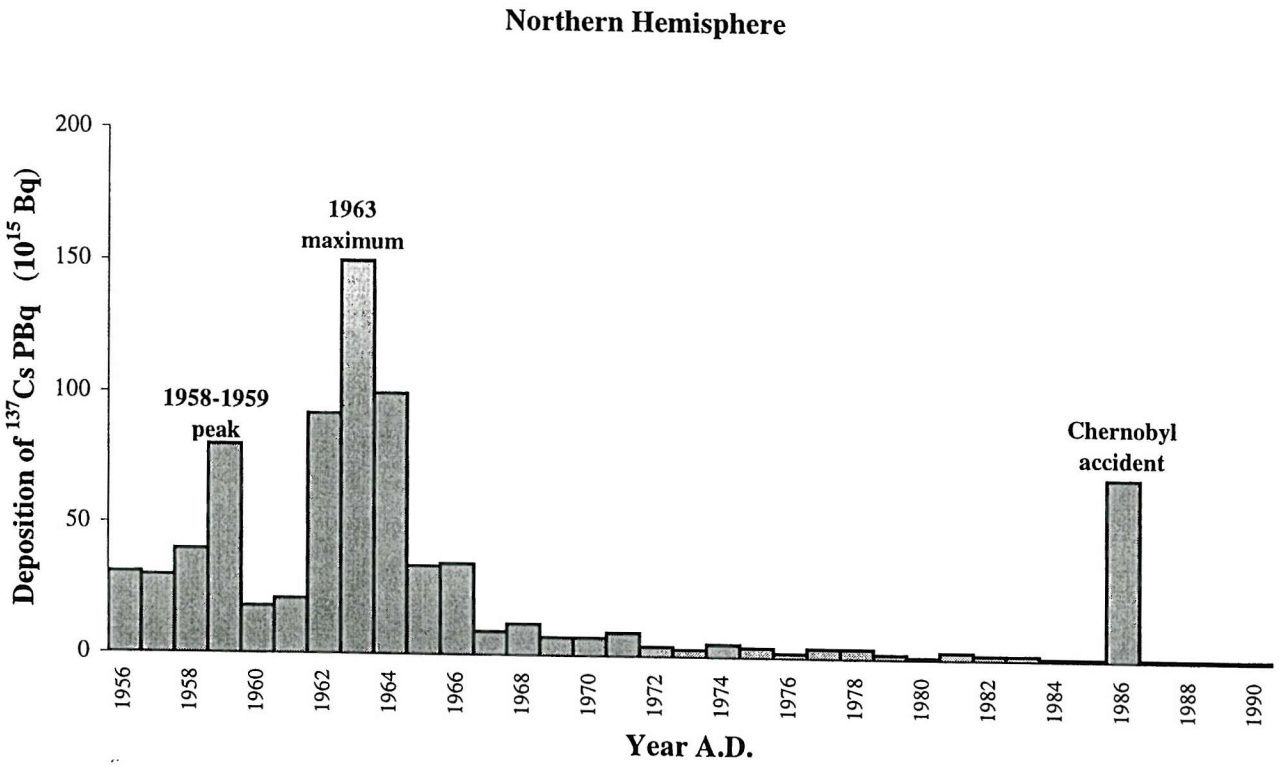

Figure 4.1:
Annual deposition of ^{137}Cs in the Northern Hemisphere (Playford *et al* 1992).

contaminated air and particles reached the UK on 2nd May 1986 and the subsequent deposition has been the subject of much scrutiny. According to Cambray *et al* (1987) the fallout from this accident has increased the pre-existing world-wide inventory of ^{137}Cs by about 5% overall, but in the UK by nearly 40% due to the proportionately higher dose received. Within different regions of the British Isles, however, the relative contribution of this radioactivity to the pre-existing contamination is very variable as a result of meteorological effects, principally non-uniform rainfall. The 1986 peak in Northern Hemisphere fallout visible in Figure 4.1 is derived from the Chernobyl plume.

The nuclear reprocessing plant and power station situated at Sellafield, on the Cumbrian coast, also represents a potential source of ^{137}Cs to Solent estuarine sediments. The isotope is routinely discharged into the Irish Sea and shows quasi-conservative behaviour in sea water (MacKenzie *et al* 1987). However, studies into the fate of Sellafield-derived caesium-137 have concluded that the discharged activity circulates in the Irish Sea before passing around the Scottish Coast into the North Sea, from which it exits via the Norwegian Coastal Current about six years after release (Prandle and Beechley 1991). Only a small fraction of the discharge is retained in Irish Sea sediments (MacKenzie *et al* 1987), with most being dispersed into more distant waters such as the Arctic Ocean (Livingstone *et al* 1982). From these studies, it may be concluded that Sellafield-derived ^{137}Cs is not accumulated to any significant extent in sediments of the southern English Coast (see also Cundy *et al* 1997, Appendix C).

4.1.2 *Environmental pathway and chemical mobility*

The deposition of caesium from the atmosphere to the surface of the Earth has been shown to be linearly correlated with rainfall for a given atmospheric concentration (Davis 1963). The resulting fallout may then arrive on to one of three principal types of surficial material: vegetation, water or soil/sediment (see Figure 4.2).

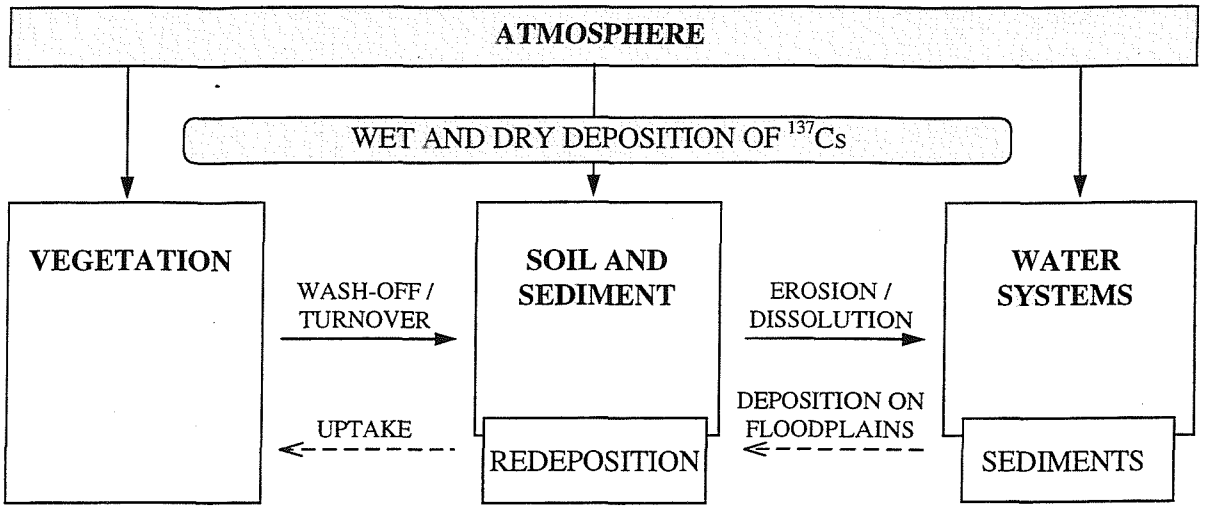

Figure 4.2:

Diagram of the ^{137}Cs cycle on the landscape
(from Ritchie and McHenry 1990).

The routing of ^{137}Cs through these environmental reservoirs is discussed below.

4.1.2.1 Vegetation

Long term storage of caesium within most types of vegetation is relatively small (Wise 1980), although this reservoir may be important on timescales of months prior to the element arriving in a more permanent sink. Rogowski and Tamura (1970) found that ^{137}Cs applied to the leaf surface of grasses was almost completely washed off into the soil after twelve months, with 75% loss reported after 153 days. It has been suggested (Wise 1980) that adsorption on to soil particles on the leaf surface rather than actual absorption by the plant is a more important control over the routing of caesium deposited on to such surfaces. The limited amount of caesium that does become absorbed by foliage will still eventually find its way into the soil as plant litter, though it may be held in the vegetation store for some time (months to years, according to plant type; upland pastures, for example, have exhibited an unexpectedly strong tendency to retain Chernobyl-derived ^{137}Cs within their nutrient cycle (Campbell and Davies 1997). Following wash-off or turnover from vegetation, caesium is strongly associated with mineral and organic soil particles and has been shown to concentrate in the upper surface of soils on which it is deposited, through firm binding to solid materials (Rogowski and Tamura 1970). In addition, these authors reported minimal uptake from the soil into new vegetative

growth, with overall loss of ^{137}Cs from the three test plots being directly correlated with soil erosion.

4.1.2.2 Water

Direct deposition on to the surface of water and rapid run-off of labelled precipitation into drainage basins can contribute to dissolved ^{137}Cs in water masses. Aston and Duursma (1973) conducted laboratory trials which demonstrated that the K_d of caesium in mixtures of suspended sediment and water is a function of the concentration of suspended particulate matter, with a strong tendency for the element to partition into the solid phase.

4.1.2.3 Soil and sediment

The dominant control on the distribution of ^{137}Cs in the environment is through binding to soil and sediment particles (Lomenick and Tamura 1965; Rogowski and Tamura 1970). Clay minerals have been shown to exhibit a high affinity for the adsorption of caesium ions (Francis and Brinkley 1976) due to the favourable interlattice spacing and the size of the Cs^+ cation. Illite in particular has been studied for its adsorption characteristics, leading to the proposal of a model for a kinetic control of this process (Comans *et al* 1991; Comans and Hockley 1992). The suggested manner in which caesium adsorbs on 2:1 clays is through instantaneous though reversible ion exchange with the edges of the mineral layers (important over timescales of days), followed by the slower, kinetically controlled, migration of the ions to interlattice sites (over timescales of years) from which they may be virtually non-exchangeable (Lomenick and Tamura 1965; Davis 1963). Indeed, the diagenetic mobility of ^{137}Cs observed in some sediment sequences has been attributed to the scarcity of weathered micaceous clay minerals, such as illite, with their abundant interlayer sites for ion exchange (e.g. Evans *et al* 1983; Davis *et al* 1984). The sediments of the Solent region contain abundant illite and montmorillonite (Gilkes 1968; Algan 1994) and are therefore likely to represent a significant sink for the isotope.

Examples of other situations which may result in the disturbance of ^{137}Cs profiles in sediments, either by chemical mobility or particle reworking, have been reported. These include:

I. increasing salinity, resulting in higher concentrations of competing ions such as Na^+, Mg^{2+} and Ca^{2+} for the exchange sites (Aston and Duursma 1973; Patel *et al* 1978; Longmore *et al* 1986);
II. release, during decomposition, of ^{137}Cs bound to organic matter (as suggested by Davis *et al* 1983 in a study of clay-deficient lake sediments);
III. under anaerobic conditions mobility may arise following the generation of cations such as NH_4^+, Mn^{2+} and Fe^{2+} leading to ion-exchange displacement (Evans *et al* 1983; Smith and Comans 1996);
IV. finally, bioturbation may result in the physical movement of particles along with their adsorbed species. The predicted effect of this is to broaden activity peaks, obliterating fine scale features, and move them deeper into the sediment (Goreau 1977).

4.1.2.4 *Salt Marsh ^{137}Cs Profiles*

The sediment accumulating in salt marshes is a mixture of atmospheric and marine-derived particles combined with plant litter from primary production (De Laune *et al* 1978). The marine contribution furthermore may be comprised of estuarine suspended material originating from atmospheric deposition, fluvial run-off, intra-estuarine surface erosion, coastal erosion and off-shore sources. All of these provenances have the potential to contribute to the ^{137}Cs inventory in the marsh sediment prism.

The application of ^{137}Cs dating relies on the identification of a maximum in the activity of the isotope at a depth which can then be correlated with a known period of deposition. The year of maximum atmospheric fallout and the year of deposition of maximum measured activity are usually assumed to be the same, but may be offset due to the time lag generated during the passage of ^{137}Cs through the environment. Studies of lake sediments have been conducted enabling calculation of the contribution of catchment erosion to the sediment ^{137}Cs inventory (Wise 1980; McHenry *et al* 1973, cited therein). These authors report that, in certain circumstances, activity peaks in eroded material occur several years after the maximum fallout during 1963. The extent to which activity profiles may deviate from the record of atmospheric fallout, due to the accretion of externally-labelled material, is dependent on the temporal variability in the relative contribution of these two sources. This may be difficult to assess, but

simultaneous application of an independent dating method and estimation of the fallout inventory for the area under study may be of benefit.

4.1.3 *Results and interpretation of Hythe ^{137}Cs profiles*

Caesium-137 activity profiles have been determined throughout the uppermost sections of three sediment cores from different locations within Hythe salt marsh. From the above discussion of fallout trends it is apparent that the features pertinent to the application of such profiles to determine sediment accumulation rates are: the 1963 fallout maximum, the 1958 fallout peak, the 1986 Chernobyl peak, and the onset of measurable deposition in the early 1950s. Attributing these event horizons to specific depths within each profile may be done with a variable degree of confidence.

The depth distribution of ^{137}Cs in the cores studied typically consists of one major peak and one or two minor peaks (Figure 4.3). The correlation of these activity profiles with the measured fallout record is relatively straightforward. Table 4.1 details the locations of the peaks within each core in terms of their suggested period of deposition along with the interpreted sediment accumulation rates. As an assessment of the error in identifying the depth of each peak, the locations of the edges of the sediment slice (1 cm thick) are used as upper and lower limits. Cores HySR2 and HySR3 each contain three activity maxima, which may be attributed to the three periods of elevated atmospheric fallout. Core HySR5, however, exhibits only two peaks in ^{137}Cs activity, with the increased deposition of the isotope due to the 1958 fallout episode apparently not preserved. The features applicable to determining the rate of sediment accumulation within the three cores are discussed below.

4.1.3.1 The dominant activity peak

The most clearly-defined peak in each of the three activity profiles is interpreted as originating from the global fallout maximum which occured during 1963. From a comparison of Figure 4.1 and Figure 4.3 a number of differences are apparent. The atmospheric fallout peak at this time is both sharper (constrained over a shorter time period) and of greater magnitude (compared to earlier and later years) than the record preserved in the salt marsh. These differences are likely to be due to a combination of the deposition of reworked ^{137}Cs-labelled sediments, both before and after the maximum fallout period, and possible diagenetic migration of $^{137}Cs^{+}$ within the sediment column. Both of these processes may lead to peak broadening and a decrease in peak magnitude. It is assumed, however, that the actual location of the sediment of maximum activity

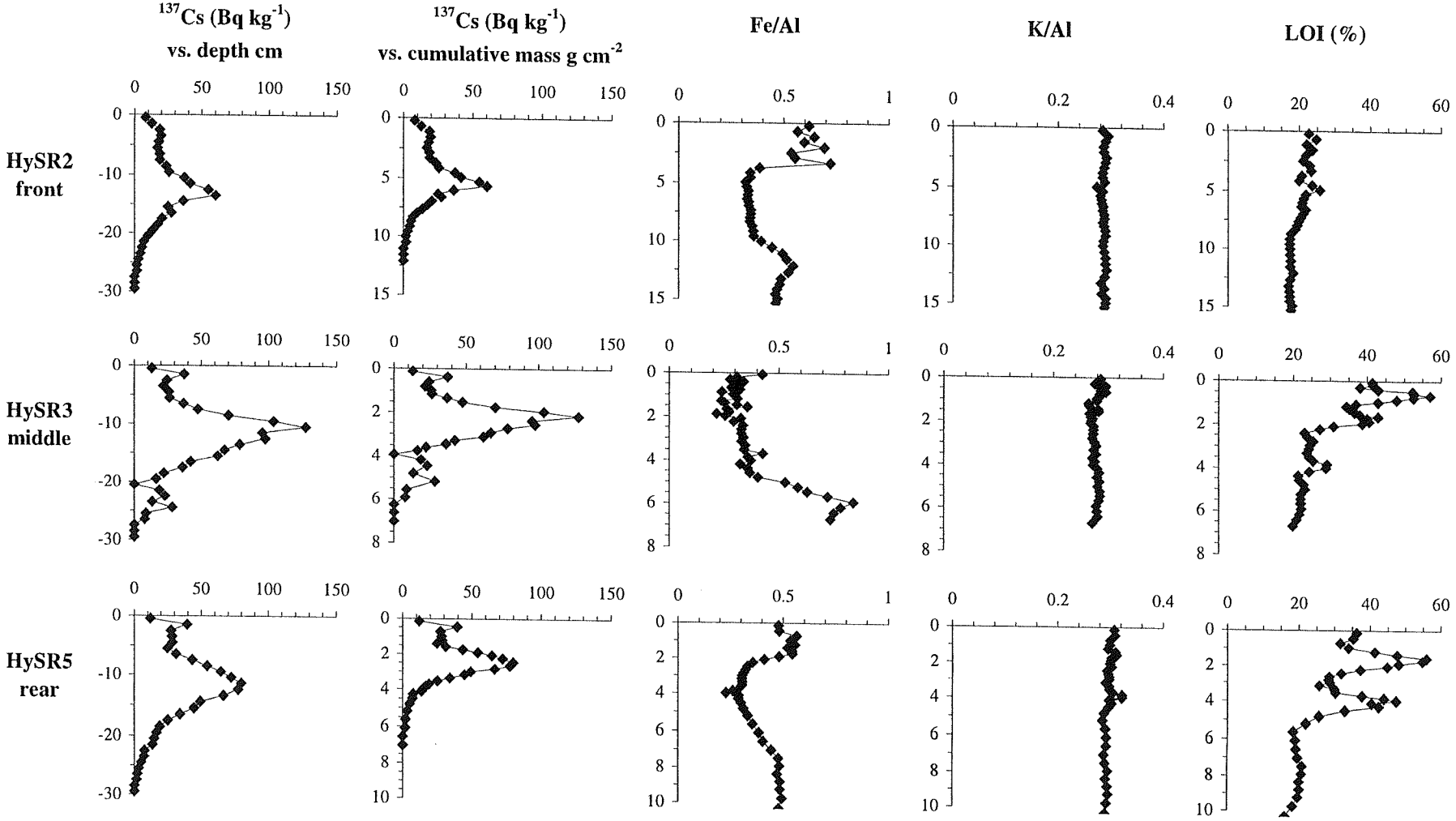

Figure 4.3:
^{137}Cs activity profiles and other geochemical parameters in three salt marsh cores.

	1963 peak	1958 peak	1986 peak	fallout onset
(a) HySR2				
Depth cm:	13-14	16-17	3-4	26-27
Accretion rates				
cm yr^{-1}	**0.45** ± 0.02	**0.47** ± 0.02	**0.50** ± 0.07	-
g cm^{-2} yr^{-1}	**0.189** ± 0.007	**0.190** ± 0.004	**0.229** ± 0.032	-
(b) HySR3				
Depth cm:	10-11	12-13	1-2	26-27
Accretion rates				
cm yr^{-1}	**0.35** ± 0.02	**0.36** ± 0.02	**0.21** ± 0.08	-
g cm^{-2} yr^{-1}	**0.072** ± 0.004	**0.073** ± 0.003	**0.054** ± 0.017	-
(c) HySR5				
Depth cm:	11-12	n.i.	1-2	27-28
Accretion rates				
cm yr^{-1}	**0.38** ± 0.03	n.i.	**0.21** ± 0.08	-
g cm^{-2} yr^{-1}	**0.082** ± 0.003	n.i.	**0.066** ± 0.022	-

Table 4.1:

Accretion rates (both cm yr^{-1} and g cm^{-2} y^{-1}) derived from the location of ^{137}Cs activity peaks in three salt marsh cores (n.i. denotes peak not identifiable).

has remained unaffected. Radioactive decay will obviously also decrease the relative magnitude of the peak, but would not result in the the extensive downcore peak tailing observed in all three cores.

4.1.3.2 The near-surface minor peak

The atmospheric deposition of Chernobyl-derived ^{137}Cs occurred over a short period during 1986 (Anspaugh *et al* 1988). Although elevated airborne activities in subsequent years have been observed, attributed to aeolian resuspension of surficial material (Cambray *et al* 1987), the majority of the fallout occurred as a relatively rapid pulse. An accreting medium, such as a salt marsh, thus ought to preserve a thin band of isotope-rich material corresponding to the sediment surface at this time. This is the case in cores HySR3 and HySR5, where the Chernobyl-derived activity seems to be constrained within a single, 1 cm thick, sample. In core HySR2, however, there appear to be several samples containing elevated activities, probably originating from the incorporation of significant amounts of externally-labelled material in this near-shore zone of the marsh. The depth of the sediments which have accumulated since the Chernobyl fallout episode is relatively small, and consequently the range of accumulation rates obtained from the top and bottom of each near-surface sample slice is considerable. Only in the case of HySR2, however, is there no overlap between the possible Chernobyl-derived accumulation rates and those rates determined from the other marker horizons (Table 4.1). This may be the result of a genuine change in the rate of sedimentation over recent decades, but is more likely to be due to inaccurate identification of the exact position of the 1986 horizon in this core due to the broadened nature of the peak.

4.1.3.3 The minor peak at depth

Cores HySR2 and HySR3 each exhibit a small point of inflection below the 1963 horizon, which is identified as being due to deposition during the 1958 peak fallout episode. As with the 1963 peak, however, the sediment profile maxima do not appear as significant as the historical fallout records would suggest, even after allowing for radioactive decay. Possible reasons for this have already been discussed above and are further explored below with respect to the diagenetic mobility of ^{137}Cs within the sediment prism. Presumably the 1958 fallout peak in core HySR5 has suffered obliteration to the degree where it is no longer identifiable within the activity profile. The accumulation rates obtained from the two identified 1958 horizons are in excellent agreement with those derived from the 1963 activity peak (Table 4.1).

4.1.3.4 The onset of deposition

Measurable levels of ^{137}Cs activity are present to depths of 26-27 cm in cores HySR2 and HySR3, and 27-28 cm in core HySR5. Utilising the sediment accumulation rates obtained from the 1963 activity maxima, these depths correspond to sediments deposited during or prior to 1940, 1916 and 1923, respectively. All three of these dates are considerably older than the initial introduction of ^{137}Cs into the environment. The cause of this apparent anomaly could either be particle reworking to a greater depth, a genuine change in the sedimentation rate (comparing the period 1950 to 1963 with 1963 to the present) or aqueous diffusion of $^{137}Cs^{+}$ cations. Within the stable sediment prism of the salt marsh the former process is not expected to be significant (McCaffrey and Thomson 1980), whereas the latter may occur as a result of competition for ion exchange sites between caesium and other cations. This is discussed further below.

4.1.4 *Mobility of ^{137}Cs in Hythe Marsh cores*

Evidence obtained from the analysis of caesium-137 activity profiles throughout the three cores suggests that the isotope may be partially labile during early diagenesis. Figure 4.3 displays the inter-relationship between the ^{137}Cs distribution, solid phase iron concentration, mineralogical variation (represented by K/Al) and organic content (closely related to the pattern of LOI). These three important geochemical parameters do not appear specifically responsible either for the location of the activity maxima or for the depth to which caesium is measurable in the cores. The migration of caesium ions is therefore likely to be occuring only on a limited scale, with much of the historical record of deposition still preserved (as evidenced by the presence of peaks correlating with fallout episodes and not with geochemical variations). This observation is consistent with the results of other investigations into ^{137}Cs exchangeability where typically only a few per cent of the isotope is available for rapid ion exchange reactions (Smith and Comans 1996).

4.1.4.1 Ion competition leading to Cs^+ mobilisation

The persistence of relatively low concentrations of solid phase iron (and elevated pore water concentrations of Fe^{2+} - see following chapter) implies the presence of sub-oxic conditions throughout much of the core section containing ^{137}Cs. The presence of such conditions has been postulated to result in the increased mobility of caesium from sediments *via* cation competition. Certain ions generated under these conditions, such as Fe^{2+} and Mn^{2+}, along with NH_4^+ derived from degrading organic matter, may displace exchangeable Cs^+ adsorbed to the sediment substrate (Evans *et al* 1983; Comans *et al* 1989). Furthermore, the presence of Na^+ in this saline environment will also enhance cation competition for exchange sites and may result in the partial release of caesium to pore waters, despite the presence of significant amounts of illite (Aston and Duursma 1973; Patel *et al* 1978). The regular inundation of the marsh by tidal waters may act to enhance the downward migration of mobilised species as waters pass through the sediment prism.

4.1.4.2 The scale of Cs^+ mobility

Fixation of caesium in association with illite occurs *via* ion exchange processes, with K^+ being the major exchangeable cation in the illite structure (Aston and Duursma 1973). As the time of exposure of caesium ions to illite particles increases, the exchangeability of the Cs^+ has been observed to decrease (Lomenick and Tamura 1965), due to the kinetically-controlled migration of the ions to inter-lattice sites, with stronger binding energies, over timescales of years (Comans *et al* 1991; Comans and Hockley 1992). The preservation of significant aspects of the depositional history of ^{137}Cs within these salt marsh sediments, despite evidence for a degree of diagenetic mobility, may be due to the fact that a considerable proportion of the Cs^+ cations are occupying inter-lattice sites and therefore remain associated to particles within the sediment column. The application of the isotope profiles to the determination of sediment accumulation rates is therefore affected but not prevented by the migration taking place, since the diffusion which is occuring does not appear to be sufficient to relocate the large solid phase concentrations present.

4.2 ^{210}Pb dating of sediment sequences

The use of lead-210 to determine rates of accretion in environmental sequences was first reported by Goldberg (1963) in relation to the accumulation of glacial ice. The technique has received a great deal of attention in the ensuing decades and has been successfully applied to a variety of sedimentary regimes including lakes (Krishnaswamy *et al* 1971), coastal marine sediments (Koide *et al* 1972; Koide *et al* 1973), and salt marshes (Armentano and Woodwell 1975; McCaffrey and Thomson 1980).

4.2.1 *Origin*

Lead-210 is present in the environment as one of the radionuclides in the uranium-238 decay series (Figure 4.4). The long half-life of the parent ^{226}Ra isotope, in combination with relatively short-lived daughters, will tend to establish a secular equilibrium in a closed system. However, a fraction of the intermediate ^{222}Rn gas diffuses out of crustal rocks and soils into the atmosphere resulting in disequilibrium from the ^{226}Ra activity. The subsequent decay of this ^{222}Rn in the atmosphere, *via* a series of short-lived isotopes, produces ^{210}Pb which is rapidly adsorbed on to atmospheric aerosols and returned to the surface of the Earth by both wet and dry deposition. The atmospheric residence time of ^{210}Pb has been shown to be of the order of days to weeks, and is short relative to its radioactive half-life (Peirson *et al* 1966; Poet *et al* 1972). The resulting flux of unsupported ^{210}Pb from the atmosphere and its ensuing decay over time is the basis for the chronological use of the isotope. The half-life of 22.26 years makes ^{210}Pb a valuable radionuclide for studying processes occurring over the last century, an important period with respect to human impact on natural systems.

4.2.2 *^{210}Pb in sediments*

The incorporation of ^{210}Pb into accumulating sediment sequences may arise from one of two distinct sources: the "supported" contribution ($^{210}Pb_{sup}$), assumed to be in secular equilibrium with its parent isotopes, originating from the *in-situ* decay of ^{226}Ra; and the unsupported or "excess" contribution ($^{210}Pb_{xs}$), derived from atmospheric fallout. As subsequent layers of sediment become buried (and cut off from further atmospheric supply) the activity of $^{210}Pb_{xs}$ decreases exponentially with depth and the interpretation of such activity profiles enables determination of the rate of accumulation of the sediment sequence. In similar fashion to the application of ^{137}Cs for dating purposes, certain conditions must be fulfilled for a meaningful chronology to be obtained. These are summarised and discussed below:

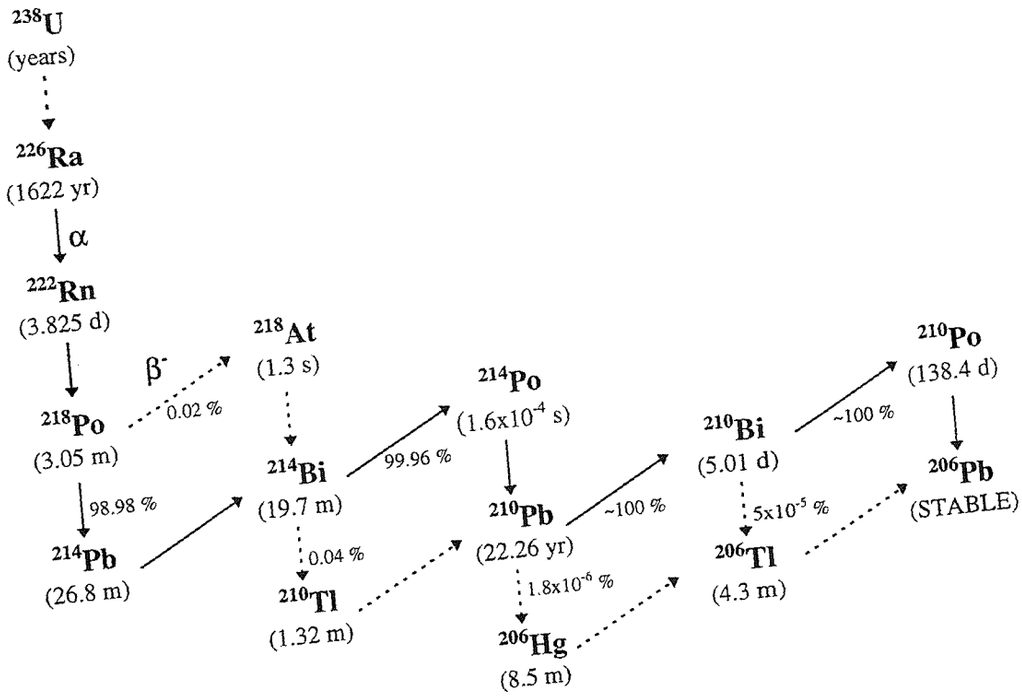

Figure 4.4:

Decay scheme of uranium-238 leading to the generation of ^{210}Pb.

I. a constant flux of $^{210}Pb_{xs}$ to the sediment surface;

II. the absence of, or ability to model, particle mixing processes;

III. insignificant chemical remobilisation of ^{210}Pb during early diagenesis;

IV. identification of the supported lead-210 activity, $^{210}Pb_{sup}$.

I. *Constant ^{210}Pb flux*

The flux of $^{210}Pb_{xs}$ from the atmosphere has been shown to be highly variable over short timescales but considerably more constant when averaged over periods of several years (Francis *et al* 1970; Zuo 1992). Since individual sediment samples may typically comprise several years of sediment accumulation it is likely that the assumption of constant flux will remain valid (Appleby and Oldfield 1992). As with ^{137}Cs, however, differences in the relative contributions from direct atmospheric fallout and the incorporation of externally-labelled material into salt marsh sediments may affect the flux of $^{210}Pb_{xs}$.

II. *Physical mixing processes*

The degree of disturbance to a sediment prism depends on the energy of the fluids moving over the surface (physical mixing) and the concentration and activity of the organisms living there (bioturbation). Salt marshes tend to accrete stable sediment profiles, often with a lack of significant particle mixing, and may therefore preserve the record of depositional inputs (McCaffrey and Thomson 1980; French *et al* 1994).

III. *Early diagenetic mobility*

In certain environments lead is known to be mobile during early diagenesis (Urban *et al* 1990; Benoit and Hemond 1991). The variation in oxidation potential throughout sediment prisms and the cycling of carrier phases (such as iron and manganese oxyhydroxides) under redox gradients can redistribute lead to different sections of the profile (Zwolsman *et al* 1993). In addition, lead has a strong tendency for complexation with organic materials, such as humic and fulvic acids, which may result in solubilisation of the metal. The effects of diagenetic remobilisation on a given ^{210}Pb profile may not readily be identifiable, although assessment of such effects is aided through the simultaneous application of an independent dating technique (such as ^{137}Cs) and the study of other geochemical variations throughout the sediment profile (particularly stable lead, redox sensitive elements and organic carbon).

IV. *Calculation of supported ^{210}Pb*

The application of lead-210 for dating purposes requires a distinction between the supported and the excess contributions to the total ^{210}Pb activity present ($^{210}Pb_{tot}$). This is usually done in one of two ways:

1) measurement of another radionuclide of the decay series that is assumed to be in secular equilibrium with the ^{226}Ra in the sediment, such as ^{214}Bi, ^{214}Pb or ^{226}Ra itself (e.g. Krishnaswamy *et al* 1971);
2) measurement of $^{210}Pb_{tot}$ at depths where the excess contribution is assumed to have decayed to zero and the measured value therefore corresponds to $^{210}Pb_{sup}$ (e.g. Goldberg *et al* 1977).

4.2.2.1 Determination of sediment accumulation rates: the simple model

If there is a constant rate of supply of accreting material (g cm^{-2} yr^{-1}) to a sediment surface then the constant flux of $^{210}Pb_{xs}$ (Bq cm^{-2} yr^{-1}) will yield a similar initial activity of each surface layer (Bq g^{-1}), such that

$$C_0 = C(0)$$

where C_0 is the initial activity for any buried sediment layer (Bq g^{-1}),
and C(0) is the activity of the surface layer (Bq g^{-1}).

Following radioactive decay,

$$C_t = C(0) \cdot e^{-\lambda(m/r)}$$

where C_t is the activity of the sediment of age t (Bq g^{-1}),
λ is the decay constant for ^{210}Pb (y^{-1}),
m is the cumulative dry mass per unit area above the sediment (g cm^{-2}),
t is the age of the sediment layer (y),
and r is the mass flux to the sediment surface (g cm^{-2} y^{-1}).

Thus,

$$\ln C_t = \ln C(0) - m(\lambda/r) \qquad \textbf{Equation 4.1}$$

and hence plotting the natural log of excess ^{210}Pb activity against cumulative dry mass of sediment should yield a linear relationship with a gradient of $-\lambda/r$. This is known as the "simple" model (Robbins 1978) or the "constant flux, constant sedimentation rate" model.

In many instances of lead-210 dating the variability of mass flux (and therefore $^{210}Pb_{xs}$ concentration in the surficial layers) over time requires the process of ^{210}Pb accumulation to be modelled more precisely. The two models which may be used to derive accurate chronologies under such conditions are known as the "constant rate of supply" (CRS) model and the "constant initial concentration" (CIC) model (Appleby and Oldfield 1992). However, the approximately linear nature of the ln $^{210}Pb_{xs}$ plots of data obtained during this study (see results below) suggests that both the sedimentation rate and the flux of $^{210}Pb_{xs}$ have been roughly constant at Hythe Marsh study site.

4.2.3 *Results and interpretation of Hythe ^{210}Pb profiles*

The variation in lead-210 activity with depth has been determined throughout four sediment cores from Hythe salt marsh. The resulting profiles, plotted against cumulative mass in order to minimise artifacts due to compaction and variations in sediment porosity, exhibit an approximately exponential decline with depth (Figure 4.5). Near the base of three of the cores, the total activity tends towards a constant value (~12-14 Bq kg^{-1}) which is assumed to represent the supported contribution, $^{210}Pb_{sup}$, in secular equilibrium with the *in-situ* decay of ^{226}Ra. This value is in agreement with previously-reported supported activities from this region of 12 ± 2 Bq kg^{-1} for mudflats and salt marshes (Cundy 1994) and ~11 Bq kg^{-1} for sub-tidal sediments (Croudace and Cundy 1995). The supported activity for each core is calculated from the mean activity of the bottom 5 samples, with the exception of core HySR2. In the latter case, the total ^{210}Pb activity does not reach a constant value at the base of the core, and hence an assumed supported activity of 12 Bq kg^{-1} is used. Logarithmic plots (Figure 4.5) of $^{210}Pb_{xs}$ activity against cumulative mass yield linear relationships (r^2 = 0.89 - 0.97) suggesting that the simple model described above is, to a first approximation, applicable to these sediments. There are, however, inflections and changes in gradient evident in these plots which cause deviations from linearity. These features may be the result of incomplete validation of the assumptions outlined above.

4.2.3.1 Accumulation rates

Linear regression, using the least-squares fit procedure, has been performed on the ln $^{210}Pb_{xs}$ profiles in order to determine the average sediment accumulation rate along the length of each sediment core using Equation 4.1. The only data points not included in the regression analysis are those with slightly negative $^{210}Pb_{xs}$ values (all close to zero) arising from using the mean of the five lowermost sample values for the determination of $^{210}Pb_{sup}$. The estimated error of each accumulation rate is derived from the standard error of the x-coefficient (Table 4.2).

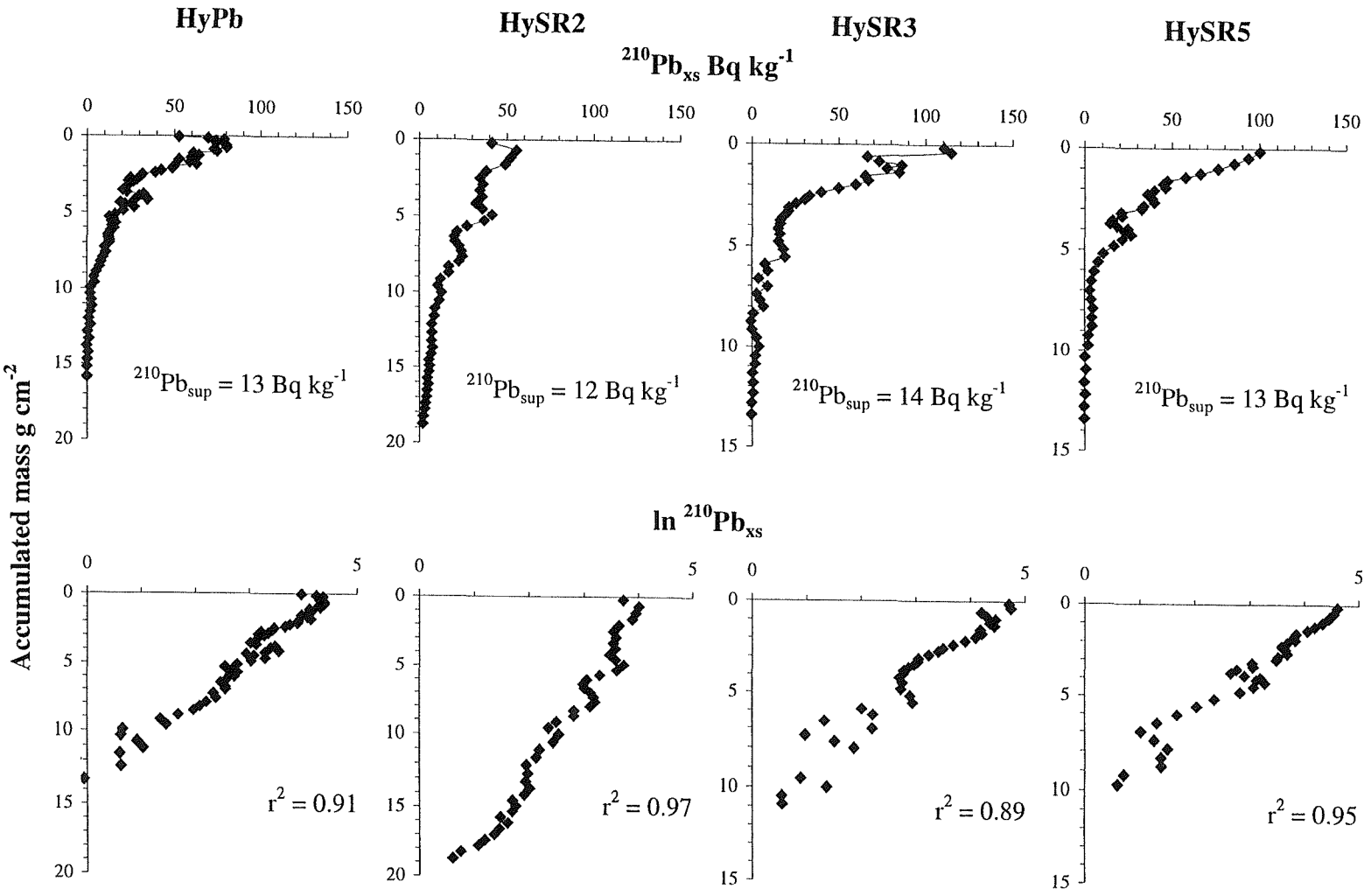

Figure 4.5:
$^{210}Pb_{xs}$ and ln $^{210}Pb_{xs}$ profiles for the four salt marsh cores.

HyPb
1-89,93

Regression Output:	
Constant	4.6
Std Err of Y Est	0.39
R Squared	0.91
No. of Observations	67
Degrees of Freedom	65
X Coefficient(s)	-0.351
Std Err of Coef.	0.014

Sediment accumulation rate
g cm^{-2} yr^{-1}

0.089 +/- 0.004

HySR3
1-34,37-43

Regression Output:	
Constant	4.8
Std Err of Y Est	0.40
R Squared	0.89
No. of Observations	34
Degrees of Freedom	32
X Coefficient(s)	-0.463
Std Err of Coef.	0.029

Sediment accumulation rate
g cm^{-2} yr^{-1}

0.067 +/- 0.005

HySR2
1-45

Regression Output:	
Constant	4.2
Std Err of Y Est	0.18
R Squared	0.97
No. of Observations	45
Degrees of Freedom	43
X Coefficient(s)	-0.171
Std Err of Coef.	0.005

Sediment accumulation rate
g cm^{-2} yr^{-1}

0.182 +/- 0.006

HySR5
1-36,38,40

Regression Output:	
Constant	4.6
Std Err of Y Est	0.26
R Squared	0.95
No. of Observations	36
Degrees of Freedom	34
X Coefficient(s)	-0.426
Std Err of Coef.	0.017

Sediment accumulation rate
g cm^{-2} yr^{-1}

0.073 +/- 0.003

Table 4.3:
Results obtained from the least-squares regression of linear ln $^{210}Pb_{xs}$ profiles. Accumulation rate errors are derived from the standard error of the x-coefficient.

4.3 Radionuclide inventories

The inventory of a particular radionuclide beneath a unit surface area may be calculated directly from the integrated sum of activity, density and sample thickness (Equation 4.2). For elements whose depositional history is known, or can be modelled, it is also possible to derive an alternative expression for core inventory based on the resulting balance of isotope addition and radioactive decay through time. The different input terms of ^{137}Cs (variable flux from 1950s to present) and ^{210}Pb (constant flux over all time) necessitate the application of both types of calculation to allow a full interpretation of the results. The relationship between inventory, flux and radioactive decay (Equation 4.3) may be also used to estimate the depositional flux of ^{210}Pb from the sediment core inventories yielded by Equation 4.2.

Radionuclide Inventory Calculations

1 Direct calculation of inventory (used for both ^{137}Cs and ^{210}Pb):

$$I = \int A_i \cdot \rho_i \cdot t_i \qquad \textbf{Equation 4.2}$$

where I is the inventory of the radionuclide within the core (Bq cm^{-2}),

A_i is the dry weight activity of each sample (Bq g^{-1}),

ρ_i is the sample density (g cm^{-3}),

and t_i is the thickness of the sample slice (cm).

2 Estimation of inventory from known constant flux (used for ^{210}Pb):

$$I = \int P(1 - e^{-\lambda t}) \cdot 1/\lambda \qquad \textbf{Equation 4.3}$$

where I is the $^{210}Pb_{xs}$ inventory (Bq cm^{-2}),

P is the depositional flux (Bq cm^{-2} y^{-1}),

λ is the ^{210}Pb radioactive decay constant (y^{-1}),

t is the time since sediment accumulation began (y).

Equation 4.2 is used to calculate the inventories of caesium-137 and lead-210 throughout each of the salt marsh cores in this study. Caesium-137 activities have been arbitrarily decay corrected to 1986 to facilitate comparison with data from other workers. The errors in the measurements are based on counting statistics (Table 4.3).

Core	Inventory Bq m^{-2}	
	^{137}Cs	$^{210}Pb_{xs}$
HyPb	n.d.	**2460** ± 90
HySR2	**2700** ± 200	**3630** ± 150
HySR3	**3050** ± 500	**2690** ± 80
HySR5	**2200** ± 200	**2470** ± 80

Table 4.3:

Radionuclide inventories determined for Hythe Marsh sediment cores (n.d. denotes not determined).

The inventory of any radionuclide in a salt marsh core will be equal to the difference between addition and loss of the isotope over the period since sediment accretion began. As previously outlined, radiocaesium and lead-210 may arrive on the marsh surface via direct atmospheric fallout and by the deposition of labelled particles from the marine and fluvial environments. Subsequent loss may occur by radioactive decay, association with eroded particles or by molecular diffusion out of the sediment into adjacent waters.

4.3.1 *Caesium-137 inventories*

Ignoring contributions from outside sources, a sediment prism that has been accumulating continuously since nuclear detonations began ought to preserve an inventory of activity representative of the cumulative fallout of ^{137}Cs onto the surface. Data obtained from AEA Technology (Playford, *pers. com.*) for the estimated annual fallout of ^{137}Cs at Milford Haven, Wales, yield a cumulative deposition of ~2950 Bq m^{-2} to 1986 (Figure 4.6). Two major studies of weapons ^{137}Cs fallout within the UK (Cawse 1983 and Cawse *et al* 1988, cited in Smith *et al*, in press) demonstrate the significant correlation between mean annual rainfall and the ^{137}Cs inventory in soil cores. Smith *et al* (in press) present a mean weapons test inventory, decay corrected to 1986, of 3160 Bq m^{-2} y^{-1} per metre of rainfall as being the UK average. Based on the long-term average annual rainfall for the Southampton waterfront area (0.754 m y^{-1}; Meteorological Office data) the predicted weapons ^{137}Cs inventory for soils and sediments of

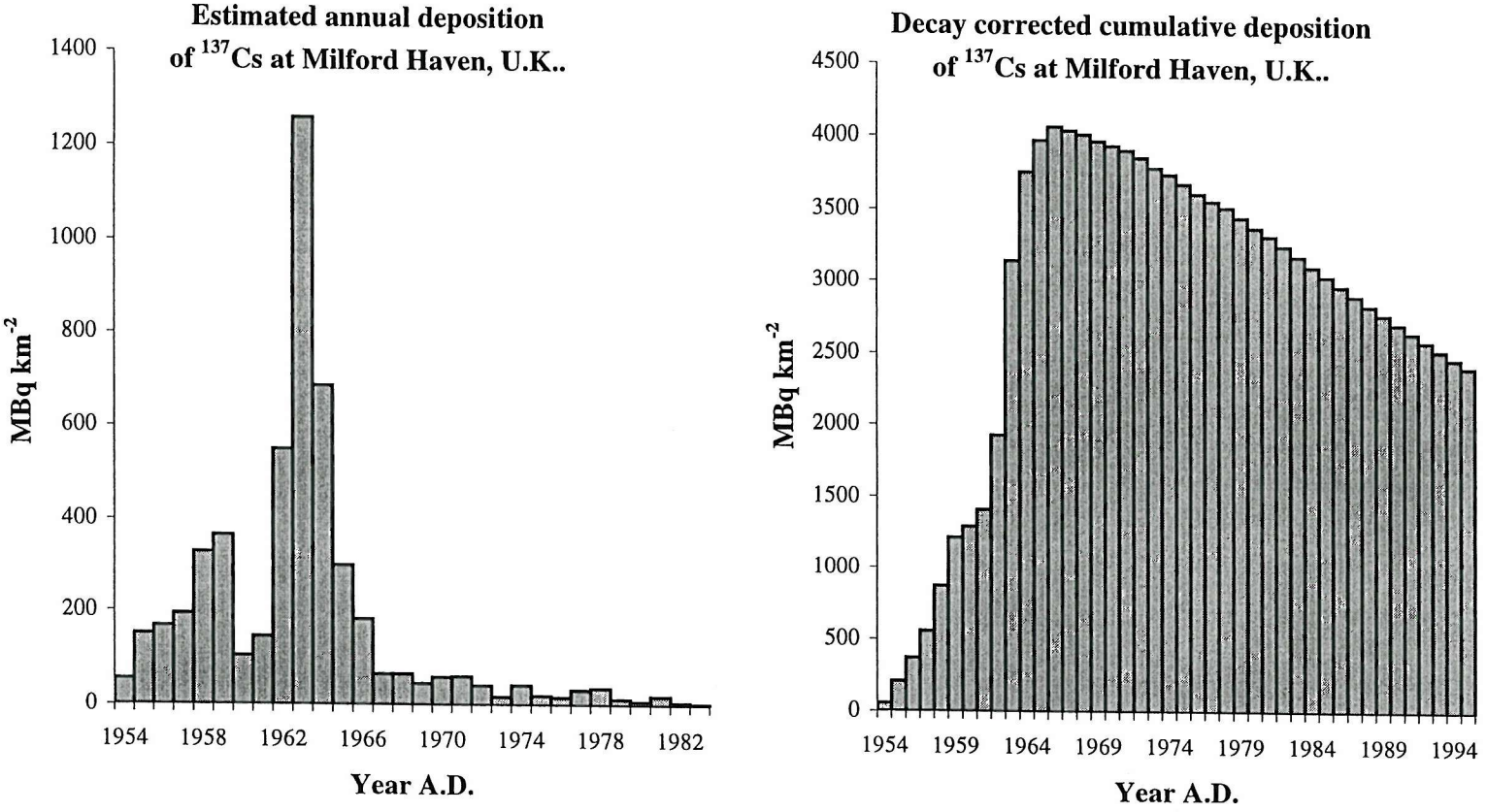

Figure 4.6:

Estimated annual deposition and decay corrected cumulative deposition of ^{137}Cs at Milford Haven, U.K.
Data from AEA Technology and Playford *et al* (1992).

this region is ~2380 Bq m^{-2} y^{-1}. Since the amount of ^{137}Cs deposition varies widely between different geographical areas these estimated inventories are subject to potential discrepancy. Nevertheless, in the absence of a weapons ^{137}Cs flux determined within the locality of the study area the estimated range of 2400-3000 Bq m^{-2} is likely to account for the true depositional flux.

The sediment core inventories (Table 4.4) agree well with the estimated history of ^{137}Cs deposition across the region, except in the case of core HySR5 which displays an inventory lower than the predicted range. Since the core inventories are not equal to one another the processes of ^{137}Cs retention within the sediment prism cannot be uniform across the marsh. A reduction in inventory must be due to the removal of ^{137}Cs through dissolution of the isotope or in association with eroded materials. Since ^{137}Cs is apparently being mobilised into Hythe marsh pore waters during early diagenesis (as exhibited by downcore penetration) some of the radionuclide is likely to be lost from the sediment prism during run-off of flood-waters. It is difficult to assess how much removal this mechanism could account for but the preservation of the pattern of weapons test deposition (see Cundy *et al* 1997; Appendix C) implies that the element has a strong affinity for the solid phase within the sediment profile. Downcore penetration of the isotope is evident but, compared to the solid phase, appears to have redistributed a relatively minor fraction of the total activity (Figure 4.3).

The overall mechanism through which accretion takes place at the surface of a saltmarsh involves processes of both deposition and erosion. During tidal inundation of the vegetated zone a portion of the surficial sediments may become resuspended in the flood waters (Stumpf 1983) and thus mixed with the existent suspended sediment load, much of which is derived from elsewhere within the estuarine system. Throughout the flood period, and in particular during the high water stand, particles may resettle on to the marsh surface or become trapped by the above-ground vegetative growth. Those sediments remaining in suspension during the ebb-flow of the tide are removed to the main channel of the estuary. The difference between the mass flux of sediment imported by the flood waters and exported during the ebb tide represents the net balance of sediment accumulated or lost by the marsh prism throughout tidal inundation. This process is likely to remove a greater proportion of the fine-grained sediments than the coarse since the former are not only more easily lifted off the sediment surface but will also remain in suspension for a longer period. The ^{137}Cs activity determined in different grain-size fractions of intertidal sediments from Poole Harbour (Cundy 1994) was highest in the <8 μm fraction and generally declined with increasing grain-size, attributed to the association of caesium with clay mineral surfaces in the fine-grained sediment fraction. The particle size sorting brought about by resuspension during flooding may therefore result in the export of ^{137}Cs activity. This may occur even when the marsh exhibits a net accretionary balance since

the deposited sediments (derived from outside the marsh) are likely to comprise the coarser component of the suspended sediment load and therefore be less radioactive than those exported.

4.3.2 *Lead-210 inventories*

The flux of radon-222 emanating from the surface of the Earth ensures a return flux of atmospheric $^{210}Pb_{xs}$ which may be considered to be approximately constant over timescales of several years or more. After a sufficient period of deposition the inventory of $^{210}Pb_{xs}$ beneath a unit area of the Earth's surface (the standing crop) ought to tend towards a constant value such that addition of the isotope is matched by radioactive decay. This may be derived from Equation 4.3 in which, as t becomes large, the parameter $(1-e^{-\lambda t})$ approaches unity (after ~150 y, Appleby and Oldfield 1992). Determination of the inventory within a sediment core (Equation 4.2) may therefore be used to estimate the mean depositional flux of $^{210}Pb_{xs}$ to the sediment surface (from $P \equiv I.\lambda$). For the derived flux to be accurate accumulation must have been taking place for a period of time sufficient to allow steady-state conditions to develop, in addition to there being no leaching of ^{210}Pb from the sediment. Calculation of the empirical flux at Hythe Marsh yields values which are in good agreement with other studies of soil and salt marsh inventories (Table 4.4).

Location	Inventory Bq m^{-2}	Calculated ^{210}Pb flux Bq m^{-2} y^{-1}	Reference
Great Britain		162	Appleby and Oldfield (1992)
Cumbria, UK		63-97	Smith *et al* (in press)
Hythe Marsh cores:			
HyPb	2460 ± 90	**76** ± 3	This study
HySR2	3630 ± 150	**113** ± 5	"
HySR3	2690 ± 80	**84** ± 3	"
HySR5	2470 ± 80	**77** ± 3	"

Table 4.4:

Mean $^{210}Pb_{xs}$ fluxes calculated from soil and sediment inventories.

Despite the similarity between the results of this and previous studies the fact that sediment cores from the same salt marsh can accumulate different inventories implies that the processes of deposition and retention of $^{210}Pb_{xs}$ (as with ^{137}Cs above) are not uniform across the marsh. This aspect may be better understood when accompanied by an assessment of the likely atmospheric flux of $^{210}Pb_{xs}$, allowing the differentiation between this and water-borne inputs of the isotope. The rate of deposition of ^{210}Pb from the atmosphere, as determined from the continuous collection of precipitation samples throughout the duration of the study, will now be considered.

4.3.3 *$^{210}Pb_{xs}$ in Southampton rainfall*

4.3.3.1 Introduction

There have been few direct measurements of the depositional flux of ^{210}Pb across the UK (Smith *et al*, in press), thus the determination of this parameter for the Southampton region ought to provide useful data for comparison to the measured sediment inventories as well as the results of these other rainfall studies. The concentration of ^{210}Pb present within precipitation depends on a complex set of factors including the history of the air mass and the intensity and duration of the storm event (Turekian *et al* 1977). During periods of low rainfall dry fallout of ^{210}Pb may also make a significant contribution, implying that the episodic collection of rainwater to determine the rate of wet deposition may yield underestimation of the total flux. However, an integrated collection regime with continuous atmospheric exposure, as used throughout this study, ought to provide samples more representative of the total ^{210}Pb flux. Assessment of the amount of rainfall is obviously important during the collection period to interpret the ^{210}Pb concentration data and this may be enhanced by consideration of the historical average rainfall for the study region.

4.3.3.2 Results

The concentration of ^{210}Pb has been determined, *via* ^{210}Po ingrowth, for 63 precipitation samples representative of three years continuous exposure to the atmosphere at Highfield, Southampton (Appendix B). Blanks determined for the analytical procedure are effectively negligible compared to the activity of the samples. The determination of ^{210}Pb activity through measurement of its grand-daughter, ^{210}Po, requires that a secular equilibrium has been established in the decay of these isotopes. However, the rapid removal of $^{210}Pb_{xs}$ from the atmosphere (days to weeks) relative to the half-life of ^{210}Po (138 days) prevents this equilibrium from being established (Peirson *et al* 1966) and the determination of the ^{210}Pb activity of the rain water thus involves a more complicated procedure. The rain water samples were processed over a period of several months, subjected to chemical separation and a period of radioactive ingrowth, and their ^{210}Po activities were determined on two occasions. The calculation of ^{210}Pb activities from these data involves a relatively straightforward application of the Bateman Equation (see Figure 4.7; from Faure 1977).

Figure 4.7: The Bateman Equation

Theoretical derivation

Consider the decay of a parent (N_1) to a daughter (N_2) which decays to a second daughter (N_3):

The rate of decay of N_1 is given by:

$$dN_1/dt = -\lambda_1 N_1 \qquad [1]$$

where N_1 is the number of atoms and λ_1 is the decay constant.

The number of atoms of N_1 remaining at any time t is:

$$N_1 = N_1^0 . e^{-\lambda t} \qquad [2]$$

The rate of decay of N_2 is the difference between the rate of production by decay of N_1 and its own radioactive decay:

$$dN_2/dt = \lambda_1 N_1 - \lambda_2 N_2 \qquad [3]$$

Substituting [2] into [3] gives:

$$dN_2/dt = \lambda_1 N_1^0 . e^{-\lambda t} - \lambda_2 N_2 \qquad [4]$$

The solution to this first order differential linear equation was first derived by Bateman in 1910:

$$N_2 = \frac{\lambda_1}{\lambda_2 - \lambda_1} . N_1^0 (e^{-\lambda 1 t} - e^{-\lambda 2 t}) + N_2^0 . e^{-\lambda 2 t} \qquad [5]$$

The first term of this equation represents the number of atoms of N_2 that have formed from the decay of N_1 but have not yet decayed themselves, whereas the second term equates to the number of atoms of N_2 remaining from an initial number of N_2^0. If N_2^0 is zero then:

$$N_2 = \frac{\lambda_1}{\lambda_2 - \lambda_1} . N_1^0 (e^{-\lambda 1 t} - e^{-\lambda 2 t}) \qquad [6]$$

Application to Hythe Marsh sediment cores

Rearranging equation [6] yields:

$$N_1^0 = \frac{(N_2 . \lambda_2 - \lambda_1)}{\lambda_1 . (e^{-\lambda 1 t} - e^{-\lambda 2 t})} \qquad [7]$$

Equation [7] may be used to calculate the activity of ^{210}Pb at the beginning of the ^{210}Po ingrowth period, since this corresponds to a time of zero ^{210}Po activity following chemical separation. These data must be corrected for the experimental yield (determined by gravimetric analysis) and may then be used to calculate the initial ^{210}Pb activity of the rain water, *via* equation [2] (note that this involves the time of the chemical separation being first time zero and then time t, depending on the decay period in question).

The ^{210}Pb depositional flux may be calculated from the product of ^{210}Pb activity in the rain water and the amount of rain having fallen (Equation 4.4):

$$P = \int A.p \qquad \textbf{Equation 4.4}$$

where P is the temporal ^{210}Pb flux (Bq cm^{-2} d^{-1}),

A is the activity of the rain at the time of deposition (Bq cm^{-3}),

and p is the rainfall flux (cm d^{-1}),

The concentration of ^{210}Pb within each sample is inversely correlated with the average amount of rainfall (Figure 4.8). Such a pattern is to be expected since periods of light rainfall tend to concentrate atmospheric ^{210}Pb to a greater extent than heavy rains (Zuo 1992). For an idealised linear model of total lead-210 deposition vs. rainfall the intercept at zero precipitation of a regression line may provide an estimate of the dry fallout (Turekian *et al* 1977). A plot of the daily ^{210}Pb flux against rainfall for all samples (r^2=0.59, n=63) yields an intercept at zero precipitation of 6.7 μBq cm^{-2} d^{-1} (Figure 4.9). This corresponds to about 40% of the total ^{210}Pb flux. The individual annual and overall mean ^{210}Pb fluxes calculated from the data are given in Table 4.5 along with uncertainties based on the counting statistics. Independent measurements of this flux for the U.K. are provided for comparison.

U.K. Study Area	^{210}Pb deposition (measured) Bq m^{-2} y^{-1}	Rainfall cm	Predicted ^{210}Pb flux (from UK average) Bq m^{-2} y^{-1}
Brotherswater, Cumbria [a]	147	210.0	151 ± 19
Milford Haven, Wales [b]	85	91.6	66 ± 8
Harwell, SE England [c]	54	65.0	47 ± 6
Southampton:			
April 93 - March 94	**75** ± 10	108.0	83 ± 15
April 94 - March 95	**70** ± 12	103.4	80 ± 15
April 95 - March 96	**41** ± 4	67.9	52 ± 10
Mean annual flux	**62** ± 8	93.1	72 ± 13
Estimated dry deposition	25 (≡ 40% of total)		

Table 4.5:

^{210}Pb deposition measured during this study along with U.K. literature values from: [a] Smith *et al* (in press), [b] Peirson *et al* (1966), [c] Burton and Stewart (1960). Predicted values are calculated using the average U.K. deposition of ^{210}Pb per metre of rainfall (see text).

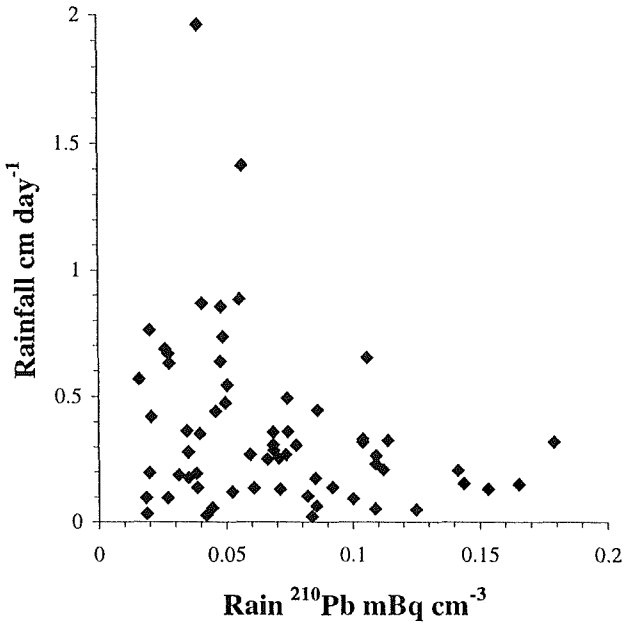

Figure 4.8:
Correlation between ^{210}Pb concentration and rainfall.

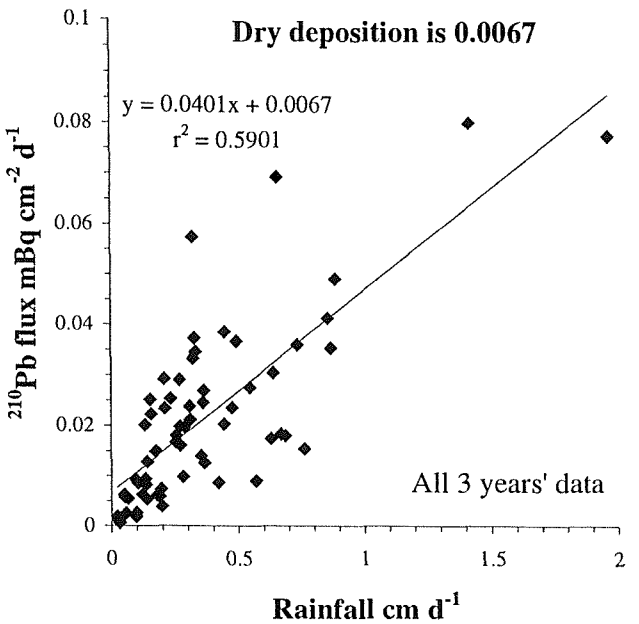

Figure 4.9:
Linear relationship of ^{210}Pb flux and rainfall.

4.3.3.3 Discussion

4.3.3.3(a) ^{210}Pb flux and rainfall

In a recent assessment of existing UK ^{210}Pb fallout data, comprising both direct measurements and calculations provided by soil and sediment inventories, Smith *et al* (in press) estimate the mean UK ^{210}Pb flux to be 77 ± 14 Bq m^{-2} y^{-1} per metre of annual rainfall. This value may be used in combination with the amount of rainfall recorded to predict the annual flux of ^{210}Pb that might be expected from the results of previous studies (Table 4.5). The values obtained for the period of collection compare favourably with the integrated ^{210}Pb flux measurements made, though in each case the mean predicted flux slightly exceeds the measured deposition on site. In a study of ^{210}Pb deposition at three locations within the northern part of the Netherlands (approximately 500 km WNW of the Hampshire Basin) a mean annual flux of 61 Bq m^{-2} y^{-1} was calculated (Zuo 1992), comparing exceedingly well with the average value of 62 Bq m^{-2} y^{-1} obtained here. Dry fallout is estimated to have accounted for ~40% of the total Southampton ^{210}Pb flux (Figure 4.9), in satisfactory agreement with the dry fallout over the Netherlands, estimated by the same procedure to be 16-38% of the total ^{210}Pb flux (Zuo 1992).

Whether the ^{210}Pb flux measured here is representative of the true average value for this region is a matter of conjecture. The annual ^{210}Pb flux varies by about a factor of two within the period of study and the data are thus subject to considerable potential error. Peirson *et al* (1966) noted that the significiant short term variability in the deposition of ^{210}Pb in rainfall may not be compensated for when averaging samples collected over a few years. Due to the effects of wind direction, air mass trajectory, storm height and other meteorological variables on the flux of ^{210}Pb at any given location, the assessment of several years' data may fix the average flux to no better than 10-50% (Turekian *et al* 1977). Distortion of the short-term flux is enhanced by the relatively short half-life of the isotope. An independent estimate of the historical deposition rate of ^{210}Pb at Southampton may be derived from the long-term average annual rainfall, calculated by the Meteorological Office to be 0.754 m y^{-1}, and the mean UK relationship between rainfall and ^{210}Pb flux (Smith *et al*, in press). This yields a theoretical long-term ^{210}Pb flux of 58 ± 11 Bq m^{-2} y^{-1}, in good agreement with the flux determined throughout the study period, increasing the likelihood that these values are representative of the true historical flux.

4.3.3.3(b) ^{210}Pb flux and saltmarsh inventories

The mean $^{210}Pb_{xs}$ flux calculated from sediment core inventories (76-113 Bq m^{-2} y^{-1}; Table 4.4) may be compared to the mean atmospheric ^{210}Pb flux (rainfall analyses and the UK correlation between rainfall and deposition yields the range 47-70 Bq m^{-2} y^{-1}). For all four cores the ^{210}Pb inventory is greater than that expected from atmospheric deposition alone (determination of the predicted inventory, assuming a ^{210}Pb flux of 58 ± 11 Bq m^{-2} y^{-1}, yields a value of 1850 ± 350 Bq m^{-2}). Sediment cores which contain additional ^{210}Pb relative to the incident flux are likely to have incorporated particles labelled with $^{210}Pb_{xs}$ elsewhere within the hydrological system. In a study of the ^{210}Pb balance within Long Island Sound, Benninger (1978) reported the rapid removal of atmospheric ^{210}Pb on to suspended particles within the estuarine water mass. A linear relationship was observed between the total ^{210}Pb concentration in water samples and the concentration of suspended solids. The incorporation of such suspended matter into the marsh, an important mechanism through which vertical accretion takes place (Stumpf 1983), is therefore an obvious route through which an increased inventory of $^{210}Pb_{xs}$ can accumulate within the sediment prism. The data of Church *et al* (1981), and references therein, show that the saltmarshes on the eastern U.S. seaboard contain up to twice the ^{210}Pb inventory expected from the known depositional flux (167 ± 33 Bq m^{-2} y^{-1}) determined from direct fallout measurements at New Haven, Connecticut.

Three of the Hythe sediment cores are marked by the similarity of their $^{210}Pb_{xs}$ inventories (2540 ± 130 Bq m^{-2}) whereas the fourth, core HySR2, contains approximately 40% more of the isotope. The unique feature of core HySR2, which may be invoked to explain the elevated inventory, is the dense nature of the sedimentary material. The mean dry sediment density throughout the section of the core containing >99% of the $^{210}Pb_{xs}$ inventory (Table 4.6) yields a value of 0.419 g cm^{-3} for core HySR2 whilst the other three core densities fall within the range 0.268 ± 0.003 g cm^{-3}.

The differences in the mean density between sediment cores are related to the relative proportion of marine-derived (mostly minerogenic) and primary-produced (organic) materials, with density being inversely proportional to organic matter content (Craft *et al* 1993). Regression analysis of the variance of radionuclide inventory as a function of mean density reveals that the pattern of inventory variation across the marsh is strongly coupled (Figure 4.10; $r^2 = 0.97$) to the sediment density, which itself is a function of the proportion of marine-derived particles present. The high $^{210}Pb_{xs}$ inventory determined for core HySR2 is the result of the increased deposition of labelled particles sourced from estuarine flood waters.

4.3.4 *Comparison of ^{210}Pb and ^{137}Cs inventories*

The results of ^{137}Cs and ^{210}Pb inventory studies carried out across the U.K. suggest a linear correlation with a 1986 decay corrected $^{137}Cs/^{210}Pb$ inventory ratio of ~1.3 (Smith *et al*, in press). The cores analysed for both of these isotopes in this study (HySR:2, 3 and 5) exhibit ratios of 0.69, 1.04 and 0.83, respectively. Caesium-137 inventories are more variable than ^{210}Pb inventories in sediment sequences, even on relatively short geographical scales, on account of localised transportational effects (Smith *et al,* in press). The range of values found here and their difference from the average U.K. ratio is indicative of the fact that salt marshes do not record the true atmospheric flux due to the influence of the marine environment. In the case of Hythe Marsh there is evidence of the marine deposition of a greater proportion of ^{210}Pb than ^{137}Cs relative to their atmospheric fluxes. Indeed, the caesium-137 budget appears to be depleted by the removal of suspended sediments during flooding and processes of dissolution.

Mean Density g cm^{-3}		
Core	**Depth cm**	**Dry ρ**
HyPb	0 - 37	0.271
HySR2	0 - 42	0.419
HySR3	0 - 38	0.270
HySR5	0 - 34	0.265

Table 4.6:

Mean dry density of that section of each sediment core containing >99% of the $^{210}Pb_{xs}$ inventory.

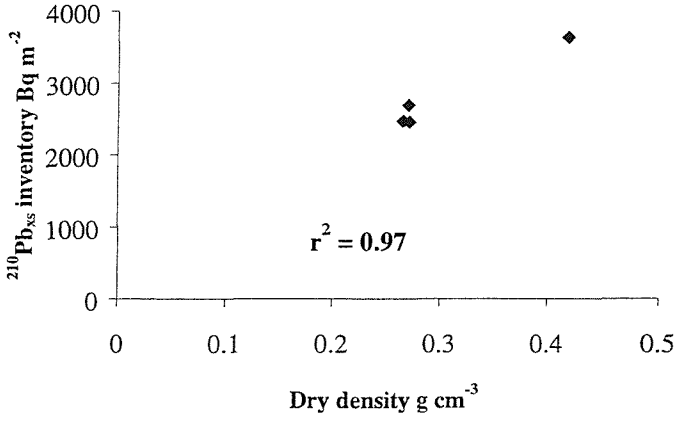

Figure 4.10:

Relationship between $^{210}Pb_{xs}$ inventory in sediment cores and mean core density.

4.4 Summary of Hythe Marsh sediment accretion

Sediment accumulation rates have been determined through the application of two dating methods (caesium-137 and lead-210) to three sediment cores from the study area, and in a fourth core using ^{210}Pb only. The values obtained from these independent radiometric techniques are in good agreement with one another (Table 4.7).

Core	Marsh zone	Sediment accumulation rate g cm^{-2} yr^{-1}	
		^{137}Cs-derived	^{210}Pb-derived
HyPb	Low	n.d.	**0.089** ± 0.004
HySR2	Low	**0.189** ± 0.007	**0.182** ± 0.006
HySR3	Middle	**0.072** ± 0.004	**0.067** ± 0.005
HySR5	High	**0.082** ± 0.003	**0.073** ± 0.003

Table 4.7:

Summary of sediment accumulation rates determined using independent radiometric techniques (n.d. denotes not determined).

Since different zones of the salt marsh accrete through the non-uniform incorporation of materials with variable densities, the mass accumulation rates depicted above (g cm^{-2} yr^{-1}) are not directly proportional to the rate of vertical accretion of the marsh surface (mm yr^{-1}). From the depth of the dominant peak in ^{137}Cs fallout the average rate of sediment build up over the past three decades may be determined (Tables 4.1 and 4.8):

Marsh zone	Low	Middle	High
Mean rate mm yr^{-1}	4.5	3.5	3.8

Table 4.8:

Mean vertical accretion of Hythe sediment cores derived from ^{137}Cs dating.

The vertical accretion of sediment is relatively constant across the marsh, differing by only one millimetre per year between the two extreme rates. This is not surprising when considering the approximately horizontal nature of the sediment surface. In accord with the results of previous studies (De Laune *et al* 1978; Craft *et al* 1993) the low (near-shore) area of the marsh exhibits a slightly higher rate of vertical accretion than areas further removed from the water. Despite existing in a higher energy environment, the exposure to a greater frequency of tidal inundation results in the entrapment of an increased amount of inorganic sediment and consequently a higher rate of vertical accretion. The mid-marsh and high-marsh areas each have similar accretion rates, which, from a comparison of their mean core densities to that of core HySR2, are due in considerable part to the *in-situ* production of organic materials.

4.4.1 *Marsh development in relation to sediment accretion*

The survival of a salt marsh ecosystem depends on the elevation of the sediment surface relative to the tidal frame. Since sea level in the Solent region is exhibiting a rising trend at the present time (Shennan 1983) it is important for Hythe Marsh to accrete at a similar rate in order to maintain the optimum conditions in which the plant species may thrive. The mean vertical accretion rates determined for the study site are all slightly lower than independent estimates of the local rate of sea level rise obtained from an analysis of tide gauge records (Woodworth 1987) of ~5 mm yr^{-1}. This net deficiency in the rate of sediment accumulation may be responsible for the significant erosion that is evident at the seaward edge of the marsh where a steep cliff has formed at the interface between the vegetated zone and the mudflat (Figure 3.2). Large blocks (up to a metre in dimension) are regularly observed to have broken from the marsh prism and lie on the mudflat being slowly disintegrated by the tide.

Independent confirmation of the erosive nature of the current phase of salt marsh formation may be obtained from a comparison of surveying conducted in 1963 with a similar survey carried out by the same researcher in 1994. The width of the survey line across the vegetated zone decreased from 180 m to 114 m during the intervening three decades (Hubbard 1994, *pers. com.*) corresponding to a retreat of approximately 2 m per year. In addition to the declining lateral extent, the geomorphological development of the marsh prism has resulted in the modern-day sediments being relatively firm and quite safe to walk on. This may be compared to the situation thirty years ago when the marsh was composed of soft waterlogged sediments which could be made to ripple over a distance of several metres by a person jumping up and down (Hubbard 1994, *pers com.*). This evolution in the condition of the sediment prism is

accompanied by colonisation of several plant species (including *Halimione portulacoides*) which were absent from the *Spartina townsendii*-dominated vegetation of the 1960s.

Degeneration of *Spartina* marshes within the Solent region has been occurring for much of the latter half of the present century (Tubbs 1980; Manners 1975) and may date from as early as the 1920s in some areas (Hubbard 1965). This die-back is characterised by the death of the aerial portion of the plants and is usually followed by the erosion of sediment particles previously entrapped by the healthy vegetation. Various reasons have been suggested to account for *Spartina* decline but the causative mechanisms are poorly understood. It would appear that during the formation of a mature marsh, one having achieved considerable elevation within the tidal frame, the introduction of fine-grained particles which settle around the roots of the vegetation may result in poor aeration of the sediments and thus oxygen starvation of sub-surface growth (Manners 1975). An alternative explanation, suggested by Tubbs (1980), is that a general lowering of the intertidal profile (caused by a change in the isostatic balance across the region) has exposed the front of the marsh prism to intensified wave attack. Further causes of decline may be related to the limited genetic variability of the ancestral plants and thus vulnerability of the modern population to infection.

4.4.2 *Core HySR1 ^{137}Cs profile*

The ^{137}Cs profile determined for core HySR1 (Fig 4.11) is worthy of discussion at this point, since it provides geochemical evidence in support of the preceding analysis of erosion at the front of the study site. The sediment ^{137}Cs activity declines very rapidly from the surface downcore, becoming undetectable in samples beneath 6 cm depth. Comparison of this profile with those obtained from the other sediment cores leads to the conclusion that approximately 20 cm of the sediment surface at the very front of Hythe Marsh has been removed as a result of erosion. Since core HySR1 therefore contains an incomplete record of the sedimentary accumulation the geochemical results are not deemed useful for the purposes of this study and have mostly been omitted from this report. It would appear that that portion of the marsh seaward of the storm-deposited shell bank is unstable under the tidal regime to which it is being exposed.

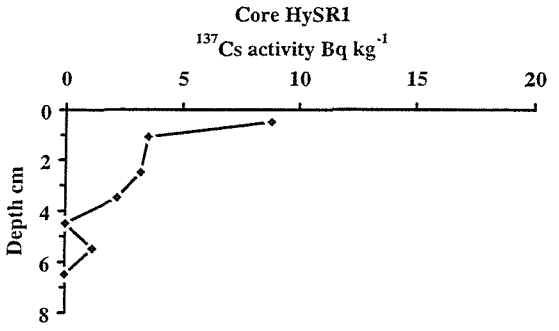

Figure 4.11:

Caesium-137 activity profile within core HySR1 revealing eroded surface layers.

4.4.3 *Core chronologies*

The sediment accumulation rates may be used to establish chronologies throughout the salt marsh cores (Fig 4.12). The resulting plots further reveal the degree of consistency between the ^{137}Cs and ^{210}Pb dating techniques, despite the different timescales which the methods rely on (Figure 4.13). It is apparent that the accumulation of sediments at the study site has been occurring for at least two centuries, and therefore may preserve a useful record of metal accumulation within the estuary over this period.

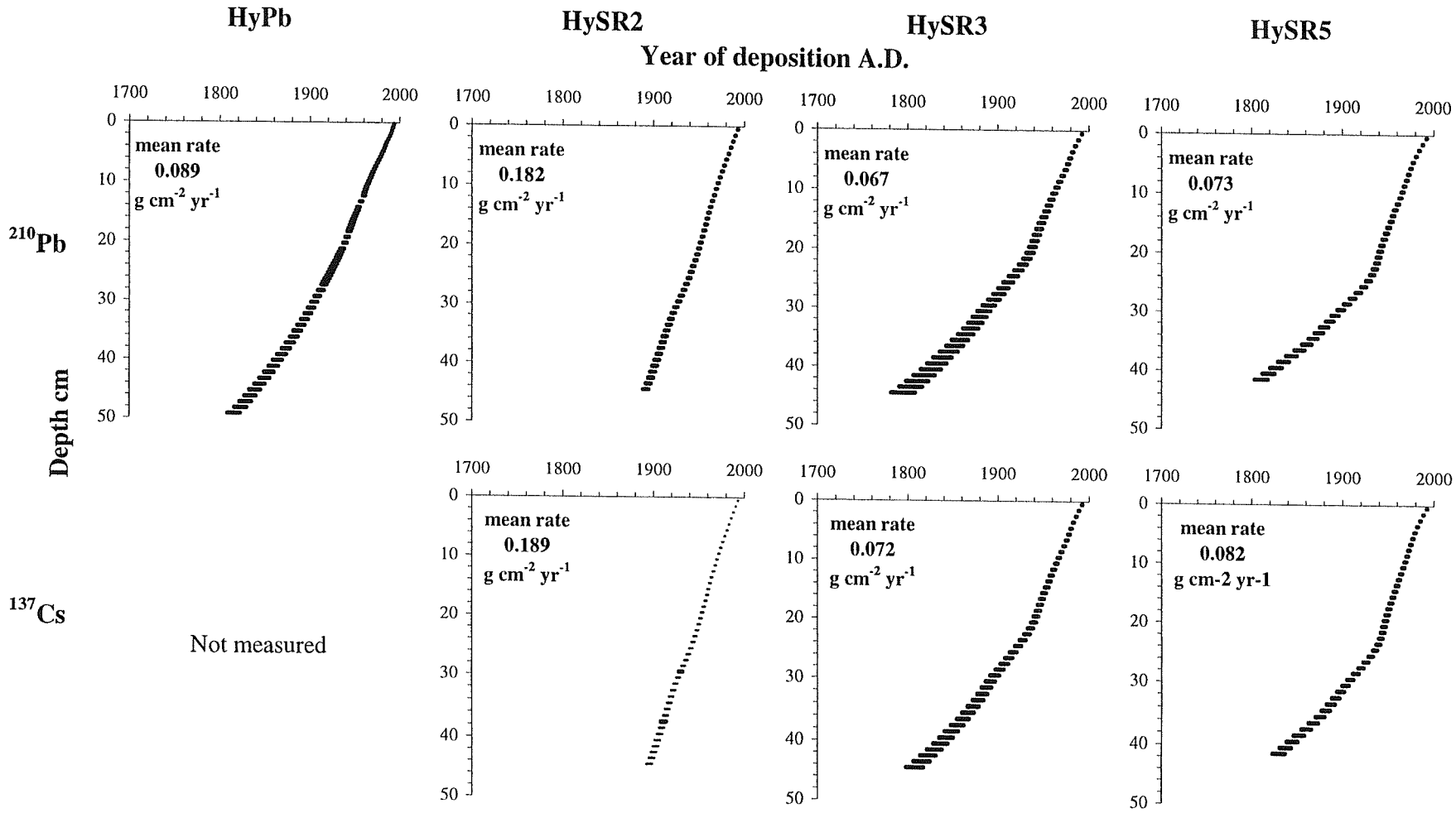

Figure 4.12:

^{210}Pb and ^{137}Cs chronologies of sediment cores derived from mean rates of sediment accumulation (errors included).

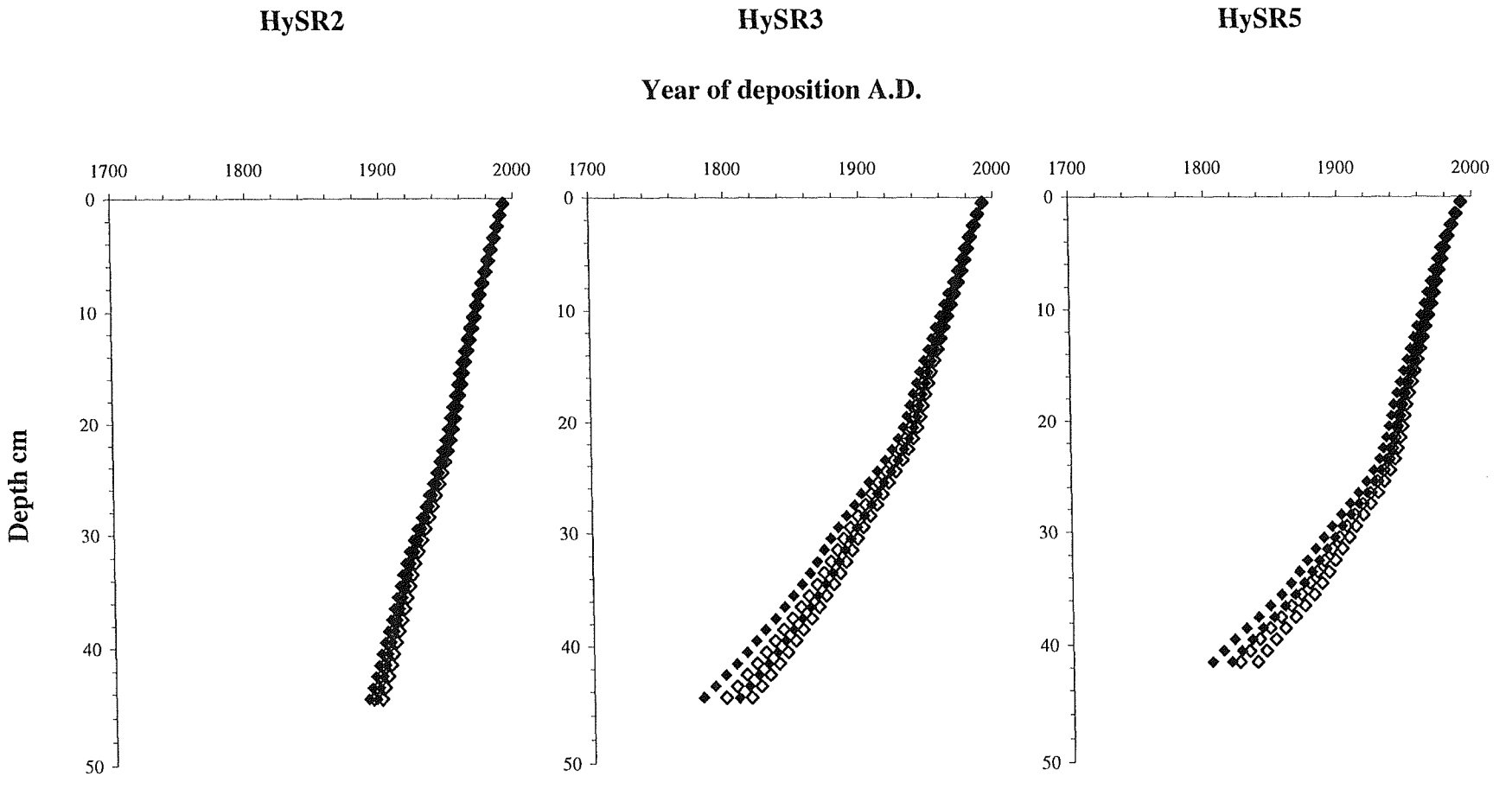

Figure 4.13:

^{210}Pb and ^{137}Cs chronologies of sediment cores derived from mean rates of sediment accumulation. Filled markers are ^{210}Pb; hollow markers are ^{137}Cs (errors included).

Chapter Five

Early Diagenesis

5.1 Early diagenesis within salt marsh sediments

Early diagenetic change in shallow sediments is dominated by the oxidation of organic carbon and associated chemical reactions (Santschi *et al* 1990). The sediment prism of a salt marsh represents a complex environment in which organic matter may decompose *via* one of several microbially-mediated pathways with the distribution of the various species of micro-organism in the sediments dependent upon the local flux of suitable electron acceptors and the rate of supply of organic substrates (Fenchel and Finlay 1995). Processes of metabolism may be divided into anabolic and catabolic categories (Berner 1980). Anabolic (assimilation) processes lead to the synthesis of protoplasm and other organism parts, whereas catabolic (dissimilatory) processes involve the breakdown of previously synthesised organic molecules to either simpler molecules or inorganic species. The energy needed for anabolism is obtained from catabolism.

5.1.1 *The oxidation of organic matter*

The mineralisation of organic matter can be defined as "the microbially-mediated oxidative breakdown of organic matter into the organic compounds - carbon dioxide, ammonium/nitrate, phosphates, plus trace constituents" (Van der Weijden 1992). Organic substrates within the sediment prism may be sourced from below-ground vegetative growth or buried following deposition on the salt marsh surface. Their subsequent degradation is mostly an oxidative process and therefore requires the consumption of electron acceptors for the reaction to proceed. The half-reaction for the breakdown of organic matter generates four moles of electrons per mole of carbon oxidised (Equation 5.1).

$$(CH_2O)_x(NH_3)_y(H_3PO_4)_z + xH_2O \longrightarrow xCO_2 + yNH_4^+ + zHPO_4^{2-} + (4x-y+2z)H^+ + 4xe^-$$

Equation 5.1 (Van der Weijden 1992).

The choice of the electron acceptor reduced in combination with this oxidation will depend on the availability of the different possible species and the electrode potential of the accompanying half-reaction. The possible half-reactions, involving reduction of a suitable electron acceptor, and the nomenclature given to the various decomposition processes, are (after Van der Weijden 1992):

Electron acceptors in bold type

1.	$\mathbf{O_2} + 4\,H^+ + 4\,e^- \longrightarrow 2\,H_2O$	(aerobic respiration)
2.	$2\,\mathbf{MnO_2} + 8\,H^+ + 4\,e^- \longrightarrow 2\,Mn^{2+} + 4\,H_2O$	(manganese reduction)
3.	$0.8\,\mathbf{NO_3^-} + 4.8\,H^+ + 4\,e^- \longrightarrow 0.4\,N_2 + 2.4\,H_2O$	(denitrification)
4.	$4\,\mathbf{FeOOH} + 1.2\,H^+ + 4\,e^- \longrightarrow 4\,Fe^{2+} + 8\,H_2O$	(ferric iron reduction)
5.	$0.5\,\mathbf{SO_4^{2-}} + 4.5\,H^+ + 4\,e^- \longrightarrow 0.5\,HS^- + 2\,H_2O$	(sulphate reduction)
6.	$0.5\,\mathbf{CO_2} + 4\,H^+ + 4\,e^- \longrightarrow 0.5\,CH_4 + H_2O$	(methanogenesis)

The expected manner in which degradation of organic matter may take place in an idealised system is for the electron acceptors to be consumed in a preferred sequence dependent on the Gibbs free energy yield per mole of carbon oxidised (Froelich *et al* 1979). In this case the most thermodynamically-favourable reaction proceeds to the point of exhaustion of reactants before the next reaction couple becomes operative. The standard Gibbs free energy for the reaction of organic molecules with each of the above electron acceptors enables prediction of the sequence in which they ought to be consumed (Table 5.1; Froelich *et al* 1979). The organic molecule used to quantify the calculation is assumed to have the Redfield (1963) stoichiometry (that of average pelagic phytoplankton), $(CH_2O)_{106}(NH_3)_{16}(H_3PO_4)$, though in coastal areas the ratios found in organic detritus may be very different from this. The Gibbs free energies are calculated for standard conditions and at the biochemical reference state (Froelich *et al* 1979).

The diagenetic sequence depicted in Table 5.1 is discussed below:

1. Oxygen consumption

Sub-aerial exposure of a salt marsh surface enables oxygen molecules to diffuse into the top of the sediment prism, both in solution and in gaseous form when the marsh dries out. Further oxygen may be introduced during tidal inundation with oxygenated water and through efflux from the roots of marsh vegetation. The ammonium ions produced from the degradation of organic matter (Equation 5.1) will, under aerobic diagenesis, be oxidised further by nitrifying bacteria to yield nitrate (Equation 5.2).

$$NH_4^+ + 2\,O_2 \longrightarrow NO_3^- + 2\,H^+ + H_2O$$ **Equation 5.2**

No.	Reaction	$\Delta G^{\circ\prime}$ kJ mole^{-1} C_{org}
1.	$C_{org} + 138\ O_2 \longrightarrow$ $106\ CO_2 + 16\ HNO_3 + H_3PO_4 + 122\ H_2O$	-56367
2.	$C_{org} + 236\ MnO_2 + 472\ H^+ \longrightarrow$ $236\ Mn^{2+} + 106\ CO_2 + 8\ N_2 + H_3PO_4 + 366\ H_2O$	-54600 (birnessite) -51596 (pyrolusite)
3a.	$C_{org} + 94.4\ HNO_3 \longrightarrow$ $106\ CO_2 + 55.2\ N_2 + H_3PO_4 + 177.2\ H_2O$	-53540
3b.	$C_{org} + 84.8\ HNO_3 \longrightarrow$ $106\ CO_2 + 42.4\ N_2 + 16\ NH_3 + H_3PO_4 + 148.4\ H_2O$	-48593
4.	$C_{org} + 212\ Fe_2O_3$ (or $424\ FeOOH$) $+ 848\ H^+ \longrightarrow$ $424\ Fe^{2+} + 106\ CO_2 + 16\ NH_3 + H_3PO_4 + 530\ H_2O$ (or $742\ H_2O$)	-24918 (Fe_2O_3) -23501 (FeOOH)
5.	$C_{org} + 53\ SO_4^{2-} \longrightarrow$ $106\ CO_2 + 16\ NH_3 + 53\ S^{2-} + H_3PO_4 + 106\ H_2O$	-6715
6.	$C_{org} \longrightarrow$ $53\ CO_2 + 53\ CH_4 + 16\ NH_3 + H_3PO_4$	-6185

Table 5.1:

Equations for the oxidation of Redfield molecules by a range of electron acceptors and the associated Gibb's free energy of each reaction (Froelich *et al* 1979).

The degradation of Redfield molecules by molecular oxygen and the subsequent oxidation of the ammonium consumes oxygen and produces acidity (Table 5.1; Equation 1). Loss of oxygen within a sediment prism also occurs through the oxidation of other reduced species (such as Mn^{2+}, Fe^{2+}, HS^- and CH_4) produced during early diagenesis.

2. Manganese reduction

Manganese oxides are usually present as solid phase coatings in sediments, and may contain Mn^{II}, Mn^{III} and Mn^{IV} species (Van der Weijden 1992). The higher valency states of the metal are very reactive oxidants, additionally able to partially oxidise ammonium to dinitrogen (Equation 5.3).

$$MnO_2 + 2\,NH_4^+ + 4\,H^+ \longrightarrow 3\,Mn^{2+} + N_2 + 6\,H_2O \qquad \textbf{Equation 5.3}$$

Manganese reduction generates dissolved Mn^{2+}, accompanied by a reduction in pore water acidity. The solubilised cations are able to migrate away from the site of reduction and often reprecipitate upon encountering oxygen; thus the metal may be preserved in sediments with an oxic top layer. It is probable that almost all of the oxidised manganese present in a typical sedimentary environment is available for microbially-mediated reduction (Froelich *et al* 1979) with the Gibb's free energy yield of the reaction dependent on the mineralogy of the Mn-oxide involved. Since this may overlap with the energy obtained from nitrate reduction (Table 5.1) the two electron acceptors may be viewed to be competing on almost equal terms for participation in the oxidation reaction and may be consumed simultaneously.

3. Denitrification

The dissimilatory reduction of nitrate and nitrite starts to become dominant at low but non-zero O_2 concentrations (Froelich *et al* 1979) and initially produces nitric (NO) and nitrous (N_2O) oxides which are further reduced to dinitrogen. The nitrogen component originating from the organic molecule may be oxidised to dinitrogen (Equation 3a) or persist in the (reduced) ammonium form (Table 5.1, Equation 3b).

4. Ferric iron reduction

Reduction of solid phase Fe^{III} renders the element soluble in the +II oxidation state, with the pore water concentration controlled by the rate of the reduction process and the solubility of Fe^{II}-mineral phases. It is likely that only a small portion of the Fe^{III} present in the sediment system is available for reduction (Froelich *et al* 1979), and this may occur as a result of

microbial catabolism (Table 5.1, Equation 4) or through non-enzymatic reactions. A prominent example of the latter process is the reaction (Equation 5.4) between Fe^{III} and sulphide ions (Van der Weijden 1992).

$$FeOOH + 4\ H^+ + 2\ HS^- \longrightarrow FeS_2 + Fe^{2+} + 4\ H_2O \qquad \textbf{Equation 5.4}$$

The importance of ferric iron reduction in salt marsh systems and the cycling of the element in combination with sulphur compounds is discussed later in this chapter.

5. Sulphate reduction

Following depletion of the electron acceptors considered so far, a variety of anaerobic bacteria may become active which rely on the dissimilatory reduction of sulphate ions to gain energy for metabolism. Other oxidised forms of sulphur may also be utilised as electron acceptors (such as SO_3^{2-} and $S_2O_3^{2-}$) forming sulphide, S^{2-}, as the product of the reduction (Krumbein 1983). On a global scale, sulphate reduction is second only to aerobic oxidation in accounting for the decomposition of organic materials (Van der Weijden 1992). The extensive involvement of sulphur compounds in early diagenesis has important consequences for the sedimentary sulphur cycle and additional implications for the cycling of other elements, particularly iron, due to the potential formation of relatively insoluble metal-sulphide phases. The relevance of these processes to the geochemical cycling of elements in salt marshes is discussed further below.

6. Methanogenesis

The electron acceptor which reduces carbon dioxide during the production of biogenic methane is derived from the organic molecule and the overall process is therefore simply the disproportionation of organic carbon to yield carbon dioxide and methane (Table 5.1; Equation 6). The reactions become prominent when practically all of the sulphate supply has become exhausted (Van der Weijden 1992). The methane generated is likely to diffuse upward and be consumed in the oxic zone, or it may alternatively be oxidised by anaerobic bacteria (Krumbein 1983).

5.1.1.1 Diagenetic zonation

The sequential utilisation of various electron acceptors for the oxidation of organic materials may lead to the establishment of different chemical zones within a sediment prism, characterised by the specific reactions that occur (Berner 1980).

The sequence of consumption of the various electron acceptors (Froelich *et al* 1979) and the subsequent zonation of the different diagenetic reaction schemes (Berner 1980) assumes that steady-state conditions are operative throughout the sediment profile and that the sediments are relatively homogeneous. Such assumptions are not strictly applicable to complex environmental systems such as salt marshes on account of the highly variable composition of the sedimentary material and the frequency with which non-steady-state diffusive processes can alter the pore water chemistry (during flooding, for example). The unique nature of the interaction of the biota, sediment and pore water needs to be explored further before a more comprehensive understanding of the system can be attained. However, the general implications of the thermodynamic calculations may be extremely useful in interpreting the observed distributions of those species involved in early diagenesis within salt marsh sediments.

Diagenetic Zone	Electron Acceptors
Oxic	O_2
Non-sulphidic post-oxic (Sub-oxic)	MnO_x NO_3^- Fe^{III}
Sulphidic	SO_4^{2-}
Non-sulphidic methanic	CO_2

Table 5.2:

Diagenetic zones resulting from the oxidation of organic matter (after Berner 1980).

5.1.2 *Diagenesis in salt marsh environments*

The regular tidal inundation of salt marshes results in the sediments being almost continuously waterlogged, except perhaps during hot summer months when surficial desiccation may occur. The diffusion of oxygen into the soil is considerably affected by this saturated condition and the subsurface environment which prevails is predominantly anaerobic (Christian and Wiebe 1978). The activity of the vegetation colonising the salt marsh surface may exert a dominant control on the flux of oxygen into the sediments through photosynthesis and root respiration (Lord and Church 1983; Cutter and Velinsky 1988) and therefore affects the seasonal redox cycling of many elements. Furthermore, the generation and maintenance of reducing conditions is dependent upon the depositional and diffusional flux of organic materials and is therefore strongly coupled to the growth and die-off of the marsh plants throughout the annual cycle (Howarth and Teal 1979; Hines *et al* 1989).

5.1.2.1 Iron and sulphur cycling in salt marshes

Due to anoxic conditions prevailing just beneath the sediment surface, sulphate reduction represents a major pathway for the oxidation of organic matter in salt marshes (Hines *et al* 1989) and the products of the associated reactions exert a significant control over the composition of the sediment and pore waters. The chemical cycling of iron and sulphur may occur over rapid timescales (of the order of days) and results in the presence of a suite of possible species. Pyrite is the only thermodynamically stable iron and sulphur compound in marine sediments (Berner 1967) and the formation of this mineral (Figure 5.1) ultimately controls the sedimentary burial of both elements (as well as many trace metals) in salt marshes (Cutter and Velinsky 1988).

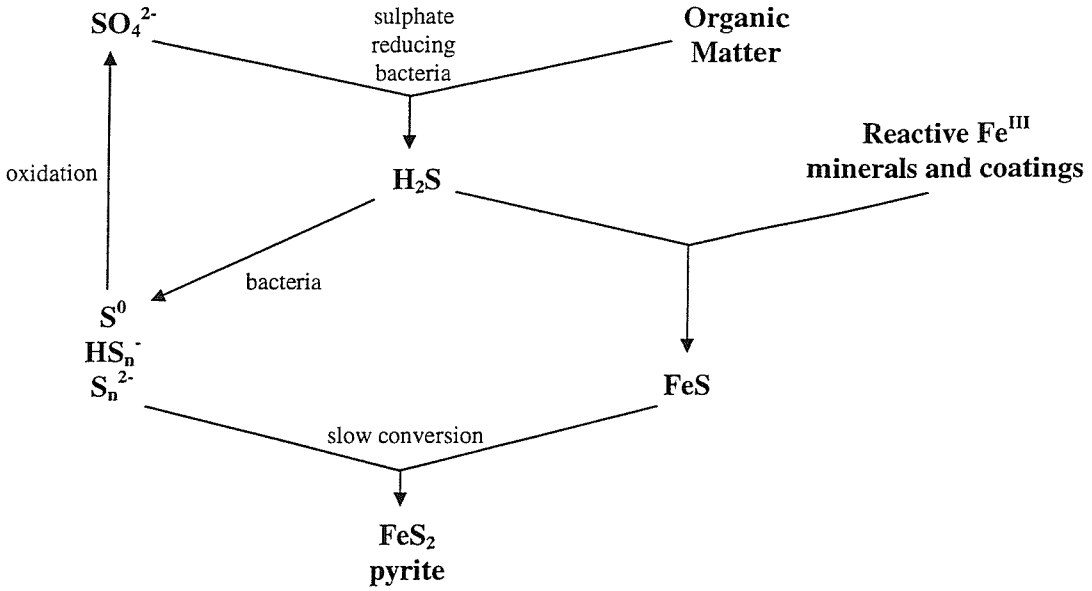

Figure 5.1:

Schematic diagram summarising the chief steps in the formation of sedimentary pyrite (after Berner 1985).

5.1.2.1(a) Sulphur compounds

Sulphate ions are regularly resupplied to pore waters during the flooding of sea water across the surface of the marsh. The ability of sulphur atoms to form a great variety of chemical compounds and to undergo changes in oxidation state over an eight electron shift results in the element being involved in many biochemical reaction schemes. It constitutes 0.1-2 % dry mass (Fenchel and Finlay 1995) of the biomass (mainly bound in proteins) but is of chief concern here in relation to its role in catabolic enzymatic processes. The bacterially-catalysed reduction of sulphate ions releases energy for metabolic processes and results in the production of hydrogen sulphide. The diffusion of the sulphide ions to more oxidising regions of the sediment prism may be followed by incomplete oxidation producing intermediary products such as polysulphide ions (HS_n^-, S_n^{2-}; n>1), elemental sulphur (S^0) and thiosulphate ($S_2O_3^{2-}$) (Boulegue *et al* 1982); complete oxidation regenerates sulphate. The variable predominance of different sulphur species throughout the pore waters of the marsh considerably dictates the distribution of authigenic mineral phases.

5.1.2.1(b) Pyrite formation

A variety of schemes have been proposed for the synthesis of pyrite in marine sediments including the reaction of iron monosulphides (FeS) with elemental sulphur or polysulphides, the dissociation of greigite (Fe_3S_4), and the direct reaction of Fe^{II} with polysulphides (Rickard 1975). The first of these mechanisms was proposed by Berner (1970) and involves the following steps: bacterial sulphate reduction, reaction of H_2S with ferric minerals to form iron monosulphides (mackinawite, $FeS_{0.94}$, and greigite, Fe_3S_4), and the reaction of iron monosulphides with elemental sulphur to form pyrite:

$$FeS + S^0 \longrightarrow FeS_2 \qquad \textbf{Equation 5.5}$$

The pyrite formed by this process crystallises slowly as minute framboidal microspheres. The time for the complete transformation of FeS to FeS_2, in the presence of abundant S^0, is of the order of several years (Berner 1970).

The persistence of two different forms of pyrite in sediments (framboidal microspheres and single crystals) led Goldhaber and Kaplan (1974) to suggest that there may be two formation mechanisms, each operative under different conditions. Experimentation yielded a mechanism for the direct precipitation of pyrite, without intermediate iron monosulphide oxidation, through the reaction of ferrous iron with polysulphides, for example *via*:

$$Fe^{2+} + S_5S^{2-} + HS^- \longrightarrow FeS_2 + S_4S^{2-} + H^+ \qquad \textbf{Equation 5.6}$$

A number of studies related to the formation of pyrite within salt marsh sediments have been conducted (Nedwell and Abram 1978; Howarth 1979; Howarth and Teal 1979; McCaffrey and Thomson 1980; Luther *et al* 1982; Lord and Church 1983; Giblin and Howarth 1984; Luther and Church 1988) and many of these have concluded that both single-crystalline and framboidal pyrite are present. Salt marsh pore waters are often undersaturated with respect to mackinawite and supersaturated with respect to pyrite (Howarth 1979; Giblin and Howarth 1984) enabling the direct precipitation of a pyrite phase. The subsequent mineralisation of two moles of sulphur per mole of iron and the buffering of pore water sulphide at a lower concentration (Table 5.3) may be of benefit to many micro-organisms and plants by reducing exposure to the toxic ions S^{2-} and Fe^{2+} (Howarth and Teal 1979). However, the formation of mackinawite and other iron monosulphides is kinetically favoured over pyrite and is expected

to dominate if the pore waters are supersaturated with respect to these minerals. Generation of pyrite will then occur gradually following reaction with elemental sulphur (Equation 5.5).

Mineral	Solubility product $[Fe^{2+}]\ [S^{2-}]$
mackinawite	2.8×10^{-18}
pyrite	2.4×10^{-28}

Table 5.3:

Solubility products of mackinawite and pyrite (Howarth 1979).

5.1.2.2 The effects of salt marsh vegetation

Salt marsh vegetation may affect the sedimentary iron and sulphur cycles in a number of ways. The seasonal variation in vegetative growth and decay dominates both the rate of supply of metabolisable organic material and also, through photosynthetic activity, the oxidative capacity of the pore waters surrounding the root zone. Consequently, the rate of sulphate reduction varies greatly over depth and time in salt marshes (Lord and Church 1983; Howarth and Teal 1979).

The growth of the root system within minerogenic sediments yields a highly non-uniform distribution of organic matter throughout the marsh prism. The oxidation and reduction reaction sequences described above are therefore not likely to be restricted to specific horizons within the sediment but may occur simultaneously in adjacent micro-environments (Lord and Church 1983; Fenchel and Finlay 1995). The areas immediately surrounding decomposing organic particles ought to be characterised by higher rates of sulphate reduction, possibly leading to the formation of small pyrite concretions (Figure 5.2; Berner 1980). At the same time adjacent active root surfaces may be sites of sulphide oxidation. These zones have additionally been found to accumulate iron, in the form of goethite, as amorphous root coatings and dispersed particles of both framboids and single crystals (Luther *et al* 1982; Boulegue *et al* 1982; Luther and Church 1988).

During early summer months subsurface oxidation is at its greatest (Boulegue *et al* 1982). The intense photosynthetic growth of the macroflora produces a flux of oxygen and other oxidants into the pore waters that destroys pyrite and releases sulphate into solution (Gleason and Zieman 1981). Ferric iron minerals may be formed through precipitation or from the pseudomorphism of extant pyrite crystals (Luther *et al* 1982). Other oxidation products may also abound, including a range of partially oxidised sulphur compounds, whilst sulphate reduction continues around microniches within the sediment body. Vegetative growth slows as the seasons advance and is accompanied by a decrease in the oxidation rate of sub-surface species. Reduction reactions consume many of the chemical species present and, as autumn approaches, the increased flux of decomposing organic detritus may contribute to the onset of a net accumulation of pyrite (Howarth and Teal 1979). Until the following spring growth the rate of pyrite oxidation is low, governed by the influx of gaseous O_2 and the activities of bacteria such as *Ferrobacillus ferrooxidans* and *Thiobacillus ferrooxidans* (Boulegue *et al* 1982).

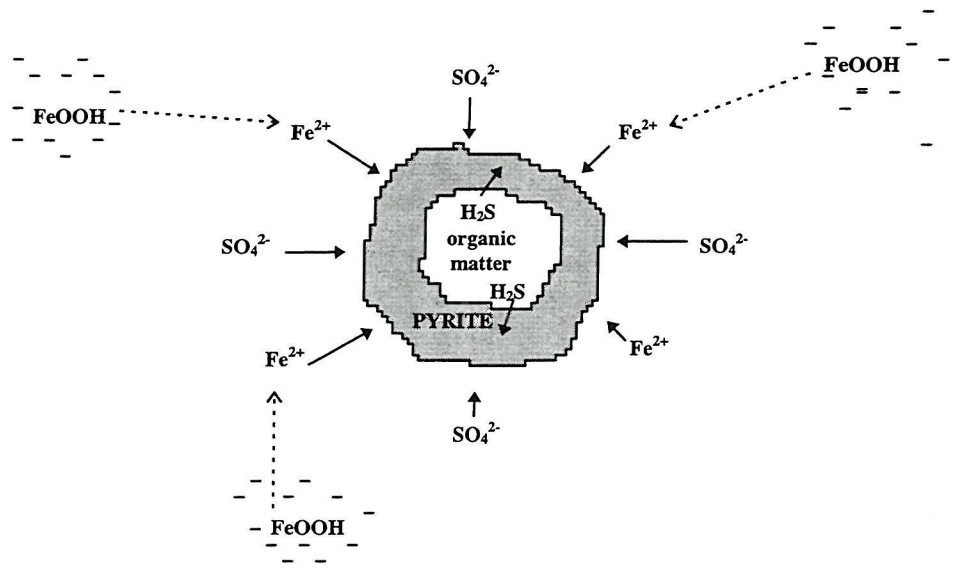

Figure 5.2:

Formation of a pyrite concretion around a decomposing clot of organic matter (after Berner 1980).

5.2 The iron, manganese and sulphur geochemistry of Hythe salt marsh cores

The cycling of iron, manganese and sulphur compounds in salt marshes involves a complex suite of geochemical interactions influenced by the sedimentological regime and the activity of the resident plant population. To interpret the concentration profiles obtained for these elements, therefore, it is helpful to consider them in concert with the sedimentary logs recorded before core sectioning (Figure 5.3).

The distribution of iron, manganese and sulphur throughout the four cores may enable the identification of different zones within the sediments where different oxidation and reduction reactions occur. The redox zonation described previously, arising from the sequential utilisation of different chemical species as electron acceptors for organic decomposition, is a useful scheme with which to interpret the observed elemental profiles. It must be remembered, however, that the heterogeneous nature of the sediment prism may preclude the formation of a theoretical or "ideal" pattern (e.g. Froelich *et al* 1979). In addition, the redox potential of any particular depth horizon cannot necessarily be expected to remain the same over even short timescales of a day or less. The solid-phase distributions measured in a sediment core refect only the net outcome of diagenetic processes at one moment in time and cannot, therefore, be used to identify all details of the diagenetic reactions taking place at any given depth (Thamdrup *et al* 1994).

The elements (S, Fe and Mn) exhibit similar distributions in all cores and are therefore described below in terms of their apparent salt marsh geochemistry throughout all four of the cores studied.

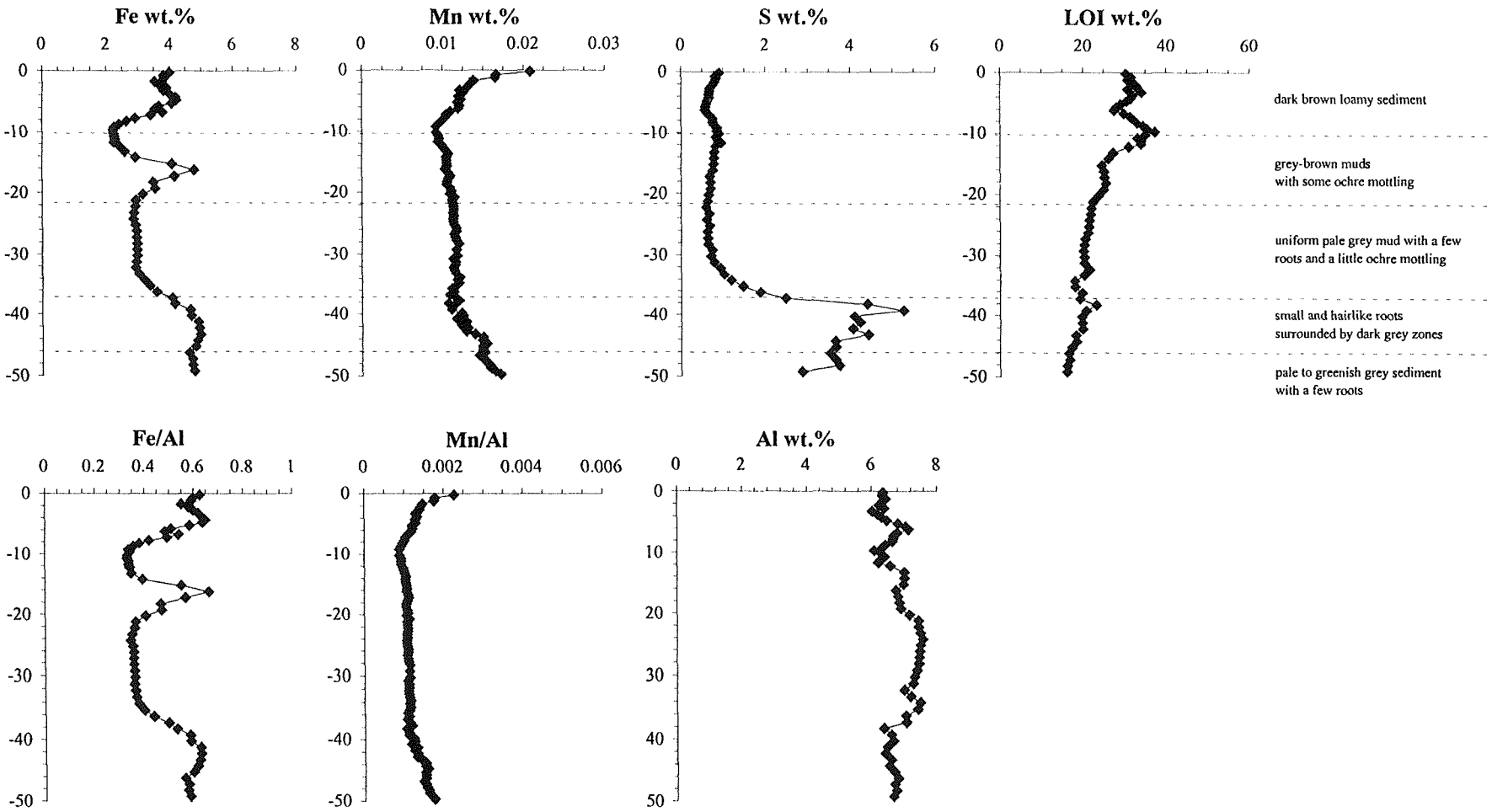

Figure 5.3(a): Core HyPb

Solid phase depth-concentration profiles of iron, manganese and sulphur in relation to core sedimentology.

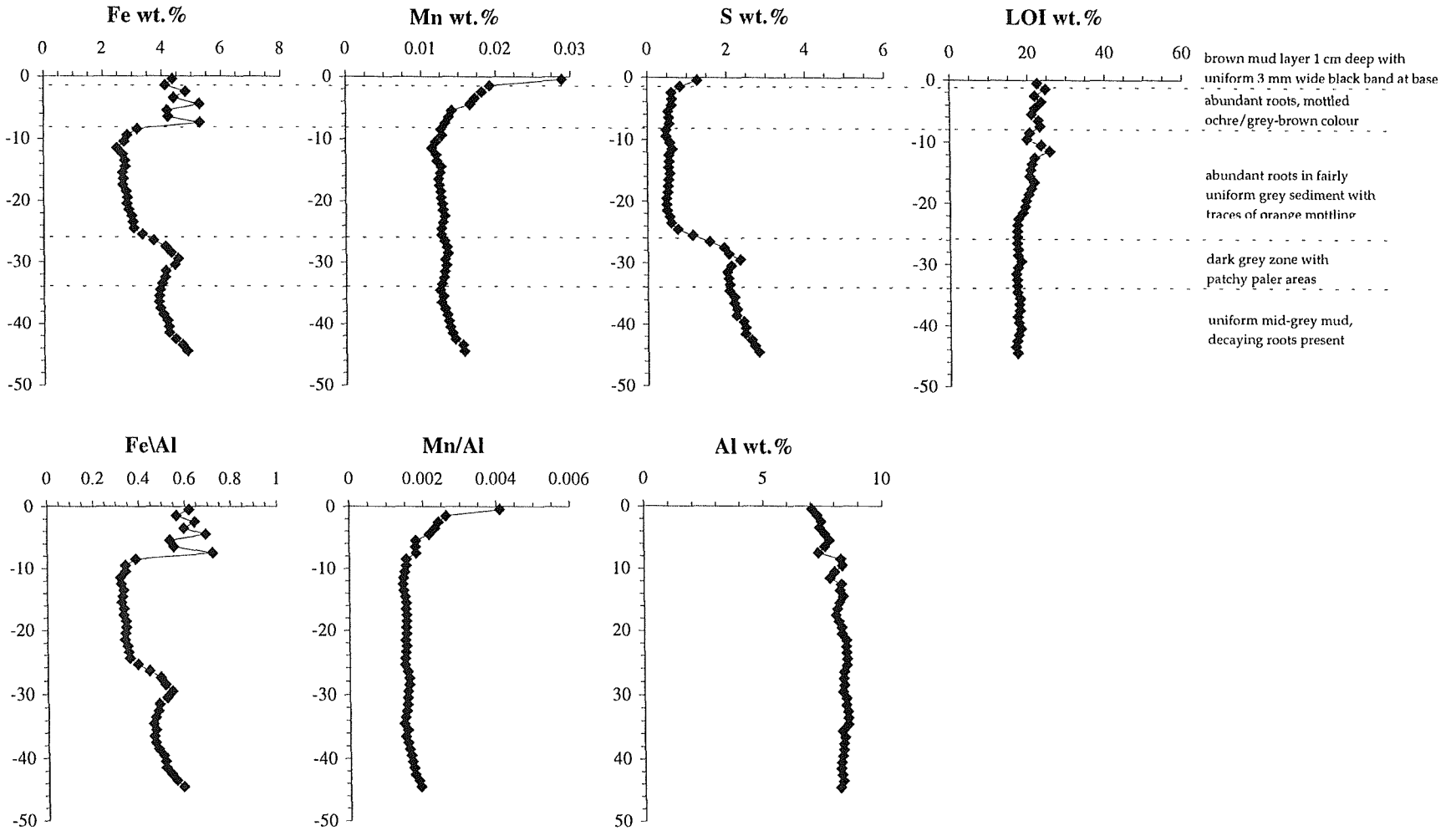

Figure 5.3(b): Core HySR2

Solid phase depth-concentration profiles of iron, manganese and sulphur in relation to core sedimentology.

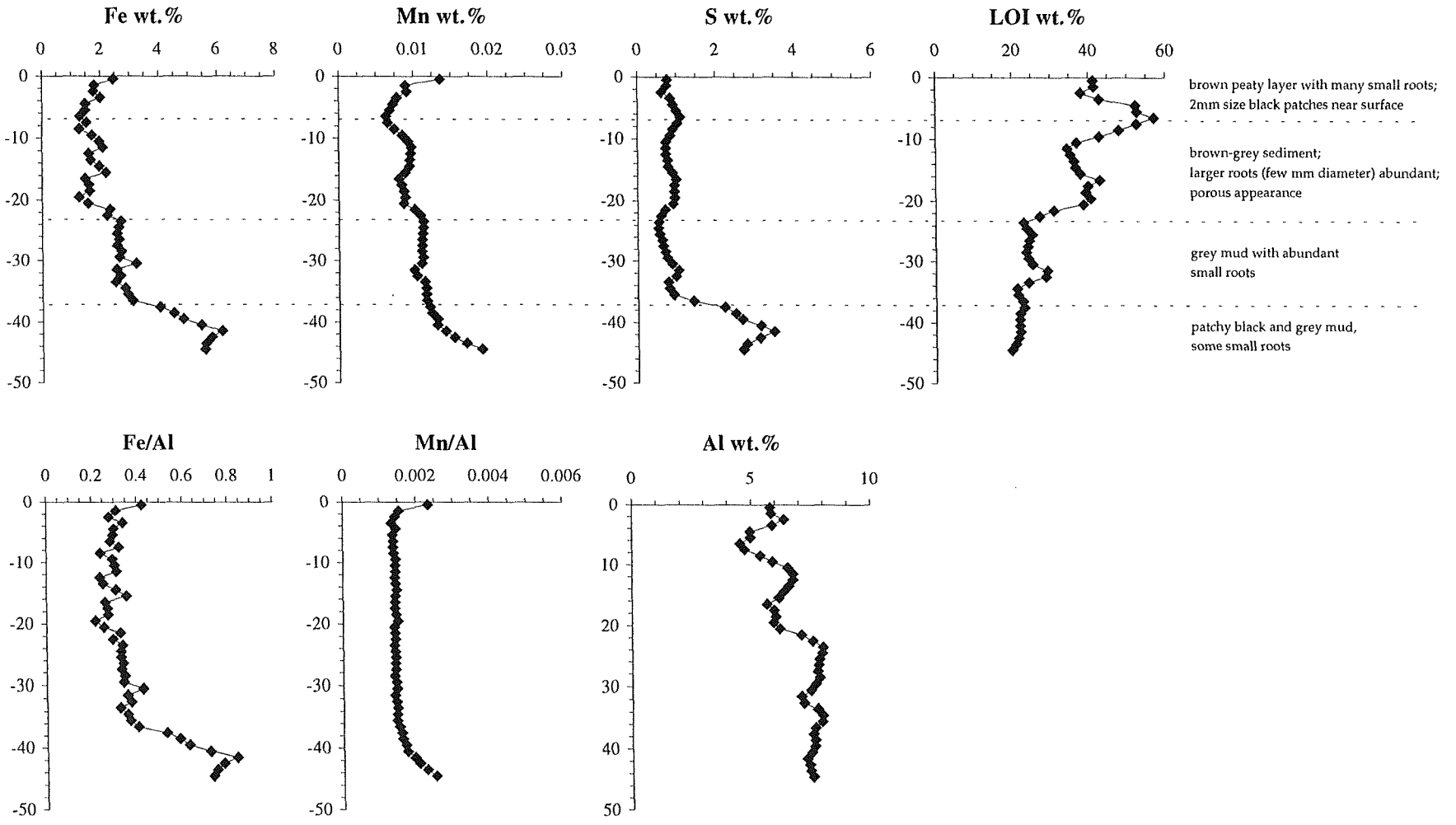

Figure 5.3(c): Core HySR3

Solid phase depth-concentration profiles of iron, manganese and sulphur in relation to core sedimentology.

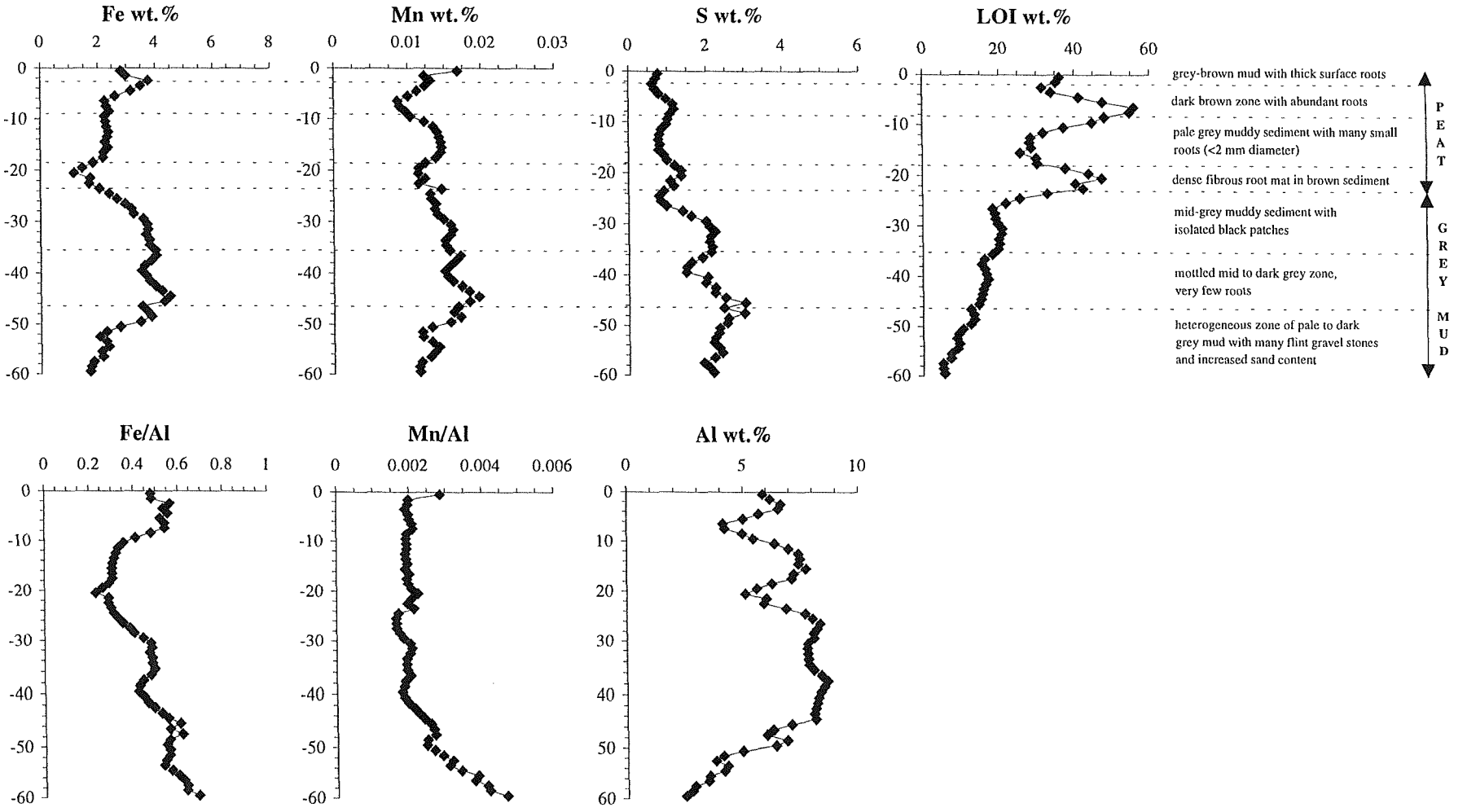

Figure 5.3(d): Core HySR5

Solid phase depth-concentration profiles of iron, manganese and sulphur in relation to core sedimentology.

5.2.1 *Sulphur*

The variation with depth of the total sulphur within a salt marsh prism is primarily due to variation in the pyrite content of the sediments (Cutter and Velinsky 1988). Lesser contributions are made by organic sulphur compounds and also the presence of sulphate-bearing waters within the pore interstices. Calculations based on the pore water profiles obtained from a Danish salt marsh (Thamdrup *et al* 1994) imply that H_2S turnover times may be less than a few minutes, at depths where sulphate reduction is known to occur, before being lost by oxidation. In order to yield a net accumulation of iron sulphides, therefore, conditions must be sufficiently reducing to enable sulphide ion involvement in mineralisation reactions, either directly (such as $Fe^{2+} + HS^- \longrightarrow FeS + H^+$) or indirectly (forming intermediate oxidation state compounds which are subsequently mineralised). Furthermore, such partially-oxidised sulphur species are precursors of pyrite formation and reaction is thus likely to be most intense where such compounds coexist along with dissolved Fe^{2+} and HS^-. The boundary between sub-oxic conditions (generating Fe^{2+} and species such as S^0, $S_2O_3^{2-}$, HS_n^-) and primarily sulphidic conditions (sourcing HS^- and S^{2-}) thus probably represents the most active zone of pyrite formation.

Assessment of each of the four Hythe salt marsh sulphur profiles reveals that similar characteristics exist in each. These may be summarised as:

I. a slightly-enriched surface layer;
II. increased concentrations in sediment layers with high C_{org};
III. abundant sulphur at depth.

5.2.1.1 Sulphur in the surface layers

The sulphur concentration in the sediments typically decreases downcore over the uppermost few cm, by about 0.5 wt.%, to a minimum value of approximately 0.6 wt.%. A similar pattern observed in salt marsh sediments from the Scheldt Estuary, Netherlands, was attributed to the deposition and subsequent loss by oxidation of sulphide-rich suspended matter originating from the upper estuary (Zwolsman *et al* 1993). The erosion and deposition of particles from the dominantly anoxic mudflats fronting the salt marsh at Hythe may be similarly responsible for these surficial enrichments.

5.2.1.2 Sulphur in organic-rich bands

Minor increases of up to 1 wt.% S are evident in all cores, forming peaks which are coincident with elevated concentrations of organic carbon. The profiles of Fe and Fe/Al indicate that the sulphur enrichments are not generally accompanied by significant iron enrichment, ruling out iron sulphide mineralisation as their mode of origin. The elevated levels may alternatively originate from the presence of organic sulphur compounds within the root-rich sediment horizons. Sedimentary organic matter is known to react with dissolved sulphur species leading to an enrichment of sulphur within marine humic acids (Ferdelman *et al* 1984). In near-surface salt marsh environments a diagenetically stable pool of sulphoxides and sulphones (in the more oxidised state) or organic sulphides and polysulphides (under more reducing conditions) may form following the reaction of organic detritus with dissolved sulphide.

5.2.1.3 Sulphur in the deeper sediments

At a variable depth (Figure 5.3) within each core, the muds become much darker and are significantly enriched in sulphur. All profiles reveal a peak, ranging from ~2.5 to ~5.5 wt.% S in different cores, beneath which the concentration decreases slightly. Examination of the Fe and Fe/Al profiles in these instances demonstrates that bacterial reduction of both sulphate and ferric iron, and the subsequent reactions which occur, result in the accumulation of authigenic sulphide minerals over these depths. An assessment of the stoichiometry of the iron sulphide phase leaves little doubt that it is FeS_2 which is predominant (Figure 5.4). The peaks which form are likely to reside just beneath the sub-oxic/sulphidic boundary, where conditions most favour the production of a pyrite phase. Such a redox boundary may also conform to a hydrological boundary, beneath which the passage of oxygenated waters during tidal flooding is greatly decreased and hence reducing conditions are better established.

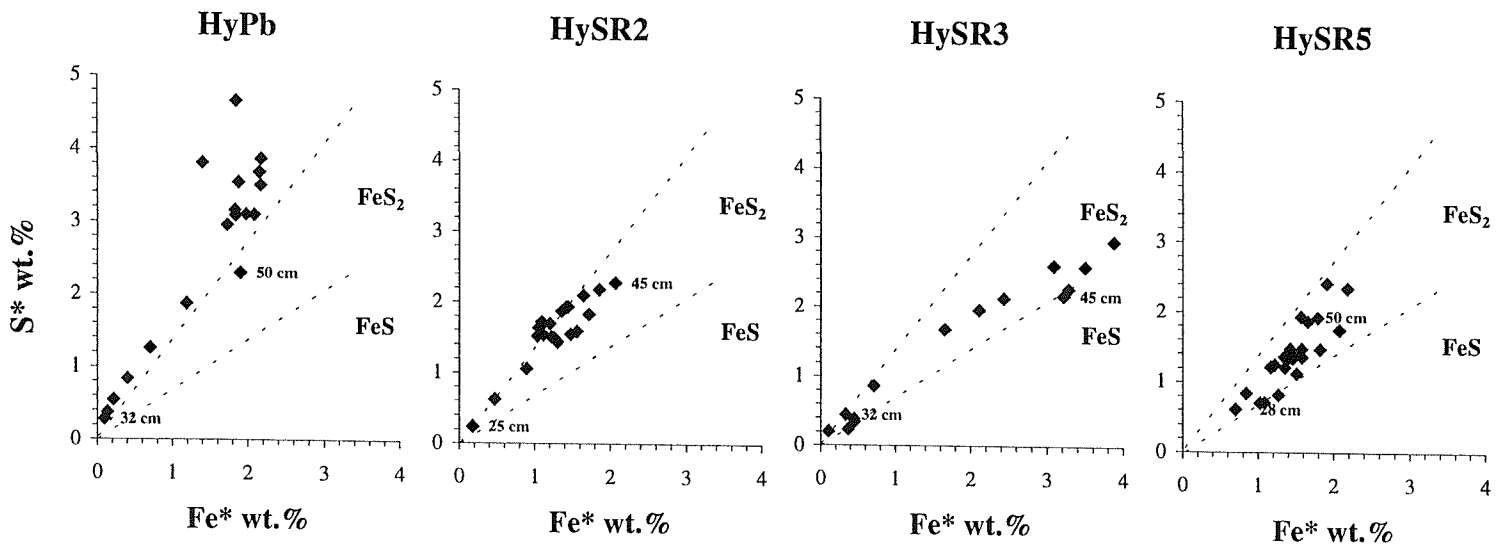

Figure 5.4:
Stoichiometric relationship between excess iron and sulphur in four salt marsh cores.

5.2.2 *Iron*

The presence of iron in salt marshes is due to the deposition of Fe-bearing particles on the sediment surface and their subsequent geochemical cycling. "Reactive" oxidised iron has traditionally been defined as that fraction of the marine sediment which reacts readily with sulphide (Kostka and Luther 1994), though this may represent only a small percentage of the total ferric iron present (Froelich *et al* 1979). The Fe-mineral assemblage is dominated by oxyhydroxide phases (both crystalline and amorphous, the latter being considerably more reactive) and sulphides (comprising monosulphides and pyrite), though vivianite, $Fe_3(PO_4)_2.8H_2O$, may also play a role (Van der Weijden 1992). Siderite, $FeCO_3$, may form as a product of iron reduction, although this is not favoured in marine sediments with high sulphide concentrations. The reaction of iron with either oxygen or sulphide species yields iron-bearing mineral phases, whilst concurrent microbial iron reduction under sub-oxic conditions may deplete the solid phase concentration to the point where only the unreactive fraction of the metal remains.

The key features of the iron distributions obtained from analysis of Hythe salt marsh cores are listed and discussed below:

I. elevated concentrations in the near-surface zone;
II. constant low concentrations within the mid-core sediments;
III. increased solid phase iron at depth.

5.2.2.1 Iron enrichment in the near-surface sediments

The uppermost section of each salt marsh core (up to a decimetre depth, except in the case of core HySR3) consists of dark-brown root-rich sediments which are typically enriched with up to ~5.5 wt.% total Fe. These elevated levels must be due to a combination of (a) burial of oxidised iron minerals deposited on the sediment surface, and (b) the authigenic formation of ferric oxyhydroxides as a result of upward diffusion and oxidation of Fe^{2+}. The presence of a patchy orange colouration suggests that ferric iron, possibly in the form of goethite, may precipitate as grain coatings within the sediments, as has been observed in salt marshes elsewhere (Boulegue *et al* 1982; Luther *et al* 1982). A study by Kostka and Luther (1994) revealed that amorphous Fe^{III}-minerals accounted for up to 50 % of the total iron present in surface salt marsh sediments, declining to less than 1 % below 10 cm depth. A similar distribution of oxidised iron is evident in these salt marsh cores, with the base of the zone of

oxidative enrichment marked by a sharp decline to roughly constant detrital levels as a consequence of reductive dissolution. This horizon is often coincident with a peak concentration of organic carbon, which causes an increased microbial demand for electron acceptors.

Core HySR3 (Figure 5.3) exhibits a much less significant zone of oxidative iron enrichment and, furthermore, a considerably more erratic iron distribution throughout much of the sediment profile. It would appear that the broader scale (cm to dm) oxic and sub-oxic diagenetic zonation evident in the other three cores remains undeveloped in this central area of the marsh. Geochemical redox control of the iron distribution is likely to be dominated by microscale variations, with iron dissolution and precipitation occurring at most depths, preventing the formation of a stable redoxcline throughout the upper 35 cm of the sediment. The pore water iron profile obtained from this area of the marsh is discussed later in this chapter.

Core HyPb (Figure 5.3) displays a prominent feature, unique amongst the four cores examined, comprising a second iron peak within the middle section of the core. This enrichment, centred at 16 cm depth, occurs between two bands of relatively low Fe content and is identified as being due to oxidative precipitation of ferric minerals, since an orange mottled colouring is recorded in the sedimentary log. There are thus two discrete horizons within this core where iron is oxidised and forms ferric phases, residing at depths of 0-9 and 12-22 cm. Conditions over the intermediate depth range (9-12 cm) preclude the precipitation of Fe^{III}-phases, perhaps as a result of the higher abundance of organic materials establishing a lower redox potential (note the peak in LOI due to organic carbon centred on 10 cm depth). In a study of salt marsh pore waters Thamdrup *et al* (1994) observed an increased rate of sulphate reduction at 8-10 cm which they similarly attributed to a layer of plant debris at that depth. The effect of the tidal pumping of oxygenated waters is likely to play a key role in the formation of the lower oxidised iron peak. The lateral transgression of flood waters through the sediment prism, particularly in this frontal marsh area, may be an important process enabling the mid-core oxidation to occur.

5.2.2.2 Constant "background" iron concentration

All of the cores exhibit depths over which the iron concentration is maintained at a reasonably constant low value (typically 2-3 wt.% Fe, corresponding to an Fe/Al ratio of ~0.3). These sediments are usually relatively uniform grey muds, with abundant small roots, incorporating traces of orange oxyhydroxide mottling. In core HySR3 the sediments are considerably browner in colour, indicative perhaps of the absence of a well-developed sub-oxic diagenetic zone. The presence of such uniformity in the other profiles suggests that the values measured represent the non-reactive iron concentration present in the cores, comprising both crystalline iron minerals and the inert lattice-bound fraction of the metal. Most of the reactive iron throughout these depth ranges appears to have been subjected to reductive dissolution thereby depleting the amount residing in the solid phase. The microbially-mediated reduction of ferric iron plays a significant role in this dissolution, additionally supplemented by non-enzymatic reactions, such as that occurring between Fe^{III} and H_2S (Canfield *et al* 1993):

$$2\,FeOOH + H_2S + 4\,H^+ \longrightarrow S^0 + 2\,Fe^{2+} + 4\,H_2O \qquad \textbf{Equation 5.7}$$

The suite of reactions which may take place within these sub-oxic sediments has a profound influence on the geochemical cycling of both iron and sulphur, as well as manganese and many trace elements. Firstly, the formation of elemental sulphur and polysulphide ions is an important precursor to pyrite mineralisation. Secondly, the upward migration of $Fe^{2+}_{(aq)}$ into sediments containing oxidised manganese minerals may result in the dissolution of the latter (Canfield *et al* 1993), via:

$$2\,Fe^{2+} + MnO_2 + 4\,H_2O \longrightarrow 2\,Fe(OH)_3 + Mn^{2+} + 2\,H^+ \qquad \textbf{Equation 5.8}$$

Similar oxidative consumption of Fe^{2+} by reaction with nitrate ions (as another alternative to oxygen) may occur (Froelich *et al* 1979). Other potential fates awaiting the Fe^{2+} sourced into solution include complexation with organic ligands, such as thiols (molecules of the type R-S-X) generated under similar conditions (Luther and Church 1988), or adsorption on to solid mineral or organic substrates. Alternatively, the presence of oxidising micro-environments in the heterogeneous sediment matrix may simply immobilise the dissolved ions through oxidative precipitation at the surfaces of active roots. The traces of orange sediment coatings observed throughout the sub-oxic zones indicate that, despite apparent reduction and depletion, the oxidation of iron does occur in the same zone with reduction in adjacent micro-environments. The regular infiltration of seawater into the marsh sediments and the diurnal cycle of

photosynthetic activity within the overlying plant population are likely to bring about rapid changes in the redox status of this section of the prism and prevent the attainment of steady-state conditions.

5.2.2.3 Iron in the deeper sediments

Coincident with the increases in sulphur content discussed previously, the iron concentration increases markedly at depth within each core. Previous studies, mostly performed on the organic-rich marshes of the eastern U.S. seaboard, have revealed the existence of two discrete zones of iron sulphide mineralisation: the upper sediments being characterised by the rapid formation and destruction of pyrite as a consequence of the prevalent fluctuating oxidative capacity, and the lower sediments exhibiting a slower net accumulation of pyrite, with iron monosulphide intermediates (Lord and Church 1983; Cutter and Velinsky 1988; Luther and Church 1988). Plots of excess iron concentration against excess sulphur for the data obtained in the present study (Figure 5.4) show that the stoichiometry of the mineral phase formed by these two elements varies across Hythe marsh.

In cores HyPb and HySR2 the presence of FeS_2 is demonstrated by the coincidence of the plotted data and the line which describes this stoichiometry. In both cores, but particularly HyPb, an additional source of sulphur is present in many samples. The peak sulphur concentration of HyPb sediments occurs at a depth of 38-39 cm and is coincident with a small peak in loss on ignition presumed to be due to the many thin (<1 mm) roots identified in this core section (see Figure 3.3). The excess sulphur above that accounted for by FeS_2 mineralisation may originate from association of this element with organic matter, as discussed above. The presence of concentric black rings surrounding decaying root fragments (prominent in core HyPb) indicates the intense sulphate reduction taking place at the decomposing surfaces to yield pyrite concretions (as depicted in Figure 5.2). It is not known whether these pyrite grains are formed from direct precipitation or through the partial oxidation of an iron monosulphide precursor. The almost pure pyrite stoichiometry observed in many samples indicates the absence of significant iron monosulphide and therefore suggests that pyrite forms through direct precipitation. This contrasts with the situation in the mid and high marsh cores, as discussed below.

In cores HySR3 and HySR5 there is evidence for the presence of both pyrite and iron monosulphides, since many data points plot between the two stoichiometric lines. The mechanism of pyrite formation is therefore likely to involve the initial formation of iron monosulphide intermediates followed by their reaction with partially oxidised sulphur compounds. Pyrite formed in this manner crystallises as framboidal aggregates of octahedral microcrystals of FeS_2 (Berner 1970). The results of the SEM analysis conducted on a fresh sediment core collected from the same location as HySR3 indicate the presence of many framboidal grains of FeS_2 (Figure 5.5), thus supporting the formation mechanism implied by the stoichiometric plots. McCaffrey and Thomson (1980) also observed such features in saltmarsh sediments and demonstrated the tendency for the mineral to associate with organic materials in the sediments. Similar features (Figure 5.5, c and d) were apparent in Hythe Marsh sediments, although chemical identification of the material inside which the pyrite grains were clustered was not possible.

The conditions within each core which favour pyrite mineralisation by either direct precipitation or slow conversion of an intermediate phase are likely to be heavily affected by the abundance of organic carbon, since this is ultimately responsible for the presence and interaction of many iron and sulphur species within the sediments (Santchi *et al* 1990). A second consideration which may be of importance is the frequency of flooding which the sediment prism experiences as this may regularly introduce oxygenated waters into the pore intersticies and thus bring about oxidation reactions. The elevated abundance of subsurface organic material due to active vegetative growth in the mid and rear marsh areas is likely to result in extensive recycling of a suite of Fe and S species and may result in supersaturation of both pyrite and iron monosulphides (see Table 5.3), in which case the kinetically-favoured precipitation of iron monosulphide phases would be expected to predominate.

In all four cores the long term storage of reduced iron and sulphur is ultimately effected through the formation of FeS_2 under conditions that are probably permanently reducing (since the accumulation consistently commences at depths beneath the active root growth). It will become apparent in later discussions that the formation of the pyritic phase at depth within Hythe salt marsh sediments has important implications for the cycling of a number of trace metals.

Figure 5.5:

Scanning electron microscope photographs of iron sulphide minerals in Hythe Marsh. Backscattered e^- imaging yielded composition to be FeS_2 (pyrite).

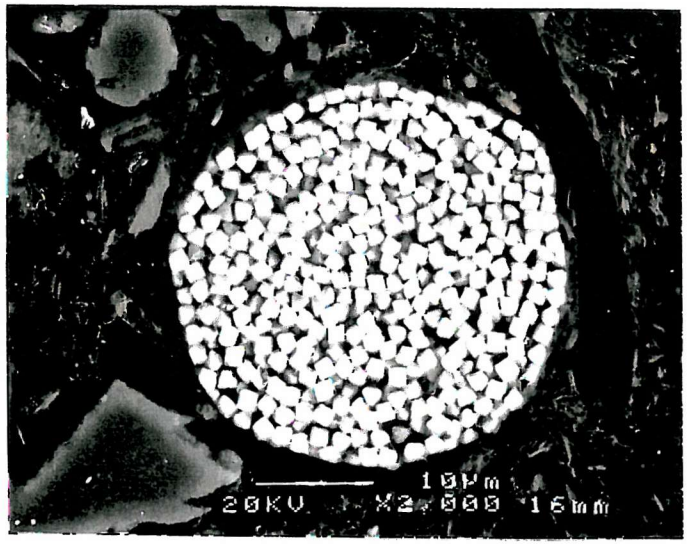

(a): Framboid of FeS_2, ~30 µm diameter.

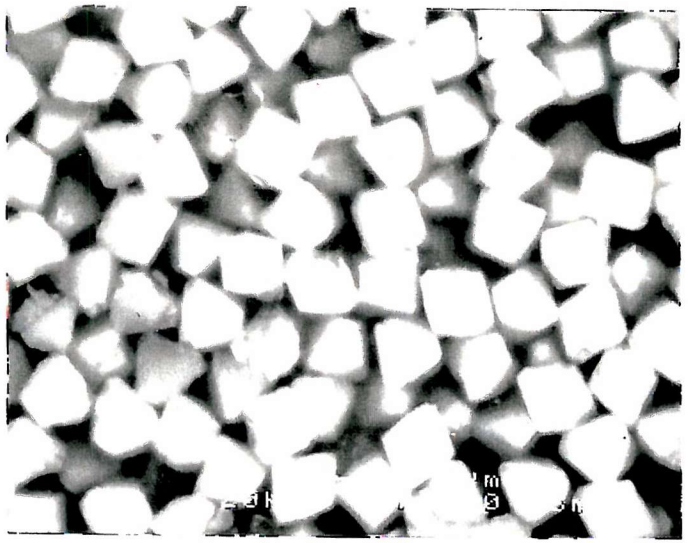

(b): Higher magnification, showing regular octahedral microcrystals.

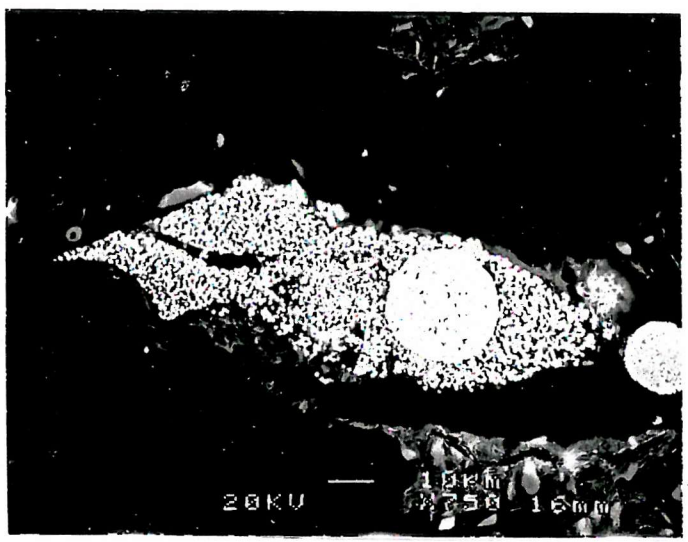

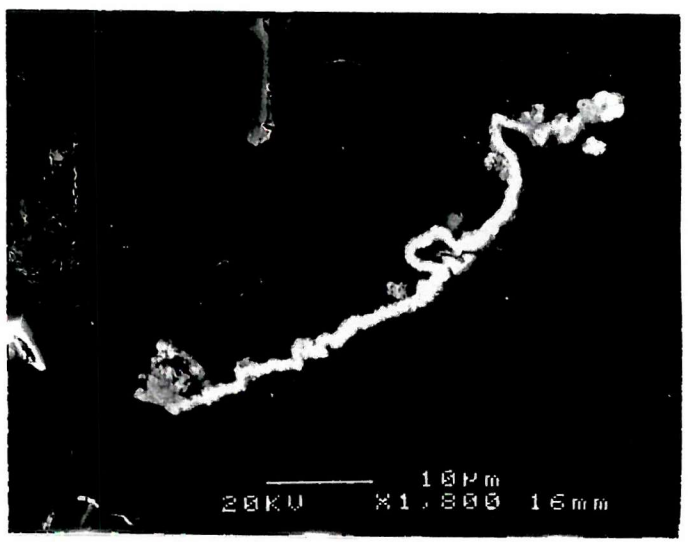

(c) and (d): Aggregation of microcrystals within the sediment matrix (possibly in association with organic materials).

5.2.3 *Manganese*

The cycling of manganese in surface sediments is dominated by reduction of the metal (rendering it soluble as Mn^{2+}) and subsequent oxidation to precipitate Mn-oxides. In a hypothetical steady-state system the dissolved and solid phase profiles of Mn ought to resemble Figure 5.6 (Froelich *et al* 1979), with the diagenetic cycling restricted to the upper (oxic and sub-oxic) diagenetic zones of the sediment prism.

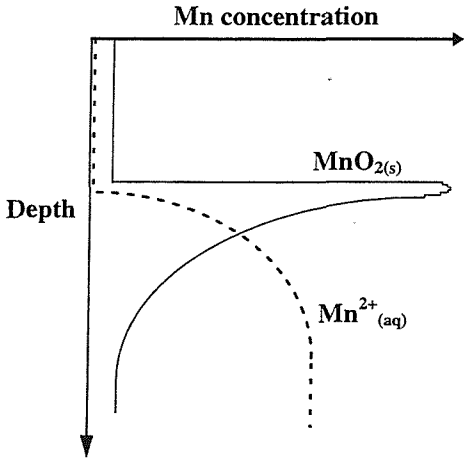

Figure 5.6:

Schematic representation of dissolved and solid- phase Mn profiles in a hypothetical steady-state system (Froelich *et al* 1979).

The formation of reduced manganese solid-phases is of much less significance than the formation of oxides, particularly since alabandite (MnS) is often undersaturated by several orders of magnitude at all depths within salt marsh pore waters (Giblin and Howarth 1984). The generation of significant amounts of alkalinity (CO_2 and HCO_3^-) as a result of intense sulphate reduction (Luther and Church 1988), however, may result in the precipitation of manganese carbonate ($MnCO_3$).

The distribution of manganese throughout Hythe marsh sediments reveals "C-shaped" profiles comprising the following features:

I. an enriched surface layer;

II. constant concentrations throughout the greater portion of each core;

III. elevated levels at depth.

5.2.3.1 Manganese in the surface layers

The concentration of manganese within the uppermost few cm of each core reaches levels of up to 300 ppm Mn and declines sharply downcore. In the more organic-rich sediments of cores HySR3 and HySR5 the Mn/Al profiles reveal that the enrichment is restricted to the surficial 1 cm, beneath which roughly constant values are attained, whereas cores HySR2 and HyPb appear to have elevated concentrations present over the whole of the upper decimetre (though still most pronounced within the upper few cm). The surficial concentrations are maintained by the deposition of Mn-bearing particles and the precipitation of authigenic Mn oxyhydroxides as upward-diffusing Mn^{2+} cations encounter the prevalent oxic conditions. Furthermore, Canfield *et al* (1993) report significant adsorption of Mn^{2+} on to the surfaces of sediments containing fully oxidised Mn-oxides, thereby reducing the oxidation state of the latter phase to an average value of 3.6, at which point such adsorption becomes negligible. The ions may thus be concentrated into the solid-phase by several different processes.

5.2.3.2 Constant manganese concentrations

Following burial the reduction of solid-phase manganese oxides may occur through a variety of reactions, including dissimilatory bacterial reduction (accompanied by organic carbon oxidation) and interaction with other reduced species such as Fe^{2+} (Equation 5.8) and H_2S. The latter reaction (Canfield *et al* 1993) may be written:

$$MnO_2 + H_2S + 2\,H^+ \longrightarrow Mn^{2+} + S^0 + 2\,H_2O \qquad \textbf{Equation 5.9}$$

The effect of manganese reduction is to deplete the solid-phase concentration such that only the non-labile fraction of the element may remain. Throughout the bulk of each core analysed the ratio of Mn/Al remains approximately constant, though differs between cores over the range 0.001 to 0.002 with a systematic increase towards the rear of the marsh.

5.2.3.3 Manganese enrichment at depth

The presence of elevated concentrations of Mn at depth within each core appears to be coupled to the reduction of sulphate ions, although the exact mechanism through which the solid-phase association takes place cannot be assessed with confidence without mineralogical investigation. Manganese may accumulate in the solid phase through adsorption and co-precipitation with iron sulphide minerals, although the observed enrichments generally seem to lie beneath the most active zone of pyrite formation implying that this is not the case. Alternatively, sulphate reduction may result in the formation of a manganese carbonate phase, due to the alkalinity generated during this process or, indeed, the direct precipitation of MnS. The latter phase has been found to be considerably undersaturated in studies carried out on organic-rich marshes of the U.S. (Giblin and Howarth 1984) but cannot be ruled out within these minerogenic sediments due to the probable relative abundance of Mn^{2+} ions. Microprobe analysis of Baltic Sea sediments, performed as a precursor exercise to this present study, identified the presence of significant quantities of MnS as an apparently authigenic phase (unpublished data; see also Lepland and Stevens 1996). The inclusion of manganese into iron monosulphides, but not into pyrite, has been reported for estuarine sediments (Luther *et al* 1980) along with the suggestion that loss of Mn may occur during the transition from Fe_3S_4 to FeS_2. It is important to realise that, whatever the exact mode of fixation, Mn may be immobilised within the deeper sediments of Hythe salt marsh, and that this appears to be coupled to the microbial reduction of sulphate ions.

5.3 Pore water Fe and Mn results

5.3.1 *Summary of sampling regime*

The concentration profiles obtained from deployments of the two different gel-based sampling devices constructed during this study provide useful although somewhat limited information on the composition of the salt marsh pore waters. Further development and testing of the equilibration apparatus could lead to significant improvements to the technique, although this has not been possible within the timescale of this project. The modes of sample collection and the data obtained from different experiments are summarised below:

5.3.1.1 Thin-film gel sampler

Field testing of the thin-film gel sampler was conducted on two occasions. During the first of these trials the gel sheet was sliced in the field immediately after retrieval from the sediments in an attempt to obtain contiguous samples containing a range of analytes. The results of this trial do not provide good quality data in terms of what we might expect to see from the known behaviour of iron within a partially reducing sediment sequence. The measured concentration of iron, for example, typically ranges from 0-200 ppb except for a few spurious samples which give readings of up to 1300 ppb. These data, obtained by GFAAS, suggest either that the gel layer did not equilibrate fully with the pore waters or alternatively suffered from interferences during the slicing operation. The apparently low values of iron concentration found (compared to the expected natural range; see results from later trials) imply either that ferrous iron from the pore waters did not accumulate within the gel slice or that it was removed by the rinsing performed prior to sectioning. The relatively short time of deployment within the marsh sediment prism, although of sufficient duration to permit equilibration as determined from laboratory experiments, is believed to have limited the transfer of solutes from the pore waters into the gel layer.

To counteract possible problems associated with the rinsing and slicing of the gel sheet a second deployment was carried out which utilised the sodium hydroxide fixing stage, as reported by Davison *et al* (1991). This method, as previously established by other workers, has been shown to yield results in good agreement with conventional pore water extraction techniques (Davison *et al* 1991; Davison *et al* 1994). The reduced uncertainty of utilising a method which has already been demonstrated to provide reliable data makes this operation a better test of the field equilibration characteristics of the device. Furthermore, the probe

remained in the sediment prism for two days as opposed to the much shorter time of 1½ hours during the initial testing. The samples obtained from this second trial were analysed for iron using GFAAS and yield a profile typical of that expected for oxic and suboxic sediments (Figure 5.7).

5.3.1.2 Chambered gel sampler

The construction of a second equilibration-based pore water sampling device, again employing a hydrated gel as the aqueous medium, focused on the need firstly to provide a larger sample size than is possible with the thin-film experiments, and secondly to isolate the gel into discrete volumes which are not able to exchange dissolved components with one another *via* diffusive processes. To permit the determination of trace element concentrations the aqueous sample must provide sufficient material for analysis. The thin-film sampling device, when sliced at 1 cm intervals, provided samples with a volume of 1 x 0.08 x 3 = 0.24 ml. The hollows milled out from the nylon bar used to construct the chambered device have a volume of about 3.5 ml, increasing the volume of sample retrieved by an order of magnitude and therefore improving the likelihood of measuring a wider range of analytes. Furthermore, with the gel divided into sections prior to deployment diffusional smearing of the concentration profiles within the apparatus is prevented following removal from the marsh. The fixing stage of the experiment is then no longer necessary and may be replaced simply by removal of the retaining membrane sheet and extraction of the different gel pieces into suitable collection vessels.

Deployment of the chambered sampling device was carried out on two occasions to investigate the concentration profiles of a range of dissolved species. Analysis of the samples obtained (at 1 cm intervals) from these experiments was carried out using ICP-AES, for iron and manganese, and FAAS, for iron only (Figures 5.7 and 5.8). Attempted measurement of the copper concentration, using GFAAS, and various trace element concentrations, using ICP-MS, yielded non-reproducible and apparently spurious results. This is believed to have arisen as a result of interferences due, especially in the latter case, to the presence of a saline sample matrix. Analysis of trace components ought to be plausible with a sampler such as the one designed during this study, although some experimental modifications may be necessary (sample manipulation, following extraction, able to "clean" the samples free of ionic interferences from Na^+ and Cl^-, for example). The ability of the apparatus to actually retrieve suitable sample material appears demonstrated by the iron and manganese profiles.

5.3.2 *Pore Water Fe and Mn Discussion*

The pore water profiles obtained from two deployments of the chambered gel device have been analysed for dissolved iron and manganese species. The role of these elements in the microbial decomposition of organic carbon has already been detailed, and the solid phase distributions measured within all sediment cores retrieved from Hythe Marsh implicate the involvement of Fe and Mn within the salt marsh sedimentary carbon cycle (Section 5.2). However, there appear to be different conditions prevalent within the cores which result in the non-uniform behaviour of these metals between sites. The two sampling areas chosen for the pore water extractions in the field (Probe #1 and Probe #2) correspond to the locations of sediment cores HySR5 and HySR3, respectively. The behaviour of iron differs considerably within these two areas of the marsh, with core HySR3 lacking the upper highly oxidised section evident in the other sediment profiles.

5.3.2.1 *Iron profiles*

The distribution of solid phase iron within Hythe Marsh reveals the presence of oxic, sub-oxic and sulphidic diagenetic zones within the uppermost few decimetres of salt marsh sediment. Both the oxic and sulphidic chemical environments represent a sink for dissolved iron through the respective formation of relatively insoluble oxyhydroxide and sulphide phases. The sub-oxic zone on the other hand ought to constitute a source of Fe^{2+} to the sediment pore waters as ferric phases are buried and incorporated into the biochemical reaction scheme of anaerobic microorganisms (Froelich *et al* 1979). Additional dissolution of solid ferric species may be brought about via complexation by organic ligands (Luther *et al* 1992). This is often accompanied by reduction of the ferric iron to Fe (II) either by the organic molecules themselves or by the reaction of these complexes with dissolved or solid phase reduced sulphur compounds. The iron sourced into the interstitial waters is able to diffuse away from the site of dissolution and may reprecipitate in either the oxic or sulphidic diagenetic zones to form ferric or ferrous iron minerals, respectively. Dissolved iron may alternatively be consumed within oxidising microenvironments juxtapositioned close to zones of reduction (Thamdrup *et al* 1994). The concentration profiles of Fe^{2+} measured following use of the thin-film sampler and two deployments of the chambered device, each in a different area of the marsh, reveal similar characteristics to one another (Figure 5.7) although some important differences are evident which may be attributed to the oxidation status of the sediments.

5.3.2.1(a) *Thin-film sampler*

The greatest concentrations of dissolved Fe^{2+} found at the location of core HyPb coincide with the depth interval over which the solid phase iron abundance is at background levels (Figure 5.7). The dissolution of ferric phases buried into the suboxic zone and the oxidative removal of reduced iron minerals formed within reducing microenvironments at these depths are responsible for the maintenance of elevated porewater concentrations of Fe^{2+}. The sharp concentration gradient over 22-26 cm depth implies the rapid removal of porewater iron following upward diffusion into more oxic sediments. Downcore of the concentration maximum Fe^{2+} persists in solution to greater than 60 cm depth indicating either the slower precipitation of sulphidic minerals as opposed to oxyhydroxides or the regeneration of porewater iron through oxidation reactions. Since this area of the marsh is close to the cliff bordering the mudflat it is likely to be inundated periodically by oxygenated waters which may remove a portion of the reduced mineral phases at depth and thus source iron into solution.

5.3.2.1(b) *Probe #1*

The first deployment of the chambered device, denoted as Probe #1, was at the location of core HySR5 towards the rear of Hythe Marsh. In this sediment core there is a clearly-defined surficial zone of iron oxidation and precipitation, extending to a depth of about 6 - 7 cm, which is characterised by an elevated solid phase iron content (Figure 5.7). The persistence of ferric iron phases within this section of the sediment profile is maintained by the deposition of Fe^{III}-bearing particles on the sediment surface and also, presumably, by the upward migration and oxidative precipitation of ferrous cations from the underlying sub-oxic sediments. Pore water studies reveal that dissolved iron concentrations are relatively low (<8 ppm) within the upper part of this oxidised zone as a result of the precipitation of ferric oxyhydroxide minerals. Downcore the solubilised iron concentration increases steadily to a maximum value of ~110 ppm at 11-12 cm depth, just beneath the zone of oxidised iron enrichment and near to the top of the presumed sub-oxic zone. Indeed, much of the depth interval where solubilised iron is concentrated (predominantly over the 5-20 cm depth interval) conforms to depths at which there is relatively little excess iron in the solid phase on account of its reductive dissolution.

5.3.2.1(c) *Probe #2*

The site from which core HySR3 was retrieved displays a rather different distribution of iron within the solid phase, there being no significant enrichment of ferric iron within the upper decimetre of this core. The effect of the relative underdevelopment of this oxidised surficial sediment layer is observable in the distribution of dissolved iron throughout the sediment prism (Figure 5.7). Of chief interest in this respect is the fact that the dissolved concentration does not fall to zero within the surface layers but is maintained at a finite value by the reduction of ferric phases at very shallow depth. This supports the previous postulate that much of this sediment core is either sub-oxic or sulphidic in character, and is subjected to a reduced amount of oxygenation compared to the other cores. This aspect is explored further below during consideration of the behaviour of manganese within these sediments.

5.3.2.1(d) *Depletion of Fe^{2+} at depth*

The onset of sulphidic conditions at depth within each sediment core is marked by the accumulation of significant quantities of both iron and sulphur into the solid phase (Figures 5.3 and 5.7). Within cores HySR3 and HySR5 this change in diagenetic zonation begins respectively at approximately 34 and 24 cm depth, although the maximum enrichment of both Fe and S within the sediments is located slightly downcore. With increasing depth through the lowermost portion of the sub-oxic zone the pore water concentration of Fe^{2+} declines steadily. However, it maintains a finite value (typically < 25 ppm) throughout the upper section of these sulphidic sediments rather than falling rapidly to near zero, as might be expected. This implies that removal of iron from solution is not accomplished completely at the interface between the sub-oxic and the sulphidic zones, and Fe-complexes are able to penetrate further downcore before forming iron-sulphide minerals. At depth within this sulphidic environment (typically about 15 cm below the onset of Fe and S enrichment) the pore water concentration of iron falls to almost zero implying the complete removal of reduced iron from the aqueous phase.

Sulphate reduction is likely to take place at a variable rate throughout much of the sediment profile in reducing micro-environments and ought to be greatest following the depletion of more favorable electron acceptors such as $Mn^{IV/III}$ and Fe^{III} (Howarth and Teal 1979). Removal of Fe^{2+} from solution will occur wherever reduced sulphur compounds and dissolved ferrous iron encounter one another, although the complete removal of $Fe^{2+}_{(aq)}$ requires a sufficiently large flux of the former species. In Hythe Marsh the lower sections of the iron concentration profiles are concave, implying the removal of Fe^{2+} over a considerable part of the lower depth

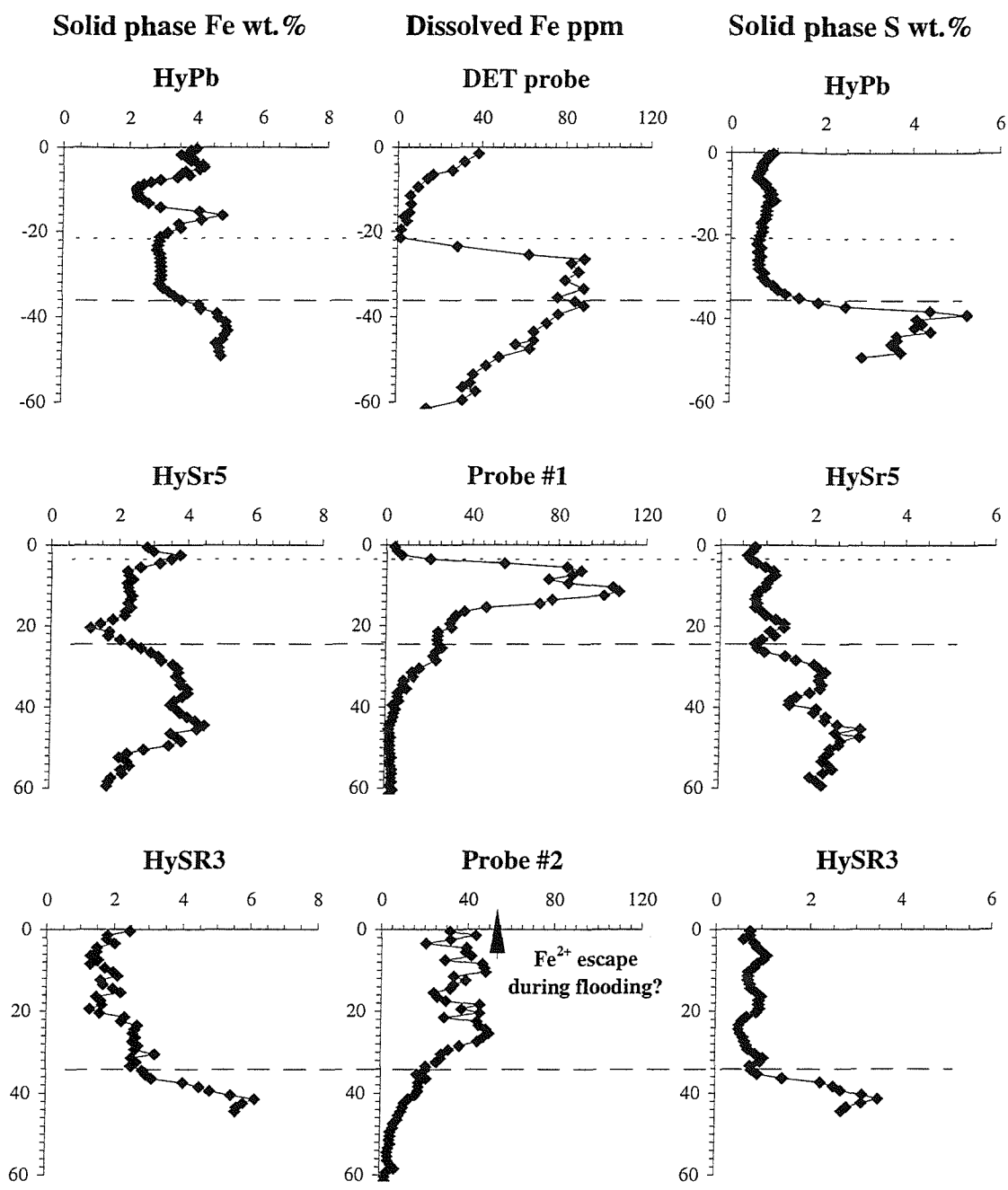

Figure 5.7:
Relationship between pore water iron and solid phase iron and sulphur at three core locations. Horizontal lines mark the approximate location of inferred oxic/suboxic (short dash) and suboxic/sulphidic (long dash) diagenetic boundaries.

range due to the upward diffusion of sulphidic species. Complete depletion is not effected, however, until greater depth within the sulphidic diagenetic zone.

5.3.2.2 *Manganese profiles*

The behaviour of manganese within Hythe Marsh, as revealed by the solid phase distribution of this element, appears dictated by the deposition and authigenic precipitation of Mn-oxides at the sediment surface. Following further burial these minerals are reduced through a variety of reaction schemes, some involving catalysis by microorganisms (Froelich *et al* 1979). Removal of oxidised manganese is completed over the surface decimetre within the low marsh cores HyPb and HySR2, but more rapidly (over 0-4 cm depth) in the case of cores HySR3 and HySR5 (Figure 5.3).

5.3.2.2(a) *Probe #1*

The Mn concentration profile obtained from probe #1 consists of a sharp increase from 80 ppb at the surface to a maximum of ~ 350 ppb, located at 5-6 cm depth, beneath which the dissolved Mn load decreases downcore (Figure 5.8). Over 40-60 cm depth the concentration is consistently low. The iron and manganese concentration profiles exhibit similar trends, although over different depth intervals. The reduction of Mn-oxide phases occurs at a higher redox potential than does the reduction of ferric iron minerals and consequently is expected to take place at shallower depths in sediments overlain by oxygenated conditions (Froelich *et al* 1979). The peak manganese concentration revealed by probe #2 (5-6 cm depth) coincides with samples exhibiting a steep Fe^{2+} concentration gradient, situated above the main Fe^{2+} maximum at 11-12 cm depth. The interaction between oxidised and reduced forms of both iron and manganese is known to involve several possible reactions which may occur spontaneously without microbial mediation (Van der Weijden 1992). Autocatalytic reactions may occur between the pairs Fe^{III}/Fe^{II} and $Mn^{IV/III}/Mn^{II}$, in addition to many reactions involving sulphur compounds (Luther *et al* 1992). The depletion of these reduced metal ions within the surface sediments is not therefore simply a case of oxidation by O_2. The oxidation of Fe^{2+} by Mn-oxides, according to Equation 5.8, can significantly inhibit the upward passage of ferrous cations within sediments (Van Cappellen and Wang 1995). The coincident depletion of Fe^{2+} and enrichment of Mn^{2+} in the interstitial waters at 5-7 cm depth revealed by probe #1 may be produced by this reaction. The variability of pore water manganese profiles in response to their reduction by Fe^{2+} is enhanced by the high relative abundance, supplied by an upward diffusional flux, of the latter species in solution.

Core HySR5 exhibits enriched (oxidised) manganese within the solid phase over a depth of 0-3 cm, coincident with the almost complete removal of iron from the aqueous phase. Manganese, however, is detectable in the pore waters at the salt marsh surface. A portion of this Mn^{2+} load is presumably derived from the dissolution of Mn-oxides at these shallow depths, whilst the remainder is sourced from the sub-oxic sediments further downcore and persists in solution following its upward migration into the oxic zone. The likelihood of dissolved manganese species being able to diffuse through oxic sediments is greater than for iron due to the faster oxidation kinetics of Fe^{2+} compared to Mn^{2+} (Zwolsman *et al* 1993). Other mechanisms which could result in Mn dissolution at these shallow depths (in reducing micro-environments) include reaction with NH_4^+ (Equation 5.3), H_2S (Equation 5.9) and microbially-mediated reduction (Table 5.1; Equation 2).

5.3.2.2(b) *Probe #2*

The most striking feature of the manganese profiles is the magnitude of concentration variation between the two probe deployments (Figure 5.8). The solutions obtained from probe #2 (diluted by a factor of ten from pore water concentration prior to analysis) contained dissolved Mn at levels of less than 5 ppb, only marginally higher than the ~1 ppb detection limit of the ICP-AES equipment. The profile obtained with probe #2 shows considerable apparent scatter and reveals the relative absence of manganese from these pore waters as compared to the other sampling area. This significant difference in pore water composition must be related to the oxidation status of the sediments in this area of the marsh. Previous discussion has considered the distribution of iron in both the solid and aqueous phases to suggest the persistence of predominantly sub-oxic conditions throughout much of the sediment prism at this location, and the absence of a well-developed oxic surface layer. It appears that this situation may enable ferrous iron in solution to diffuse across the sediment-water interface during tidal inundation, since the pore water concentration remains relatively high (~ 30 ppm Fe) at the surface. Due to the slower oxidation kinetics of Mn it seems likely that this element may also be able to escape from the sediment prism. Factors governing the oxidation status of the sediments at any given location are many, but are likely to be influenced to a large extent by the degree of diffusion of O_2 into the sediment prism, the amount of oxidisable organic matter present and the activity of the overlying plant population as well as the sub-surface microbial population. The solid and aqueous phase distributions of iron and manganese within core HySR3 and probe #2 are complementary in that they suggest a consistent pattern of extensive metal oxide reduction within the sediments, accompanied by the loss of solubilised species due to diffusion.

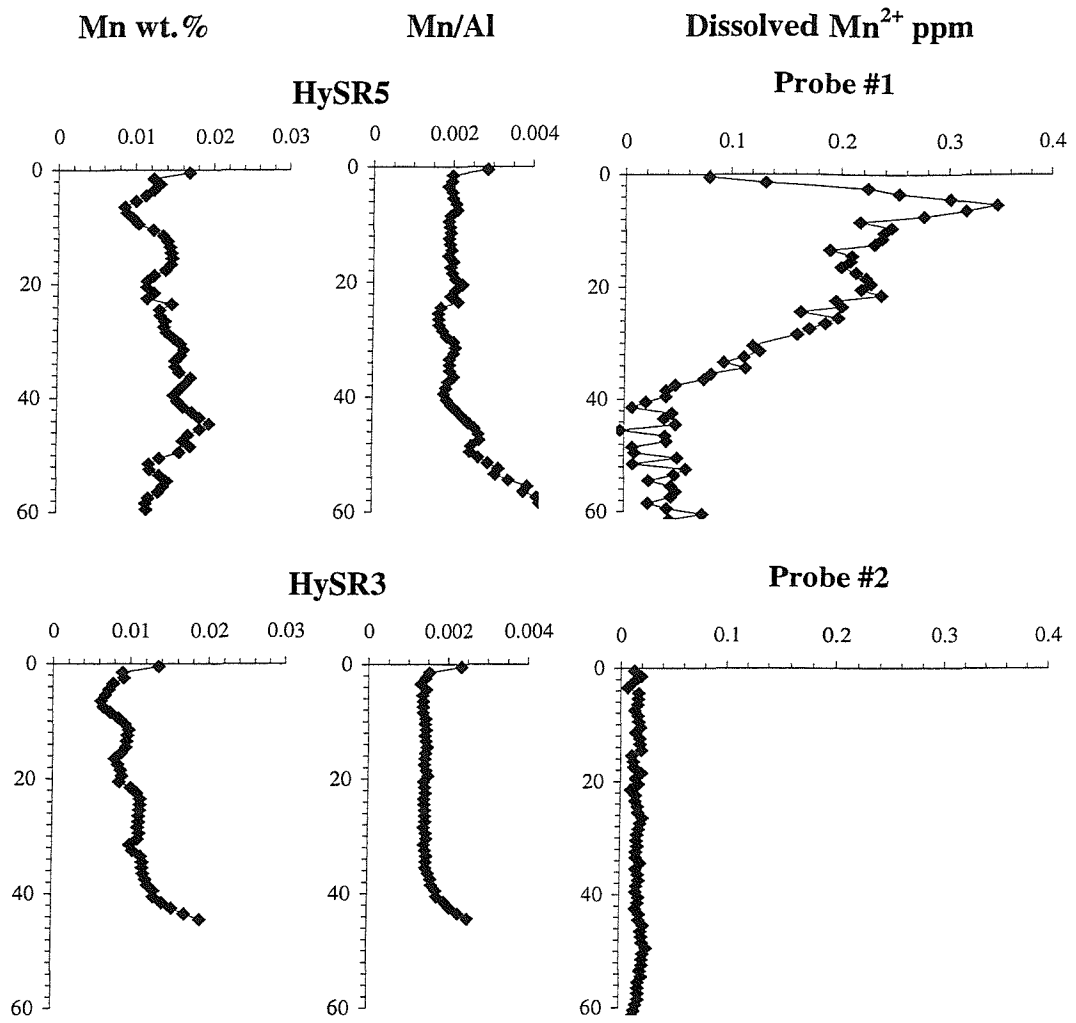

Figure 5.8:
Relationship between solid phase and pore water manganese at two core locations.

5.4 Diagenetic zonation

From the above analysis of the salt marsh cores it may be concluded that, despite the heterogeneity of the sediment matrix creating apparent excursions from the ideal situation, some definite chemical zonation of the pathway for the degradation of organic matter is exhibited by these sediments. It must be remembered, however, that the mutual exclusion of the respective chemical reactions into specific vertical zones of the sediment prism is not to be expected since small-scale variations in composition may create adjacent micro-niches with differing redox characteristics.

5.4.1 *Oxic zone*

The introduction of oxidants (particularly O_2) down through the surface results in the precipitation of oxyhydroxide mineral-phases to yield brown upper sediments. These oxic sediments typically contain high levels of both iron and manganese, often with abundant roots. The oxidative capacity of salt marsh plant roots has been described in several previous studies (e.g. Boulegue *et al* 1982; Luther *et al* 1982; Luther and Church 1988) and is known to have a seasonal dependence. Manganese tends to be most concentrated in the upper portion of the zone of iron enrichment, as observed in other salt marsh systems (Zwolsman *et al* 1993). This arises from the fact that microbial reduction of manganese precedes iron reduction. The onset of more reducing conditions at the base of the oxic zone is frequently associated with an increased content of organic matter within the sediment. There appears, therefore, to be a balance between the enhanced oxidative capacity of the root-rich sediments and the increased reduction brought about by the presence of elevated levels of organic detritus within the sediment, and this may be expected to display seasonal variability.

5.4.2 *Sub-oxic zone*

At some near-surface depth (cm to dm) the depletion of oxygen by organic decay results in the bacterial utilisation of both Fe^{III} and Mn^{IV} phases as electron acceptors. The abundance of these elements in the sediment typically declines sharply to constant levels, defining the sub-oxic zone, which may persist for several decimetres downcore. Throughout this zone the dissolution of oxidised iron and manganese mineral phases provides a source of dissolved metal ions to the pore water which may fuel the precipitation of oxides in the layers above and sulphides at depth. The persistence of orange grain coatings within these sediments (as visually evident in HyPb and HySR2) however, suggests that the precipitation of oxides can occur locally within

the zone of reduction, perhaps related to periods of tidal inundation or the presence of oxidising micro-environments or even discrete sedimentary horizons (as with HyPb). Oxidative loss of both Fe^{II} and Mn^{II} may also be brought about by autocatalytic reactions involving oxidised Fe^{III} and $Mn^{IV/III}$ mineral phases.

5.4.3 *Sulphidic zone*

All four cores exhibit a pronounced accumulation of iron and sulphur (also manganese, though to a lesser extent) throughout the basal section, which typically commences at about 25 to 35 cm depth. These enrichments denote areas within the sediment where the decomposition of organic materials via sulphate reduction generates significant dissolved sulphide species and results in mineral precipitation. The molar ratios of iron and sulphur, as calculated from the XRF data, suggest that the dominant stoichiometry present is FeS_2. Long-term storage of iron and sulphur in the most thermodynamically stable form, pyrite, rather than as iron monosulphides, has been demonstrated to take place in the organic-rich marshes of the U.S. (Howarth 1979; Howarth and Teal 1979; Luther *et al* 1982; Lord and Church 1983; Luther and Church 1988) as well as in many other marine sediments (Berner 1970) and can now also be identified within these shallow minerogenic marshes.

Chapter Six

Trace Elements

6.1 Trace elements in salt marshes

6.1.1 *Rationale for the present study*

Trace element cycling in natural systems is the focus of much research at the present time, motivated by the significant impact of anthropogenic activities on the cycling of many metals within the hydrosphere (Salomons and Förstner 1984) and the potential ecotoxicological effects this may have (Calmano and Förstner 1996). Estuaries, in particular, have long been the focus for human industrial activities and hence diluted and dispersed contaminants discharged into the nearshore environment. As a result, estuarine sediments are often significantly contaminated with anthropogenically-derived element loadings (Williams *et al* 1994).

The study of trace element distributions, particularly those of metals, within salt marshes may be carried out in an attempt to elucidate the temporal variability in the flux of elements to the sediment prism (e.g. McCaffrey and Thomson 1980; Allen and Rae 1986; Zwolsman *et al* 1993). Post-depositional processes, resulting in the redistribution of elements and thus preventing the preservation of an historical record within sediment sequences (Ridgway and Price 1987), are also worthy of investigation since they are important controls on the fate and bioavailability of these important constituents. There is a shortage of detailed information regarding the distribution and behaviour of trace elements in the salt marshes of the Solent region (Cundy 1994), an estuarine system otherwise extensively studied (e.g. Tubbs 1980) due to its unique geographical nature. The present study addresses some aspects of this issue through the detailed analysis of geochemical properties within several salt marsh cores from Hythe Marsh, Southampton Water.

6.1.2 *Sources of trace elements to salt marshes*

Through strong binding within mineral lattices much of the elemental load delivered from the catchment area is unreactive during transportation and early diagenesis. The dominant reactive trace element fraction within many hydrological systems is derived from anthropogenic discharges, with the released elements partitioning amongst the main carrier phases present in the aqueous environment (Table 6.1). The role played by these secondary phases, for example through complexation by organic materials and adsorption to clay mineral and metal oxide surfaces, is highly significant and may dictate the geochemical behaviour of many trace elements (Salomans and Förstner 1984). These phases themselves occur in a variety of forms and the environmental partitioning of a given element has been found to be strongly dependent

on the prevalent physico-chemical conditions, most notably pH and Eh (Bendell-Young and Harvey 1992). The interaction and exchange of metals between different chemical species is a continuous process throughout the cycle of transportation and deposition as the components respond to changing conditions within a variety of physically and chemically distinct environments (atmosphere, river, estuary, sedimentary deposit, and so on).

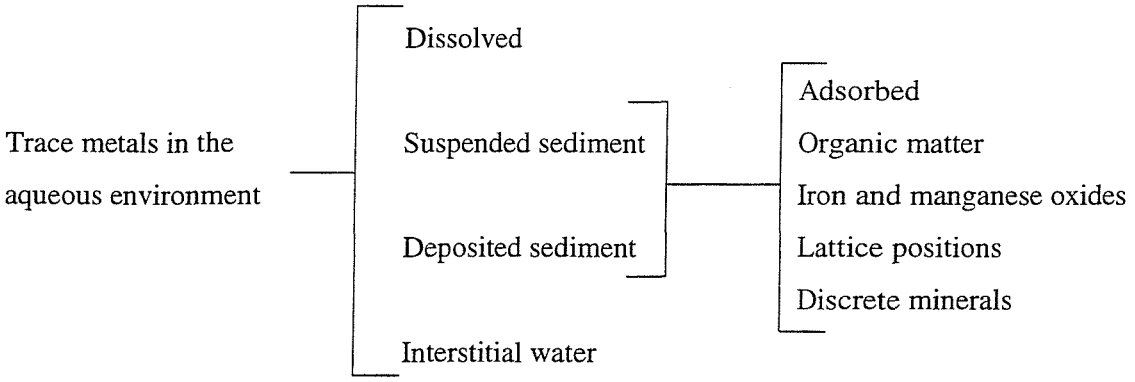

Table 6.1:

Speciation of trace metals in the aqueous environment.

The suspended material within estuarine waters is known to scavenge trace metals effectively through binding to mineral surfaces and reactive particle coatings (Salomans and Förstner 1984). Consequently, the incorporation of these elements into the sediment prism of a salt marsh often reflects the deposition of fine-grained materials during the tidal high water stand (Stumpf 1983). Other elements (especially Br and I) are dominantly sourced from sea water and may be added to the sediments during tidal inundation followed by uptake into the solid phase or persistence in pore waters. For some elements deposition from the atmosphere during sub-aerial exposure may represent the most significant route into salt marsh sediments. Lead in the urban environment is often derived predominantly from exhaust emissions (Dörr *et al* 1991; Sugden *et al* 1993) and this atmospheric source may contribute directly to the lead loading of salt marsh sediments (Williams *et al* 1994). Obviously the hydrodynamic regime operative across a given marsh and the proximity of different sources for individual elements show high regional variability and thus make it difficult to compare contaminant levels from separate areas. Indeed, differences in the nature of the sedimentary material and related physico-chemical parameters often reduce the ability to compare sediment metal loadings even from within the same marsh (Williams *et al* 1994).

6.1.3 *Post-depositional modification of trace element profiles*

The sediments and pore waters constituting salt marsh environments are subjected to a high intensity of early diagenetic processes, driven by the decomposition of organic matter (Howarth and Teal 1979; Lord and Church 1983). This results in the zonation of geochemical redox conditions and affects the distribution of major sedimentary components such as Fe and Mn oxyhydroxides, iron sulphides, and organic materials. Each of these secondary phases is known to have the potential to scavenge trace metals under suitable conditions (Shaw *et al* 1990). Following incorporation into the sediment body, therefore, whether through the deposition of particulate materials or via precipitative and adsorptive mechanisms sequestering elements directly from solution, trace components may also be subjected to redistribution as a consequence of the changing physico-chemical conditions throughout the sediment profile (Santschi *et al* 1990). The formation of primary trace element mineral phases (e.g. zinc sulphide) does not usually exert significant control on trace element distributions compared to their associations with other sedimentary phases, such as pyrite (Ridgway and Price 1987; Shaw *et al* 1990). This often results in a difficulty in assigning individual adsorption processes to particular components in complex systems in which clay minerals, pyrite, metal oxyhydroxides, and organic matter, either as particles or coatings, compete as substrates for trace element adsorption (Tessier *et al* 1996).

6.1.4 *Sources and sinks during early diagenesis*

The redistribution of elements within sediment sequences involves dissolution, diffusive transport and precipitative processes that deplete and enrich different sedimentary phases according to kinetic and thermodynamic requirements. Minor components may be supplied to pore waters during the dissolution of carrier phases or alternatively be introduced during the percolation of flood waters through the sediment prism (Williams *et al* 1994). During the microbial decomposition of metabolisable organic matter, for example, trace elements associated with the organic materials are likely to be released into pore waters. The reductive dissolution of ferric and manganese oxide carrier phases, as they react in the sub-oxic diagenetic zone (Froelich *et al* 1979), may also supply the dissolved trace metal load (Shaw *et al* 1990).

The solubilised species undergo diffusive transport within the sediment profile, migrating along concentration gradients, to zones where they are incorporated once more into the solid phase (Li and Gregory 1974). Such sinks may arise due to a variety of interactions between dissolved and solid constituents involving mechanisms of adsorption, complexation and co-precipitation. The flooding and subsequent drainage of waters within a salt marsh acts as a tidal pump, introducing and redistributing dissolved constituents. The most important phases governing trace metal behaviour in salt marshes are outlined below:

6.1.4.1 Metal oxides

The cycling of iron across oxic/sub-oxic boundaries involves its reductive dissolution and oxidative precipitation (Froelich *et al* 1979). Several studies in recent years have demonstrated that arsenic and phosphorus, in particular, can become coupled with the sedimentary recycling of iron and reveal similar distributions to this carrier phase in continental shelf sediments (Thomson *et al* 1995), estuaries (Maher 1985; Peterson and Carpenter 1986) and freshwater lakes (Carignan and Fleet 1981; Farmer and Lovell 1986; Belzile and Tessier 1990). The reasons for this coupling may be attributed to the complexation of dissolved arsenate (Maher 1985; Peterson and Carpenter 1986) and phosphate (Carignan and Fleet 1981) species by the positively charged surfaces of the oxyhydroxides, for example via:

$$FeOH_2^+ + AsO_3^- \text{ or } H_2PO_4^- \longrightarrow FeOAs(\text{or P})O(OH)_2 \qquad \textbf{Equation 6.1}$$

The elements bound by this process will be released to the pore water when the substrate is subjected to reductive dissolution during burial. Ferric oxyhydroxides precipitating within the upper sediments are then likely to readsorb dissolved arsenate and phosphate as they migrate upward out of the post-oxic zone. Other trace elements, such as zinc, nickel, lead, copper, and cadmium are also known to associate with hydrous ferric oxide phases through processes of adsorption and coprecipitation (Lee 1975; Tessier *et al* 1985; Johnson 1986; Bendell-Young and Harvey 1992; Tessier *et al* 1996).

Manganese oxides have considerable capacity to act as substrates for the adsorption of a wide range of trace metals, since divalent iron, cobalt, nickel, zinc and cadmium, as well as Pb^{4+}, are easily accomodated within the Mn-oxide lattice (Hem 1978). The concentrations of these and other metal ions in natural waters may therefore be controlled by sorption processes on to Mn-oxide surfaces (Shaw *et al* 1990). In salt marsh systems the active cycling of Mn-oxides in the

surface layers has been shown to control aspects of the distribution of Zn, Ni, Co and Cd (Zwolsman *et al* 1993).

6.1.4.2 Metal sulphides

The formation of insoluble metal sulphide phases can control the solubility of many metals in anoxic sediment systems where sulphide ions are generated (Suess 1979; Skei *et al* 1988). The thermodynamically stable mineral forms of zinc, lead and nickel sulphide are predicted to form in anoxic salt marsh sediments (Luther *et al* 1980) although direct evidence for this is rarely obtained. Estuarine sediments have, however, been found to contain framboids of mixed zinc and iron sulphide minerals, as well as revealing the incorporation of nickel into pyrite (Luther *et al* 1980).The scavenging ability of iron sulphides for several trace metals has been shown to be great (Jean and Bancroft 1986), sedimentary pyrite being an important sink for a number of trace metals, especially As, Mo and Ni (Belzille and Lebel 1986; Huerta-Diaz and Morse 1992; Morse 1994; Wallman *et al* 1996). Downcore variations in the geochemical behaviour of arsenic, zinc and copper have been reported by Moore *et al* (1988), involving a clear shift in the partitioning of all three elements into sulphidic phases at depth within the reducing sediments, as compared to association with organic and oxide phases in the oxic upper layers.

6.1.4.3 Organic materials

The control of trace metal distribution by the abundance and nature of organic materials, in both dissolved and particulate forms, may be effected through a variety of mechanisms. The remineralisation of organic matter is the driving force behind early diagenetic change (Santschi *et al* 1990) and the reactions involved in this overall process dominate the chemistry of shallow sediments and pore waters, thus affecting all components within the system. Additionally, organic materials affect trace elements directly through their strong binding capacity for metal ions (e.g. Swanson *et al* 1966; Rashid and King 1969; Picard and Felbeck Jnr. 1976; Bendell-Young and Harvey 1992; Tessier *et al* 1996; Luther *et al* 1992).

The organic component of recent marine sediments is dominated by humic substances (Rashid 1985). The process of humification, beginning with carbohydrates, lipids, proteins, lignins, and other organic molecules, involves a series of microbially-mediated reactions, and produces complex polymers with molecular weights ranging from a few hundred to several hundred thousands (Rashid and King 1969). The degree of humification of such materials is usually positively correlated with their metal absorption capacity due to the increasing concentration of reactive functional groups. These are responsible for the interaction of humates not only with trace metals, but also with clay mineral surfaces (Picard and Felbeck Jnr. 1976) and ferric oxyhydroxides (Tipping 1981; Bendell-Young and Harvey 1992; Tessier *et al* 1996). The three dominant mechanisms underlying the association of metals with humic substances, whether in dissolved, colloidal or particulate form, are outlined below (after Rashid 1985). The solubility, migration and redistribution of metal ions within sediment sequences are significantly influenced by these reactions:

- *Physical adsorption:* arising from weak van der Waals forces or electrostatic attraction. The cations in such sites are easily replaced, though alternatively may migrate to other sites within the organic molecule.
- *Cation exchange:* the replacement of hydrogen ions within the organic molecule by metallic cations (dominant H^+ loss is from carboxyl and phenolic hydroxyl groups). The degree of exchange tends to increase with increasing pH due to greater ionisation of the functional groups.
- *Chelation and complexing reactions:* resulting in the firm bonding of metals through electron transfer and the formation of organo-metallic ring complexes.

6.1.4.3(a) Organic metal enrichment

The enrichment of metals within humic fractions is reported to be considerable (Swanson *et al* 1966; Rashid and Leonard 1973) but is a complex process subject to external control by the physico-chemical environment. Humic materials may operate to sequester metals into the solid phase through direct association with particulate organics or through the flocculation of dissolved and colloidal complexes (Bendell-Young and Harvey 1992; Tessier *et al* 1996). On the other hand the dissolved humic pool may enhance metal dissolution through the formation of stable dissolved organo-metallic complexes, considerably increasing metal solubility (Rashid and Leonard 1973). The accumulation of metals in sediments has generally been found to be greater in those areas enriched with organic matter (Rashid and Leonard 1973; Rashid 1985). A number of geochemical studies performed on salt marsh environments have revealed significant

correlations between sediment organic loading and concentrations of Pb, Cu, Zn, Ni and Cd (Guerzoni *et al* 1984; Di Giulio and Scanlon 1985; Allen *et al* 1990; Caçador *et al* 1996).

6.1.4.3(b) Organic enrichment of I and Br

The distribution of bromine and iodine within sediment sequences is often dictated by the abundance and nature of the organic fraction (Price and Calvert 1977). Marine organisms have been found to concentrate both of these elements to considerable levels, typically to around 200-300 ppm, and loading of these halogens usually correlates well with the organic content of nearshore and continental shelf sediments (Pedersen and Price 1980). The case for estuarine sediments is often more complex due to the dynamic nature of the redox environment and the influence of terrigenous organic materials (Malcolm and Price 1984). Published investigations of bromine and iodine distributions within salt marsh sediments are noticeably few.

Redox chemistry

The marine geochemistry of iodine involves both iodate and iodide species. In oxic and anoxic environments the IO_3^- and I^- species each have their respective dominance and the consequent geochemical changes may redistribute this element within sediments (Thomson *et al* 1995). The conversion of iodate to iodide (at pH 8.1) occurs at a pE of 10.5, just below that of nitrate reduction:

$$IO_3^- + 6H^+ + 6e^- \longleftrightarrow I^- + 3H_2O \qquad \textbf{Equation 6.2}$$

Iodine may therefore be used either as an electron acceptor or electron donor during microbial metabolic activity (Shimmield and Pedersen 1990). This may lead to a variable relationship between iodine concentration and organic carbon dependent on the oxidation status of the sediment (Price and Calvert 1977). Bromine, on the other hand, existing only with an oxidation state of -1, is not susceptible to redox-related speciation changes and therefore often conforms more closely to the pattern of organic carbon distribution.

Organic association

The mechanisms which bind both iodine and bromine to organic substrates are poorly understood, particularly in the case of the latter element, and may be several. Harvey (1980) used a series of extractions to conclude that bromine exists in a variety of water-soluble and organic-soluble forms within marine sediments. Experiments conducted by Francois (1987) show that humic substances can reduce iodate to electropositive species such as HOI and I_2 which then substitute on to the organic molecules. Organic materials did not take up significant iodine when exposed to iodide-bearing solutions (as found in the interstices of reducing sediments). Hypoiodous acid and I_2 may, however, be produced from iodide *via* oxidation by iodide oxidase, an enzyme present in the early degradation products of plankton (Price and Calvert 1977). The presence of free oxygen is required for this enzymatic reaction to proceed and the mechanism is thus thought to be absent under reducing conditions (Shimmield and Pedersen 1990). The reaction between IO_3^- and HS^- also yields HOI and I_2. Since the predominance of either I^- or IO_3^- depends on the oxidation condition of the waters then the enrichment of iodine within the organic fraction can be attributed to redox-controlled sorption processes (Shimmield and Pedersen 1990). These involve the generation of strong electrophiles either through enzymatic utilisation of O_2 and I^- or reactions involving IO_3^-, and are thus likely to occur at or near the sediment water interface (Francois 1987). Enrichment of iodine within oxic sediments as opposed to anoxic sediments has been frequently reported (Price and Calvert 1977; Upstill-Goddard and Elderfield 1988).

Halogen/C_{org} ratios

The ratio of halogen to organic carbon within surficial marine deposits is dependent on the nature of the organic matter and the oxidation status of the sediment. Marine organisms, particularly plankton, are known to concentrate both iodine and bromine to greater levels than either marine plants or terrestrial vegetation (Upstill-Goddard and Elderfield 1988). Malcolm and Price (1984) determined the efficiency of organic matter to sorb iodine in the presence of oxygen (no measurable iodine was sorbed by any of the organic materials under oxygen-free conditions) as being in the order: terrigenous floc << aged terrigenous floc < plankton << aged plankton. Since estuarine environments are characterised by the mixing of terrigenous and marine organic materials they often display lower halogen to organic carbon ratios than offshore sites. Large variations in Br/C_{org} are found between different geographical locations but the ratio at any given sample site is usually roughly constant, although this is not true of all estuaries (ten Haven *et al* 1988). Examples of typical I/C_{org} and Br/C_{org} values reported for nearshore and estuarine surficial sediments are presented in Table 6.2.

Location	I/C_{org}	Br/C_{org}	Reference
Barents Sea	380	120	Price *et al* (1970)
Namibian Shelf	20-250	40-130	Price and Calvert (1977)
Panama Basin	50-395	146	Pedersen and Price (1980)
Continental margins	265	131	Shimmield and Pedersen (1990)
Loch Etive estuary, U.K.	160	180	Malcolm and Price (1984)
Tamar estuary, U.K.	20-65	5-35	Upstill-Goddard and Elderfield (1988)
Hythe Marsh, U.K.	≤15	≤60	Present study

Table 6.2:

Typical reported values of iodine and bromine ratios to organic carbon in marine sediments. Units are (ppm halogen / wt.% organic carbon) x 10^{-4}.

The frequently-observed exponential decline of I/C_{org} with depth (e.g. Pedersen and Price 1980) is indicative of the preferential release of iodine during microbial decomposition. Sediment redox zonation may also influence the behaviour of iodine under suitable conditions and can decouple the relationship of I to Br and C_{org} (Thomson *et al* 1995). A less dramatic decline or even a slight increase in the Br/C_{org} ratio with depth appears typical of continental shelf and margin sediments (Price and Calvert 1977) revealing that bromine is more strongly bound to organic carbon than iodine. The persistence and further enrichment of bromine within the organic fraction at increased depth (e.g. Shimmield and Pedersen 1990) has been ascribed to a residual enrichment process by Mayer *et al* (1981) where loss of carbon occurs relative to bromine during degradation. This may be promoted by the bactericidal action of brominated compounds causing them to be concentrated within the refractory organic carbon pool (Flury and Papritz 1993). The release of both elements from organic materials may additionally result from their substitution by nucleophilic species such as thiosulphate or sulphide ions (François 1987).

6.1.5 *The reconstruction of historical depositional fluxes*

Provided that the degree of trace element mobility within a given sediment sequence is of minor consequence to the overall distribution of that particular element, the opportunity may arise to investigate the depth-concentration profile in terms of its temporal dependency (Goldberg 1976). Sediment layers at depth in the prism may retain the chemical composition inherited during their formation at the surface implying that certain element profiles may record variations in the depositional flux over time. Establishing a representative chronology for such a sequence permits resolution of the accumulative timescale and thus relates the depth-concentration profile to a temporal scale of reference. Reconstructions such as this may yield important information regarding anthropogenic discharges over previous decades or even centuries and also help to understand the consequences of recent pollution controls (Ravichandran *et al* 1995).

The fundamental requirement which must be fulfilled in order to achieve a meaningful historical interpretation is that of chemical and physical immobility of the elements under consideration (McCaffrey and Thomson 1980). As discussed above, this assumption is not always valid within diagenetically active sediment sequences, in which case an attempt to utilise the concentration profiles for such a purpose would yield misleading results. Successful applications of this technique, where the authors were satisfied that remobilisation processes were limited, can be found, for example, in Goldberg *et al* (1977), McCaffrey and Thomson (1980), Allen and Rae (1986), Valette-Silva (1993), Kerfoot *et al* (1994) and Ravichandran *et al* (1995).

6.2 Trace element results and calculations

The concentrations of As, Br, Cu, I, Ni, P, Pb and Zn have been determined along several short sediment cores from Hythe Marsh, Southampton Water (Figures 6.1 - 6.3). The analysis of these components by XRF yields bulk concentration data in $\mu g\ g^{-1}$ of dry sediment.

6.2.1 *Excess concentrations*

The fraction of each element which is occupying lattice positions in the detrital mineral portion of the sediment has been calculated according to Equation 3.2 and subtracted from the total to yield the excess concentration, denoted with an asterisk. Note that the total element concentration used for those elements with significant potential input from saline waters (I and Br) is the salinity corrected value. This has been determined in the same manner as for major elements (Equation 3.1).

6.2.2 *Inventories*

The inventory of any element within a sediment core may be derived from the expression:

$$I = \Sigma_0^i C_i \cdot \rho_i \cdot t_i$$

Equation 6.3

where I is the inventory ($\mu g\ cm^{-2}$),
C_i is the element concentration at depth i ($\mu g\ g^{-1}$),
ρ_i is the sample density ($g\ cm^{-3}$),
and t_i is the sample thickness (cm).

The inventories calculated using this expression for different elements within each of the four sediment cores reveal several distinct patterns of variation across the marsh (Figure 6.4). These patterns may be compared to the physical sedimentary characteristics (density, total accumulated mass) and other inventories (those of ^{137}Cs, ^{210}Pb and Al) in order to interpret the observed variations (see later discussion).

6.2.3 *Flux calculations*

The data may be used to calculate the initial flux of a particular element to the marsh surface over the period represented by the accumulation of the sediment prism. In the absence of early diagenetic redistribution the derived flux allows the identification of variations in the deposition of different species. Calculation of the flux is obtained from:

$$F_i = C_i \cdot s \cdot \rho_i$$

Equation 6.4

where F_i is the flux at depth i ($\mu g\ cm^{-2}\ yr^{-1}$),
C_i is the concentration ($\mu g\ g^{-1}$),
s is the mean sedimentation rate ($cm\ yr^{-1}$),
and ρ_i is the sediment density ($g\ cm^{-3}$).

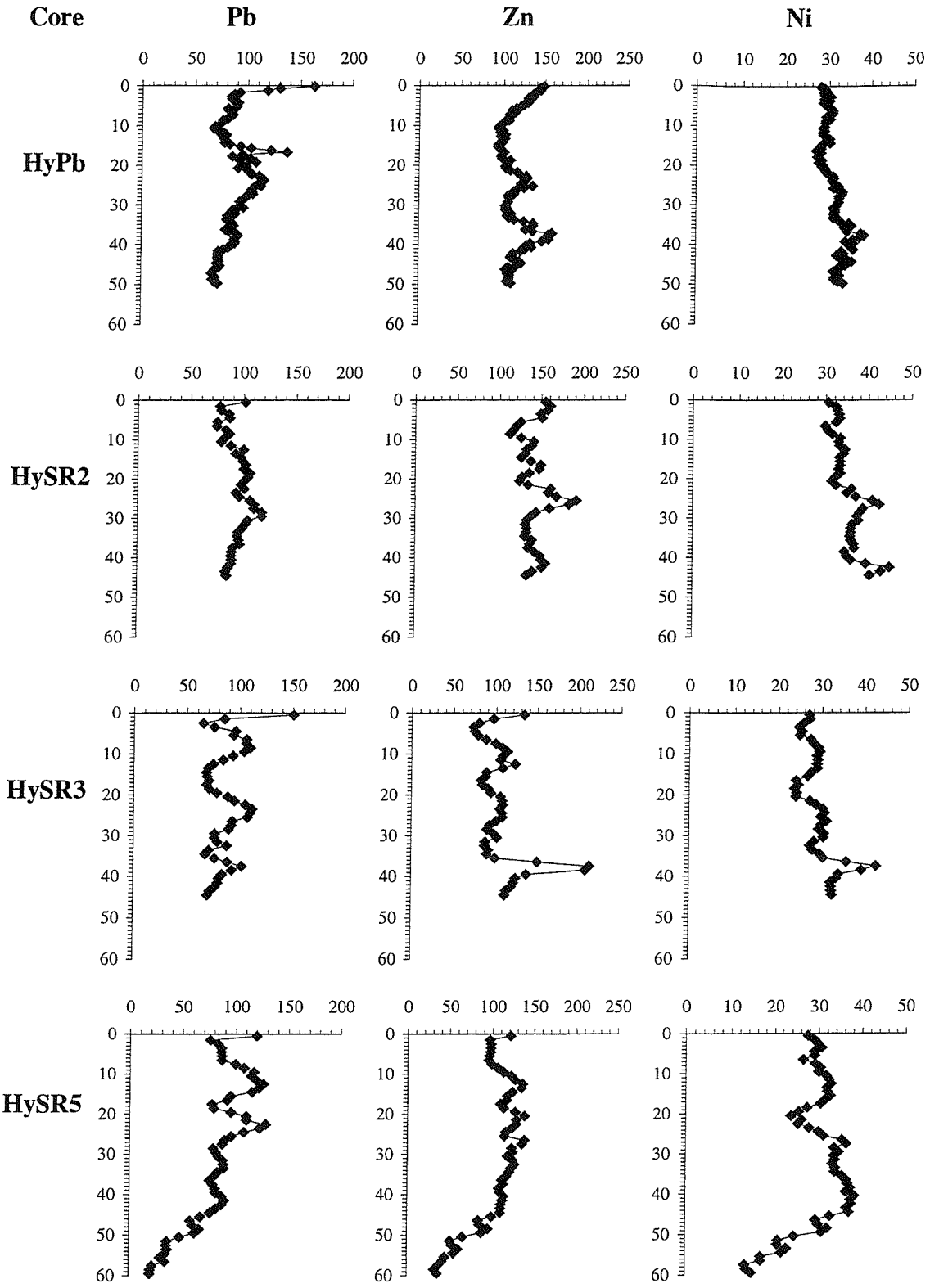

Figure 6.1 (a):
Depth-concentration profiles (total element load) of lead, zinc and nickel.

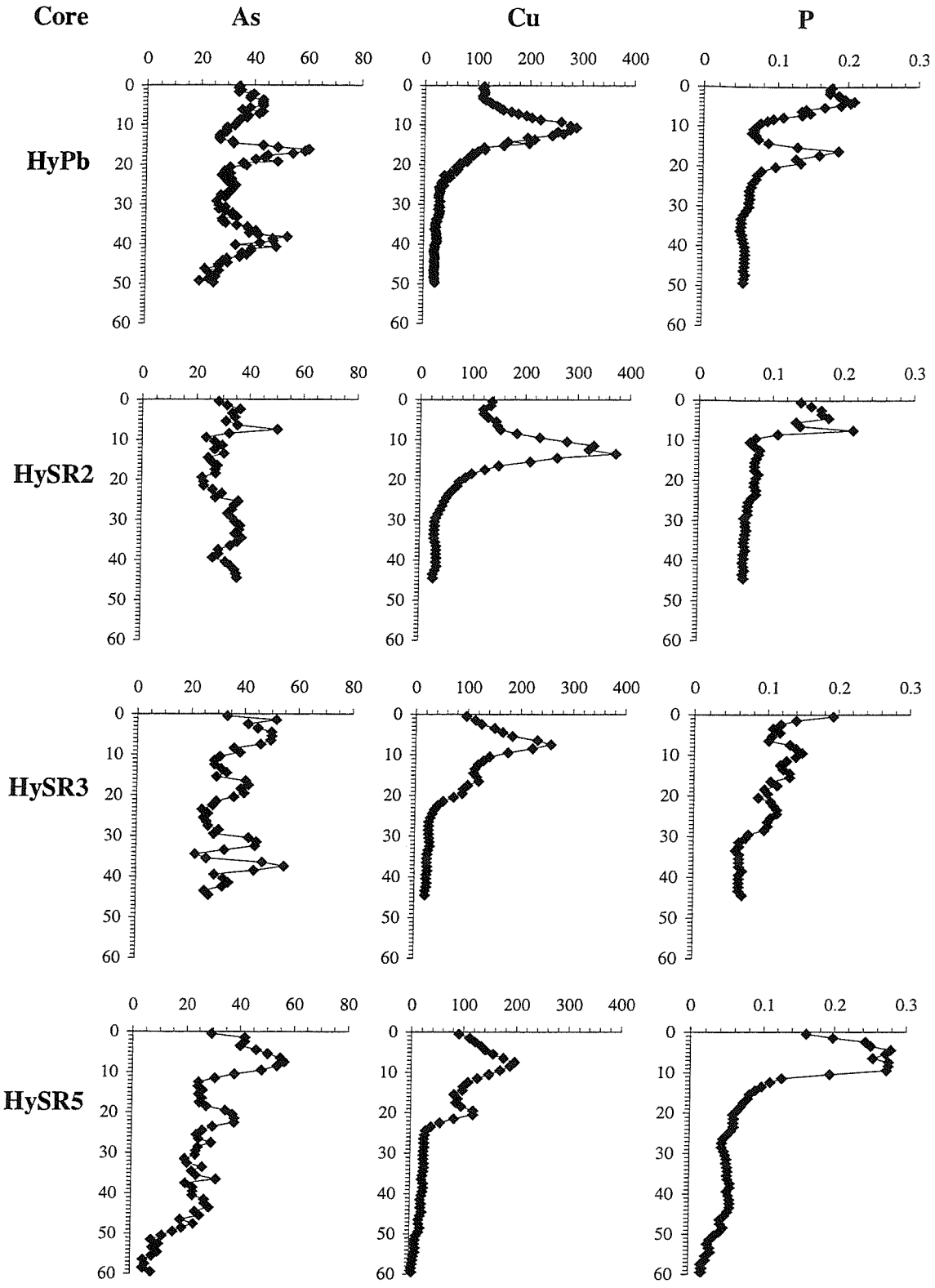

Figure 6.1 (b):
Depth-concentration profiles (total element load) of arsenic, copper and phosphorous.

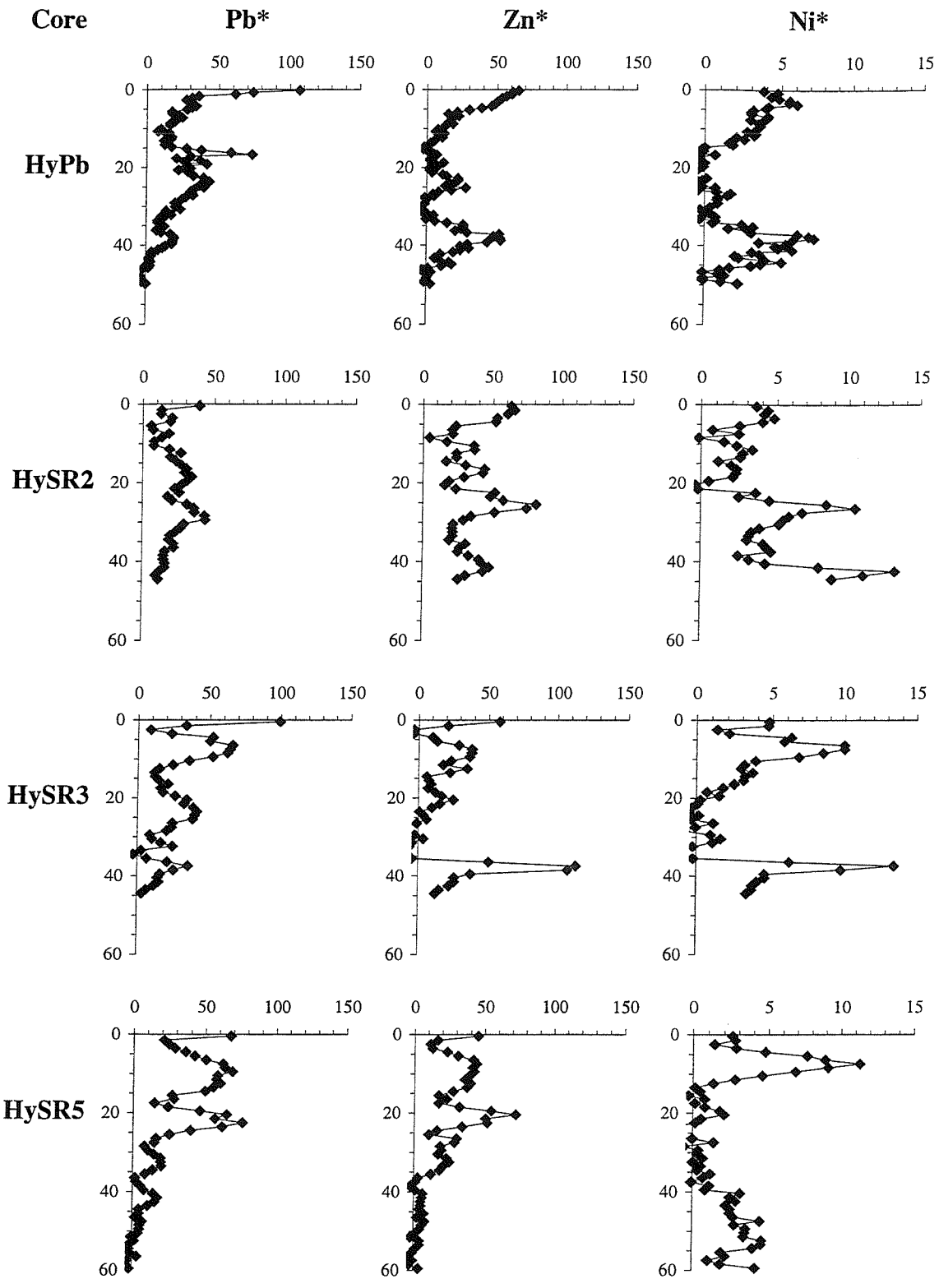

Figure 6.2 (a):
Depth-concentration profiles (excess element load) of lead, zinc and nickel.

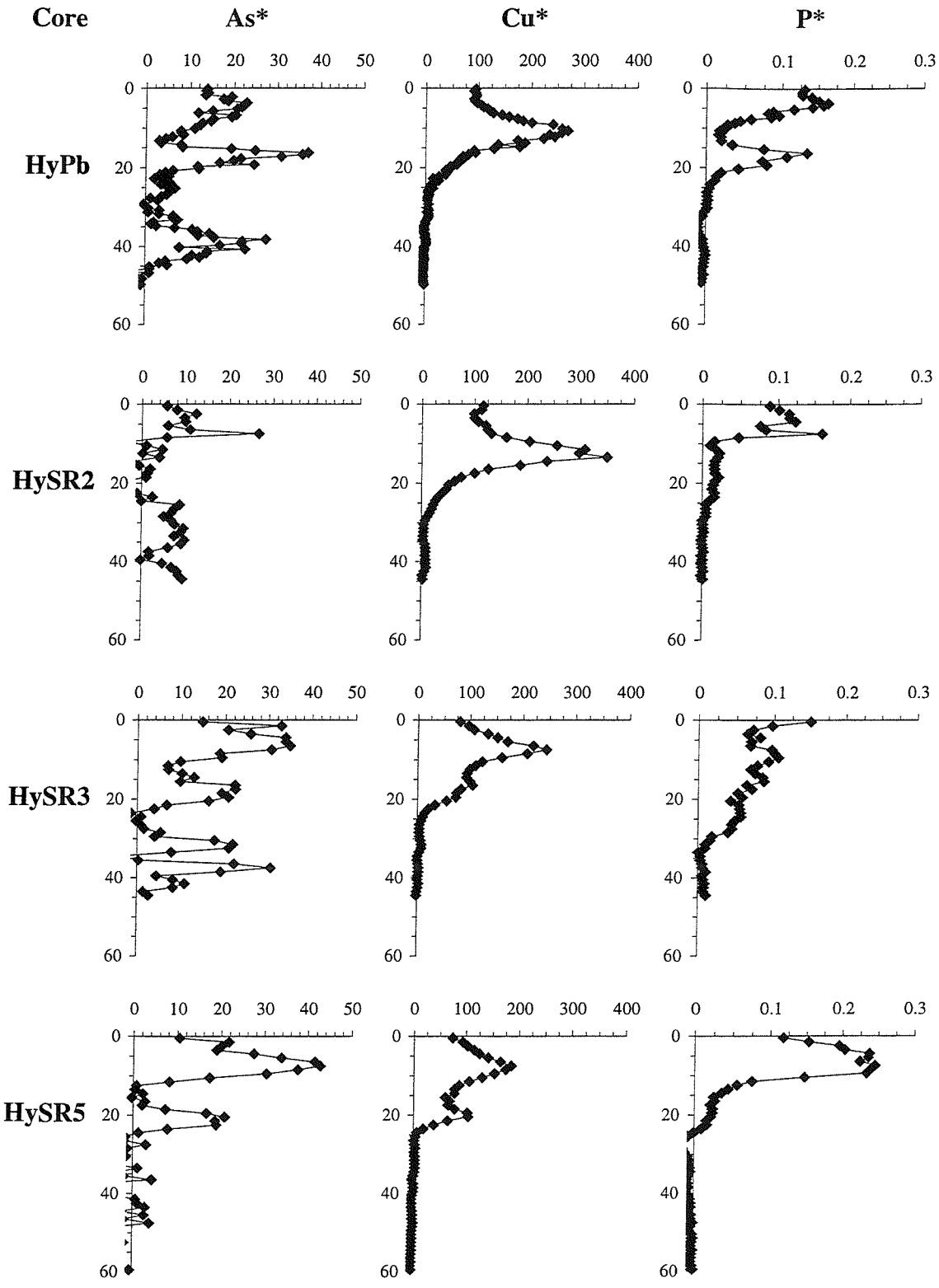

Figure 6.2 (b):
Depth-concentration profiles (excess element load) of arsenic, copper and phosphorous.

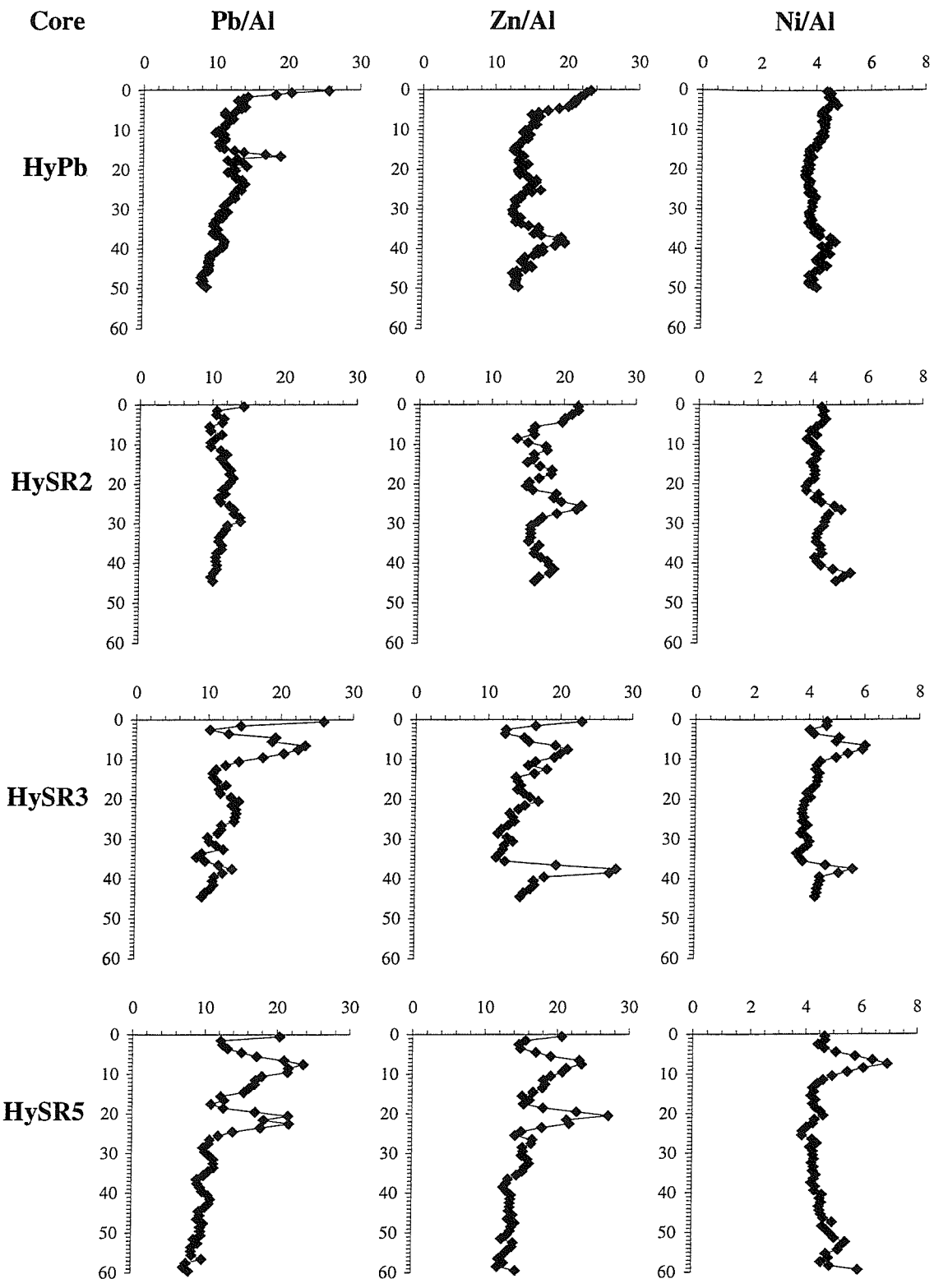

Figure 6.3 (a):
Depth-concentration profiles (normalised to aluminium) of lead, zinc and nickel.

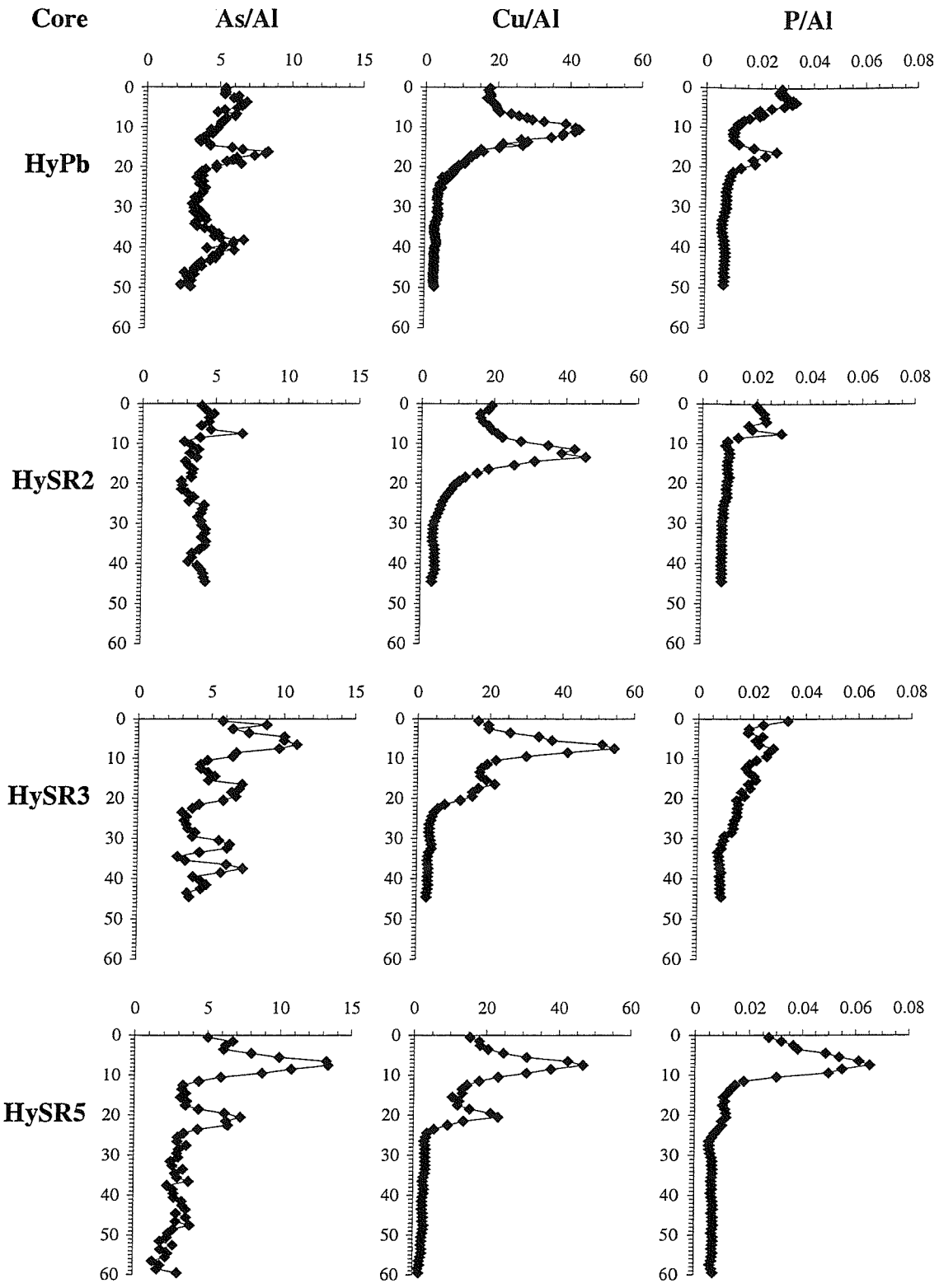

Figure 6.3 (b):
Depth-concentration profiles (normalised to aluminium) of arsenic, copper and phosphorous.

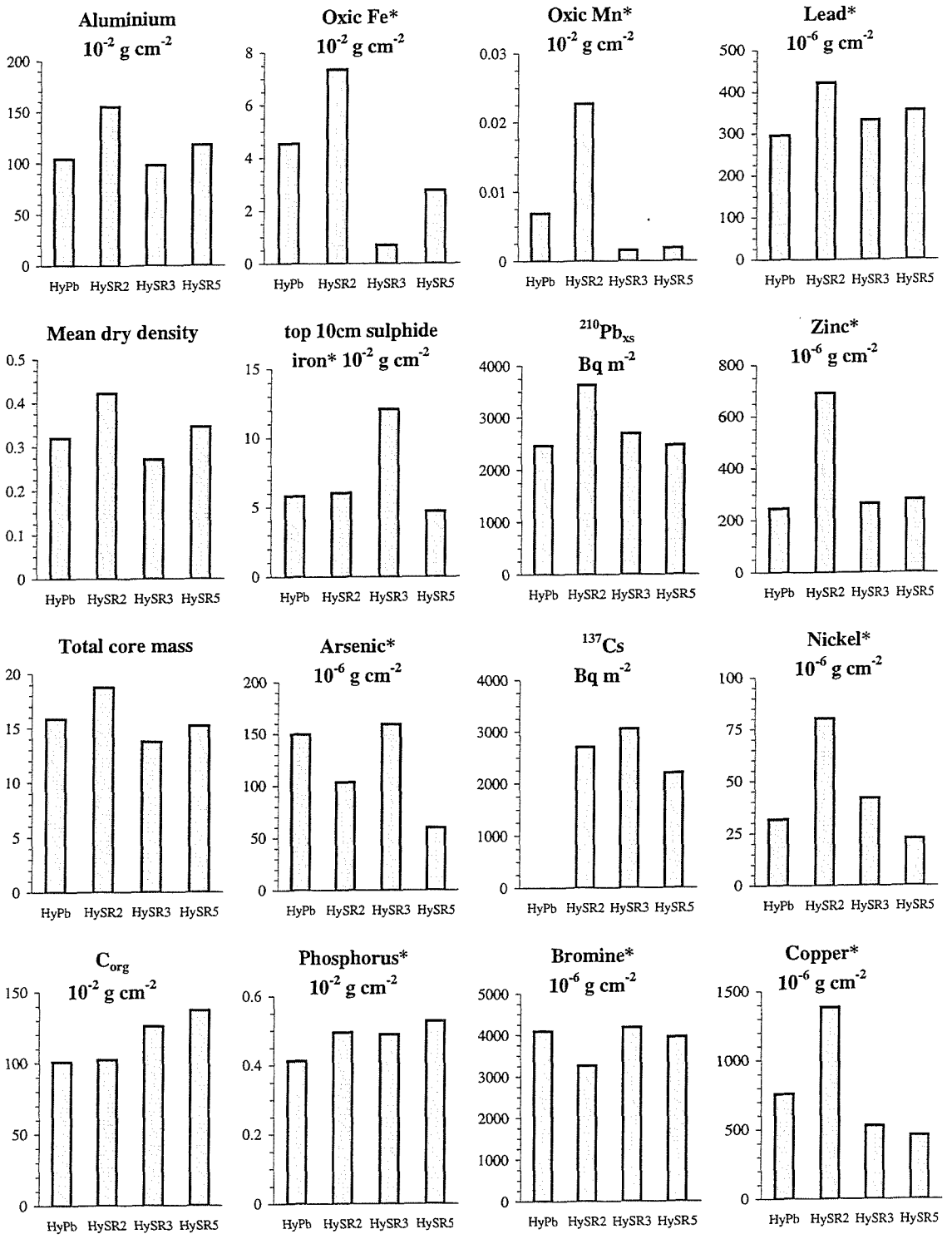

Figure 6.4:
Inventories of elements in the 0-45 cm depth interval of each sediment core;
* denotes excess element inventory.

6.3 Trace element distributions within Hythe Marsh

The distinctive geomorphology of a salt marsh is the result of an equilibrium between depositional and erosive processes (Pethick 1992). The introduction of particulate material is the main route through which most elements accumulate within the sediment prism, arriving in association with a variety of carrier phases. Intertidal sediments of this nature are known to be a predominant sink for particle reactive species, particularly trace metals, although they need not necessarily represent a permanent reservoir. Instances of metal release from such sediments are not unknown (e.g. Zwolsman *et al* 1993) and result from changes in metal speciation during burial. The fact that many trace elements are scavenged from natural waters by metal oxides, organic coatings, clay particles and other surfaces and that these constituents are subsequently involved in early diagenetic processes within sediments results in trace element phase transitions following deposition (Shaw *et al* 1990). Pore water profiles of species are therefore useful to help determine diagenetic pathways, although in this study such data are limited for minor components despite significant efforts made in this respect. Much of the information regarding trace elements is therefore restricted to the solid phase, this being more relevant to the eventual rate of burial of the chemical constituents.

A number of studies into the fate of trace elements in intertidal sediments have concluded that remobilisation occurs on a widespread scale (Ridgway and Price 1987). This may be sufficient to remove the record of deposition within sediment sequences, and furthermore may result in the potential loss of a portion of the elemental load from the sediments. The analyses carried out on the sediment cores retrieved from Hythe Marsh allow the distribution of many trace elements, in terms of their concentration-depth profiles, to be described. The processes which have resulted in the observed patterns may, in many cases, be inferred from comparison of the trace element distributions with those of known important carrier phases, along with knowledge of their likely patterns of geochemical behaviour.

6.3.1 *Diagenetic remobilisation*

The presence of hydrous oxides of iron and manganese, sulphidic mineral phases and particulate organic materials, each being extensively recycled within the salt marsh environment, exerts an influence upon many minor components of the system causing their concentration profiles to become uncoupled from the depositional history. This effect is neither the same for each element nor uniform across the marsh due to differences in the geochemical behaviour of elements and sedimentary constituents between cores.

The correlations observed between trace metal enrichments and the abundance of the secondary carrier phases appears sufficient evidence to implicate the mechanisms resulting in remobilisation and enrichment of particular species within certain horizons. The main factors responsible for concentrating trace elements have already been disclosed and these are now discussed in turn in relation to the trace element distributions they appear to influence.

6.3.2 *Association with oxide phases*

6.3.2.1 Ferric oxyhydroxides

The formation of hydrated ferric oxyhydroxides within the upper decimetre of Hythe Marsh has been considered previously (Chapter 5). These mineral phases are continuously cycled within the surficial sediments as subsequent layers are buried and become exposed to reducing conditions. A number of features of the concentration profiles obtained for Fe, As and P reveal intimate association of these elements in Hythe Marsh (Figure 6.5 and Figure 6.6). This is most prominent when considering the upper 25 cm of core HyPb and the upper 10 cm of core HySR2, involving the transition between oxic and sub-oxic sediments.

6.3.2.1(a) Cores HyPb and HySR2

Both arsenic and phosphorous are implicated in a variety of biological processes, and are known to be cycled similarly in near-shore marine environments (Sanders 1980). The reductive dissolution of solid phase iron, upon burial to sufficient depth within sediment sequences, also releases any adsorbed As and P to the pore waters. All three species are then free to diffuse throughout the sediment prism to sites where precipitation or readsorption into the solid phase can take place. Alternatively, in the absence of a capture mechanism, loss from the sediment prism could occur. In the oxic upper layers of Hythe Marsh the formation of authigenic ferric iron minerals is of considerable significance and appears to concentrate both As and P following their release within the post-oxic zone of the sediment prism. The depths at which ferric iron minerals are deemed to be actively precipitating (core HyPb 0-10 cm and 14-22 cm; HySR2 0-10 cm) are also enriched with arsenic and phosphorous. The elevated concentration of both of these elements, coincident with solid phase iron, apparent at 8 cm depth in core HySR2 indicates the considerable upward migration of dissolved species from the lower, more reducing, zones of the sediment before being readsorbed at the oxic/sub-oxic boundary (also reported for Loch Lomond sediments by Farmer and Lovell 1986). The extent to which

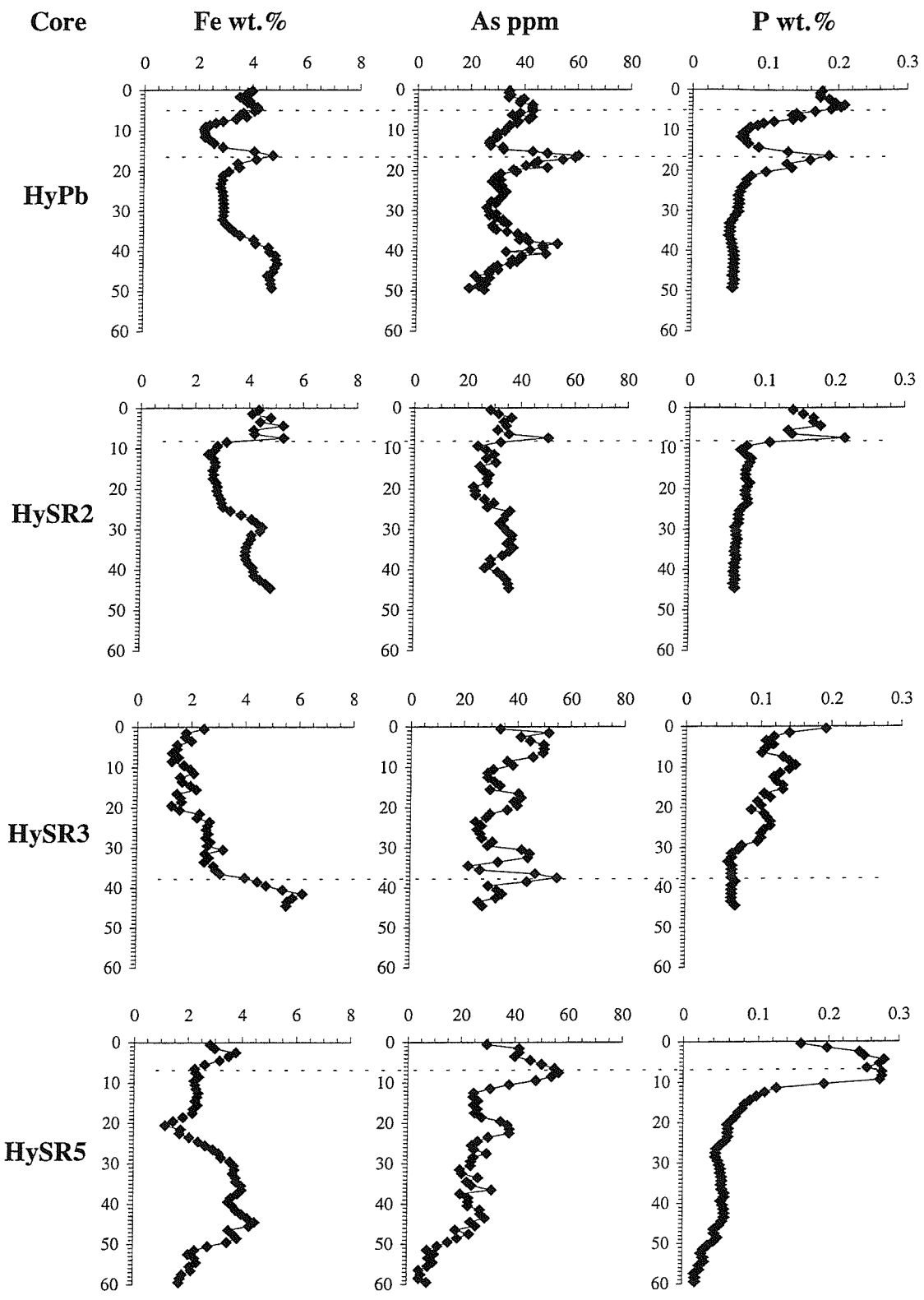

Figure 6.5:
Horizontal correlations between Fe, As and P.

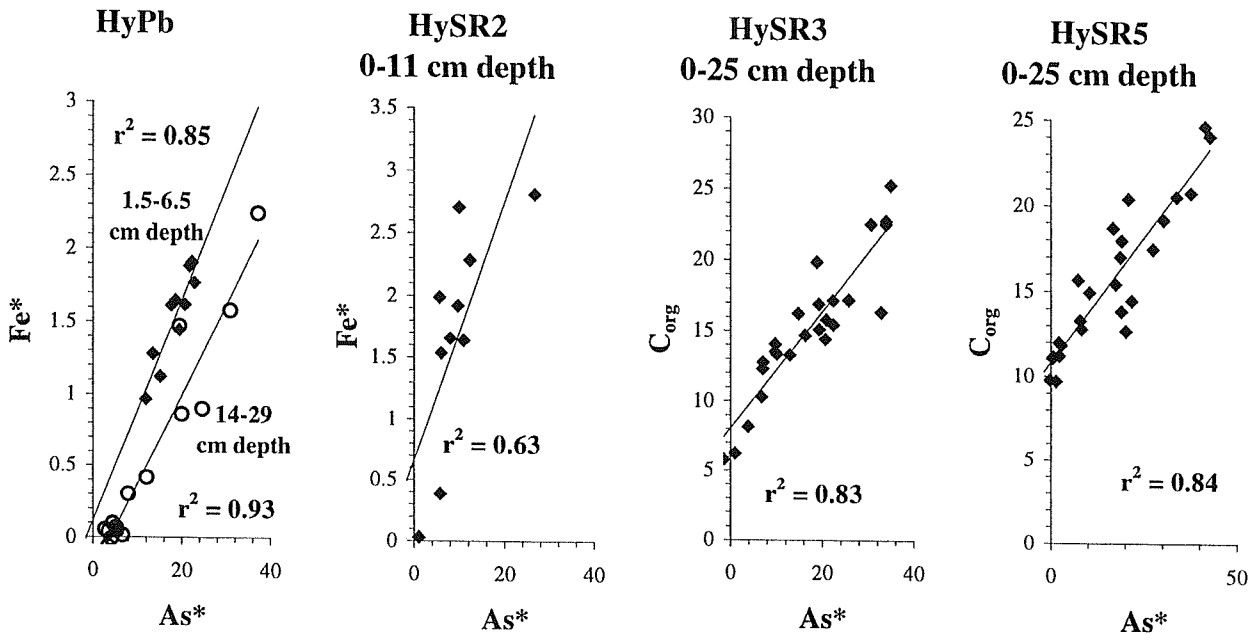

Figure 6.6:

Correlation of excess arsenic with Fe* (cores HyPb and HySR2) and C_{org} (HySR3 and HySR5).

historical deposition records may be smeared or even totally removed by such remobilisation processes appears severe (Widerlund and Ingri 1995).

6.3.2.1(b) Cores HySr3 and HySR5

In core HySR3 the abundance of oxidised iron is depleted relative to the other cores and does not allow the identification of a distinct oxic to post-oxic boundary, although the brownish colour of the sediments implies the presence of at least periodically oxidising conditions down to a depth of 23 cm (Lyle 1983; Zwolsman *et al* 1993). The persistence of minor amounts of ferric iron mineralisation throughout this core section is implied by the colour of the sediments and this is thought to be responsible for the observed phosphorous distribution. At the same depth (33 cm) as sulphide mineralisation commences the excess P concentration falls to zero, supporting the argument that it is the presence of oxidised iron phases which sequester phosphorous within the bulk of the core (Maher 1985).

The control over P within core HySR5 is similar to cores HyPb and HySR2, since the enrichment of phosphorous is confined to that oxic upper section of the core clearly also abundant in solid phase ferric iron (extending to a depth of 12 cm). The distribution of arsenic, on the other hand, within both HySR3 and HySR5 bears a lesser degree of resemblance to that of phosphorous than is the case for the other cores. Sub-surface peaks in the excess concentration of arsenic are apparent within HySR3 and HySR5 which are coincident with the organic-rich root horizons (see Figure 6.6). Within the middle and rear sections of the salt marsh, where the organic carbon content increases considerably, the role of hydrous ferric oxides in regulating the distribution of arsenic appears to be secondary to complexation by the organic material itself. Maher (1985) similarly found the amount of organically-bound arsenic to increase with an increasing organic content of the sediments; this is discussed further below.

6.3.2.2 Manganese oxides

In all cores studied the diagenetic cycling of manganese within the surficial sediments is evident from the solid phase profiles. The distributions of lead, zinc and, to a lesser extent nickel, in the upper few cm of each core (with the exception of HySR2) approximately mimic those observed for manganese (Figures 6.1-6.3). The excess concentrations of both lead and zinc show considerable correlation (r^2 = 0.90 and 0.79, respectively) to excess manganese throughout the zone of Mn-oxide enrichment within core HyPb (Figure 6.7). There can be little doubt that the distribution of manganese within these surficial sediments is governed by the

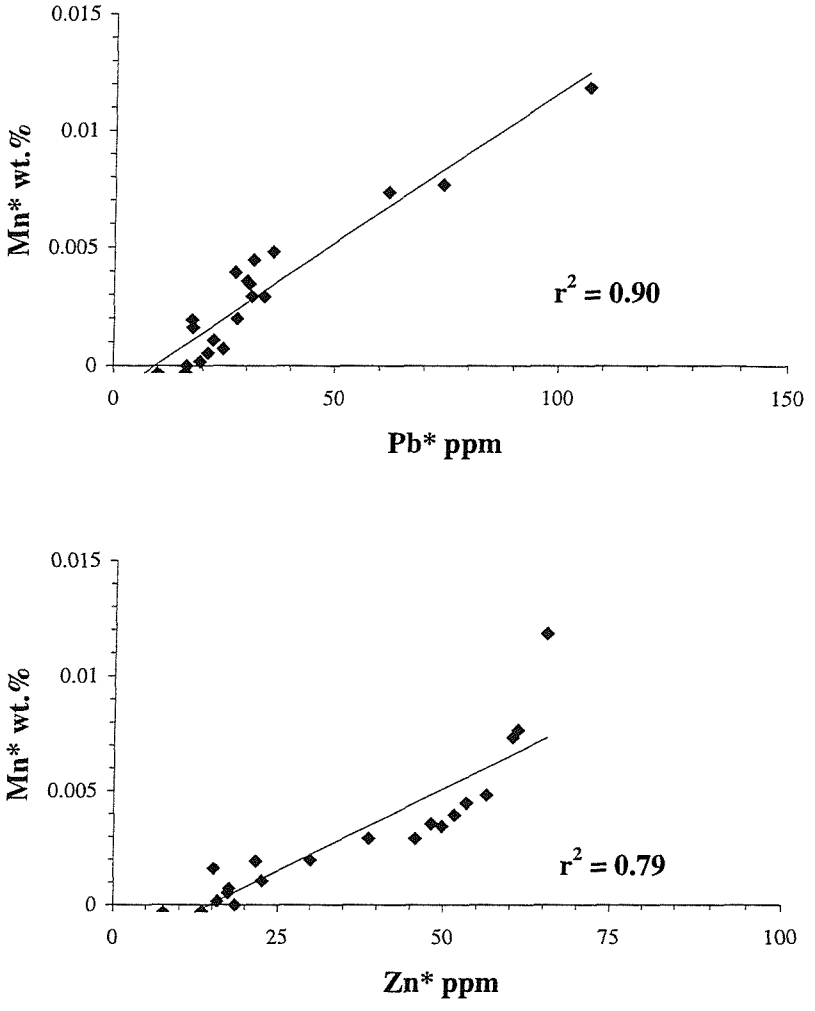

Figure 6.7:
Correlation between manganese and the trace metals lead and zinc within the surficial 10 cm (zone of Mn-oxide enrichment) of core HyPb.

diagenetic cycling of this element along the redox gradient (Froelich *et al* 1979; Santschi *et al* 1990) leading to the conclusion that both Pb and Zn in the surface zone of Hythe Marsh are subjected to similar redistributive processes. In core HySR2 (also exhibiting a decimetre scale surficial zone of Mn enrichment) the distribution of both Pb and Zn is somewhat decoupled from that of manganese, perhaps due to the competition for adsorption sites by ferric oxides. Cores HySR3 and HySR5 contain relatively little Mn-oxide material and this phase therefore plays a reduced role in governing the trace metal distribution. Surficial (1-2 cm depth) enrichments of the metals Pb, Zn and Ni within these two cores may signify adsorption onto Mn-oxide surfaces, or alternatively simply reflect the liberation of dissolved trace metal species following burial to shallow depth and the subsequent degradation of various carrier phases.

In riverine and estuarine waters the suspended particulate material actively scavenges many trace metals (Salomans and Förstner 1984) and it is therefore probable that both lead and zinc arrive at the surface of the marsh in association with the solid phase. In order to be implicated in the redox cycle of manganese, then, both of these metals must become solubilised at some point after deposition. This is most likely to occur through the reduction of metal oxide carrier phases or the decomposition of complexing organic materials during intense early diagenesis. Shaw *et al* (1990) report the release of a number of transition metals into the surficial pore waters of sediment sequences as a result of the degradation of particles which have scavenged metals from the water column. Once the ions have become associated with the Mn-oxide in the surficial sediments they will be released to the pore waters during microbial reduction (along with Mn^{2+}) and may be readsorbed during oxidative precipitation of the manganese (Williams 1993). Similar remobilisation of these trace metals in surficial salt marsh sediments has been reported by Zwolsman *et al* (1993). Whether a portion of either of these metals is lost from the sediment prism during this diagenetic cycling cannot be assessed from the data available, although pore water profiles of iron and manganese suggest that such loss may occur in core HySR3.

6.3.3 *Association with sulphidic phases*

The concentration profiles obtained during the present study indicate that As, Ni, Zn and Pb are all enriched to a variable degree within those sediments containing elevated levels of reduced iron and sulphur. The interpretation of these peaks as probable diagenetic features rather than as resulting from variations in the depositional flux is based on the known association of trace metals with sulphide minerals in certain depositional environments and the apparent lack of a consistent depositional record, as preserved in the different sediment cores from Hythe Marsh.

The abrupt increase in excess element concentration, particularly evident for Ni and Zn at 36 cm depth in core HySR3, is more plausibly explained when considering the shift in the redox condition of the sediment than by abrupt variations in the supply of these elements to the marsh surface over time.

6.3.3.1 Arsenic

The enrichment of arsenic into the solid phase, forming peaks which indirectly indicate the association of this element with sulphide mineralisation, is evident in cores HyPb (35 - 45 cm depth), HySr2 (25 - 40 cm) and HySR3 (35 - 45 cm). The arsenic concentration profiles within the sediments of Hythe Marsh reveal the significant control exerted by the nature of the sedimentary material on the distribution of this labile element. Each of the three peaks detailed above has, as its upper limit, the depth at which iron sulphide mineralisation commences in the sediment core (as observed by Wallman *et al* 1996). Furthermore, the arsenic enrichment appears to reach a maximum slightly above the peak in iron suggesting that the former element is migrating downcore before partitioning into the solid phase. A clear shift in the partitioning of arsenic from association with metal oxide and organic phases in the upper (oxidising) zones into sulphidic phases at depth has been reported by Moore *et al* (1988). In that study, arsenate was found to dominate the pore waters of the oxic zone, whereas arsenite was most abundant in the reduced zone of the sediments. A strong relationship between pyrite iron and arsenic has also been reported by Belzille and Lebel (1986).

6.3.3.2 Nickel and Zinc

The distributions of nickel and zinc in the sediments are similar in all cores analysed (Figures 6.1-6.3). These elements are apparently associated with the cycling of manganese in the upper sediments, as discussed above, and at depth within each core (except HySR5) appear to respond to the onset of sulphide-generating conditions through association with the solid phase. An attempt was made in the present study to investigate the elemental composition of the sedimentary pyrite framboids using backscatter electron microscopy, although this failed to provide evidence of any significant trace metal association, possibly as a result of insufficient detection limits. The evidence for sulphide mineralisation of these elements, therefore, is restricted to that obtained indirectly from comparison of the solid phase profiles of iron, sulphur and the respective trace elements. The incorporation of these elements within authigenic sulphidic phases has been observed in other studies of reducing sediments through

the application of a variety of techniques, including sequential extraction schemes and electron backscatter analysis (Luther *et al* 1980; Moore *et al* 1988; Skei *et al* 1988)

6.3.3.3 Lead

The extent to which lead has partitioned into the sulphidic phase is less than for the other trace elements considered so far (Figures 6.1-6.3). Minor peaks are observable in cores HyPb and HySR3 (at depths of approximately 35-40 cm in each case) which are lesser features of the overall concentration profiles. In core HySR2, however, the Pb maximum measured at approximately 30 cm depth is the most enriched section of the core, apparently due to association with iron sulphides forming at these depths (Jean and Bancroft 1986; Huerta-Diaz and Morse 1992). A more complete discussion of the overall behaviour of lead within Hythe Marsh is given during consideration of its isotopic composition (Chapter 7).

6.3.4 *Association with organic materials*

The middle and high marsh cores, HySR3 and HySR5, contain a high proportion of particulate organic material as a result of the increased vegetative productivity of these areas and the reduced export of detritus by ebbing waters (Figure 3.4). The decomposition of the root system of the marsh plants is an important source of organic carbon to the sub-surface microbial communities (Gardner *et al* 1988) and is known to yield fulvic and humic acids within the sediments (Pellenbarg and Church 1978). As a consequence of the dominance of organic materials, both living and dead tissue, the sediments are composed of a lesser amount of minerogenic sediment. Not only the sediment matrix is unique in these root-rich zones, however, since the redox environment is considerably altered (compared to less vegetated sites) by the decay of the organic fraction.

The control on the sedimentary cycling of trace metals exerted by the rate and mechanism of organic decomposition is believed to be considerable (Lord and Church 1983), and humic substances play a significant role in this due to their predominance within the sediment column and high surface activity (Rashid 1985). This may be further enhanced in salt marshes by the formation of a diagenetically stable pool of organic-thiol complexes following the reaction of sedimentary organic matter with dissolved sulphide (Ferdelman *et al* 1991). These sulphur-bearing functional groups have been shown to form complexes with uranium (Church *et al* 1996) and are believed to exert a major control on the cycling of many metallic species within salt marshes (Ross-Carre, cited Church *et al* 1996). Pellenbarg (1978) experimented with

Spartina litter and found it to bind a number of metals firmly leading to considerably enriched detritus. In addition to the humic materials there are also likely to be high densities of microbes associated with the rhizosphere and these may also act as sites for trace metal adsorption (Williams *et al* 1994).

The root-rich layers of sediment in cores HySR3 and HySR5 contain elevated levels of As, Br, Cu, Pb, Ni, and Zn, each to variable extent (Figures 6.1-6.3). The speciation of the trace elements within these sediments is unknown but appears closely correlated with the growth of the root system. Mechanisms by which trace metals may become associated with particulate organics are several and also lead to the formation of metal-enriched organic coatings on sedimentary particles (Tessier *et al* 1996). The distribution of many trace elements around the sub-surface vegetative growth implies a dominant control mechanism being exerted by the rhizosphere. The steep diagenetic gradients encountered and the abundance of organic molecules in the sediments result in changes in the speciation of many components, bringing about their redistribution within the profile. The brown-orange colouration of the sediments between the roots gives an indication of their periodically oxidising nature (Zwolsman *et al* 1993). They are also likely to be more acidic than the lower areas of the marsh (Church *et al* 1996) due to the oxidative capacity of the roots, generating SO_4^{2-} through sulphide oxidation, and the reduced inundation of alkaline tidal waters.

Previous studies have also concluded that metal enrichments in salt marshes often occur within organic-rich silt-clay fractions of the sediment (Williams *et al* 1994) since these exhibit high ion exchange capacities. In particular, Caçador *et al* (1996) report increased loadings of lead, zinc and copper in sediments trapped between dense root mats within salt marshes. Utilising a sequential extraction scheme Caçador *et al* (1996) concluded that a greater percentage of the metals (as compared to non-vegetated sites) was present in the residual fraction (possibly residual organic matter unaffected by the H_2O_2/HNO_3 reaction stage). Binding of the metals to root mucilage was suggested as a possible mechanism for these enrichments. Following an investigation into metal speciation amongst the particulate phases in lake sediments Tessier *et al* (1996) report the complexation of trace metals on to the functional groups of organic coatings adsorbed on iron oxyhydroxides in the more acidic (pH 4.8) lake. This was not significantly apparent in the circumneutral lakes sampled where complexation by the OH groups of Fe and Mn oxyhydroxides was responsible for immobilising most of the trace metal load. The adsorption of humic substances on to Fe-oxyhydroxides and the precipitation of iron-humic complexes increases with decreasing pH (Bendell-Young and Harvey 1992). Despite the reduced ionisation of organic functional groups with decreasing pH, therefore, it would appear

that in systems containing significant organic loads as well as ferric iron minerals the binding of trace metals into the solid phase is facilitated under more acidic conditions (such as those at the rear of the marsh). The brown and orange colouring throughout these peaty, organic-rich zones implies the presence of a minor oxidised iron fraction in the sediments which may assist in the precipitation of trace metals through humic complexation reactions.

The degree of correlation between the organic carbon content of these organic-rich sediments and trace metal loading varies considerably for the different elements studied (Table 6.3). These general correlations have been calculated for the upper 25 cm of cores HySR3 and HySR5 (incorporating the two upper root-rich horizons). It is known, however, that many other control mechanisms exist within the sediments which affect the distribution of minor components (see, for example, the above discussion on the role of Fe and Mn oxides). Despite the coincidence of trace metal enrichment and organic carbon content, therefore, this represents another controlling factor in a complex system where several different phases may compete for the adsorption of trace elements. In the higher marsh areas the role of organic materials in governing trace element distributions is considerable but cannot be invoked to explain completely their speciation within the sediments. The significance of oxide and sulphide phases is still apparent in these cores and the additional potential for relicts of the depositional history to persist cannot be ignored.

Element:	**As***	**Br***	**Cu***	**Pb***	**Ni***	**Zn***
HySR3	**0.83**	**0.61**	**0.77**	0.16	**0.67**	0.13
HySR5	**0.84**	**0.61**	0.53	0.16	**0.66**	0.34

Table 6.3:

Pearson r^2 values determined for the correlation between organic carbon and excess element concentration over the upper 25 cm (peaty section) of sediment cores HySR3 and HySR5.

6.3.5 *Summary*

The preceding interpretation accounts for many of the features observed in the trace element concentration profiles within Hythe Marsh. Variations in the distribution and recycling of the three dominant sedimentary phases (oxides, sulphides and organics) may be invoked to account for much of the observed trace element distributions. A summary of the response of the various trace elements to the distribution of these carrier phases follows:

6.3.5.1 As and P

Arsenic appears to be subjected to reconcentration by all three phases, and is revealed as a labile element exhibiting active post-depositional mobilisation. No part of the profiles for this element can be attributed to the preservation of a depositional record. Iron oxides and sulphidic conditions are most important in governing this element within the more minerogenic cores (HyPb and HySR2), whereas in the peaty sediments of the middle and rear marsh these controls are of lesser importance than apparent complexation by organic materials (though the role of iron in the formation of humic complexes may still be important). Phosphorous, on the other hand, is distributed solely according to the abundance of ferric oxyhydroxide phases throughout each core analysed.

6.3.5.2 Pb

The coupling of lead with manganese within the surficial few centimetres of the sediments of each core is indicative of the considerable recycling experienced by these two elements at shallow depths where intense diagenetic gradients are likely to be prevalent. Lead is also concentrated in the lower ferric iron peak (14-22 cm depth) within core HyPb indicating some association with this phase, as well as potential organic associations within the higher marsh areas. Sulphide mineralisation of lead is apparent (particularly within core HySR2) though of lesser significance. However, a number of features of the lead profiles cannot be attributed to variations in these geochemical parameters (for example, HyPb 20-35 cm depth, HySR2 10-25 cm depth and HySR3 20-30 cm depth). Indeed, the use of stable lead isotope analysis supports the partial preservation of the depositional record of lead, since it yields variations in the isotope signature throughout the sediment prism which are attributable to different source inputs over time (see Chapter 7).

6.3.5.3 Zn and Ni

The distributions of zinc and nickel are remarkably similar in each of the cores. Most of the features observed are caused by association of these elements with manganese oxides, sulphidic minerals and organic loadings. Overall it would appear that these two elements are extensively recycled into authigenic phases following their incorporation within the sediment prism.

The following discussion summarises the most important aspects remaining to be considered regarding the distribution of trace elements within Hythe Marsh sediments.

6.3.6 *Depositional flux of copper*

The maximum concentration of copper measured (374 ppm, core HySR2) indicates considerable concentration of this element into the sediments of Hythe Marsh, especially considering the average shale value of 45 ppm reported by Turekian and Wedepohl (1961). The sediments contain constant background levels of ~20 ppm at depth and exhibit elevated concentrations within the upper decimetres of each core (Figures 6.1-6.3). Calculation of the excess copper concentration according to Equation 3.2 (mean detrital ratio of Cu/Al = 2.9 ppm Cu per wt.% Al) reveals that cores HyPb and HySR2 exhibit essentially single-peaked profiles whereas those within HySR3 and HySR5 contain two distinct maxima. Analysis of these profiles in concert with the known anthropogenic use of copper for local industrial purposes suggests that the sedimentary record preserves, at least partially, the depositional flux. However, the disparity between features observed in different areas of the salt marsh implies that post-depositional processes do redistribute a portion of the copper load during early diagenesis.

6.3.6.1 Source of copper

The discharge of copper from the oil refining and chemical industry complex situated at Fawley, built in considerable part on reclaimed intertidal land in close proximity to Hythe Marsh, has been a major feature of metal contamination in Southampton Water for several decades (Ármannsson *et al* 1985; Dicks and Levell 1989; Sharifi 1991; Croudace and Cundy 1995). The site first came into industrial use in 1921 followed later by significant expansion during the 1950s, with concurrent increases in the levels of contaminants (hydrocarbon and trace metal) being released into the local estuarine system (Croudace and Cundy 1995). The copper discharged along with other industrial effluents is likely to associate with the suspended

particulate load in the estuary and thereafter become distributed within the sediments of Southampton Water.

6.3.6.2 History of local Cu pollution and the sediment load

From the product of concentration ($\mu g\ g^{-1}$) and sediment accumulation rate ($g\ cm^{-2}\ yr^{-1}$) the annual flux of Cu ($\mu g\ cm^{-2}\ yr^{-1}$) to the salt marsh surface may be derived (Equation 6.4). Comparable results are obtained through the application of each independent radiometric dating technique and these reveal interesting parallels with the known pattern of anthropogenic copper use in local industries. Copper concentrations significantly above the local background level are first apparent at 25-30 cm depth within each core (Figures 6.1-6.3). Comparing the flux data to the time of deposition of the sediments (Figure 6.8) reveals that increased deposition of copper commenced during the 1930s. This is consistent with the known initiation of oil refining and other industrial operations in the immediate vicinity and is likely to represent predepositional labelling of these sediments with the metal. Increases in Cu concentration within sediments deposited after this date are primarily due to greater anthropogenic release into Southampton Water, particularly accompanying the expansion of the industrial site during the 1950s. This appears to be recorded in the salt marsh sediments by the sharp increases in copper flux evident within sediments deposited during this period. Discharge of refinery effluents was reviewed during the 1960s and 1970s and a number of measures were introduced over these decades to decrease the amount of pollution being released (Dicks and Levell 1989). All four of the salt marsh records reveal a maximum depositional flux of copper between the early 1960s and 1970s, and thereafter exhibit a significantly declining load toward the sediment surface. The history of copper discharge into Southampton Water and the flux recorded within Hythe Marsh sediments are therefore in reasonable accord throughout the whole of the sedimentary profiles. The conclusion of Shaw *et al* (1990) that copper appears less sensitive to redox-driven redistribution than many other transition metals within sediment sequences further supports this observation.

6.3.6.3 The effect of organic matter on the Cu profiles

The distributions of copper observed within the sediments may be divided into two categories. The first of these is to be found within cores HyPb and HySR2 and consists of a single major peak in concentration (corresponding to deposition during 1963-66 and 1962-65, respectively). This peak, along with the remainder of the Cu profile, exhibits apparent independency from other geochemical parameters within the cores (such as organic carbon content) and, due to the

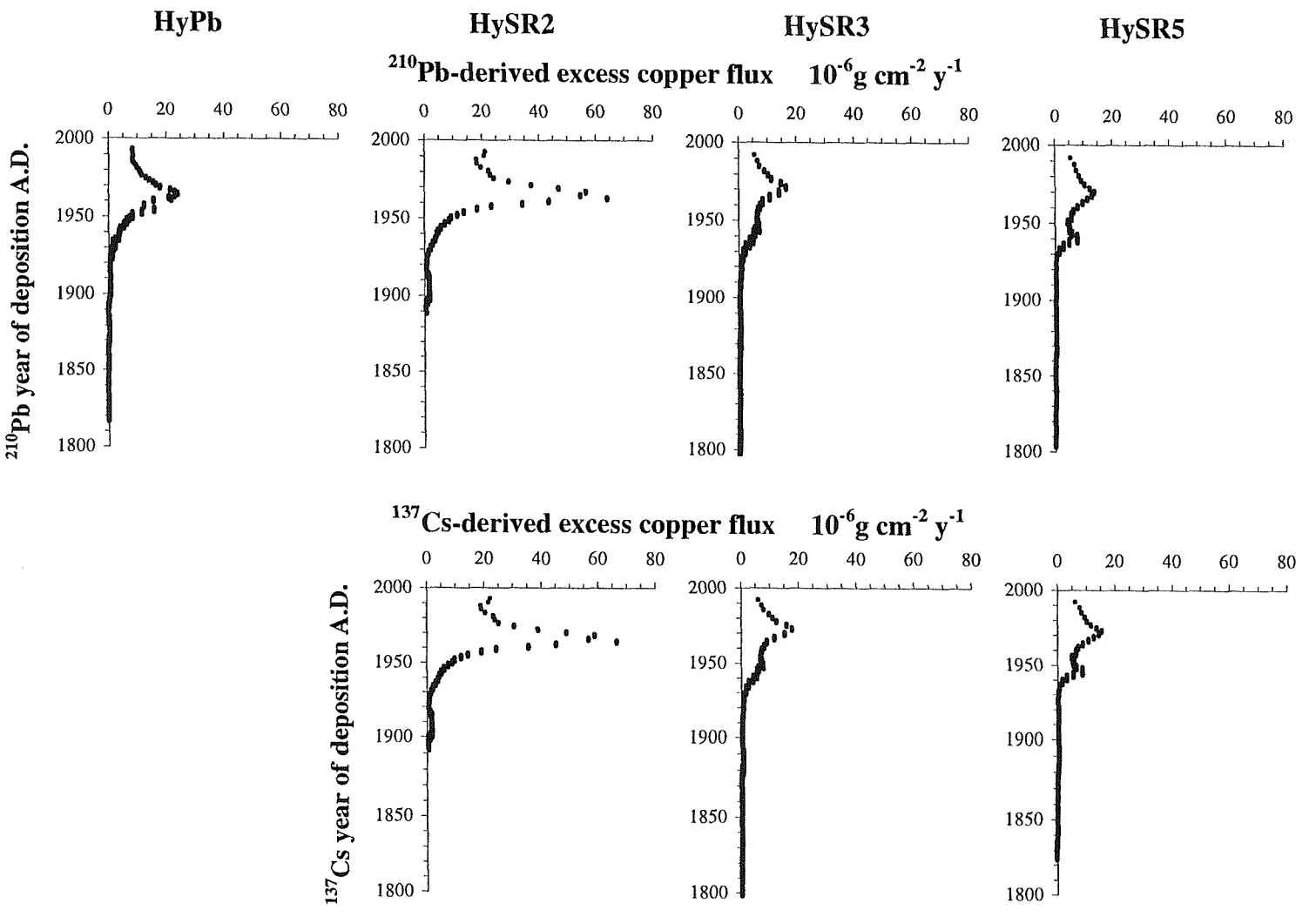

Figure 6.8: Copper flux data and sediment accretion chronologies from ^{210}Pb and ^{137}Cs..

correlation it observes with the known anthropogenic discharge pattern, is interpreted as resulting from variations in the depositional flux. The second type of copper profile, as revealed in cores HySR3 and HySR5, consists of two significant concentration maxima at depths coincident with elevated abundances of organic carbon. The single "pollutant spike" nature of the copper distribution as inferred from cores HyPb and HySR2 appears to have become altered, resolving the Cu profile into two distinct peaks. The upper peaks (7-8 cm depth in both HySR3 and HySR5) and the lower peaks (~17 cm and ~ 21 cm depth , respectively) are not considered to be reliable indicators of depositional flux since they are clearly correlated with the root-rich horizons within the sediments. Despite the strong case for preservation of the depositional record at other sites on the marsh the profiles obtained for cores HySR3 and HySR5 exhibit signs of post-depositional redistribution of Cu within the sediments, increasing the amount of metal present within the organic-rich layers. The overall concentration profile obtained is probably a superimposition of the depositional flux and subsequent diagenetic remobilisation leading to enhanced copper concentrations within certain horizons. The increased abundance of organic materials appears to be the parameter responsible for the redistribution, perhaps driven by complexation to form humic-copper complexes (Rashid 1985) and subsequent immobilisation on to the solid matrix within organic-rich sediments (Williams 1994).

6.3.7 *Halogen distribution*

6.3.7.1 Bromine

6.3.7.1(a) Source

Bromide is a major anion in sea water, typically present at ~ 70 ppm (Malcolm and Price 1984), hence the flood waters which drain the sediment prism regularly introduce a large quantity of this element into the pore interstices, and probably represent the single largest source of bromine to Hythe marsh. Concentrations up to 801 ppm in estuarine sediments from Loch Etive (Malcolm and Price 1984) and 278 ppm in Panama Basin sediments with less than 2.5 wt.% organic carbon (Pedersen and Price 1980) warrant the expectation that the organic-rich sediments of the rear-marsh will be highly brominated (Edmunds 1996). The enrichment of bromine relative to chlorine in marine aerosols and rainfall is known to be a consequence of the increased concentration of organic carbon present at the sea surface (Edmunds 1996). The interaction of this bromine-rich surface microlayer with vegetation and sediment as flood waters enter and leave the marsh may exert a significant effect on the deposition of brominated

materials (as observed for some metals by Pellenbarg 1984). Aeolian deposition of marine aerosols and precipitative introduction of brominated rain water also represent likely routes for the transport of Br into the salt marsh sediment prism. A further source of bromine requiring mention is that derived from the combustion of fossil fuels, particularly coal, since this is known to result in elevated atmospheric concentrations in some areas, such as the Trent Valley (Edmunds 1996). The nearby fossil fuel power stations at Marchwood and Calshot thus represent a potential source of anthropogenic bromine, as does the Exxon bromo-butyl rubber plant within the nearby chemical works, although the amount of this element derived from either natural or industrial sources cannot be determined here.

6.3.7.1(b) Behaviour

Sediments with the least Br enrichment (<200 ppm excess concentration) are to be found within the lower section of each core and across major redoxclines, whilst the upper decimetres, with their more organic-rich matrices, are characterised by elevated bromine concentrations (Figure 6.9). Correlative plots of bromine against organic carbon (Figure 6.10) show reasonable agreement in the case of three cores (HyPb, HySR3 and HySR5; r^2 = 0.65, 0.77 and 0.87, respectively) and are not significantly correlated within the most minerogenic core, HySR2 (r^2 = 0.12). Significant control appears to be exerted on the Br distribution through absorption by organic molecules. The regular flux of saline waters through the salt marsh introduces bromide ions to all areas of the marsh prism. Some of these anions may then be removed on to the sediment matrix, *via* processes dependent on the abundance and nature of the organic portion (Edmunds 1996).

Within core HySR2 the correlation between organic carbon and bromine is weak (r^2 = 0.12) and the overall enrichment of bromine is smaller than in other cores (< 300 ppm throughout). Minima centred at 10 and 26 cm depth (Figure 6.9) are coincident with depths over which major diagenetic zone changes occur, as revealed by the iron profile (a similar feature is also apparent in core HyPb at about 12 cm depth). The upper minimum in core HySR2 represents the boundary between oxic and post-oxic conditions (ferric iron is removed at 10 cm depth) whereas the lower minimum marks the depth of change from post-oxic to sulphidic conditions (iron increases markedly over 25-29 cm depth). The sharp decreases in Br/C_{org} also evident at these depths indicate that bromine is lost from the sediment to greater extent than concurrent loss of organic carbon. The complex suite of geochemical species likely to be present at these redox fronts, including hydrogen sulphide ions and intermediate oxidation state sulphur

compounds, may bring about the loss of bromine through their nucleophilic substitution on to the organic molecule and the displacement of bromide ions (Francois 1987).

6.3.7.1(c) Br/C_{org} ratios

The Br/C_{org} values determined for Hythe Marsh sediments (Figure 6.9) are at the lower end of previously reported ranges (Table 6.2) reflecting the terrestrial nature of the organic fraction within the sediments. The uptake of bromine by marine plankton is known to result in much higher Br/C_{org} ratios than found within terrigenous organic materials, therefore suggesting that halophytic salt marsh vegetation ought to contain lower ratios than present in offshore sites having abundant planktonic seston (Malcolm and Price 1984). Despite the large increase in organic carbon concentration towards the rear of the marsh, the ratio of Br/C_{org} in the sediments is restricted to a relatively narrow range (0-60) for all samples. The vertical distributions of Br/C_{org} within each core show broadly similar features, consisting of higher ratios within the oxic upper layers, low values across major redoxclines (in cores HyPb and HySR2) and declining values within the sulphidic sediments. Throughout the post-oxic zones the Br/C_{org} ratios are variable (between 20-50) though they exhibit a general decrease with depth. At a given location on the marsh the Br/C_{org} ratio throughout the sediment profile may vary as a consequence of several processes:

- variation in the rate of supply of bromine from flood water to areas of the sediment;
- variable composition of organic material, affecting its ability to absorb Br;
- a disparate rate of release of Br relative to C_{org} from degrading organic matter.

Organic materials are produced within the sediment body, as well as being imported and exported during tidal flushing. Consequently, the ratio of Br/C_{org} present within a material at the initial time of incorporation into the sediments is expected to exhibit great variability, from relatively bromine-rich marine detritus to the bromine-poor terrestrial primary production.

6.3.7.2 Iodine

6.3.7.2(a) Source

Iodine is present in sea water at a much lower concentration than bromine ([I] ~60 ppb, [Br] ~70 ppm; Malcolm and Price 1984) but may be concentrated to greater levels within marine organisms - up to 10,000 ppm in some cases (Pedersen and Price 1980). Excess iodine concentrations have been calculated in similar fashion to bromine above (Equations 3.1 and 3.2). Hythe Marsh sediments contain up to 75 ppm excess iodine, equivalent to total sediment I concentrations of up to 130 ppm. As with Br these are at the lower end of concentrations reported for the Loch Etive estuary (208-721 ppm I; Malcolm and Price 1984) and Panama Basin sediments (76-861 ppm I; Pedersen and Price 1980) suggesting that the removal of this element from waters flooding the marsh is less efficient than its removal by planktonic debris, believed to take place at or near the sediment-water interface in offshore locations (Shimmield and Pedersen 1990).

6.3.7.2(b) Distribution

The influence of the redoxcline within sediments has the potential to decouple the relationship between iodine and organic carbon as the two elements are subjected to different redistributive processes. The spatial favourability of different oxidation states of iodine, ranging from -1 (iodide) to +5 (iodate), depending on the prevalent redox climate, causes iodine to behave in a more dynamic fashion than bromine during early diagenesis (Thomson *et al* 1995). The mechanisms considered previously through which organic matter may concentrate iodine, are known to predominate in the presence of free oxygen (Shimmield and Pedersen 1990) partly explaining the observed enrichments of I within oxic sediments (e.g. Price and Calvert 1977). Laboratory experiments have also concluded that iron oxyhydroxides readily take up iodine species from solution (Shimmield and Pedersen 1990) and the abundance of this phase in Hythe salt marsh sediments also needs to be considered.

The excess iodine concentration profiles determined for the four sediment cores reveal that the element does indeed respond actively to the physico-chemical environment of deposition, exhibiting features which often parallel the apparent redox condition of the cores (Figure 6.9). The dependency of sedimentary iodine concentration on the abundance of iron and organic carbon (Figure 6.10) within Hythe Marsh differentiates the rear marsh area from the other sample sites; only in core HySR5 do iodine and C_{org} exhibit any significant correlation. Within

the other three cores diagenetic processes appear to dominate the post-depositional cycling of iodine and uncouple its distribution from that of the organic fraction (Table 6.4).

Core:	HyPb	HySR2	HySR3	HySR5
Depth:	0-20 cm	0-11 cm	0-30 cm	0-13 cm
r^2 vs. Fe* wt.%:	**0.68**	**0.89**	0.31	0.24
Over whole core:				
r^2 vs. C_{org} wt.%:	0.04	0.05	0.11	**0.82**

Table 6.4:

Relationship between iodine concentration and that of iron (oxidised sediments only) and organic carbon.

6.3.7.2(c) Ferric iron

The close agreement exhibited by the distributions of iodine and ferric iron in cores HyPb and HySR2 (r^2 = 0.68 and 0.89, respectively), along with the disparity observed between I and C_{org}, demonstrates the sedimentary redistribution of this halogen according to the redox zonation. The two elements (I and Fe) do not conform to one another throughout the whole length of these cores, however, since iodine is enriched to relatively high levels throughout the post-oxic zone which is effectively free of excess iron. Nevertheless, the oxidised surface sediments contain a pronounced relationship of iodine to ferric iron which may be the result of a direct phase association between the two species or caused indirectly by independent redox control over both elements. Observing an absence of iodine enrichment to be paralleled by an absence of iron within calcareous sediments led Ullman and Aller (1985) to argue that adsorption of iodate by ferric oxyhydroxide surfaces was responsible for surficial I enrichments. Core HySR3 is unique in that it contains a much lesser abundance of both iodine and ferric iron, from which observation a similar mechanism to that postulated by Ullman and Aller (1985) appears probable. Chemical leaching experiments conducted by Francois (1987) yielded inconclusive results regarding the speciation of iodine in surficial sediment samples due to difficulties in identifying the iodine extracted from different phases. Although ferric oxyhydroxides appeared

to be of secondary importance in governing the iodine distribution, it was recognised that relatively high concentrations of I could still be associated with this phase.

The mechanism whereby iodine partitions into the solid phase in the less organic sediments found across the front of Hythe Marsh cannot be deduced from the extent of the present study but appears to be related to the availability of ferric iron. Of course, since this in turn depends upon the availability of oxygen (and other oxidants) the ferric iron distribution may only be a proxy signal for an alternative control process affecting both elements in a similar fashion. Although more research is necessary before the interdependency of these two elements can be deduced in more detail, the results obtained from cores HyPb, HySR2 and HySR3 suggest that the laboratory-demonstrated adsorption of iodate ions by iron oxyhydroxide surfaces may well occur within salt marsh sediment sequences.

6.3.7.2(d) Organic carbon

In the case of core HySR5, unique amongst the four cores studied, the distribution of iodine within the sediments is closely correlated ($r^2 = 0.82$) with that of organic carbon (Figure 6.10). The mechanism of this association is believed to involve electropositive iodine species such as HOI and I_2 (Francois 1987), perhaps formed through the reduction of iodate by the humic substances abundant within this area of the marsh. Clearly the dominance of controlling processes relating either to association of I with ferric or organic materials is altered in traversing the marsh. Since the degree of reaction between iodine and organic substrates is known to be related to the prevalent redox condition (e.g. Upstill-Goddard and Elderfield 1988) it is likely that differences observed between the cores are due to variations in the oxidation status of the sedimentary prism. The paucity of ferric iron within core HySR3 implies the persistence of relatively reducing (post-oxic) conditions throughout much of the profile, under which there is typically little association between iodine and organic carbon (Price and Calvert 1977). Within the two lower marsh cores, HyPb and HySR2, the surface sediments are characterised by abundant oxidised iron minerals and a reduced amount of organic matter relative to core HySR5. The different abundances of such major sedimentary phases may be sufficient explanantion of the observed phase associations of iodine, although the oxidation potential of the sediments probably enhances the variation across the marsh. Core HySR5 consists of a peaty upper section above 26 cm depth through which oxygen is likely to diffuse more freely than within more minerogenic core sections. The mingling of both iodine and oxygen species within these sediments promotes the likelihood of reaction between I and C_{org} through the generation of suitable electropositive species.

6.3.7.2(e) I/C_{org} ratios

As with the Br/C_{org} ratios discussed above, values of I/C_{org} within Hythe Marsh sediments are at the lower end of the range found within the literature. In the present study, the values of I^*/C_{org} measured throughout the cores range from 0 - 12 (ppm I#*/wt.% C_{org}) for excess iodine (Figure 6.10), equivalent to a total iodine to organic carbon ratio ranging from 0 - 30. These values are lower than other reported values (Table 6.2) presumably as a consequence of the terrestrial nature of the organic material present within the salt marsh sediments (Upstill-Goddard and Elderfield 1988). The variation with depth exhibited by these ratios closely follows the pattern of excess iodine distribution and does not conform to the exponential decrease often observed within marine sediment sequences (e.g. Pedersen and Price 1980). The sediments considered throughout this study are morphologically distinct from those found in submarine locations on account of the predominance of sub-surface organic growth. This results in the presence of not only decaying organic carbon beneath the sediment surface but also freshly produced organic matter. The relationship between iodine and organic carbon found elsewhere (suggesting the preferential release of iodine from organic substrates during degradation) is therefore not as obvious within salt marshes as a consequence of the simultaneous decay (and therefore release of iodine) and growth (along with potential I uptake) of organic materials throughout much of the sediment prism.

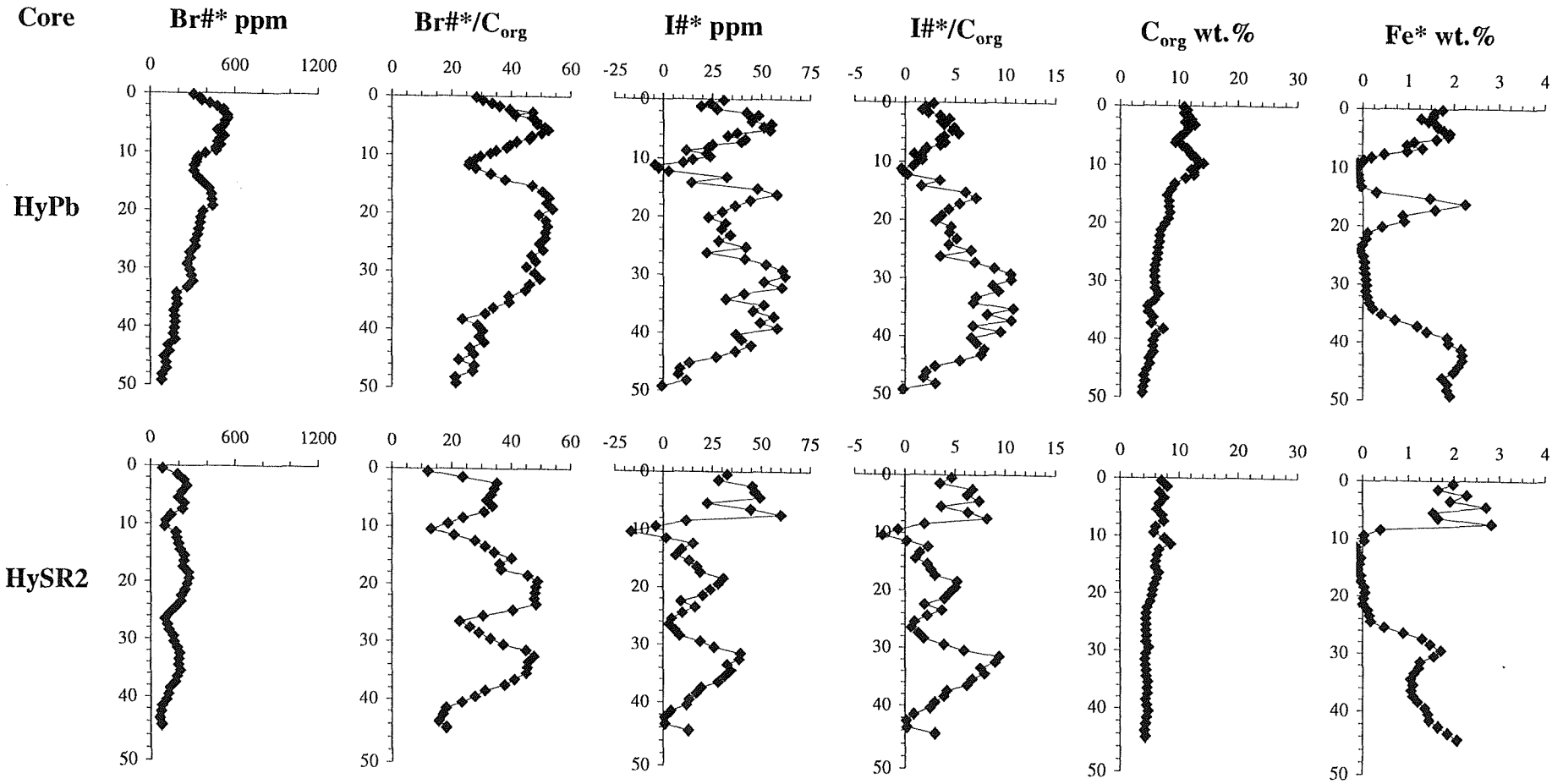

Figure 6.9 (a):

Depth-profiles of excess bromine, excess iodine and halogen/C_{org} ratios. Organic carbon and iron profiles shown for comparison.

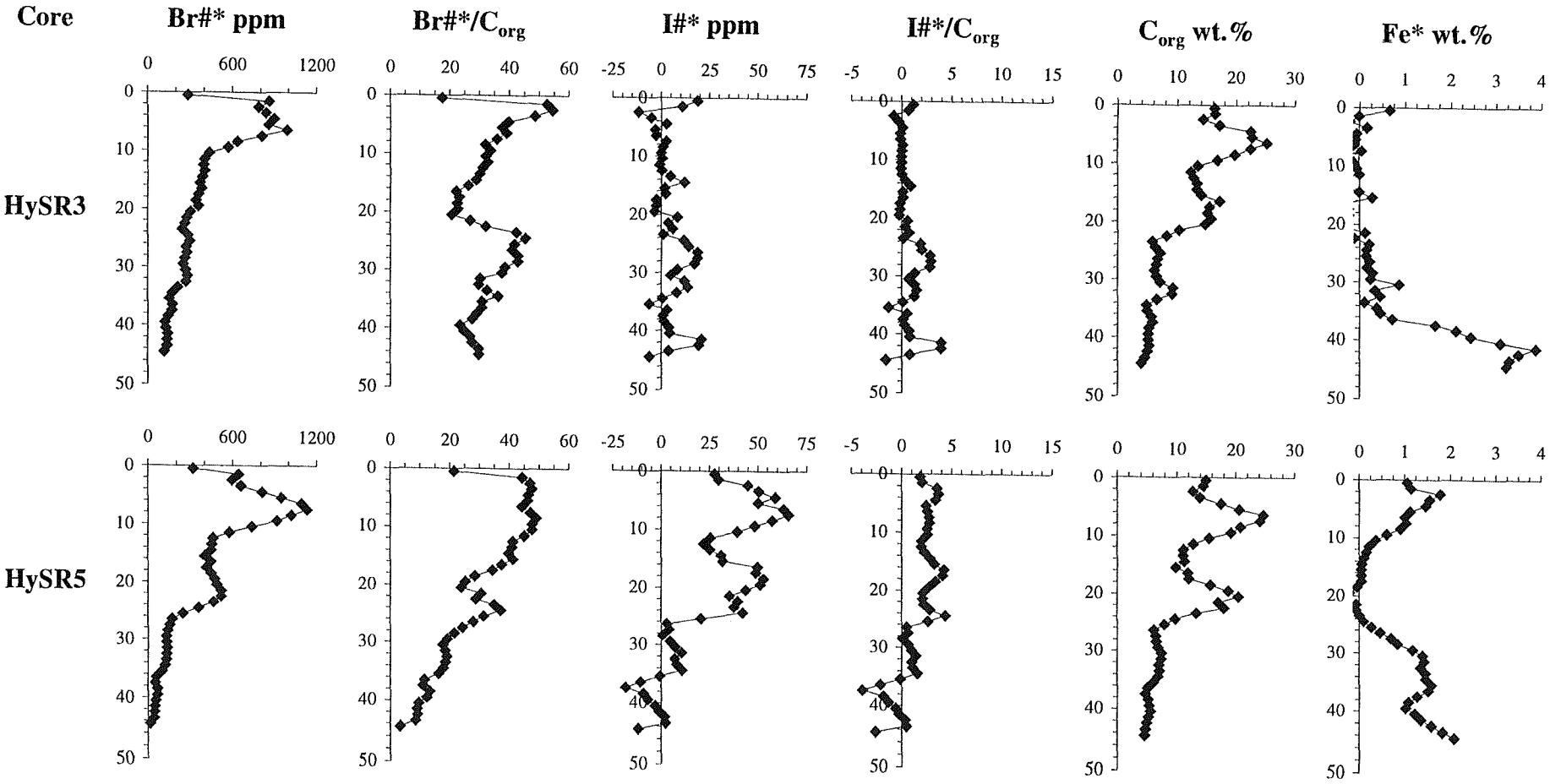

Figure 6.9 (b):

Depth-profiles of excess bromine, excess iodine and halogen/C_{org} ratios. Organic carbon and iron profiles shown for comparison.

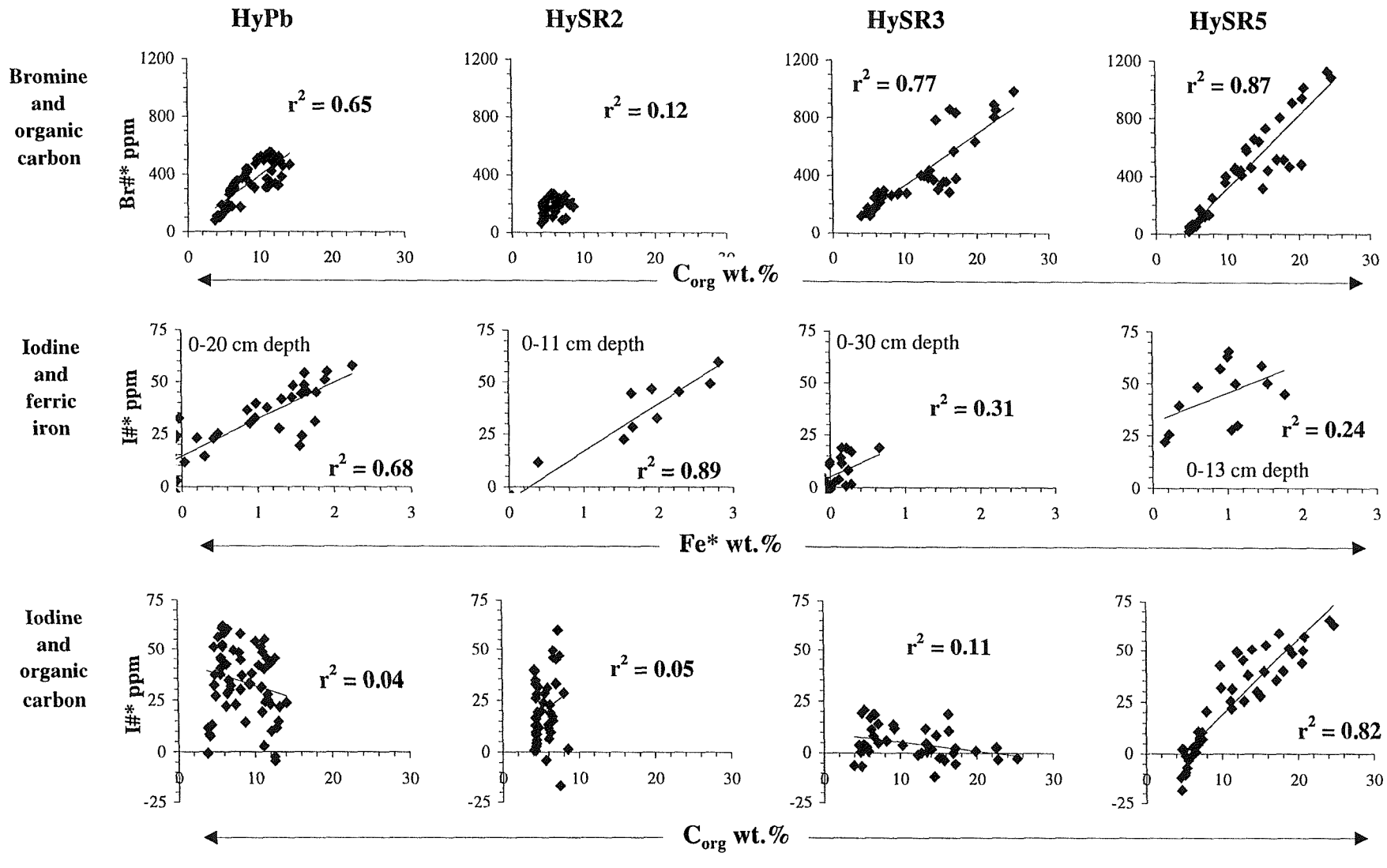

Figure 6.10: Correlative plots between excess halogen concentration, iron and organic carbon.

	As*	Cu*	Pb*	Zn*	Ni*	Oxic Fe*	P*	Oxic Mn*	Br*	Dry density	Al	^{137}Cs	^{210}Pb	C_{org}
As*		0.00	0.27	0.07	0.00	0.06	0.51	0.01	0.18	0.33	0.26	0.97	0.01	0.20
Cu*	0.00		0.51	0.87	0.85	0.83	0.01	0.99	0.82	0.68	0.74	0.03	0.84	0.58
Pb*	0.27	0.51		0.84	0.63	0.36	0.38	0.58	0.84	0.68	0.86	0.02	0.79	0.01
Zn*	0.07	0.87	0.84		0.88	0.66	0.07	0.91	0.96	0.78	0.92	0.00	0.96	0.22
Ni*	0.00	0.85	0.63	0.88		0.48	0.01	0.84	0.73	0.47	0.65	0.18	0.97	0.33
Oxic Fe*	0.06	0.83	0.36	0.66	0.48		0.03	0.86	0.75	0.83	0.72	0.04	0.52	0.55
P*	0.51	0.01	0.38	0.07	0.01	0.03		0.00	0.08	0.06	0.12	0.93	0.05	0.53
Oxic Mn*	0.01	0.99	0.58	0.91	0.84	0.86	0.00		0.89	0.77	0.82	0.01	0.85	0.50
Br*	0.18	0.82	0.84	0.96	0.73	0.75	0.08	0.89		0.91	0.99	0.02	0.85	0.19
Dry density	0.33	0.68	0.68	0.78	0.47	0.83	0.06	0.77	0.91		0.95	0.16	0.60	0.17
Al	0.26	0.74	0.86	0.92	0.65	0.72	0.12	0.82	0.99	0.95		0.06	0.78	0.14
^{137}Cs	0.97	0.03	0.02	0.00	0.18	0.04	0.93	0.01	0.02	0.16	0.06		0.08	0.17
^{210}Pb	0.01	0.84	0.79	0.96	0.97	0.52	0.05	0.85	0.85	0.60	0.78	0.08		0.23
C_{org}	0.20	0.58	0.01	0.22	0.33	0.55	0.53	0.50	0.19	0.17	0.14	0.17	0.23	

Shading	r^2
	< 0.65
	0.65 - 0.9
	> 0.9

Table 6.5:
Correlations between the sediment core inventories of different parameters within Hythe Marsh.

6.3.8 *Inventories*

The inventory of any stable element within a given length of sediment core (Equation 6.3) is a function of the nature of the sedimentary material, and the net import and export of that element to and from the accreting sediments at each location sampled. The pattern of variation observed for different element inventories between sediment cores may allow information to be gathered regarding the input of each element to the marsh prism. To allow comparison between cores the inventories discused in this section are all derived from the 0-45 cm depth interval of each core (Figure 6.4).

6.3.8.1 Aluminium

The inventory of aluminium increases in the order HySR3 < HyPb < HySR5 < HySR2, and is dependent upon the amount of minerogenic material incorporated into the sediment prism in combination with organic matter produced by the marsh vegetation. The variation of mean dry density and total mass of sediment accreted (g cm^{-2}) closely follows the variation in aluminium inventory (r^2 = 0.95 for Al inventory and mean dry density; Table 6.5). A number of trace elements also have inventory variations across the marsh which conform to the pattern of variation of aluminium and mean core density. This is likely to be due to the fact that all of these elements are deposited on the sediment surface in association with the same sedimentary material from the estuarine environment. Strong correlations (r^2 > 0.90) exist between aluminium, zinc and bromine (Table 6.5) whereas aluminium is moderately correlated (0.65 < r^2 < 0.90) with copper, lead, nickel, oxic iron, oxic manganese and ^{210}Pb inventories. The most likely explanation for the observed inventory variations is that these elements arrive on the surface of the marsh in association with marine-derived sedimentary particles (material from the estuarine suspended sediment load) and therefore accumulate in greatest amounts where the deposition of such material is highest. Note that this variation is not strictly dependent upon the distance of the accumulating sediment from the estuarine water mass and must therefore be subjected to highly localised effects related to the buoyancy of the sediments and the ability for sediment particles to become trapped in different areas of the marsh.

6.3.8.2 Iron and manganese

The distribution of iron and manganese inventory across the marsh follows the sequence HySR3 < HySR5 < HyPb < HySR2 with these two elements exhibiting a reasonably strong correlation ($r^2 = 0.86$). Despite the fact that this pattern of variation is identical to that observed for aluminium the variability of the magnitude of sediment inventory is much greater for Fe* and Mn* than for Al and the other elements listed above. The mid- and rear marsh cores (with elevated organic carbon contents) contain a reduced amount of both of these redox-sensitive metals in the surface layers, and this phenomenon is likely to be related to the oxidation status of the sediment prism. The pore water profiles obtained from the sites of sediment cores HySR3 and HySR5 imply that considerable differences exist between the two locations. The lowest inventory found in the marsh for both Fe* and Mn* corresponds to the sediment core which lacks a well-developed oxic surface layer and the postulated escape of these elements into overlying waters thus appears supported by the inventory data. Furthermore, the inventory of sulphidic iron, as determined throughout the uppermost 10 cm of the enriched iron and sulphur zone at depth within each core, is far greater within core HySR3 than in the other three cores. The lesser importance of surficial oxidation within this core has resulted in the accumulation of an increased amount of iron in the sulphidic zone and suggests the persistence of more reducing conditions throughout the sediment profile.

Chapter Seven

Stable Lead Isotopes

7.1 Introduction

7.1.1 *Anthropogenic lead use*

The industrial use of lead for human purposes has been taking place since about 2500 B.C. (near the end of the Chalcolithic era) when ores were first mined and smelted to yield useful alloys (Patterson 1971). The widespread advent of coinage amongst early civilisations, starting at about 650 B.C., utilised silver obtained from the cupellation of lead metal (producing ~400 tonnes of lead oxide for every tonne of silver) and initiated the considerable expansion of world lead production. This continued until the fall of the Roman Empire whereupon the generation of lead metal declined markedly. Following the Industrial Revolution world lead production rose exponentially, with a multitude of uses being found for the metal such as the manufacture of water pipes, paint additives and as ships ballast. More recently, with the advent of the internal combustion engine, alkyl lead derivatives have been added to petroleum fuels. The discharge of lead in vehicle exhaust fumes now represents the largest source of the element in urban locations, sourcing lead to the environment predominantly in aerosol form. The residence time of lead in atmospheric aerosols is reckoned to be of the order of a few weeks (Shirahata *et al* 1980), sufficient time to have profoundly influenced the atmospheric cycle of lead (Nriagu 1989) and to have resulted in the worldwide dispersal of lead from smelter and exhaust emissions (Ng and Patterson 1982).

7.1.2 *Lead source reconnaissance using stable isotope ratios*

Lead has four stable isotopes, each with a different average crustal abundance, ^{204}Pb (1.35%), ^{206}Pb (25.3%), ^{207}Pb (21.1%) and ^{208}Pb (52.2%). The first of these isotopes is termed primordial lead since it has not been produced through any known radioactive decay scheme. The three heavier isotopes, however, are all radiogenic and are continuously produced by the respective decay schemes of ^{238}U, ^{235}U and ^{232}Th (Figure 7.1). Their abundances may vary considerably throughout the Earth's crust due to variations in the concentration of their parent radionuclides and differences in the age of distinct geological units. Lead ores tend to contain no uranium or thorium, and are therefore likely to have their isotopic composition fixed at the time of ore formation. The resulting isotope characteristics will therefore depend upon the concentration of uranium and thorium within the parent material and the time of segregation of the ore minerals (Chow *et al* 1975). Ores formed more recently within the Earth's history ought to have an isotopic composition which is more radiogenic than older lead ore bodies (see Table 7.1). The extraction of lead ores for anthropogenic consumption results in the distribution of a wide range

U	Pa	Th	Ac	Ra	Fr	Rn	As	Po	Bi	Pb	Tl
92	91	90	89	88	87	86	85	84	83	82	81

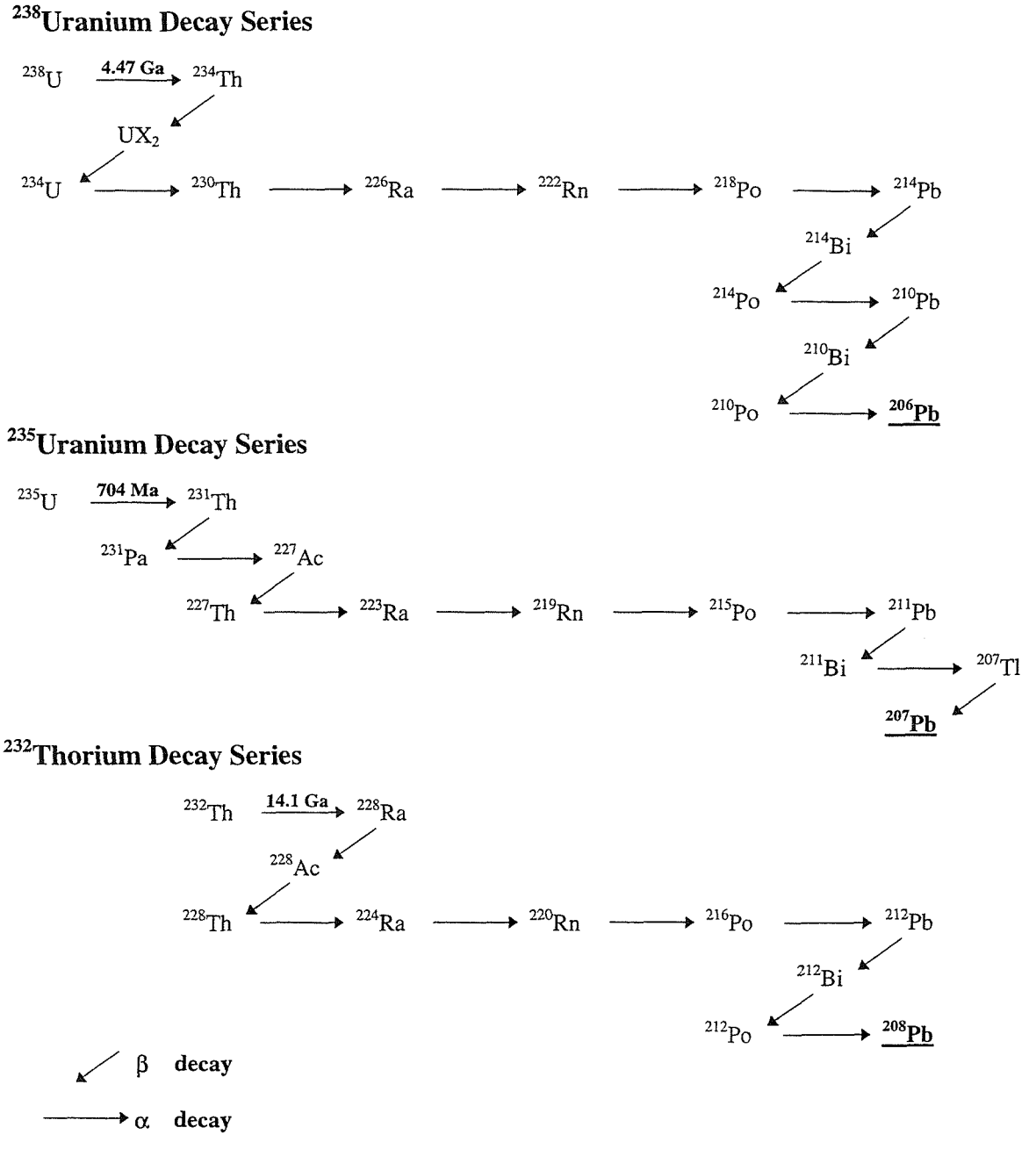

Figure 7.1:
The uranium and thorium decay schemes with the parent nuclides ^{238}U, ^{235}U and ^{232}Th leading to the formation of the stable end-members ^{206}Pb, ^{207}Pb and ^{208}Pb, respectively (from Kersten *et al* 1992).

of materials, each of which may have a characteristic isotopic composition. The dispersal of this lead into the environment does not in itself bring about further isotopic fractionation (due to the identical chemical behaviour and similar masses of the isotopes) and it therefore may be possible to detect the anthropogenic release of lead from a particular ore body through the application of lead isotope analysis.

During the mixing of multiple lead sources, each with a different isotopic signature, the overall composition of the host material will be equal to the weighted mean of the individual source terms. In settings where the local, natural lead isotopic composition is similar to that of lead deposited from anthropogenic activities it is not possible to distinguish between these two sources through the analysis of lead isotope abundances. This has been problematic in parts of North America where a restricted range of lead isotope ratios may be present (e.g. $18.70 < {}^{206}Pb/{}^{204}Pb < 18.95$), despite large variations in the total lead concentration due to anthropogenic release (Hamelin *et al* 1990). However, should the various sources of lead to any particular environmental sample have suitably different isotopic compositions, then analysis of the material may permit source apportionment (Kersten *et al* 1992). In Europe such differentiation is facilitated by the tendency for industrial lead to be derived from ancient, unradiogenic lead ores, such as those from Broken Hill and Mount Isa (Australia) and British Columbia (Canada), which have widely different isotopic compositions from local crustal lead and European lead ores (Hamelin *et al* 1990; Kersten *et al* 1992).

7.1.3 *Petrol lead*

The origin and rate of consumption of the lead ores used to manufacture petrol additives is of concern to any contemporary isotopic study due to the predominance of this source in many localities. The Associated Octel Company Ltd, principal supplier to the British market, have mostly used a mixture of Australian and Canadian ores in recent years (Delves 1988), though in the past have also purchased lead from the USA (Associated Octel, *pers. com.*). Further complication derives from the fact that Associated Octel is not the only supplier of lead alkyls to UK refineries since some purchase their additives directly from US manufacturers. Over recent decades legislation has been introduced to combat rising lead contamination amidst fears about the potential health risks posed by exposure to this highly toxic metal. The average lead concentration in gasolines sold within the UK, for example, has fallen approximately six-fold over the past thirty years (Figure 7.2; data from Associated Octel, *pers. com.*). Statistics from the Department of Trade and Industry (cited in Farmer *et al* 1996) suggest that lead emissions from petrol combustion peaked during 1976. The predicted isotopic ratio of such lead released

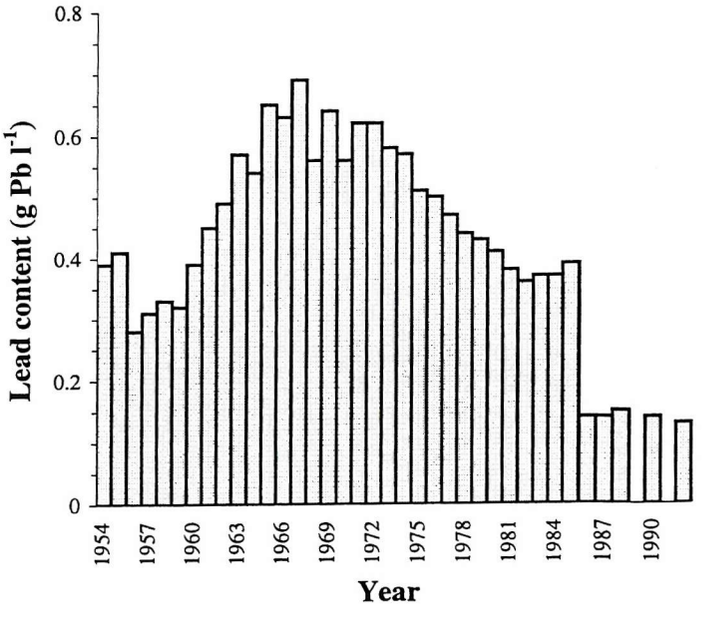

Figure 7.2:
Average lead levels of premium U.K. petrol.
Data from Associated Octel Co. Ltd.

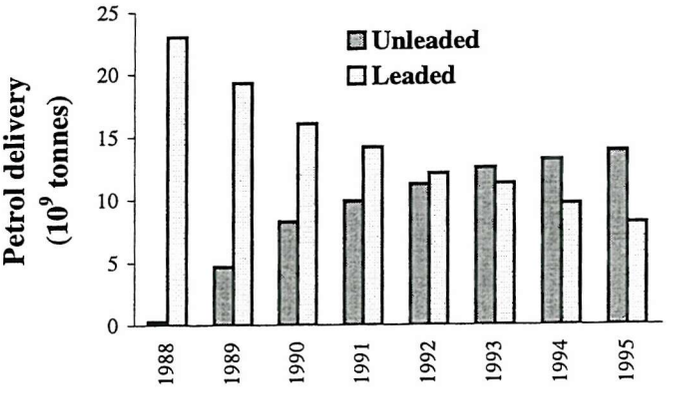

Figure 7.3:
Delivery of leaded and unleaded petrol by year.
Data from Associated Octel Co. Ltd..

in the UK may be estimated by assuming that a mixture of Australian and British Columbian ores is used in a ratio of 70:30, yielding an average $^{206}Pb/^{207}Pb$ ratio of 1.076. Petrol samples collected directly from pumps within the Southampton region and analysed by ICP-MS during the course of this study yield $^{206}Pb/^{207}Pb$ ratios in the range 1.059 ± 0.003 to 1.079 ± 0.003 (Monna *et al* 1997; Appendix C). These results are in good agreement with determinations made by Delves (1988) for the Southampton and Edinburgh regions (1.065 ± 0.003) and Sugden *et al* (1993) for the Edinburgh region (1.056 to 1.093; n=9) and are useful in assigning an approximate isotopic ratio to this important lead source.

Country	1972 tonnage	Major district	Host rock age	$\frac{^{206}Pb}{^{204}Pb}$	$\frac{^{206}Pb}{^{207}Pb}$	$\frac{^{206}Pb}{^{208}Pb}$
USA	619000	Missouri	Pennsylvanian	21.78	1.385	0.5342
		Idaho	Precambrian	16.45	1.052	0.4525
Australia	451000	Mt. Isa and Broken Hill	Precambrian	16.08	1.037	0.4465
Canada	419000	British Columbia	Precambrian	16.68	1.064	0.4557
		New Brunswick	Ordovician	18.39	1.160	0.4770
Peru	208000	Cerro de Pasco	Miocene	18.86	1.200	0.4816

Table 7.1:

Lead isotopic data of major ore bodies (from Chow *et al* 1975).

7.1.4 *Lead isotopes in saltmarsh sediments*

Lead in the natural environment may be present as several different chemical species and it is to be expected that lead sourced from different provenances may be preferentially incorporated into particular environmental materials. Natural mineral lead, for example, is present chiefly in lattice-bound sites whereas anthropogenic lead is more likely to occupy exchangeable locations in oxide and organic phases (Shirahata *et al* 1980; Hamelin *et al* 1990). The lability of the anthropogenic lead fraction during post depositional chemical processes is therefore typically enhanced compared to the natural fraction (Kersten *et al* 1992) and such diagenesis may further enhance the segregation of the two components into different sedimentary phases. Variations in the isotopic composition of lead being deposited within a salt marsh arise when the relative contributions derived from a number of different lead sources, each having its own characteristic isotope signature, are not constant over time. The complex mixture of lead ores

used for industrial puposes in variable amounts at different times, presumably dictated by their availability and cost, has been revealed by reconstructions based on snow, soil and sediment records (see *Geochim. Cosmochim. Acta,* 1994, v.58). An accreting sediment prism, such as a salt marsh, may record within its layers the changing isotopic signature of lead entering the estuarine environment over the period since sediment accretion began.

The interpretation of vertical profiles of lead isotope abundances in terms of the historical record of lead use preserved within the sediment sequence assumes the relative immobility of lead following deposition. Since several studies have implicated lead to be involved in geochemical cycles taking place during early diagenesis (e.g. Urban *et al* 1990) the likely effects of any redistribution of this element within the sediment sequence under scrutiny must be investigated prior to considering the sediment record as representative of the historical flux (Cundy *et al* 1997; Appendix C).

The complex historical pattern of lead use in Europe implies that any reservoir for this element in the environment may potentially accumulate an overall isotopic signature that changes over relatively short timescales. Kersten *et al* (1992) were able to distinguish between two types of air mass moving over the German Bight according to the isotopic composition of aerosols collected there. The ratio of $^{206}Pb/^{207}Pb$ varied from background modern lead values of 1.20 (air masses having passed almost exclusively over the North Sea) to anthropogenic signals as low as 1.10 (air masses having crossed the UK mainland). The Southampton Water region may therefore be expected to receive lead from a variety of widespread sources, including other European industrial emissions, due to the movement of air masses across the continent.

Historical pattern of lead use

Year	Period	Anthropogenic events	^{206}Pb / ^{207}Pb
~1976	Industrial	Reduction in petrol lead reduces main source of Pb to atmosphere	...increasing...
~1930	Industrial	Internal combustion engines use Pb from imported ores	Precambrian Pb ores **1.04 - 1.06**
~1800	Early-industrial	Major smelting of domestic ores; many industrial uses of lead	U.K Pb ores and coal **1.17 - 1.19**
pre-1800	Pre-industrial	Comparatively minor use since Roman times	Background values ≈ **1.18** in study area

Table 7.2:

General trend of $^{206}Pb/^{207}Pb$ ratio in Europe as a result of anthropogenic lead use.

7.2 Results

Detailed investigation of the isotopic composition of lead in core HySR5 has been performed at a sampling resolution of one centimetre (Figure 7.4). In order to interpret these data fully it is necessary to consider the measured isotopic variability in concert with the following parameters:

- total lead concentration within the core,
- the relative contributions of lead from natural and anthropogenic sources,
- the timescale of sediment accretion,
- the diagenetic behaviour of lead within this area of the marsh.

The technique used to prepare samples for introduction into the ICP-MS involves a double acid leach of the sediments, using *aqua regia* followed by hydrochloric acid. This procedure may not quantitatively extract all of the lead from the sample and this aspect also requires consideration (see discussion below).

7.2.1 *Sample preparation*

In determining the isotopic composition of lead extracted from these sediment samples it is important to consider which fractions, if not all, of the total lead present within the sample pass through the preparation stages and are available for analysis. The lead fraction analysed here by ICP-MS is that portion removed from the sediments during refluxing with *aqua regia* followed by 6N HCl. No effort was made in this study to quantify the efficiency and nature of lead removal from the sediments because the procedure used is similar to that adopted by Cundy (1994). Despite slight differences in the experimental method (Cundy's use of a double *aqua regia* leach rather than introducing hydrochloric acid during the second stage) the results obtained for sediments from the River Hamble salt marsh (Cundy 1994) demonstrate the efficiency of the acid extractions and their effect on the measured lead isotope ratios (Table 7.3). Three different sediment samples were each subjected to two sequential *aqua regia* extractions, followed by complete HF digestion of the residue, to compare the lead isotopic compositions obtained during these individual stages with the overall value obtained from the standard preparation (Cundy 1994).

Sample	$^{206}Pb/^{207}Pb$			
	1st Aqua Regia	2nd Aqua Regia	HF Digestion	Standard Procedure
HB2/6	1.12	1.11	1.20	1.12
HB2/7	1.11	1.11	1.20	1.12
HB2/9	1.12	1.12	1.20	1.12
% total Pb	87	11	2	98

Table 7.3:

$^{206}Pb/^{207}Pb$ isotopic composition of different chemical extraction stages (from Cundy 1994)

The chemical leach removes almost all of the lead from the sediment, leaving unaffected a residual fraction with a high $^{206}Pb/^{207}Pb$ ratio corresponding closely to that of local inherent mineral lead. The lead isotope ratios determined for samples which have passed through the similar method employed in this study are therefore likely to similarly represent the weighted mean of ~98 % of the sedimentary lead load, which may be assumed to consist of all of the anthropogenic fraction and most of the detrital component.

The ratio of $^{206}Pb/^{207}Pb$ has generally been adopted as the most sensitive to change in environmental samples and it is also the easiest ratio to determine reliably by the ICP-MS technique (Bacon *et al* 1996). Analysis of lead isotope ratios using thermal ionisation mass spectrometry (TIMS) is superior in precision but such a facility was not available within the Geology Department at the time of this study. To facilitate presentation and discussion of the data, only the $^{206}Pb/^{207}Pb$ ratio needs to be considered for examination of the vertical variation in the lead isotope composition. The interdependency of pairs of isotope ratios (such as $^{206}Pb/^{208}Pb$ against $^{206}Pb/^{207}Pb$) are used to interpret the effects of variable contributions from different lead sources (Figure 7.5). Such plots may permit the identification of a single lead source if data points form a cluster, multiple sources if several clusters are obtained, or from a mixing of sources if data points form linear arrays (Hurst *et al* 1996). The inclusion of various known source ratios within these charts may greatly assist the interpretation of the measured compositions.

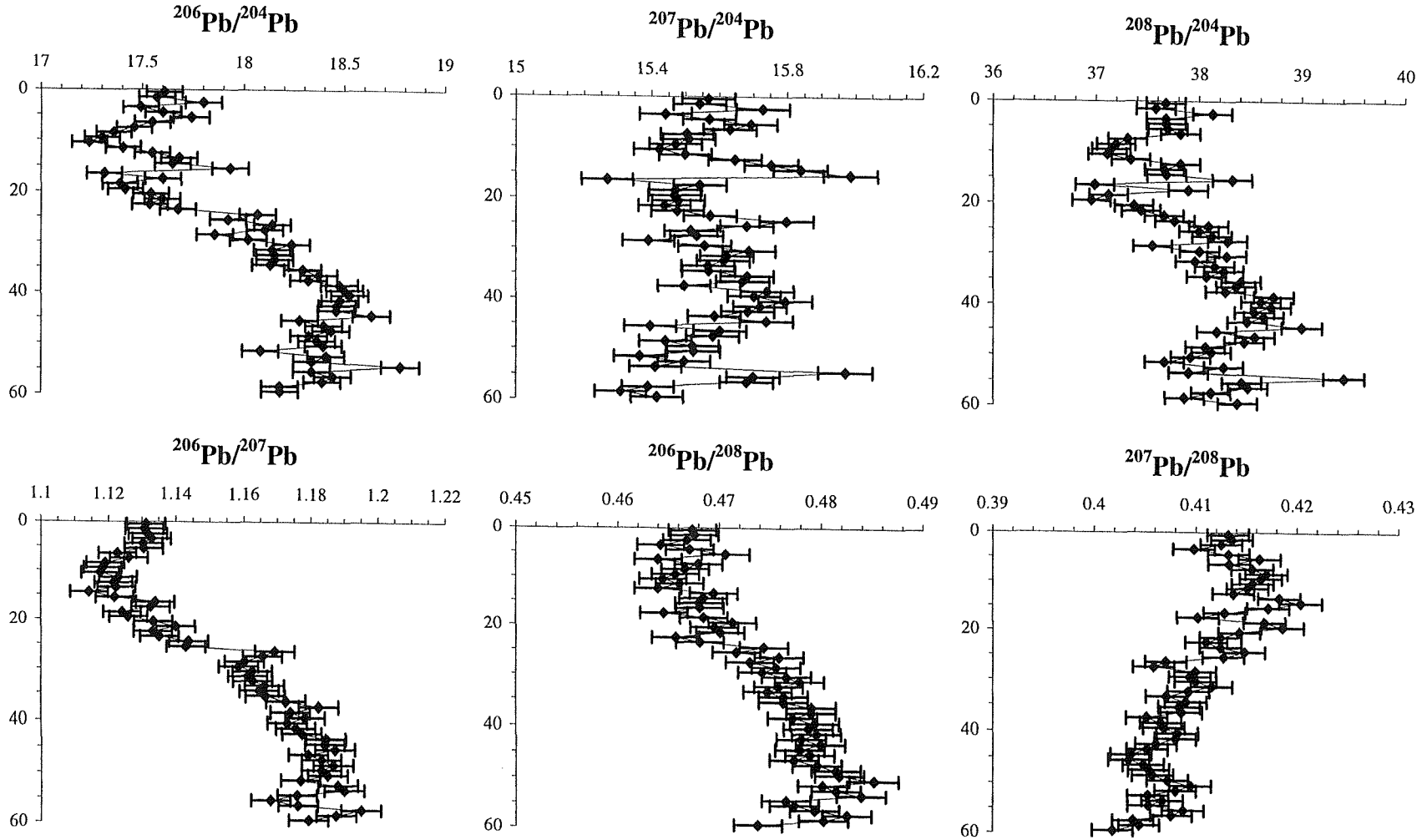

Figure 7.4: Variation of stable lead isotope ratios with depth in core HySR5. Error bars are drawn at 0.5% (~1 standard deviation) of the measured ratio.

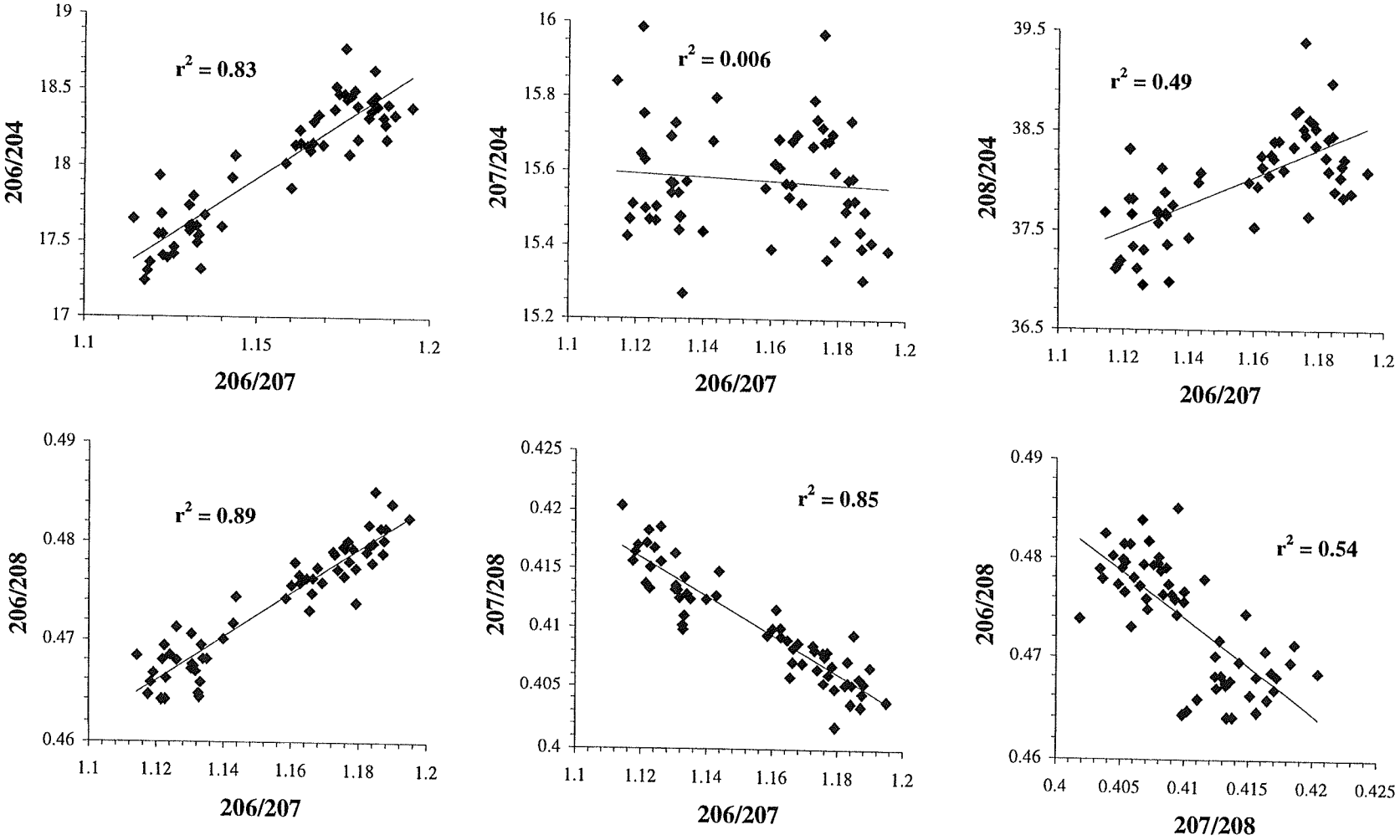

Figure 7.5:
Correlative plots of different stable lead isotope ratios.

7.3 Discussion

The isotopic composition of lead within core HySR5 is not uniform throughout the length of the core revealing that a number of isotopically distinct sources have supplied lead to the accreting sediment prism. The various lead isotope ratios exhibit different sensitivities to the mixing of multiple lead sources (Figures 7.4 and 7.5). Due to the lower abundance of ^{204}Pb and associated errors of measurement the scatter within the data involving this isotope is greater than that of the other ratios. For this reason contemporary isotope data are often presented as plots of only the most useful isotope ratios, particularly $^{206}Pb/^{207}Pb$ (e.g Farmer *et al* 1996). A similar practice is adopted throughout the following discussion when considering the vertical distribution of lead within the sediments. Plots of $^{206}Pb/^{207}Pb$ vs. $^{206}Pb/^{208}Pb$ and $^{206}Pb/^{207}Pb$ vs. $^{206}Pb/^{204}Pb$ are useful for the identification of different end-member lead sources and demonstrating the mixing of anthropogenic and natural lead.

7.3.1 *Vertical distribution*

7.3.1.1 40-50 cm depth

The mean isotopic composition of the basal section (40-50 cm depth) of core HySR5 (Figure 7.4) may be taken to represent the value of local lead prior to widespread contamination by anthropogenic lead. The increased scatter of the data below 45 cm depth is probably due to the inclusion of variable amounts of a separate sedimentary phase (gravel present amongst the mud) during sample processing. Should this gravel contribute an additional source of lead to the sample material then the measured overall ratios are likely to be affected at random. No gravel fragments were detected at depths shallower than 42 cm. Chronological determinations reveal that the sediments at 40-50 cm depth were deposited during the early to mid-nineteenth century and therefore might be expected to preserve an isotopic signature characteristic of the environmental lead load for this period. Comparison of $^{206}Pb/^{207}Pb$ and $^{206}Pb/^{208}Pb$ isotope ratios for core HySR5 with literature values pertaining to the early-industrial use of lead, as well as independently determined natural mineral lead ratios for the Southampton Water region, reveal their "background" composition (Table 7.4).

Material	$^{206}Pb/^{207}Pb$	$^{206}Pb/^{208}Pb$	Reference
HySR5 sediment; mean 40-50 cm depth	1.18	0.48	This work
So'ton Water, pre/early -Industrial sediment	1.18	0.48	Croudace and Cundy 1995 Cundy *et al* 1997
UK ore galena	1.17 - 1.18	0.48	Moorbath 1962
British lead ore and Scottish coal	1.17-1.19		Sugden *et al* 1993 Farmer *et al* 1996
British 19th century aerosols	1.170		Bacon *et al* 1996
Pre-industrial European river deposits	1.19 - 1.21		Kersten *et al* 1992
Pre-industrial European aerosols	1.21	0.49	Grousset *et al* 1994

Table 7.4:
Background lead isotope data.

The isotopic composition of background lead within the European continent appears reasonably well constrained within the range $1.18 < {}^{206}Pb/^{207}Pb < 1.21$, and the deeper sediments of core HySR5 display good agreement with this natural value. It is likely that the ratios at the base of core HySR5 may represent the mixing of the natural lead component with an industrial anthropogenic component derived dominantly from domestic British lead ores and coal. Calculations (see below) reveal that approximately 40-50% of the lead present in this section of the core is anthropogenic in origin. Early-industrial aerosols containing appreciable amounts of anthropogenic lead, collected since 1856 at the Park Grass experimental site, Rothamstead, UK, yield average $^{206}Pb/^{207}Pb$ ratios of 1.17, similar to unpolluted materials in that locality (Bacon *et al* 1996) and similar to lead ore from Scottish mines (Sugden *et al* 1993). Anthropogenic lead derived from the smelting of domestic ores and the burning of local coal is difficult to distinguish from natural European mineral lead on the basis of isotopic characteristics alone and thus these sources may be conveniently grouped together as pre/early-industrial lead (Croudace and Cundy 1995).

7.3.1.2 26-40 cm depth

Immediately above the basal section of core HySR5 the $^{206}Pb/^{207}Pb$ ratio declines upwards through the sediment profile. An inflection at 30 cm depth gives rise to a slight increase in the isotope ratio, above which, over 25-27 cm depth, the decrease from 1.169 to 1.143 is very

sharp. This depth horizon corresponds to a major change in the sedimentary facies from grey minerogenic sediments beneath to brown and grey-brown organic-rich peats above. The total lead concentration of the core samples also shows a relationship to this boundary with a marked increase in concentration commencing immediately above it. The correlation between the shift in lead concentration, isotopic characteristics and sedimentary facies may be significant or may simply be a random coincidence. The declining $^{206}Pb/^{207}Pb$ ratio is indicative of the introduction of a lead source with an isotopic composition different from that of the pre/early-industrial component. The rising dominance of this source takes place gradually over depths of 40-26 cm followed by a sudden increase above the facies boundary, as also revealed by the increasing concentration of excess lead in the lower section of the peat (Figures 6.1-6.3). This increase in the lead load may be due to increased deposition at the sediment surface during accretion or alternatively may be caused by post-depositional migration of the element during early diagenesis. Both of these processes are able to bring about changes in the isotopic composition of the total lead present at any given depth, in the former case through the adddition of different amounts of isotopically distinct lead sources, and in the latter case through the increased lability of anthropogenic lead over the natural lead fraction.

Humic substances are known to represent a major reservoir for anthropogenic lead released into the environment (Shirahata *et al* 1980) due to the affinity of the metal for the many binding sites found on the organic molecules of which they are composed. The correlation observed between lead concentration and organic matter content within the peaty section of this sediment core, however, does not reveal a strong association (Table 6.3). However, the similarity between the profiles of Pb/Al and C_{org} (Figures 6.1-6.3 and 3.5) is suggestive of the concentration of lead within the organic-rich bands. This matter is discussed at the end of this chapter following consideration of a second lead isotope profile from Hythe Marsh.

7.3.1.3 0-26 cm depth

The $^{206}Pb/^{207}Pb$ ratio of HySR5 sediments within the surficial core section exhibits a c-shaped profile (Figure 7.4). The lead concentration displays a peak at the base of the upper organic-rich horizon (12-13 cm depth) where the lead isotope ratio forms a broad minimum from 10-16 cm depth. This observation is consistent with the mixing of a low $^{206}Pb/^{207}Pb$ ratio anthropogenic source with the natural lead present in the detrital mineral phase, which yields an overall isotopic composition equal to the weighted mean of the various source terms. The effects of this mixing are greatest where the anthropogenic lead concentration is at its highest. Towards the surface of the core the $^{206}Pb/^{207}Pb$ ratio increases to 1.131-1.133 revealing the declining

dominance of the low ratio source. The range 1.12 < $^{206}Pb/^{207}Pb$ < 1.14 agrees well with previously published data for recent subtidal sediments from this region (Croudace and Cundy 1995; Cundy *et al* 1997).

7.3.1.4 Influence of diagenetic processes on the vertical profiles

The lead present in any particular environmental sample may originate from a mixture of sources, each with a characteristic stable isotopic composition. In an estuarine setting the inherent local mineral lead and any anthropogenic industrial lead are likely to become mixed during estuarine processes, although they may still occupy distinct phases within the sedimentary materials. The variable relative abundance of the four stable lead isotopes throughout core HySR5 implies non-constancy of the isotopic signature of lead supplied to different depths of the sediment profile. Such variability may result either from temporal changes in the source of lead to the surface of the accreting sediment or through post-depositional processes favouring the accumulation of lead from a particular source within certain depth horizons. The overall measured profile of the lead isotopic abundance almost certainly results from a combination of these two effects. Whilst such diagenetic processes may interfere with any attempted correlation of depth with the historical flux of lead to the marsh they should not affect the ability to distinguish between anthropogenic and natural lead sources, provided that suitable end-members can be identified.

7.3.2 *Correlation between isotope ratio pairs*

The plotting of one isotope ratio against another may reveal the mixing of lead derived from different sources. The most useful relationships in the case of core HySR5 are $^{206}Pb/^{204}Pb$ vs $^{206}Pb/^{207}Pb$ and $^{206}Pb/^{208}Pb$ vs $^{206}Pb/^{207}Pb$ (Figure 7.6) thereby accounting for all four of the stable isotopes. The position of the local natural lead component may be plotted from the data of Croudace and Cundy (1995) along with data for lead ores known to be imported and consumed within Britain (Table 7.1). The sediment samples exhibit a pattern of isotope variation which reveals the progressive mixing of anthropogenic Precambrian ore lead with the early-industrial component (natural and domestic ore lead) present at depth. The local release of such Precambrian lead ore is likely to be significantly derived from the burning of alkyl-leaded fuels in internal combustion engines (Sugden *et al* 1993), providing an anthropogenic lead load dominantly in aerosol form, although discharge of lead directly into estuarine waters from local industry is also probable. Both of these provenances are able to contribute lead with an isotope signature characteristic of imported ores. The scatter of the isotope ratio dataset

determined for Hythe Marsh probably arises from short term fluctuations in the deposition of lead from many potential sources.

7.3.3 *Lead isotopes and lead concentration*

7.3.3.1 The total lead fraction

The mixing of anthropogenic and natural lead sources within the matrix of an accreting sediment prism ought to result in a perturbation of the natural isotopic signature in direct proportion to the amount of non-local lead introduced. Plots of the isotopic composition of the salt marsh samples against $1/Pb_{tot}$ thus may be useful in revealing the relationship between the proportion of industrial lead in the sediments and their resultant lead isotope characteristics (Figure 7.7).

In the case of core HySR5 these plots yield data with considerable scatter and hence reveal the non-proportionality between the overall lead isotope ratios of the sedimentary material and the concentration of lead therein. There are two factors which may be invoked to account for this observation. Firstly, separate sediment samples which contain the same total Pb concentration may each be comprised of a different proportion of natural lead due to variations in the predominance of detrital mineral particles throughout the core profile. The total lead concentration of the sediments is therefore not strictly proportional to the concentration of anthropogenic lead residing within any given sample. Secondly, the isotopic composition of the excess lead being incorporated into the salt marsh cannot be expected to have remained constant over the period of sediment accumulation, thus giving rise to a variable effect upon the sediment isotopic signature dependent on the mean source ratio. For example, the mixing, in equal proportions, of natural lead from the study region ($^{206}Pb/^{207}Pb \approx 1.18$) with lead derived either from domestic lead ores ($^{206}Pb/^{207}Pb \approx 1.17$) or from imported Australian ores ($^{206}Pb/^{207}Pb \approx 1.04$) can yield similar sedimentary lead concentrations with widely differing overall isotope ratios of 1.175 and 1.110, respectively. It is therefore not only the quantity of excess lead mixing with local lead which is of concern, but also the nature of the original source of this excess lead and its intrinsic isotope characteristics.

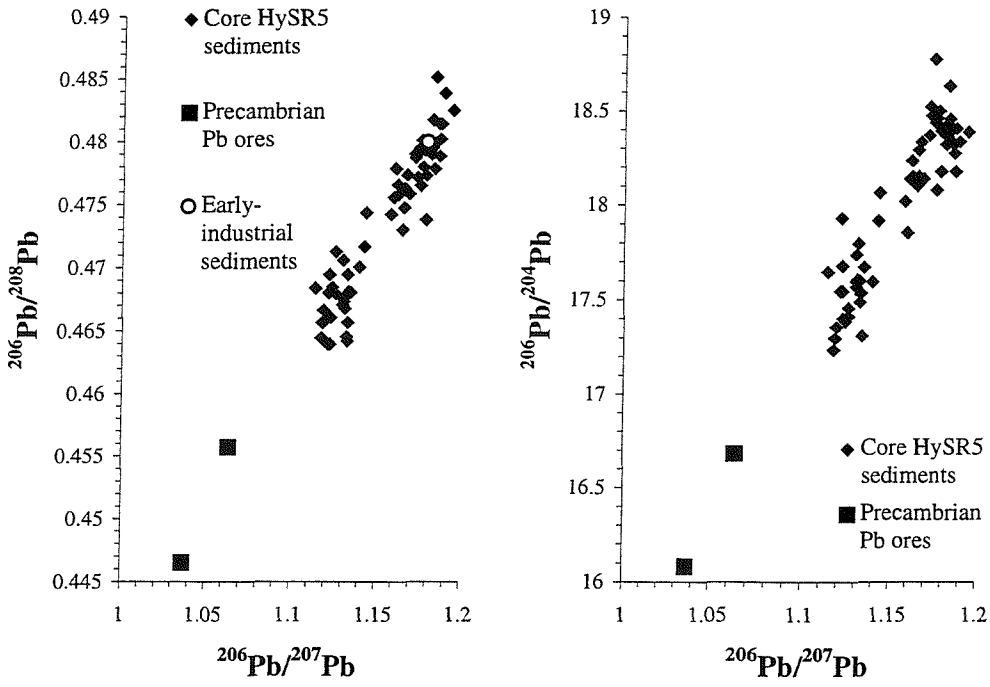

Figure 7.6:
Lead source mixing plot for lead isotopes in core HySR5.

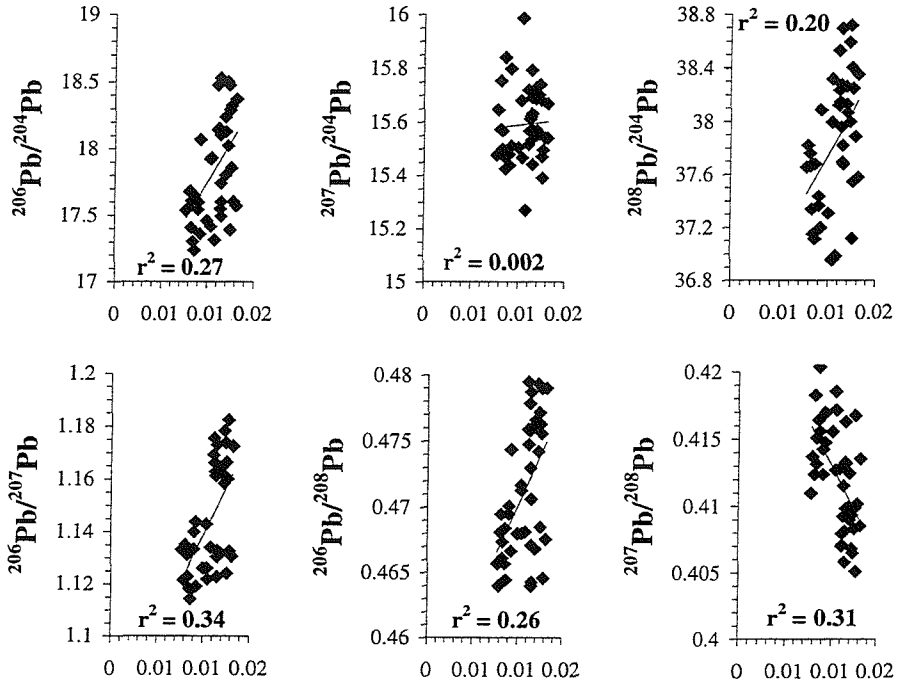

Figure 7.7:
Plots of stable lead isotope ratio vs. $1/Pb_{tot}$ for core HySR5.

7.3.3.2 The natural and excess lead fractions

The sediments found at depth within core HySR1, the deepest sediments obtained from Hythe Marsh, yield a mean lead concentration of 46 ppm and a Pb/Al ratio of 5.85 (ppm/wt.%) as being typical of the detrital mineral component. This may be useful in examining the other sediment cores where the detrital component cannot be estimated due to the absence of a constant value at depth. Establishing the detrital ratio of lead to aluminium allows discrimination between the excess and detrital lead concentrations (Equation 3.2):

Calculation of the inherent mineral lead concentration throughout core HySR5 reveals a pattern arising from variations in the mineral composition of the sediments (Figure 7.8). The most significant features of this profile are the decreased concentrations of natural lead apparent within the upper portion of the core, where the sediments are dominated by organic-rich horizons which dilute the mineral phase, and the basal section, where a siliceous sedimentary component is present. The overall isotope signature of the sediments is obviously affected by the variation of the inherent mineral lead content throughout the profile as this represents a significant source of lead to the marsh (20-80% of the total lead) and has a relatively distinct radiogenic isotope signature. The excess lead concentration profile for core HySR5 (calculated using Equation 3.2) reveals two large concentration peaks in the upper core section accounting for between fifty and eighty per cent of the total lead content (Figure 7.8). The mixing of natural and anthropogenic lead sources in Hythe Marsh is evident from plots of the measured isotope ratio against the percentage of natural lead (Figure 7.9). This also further reveals the different sensitivities of the various isotope pairs to such a mixing of sources and hence their respective applicability for source apportionment.

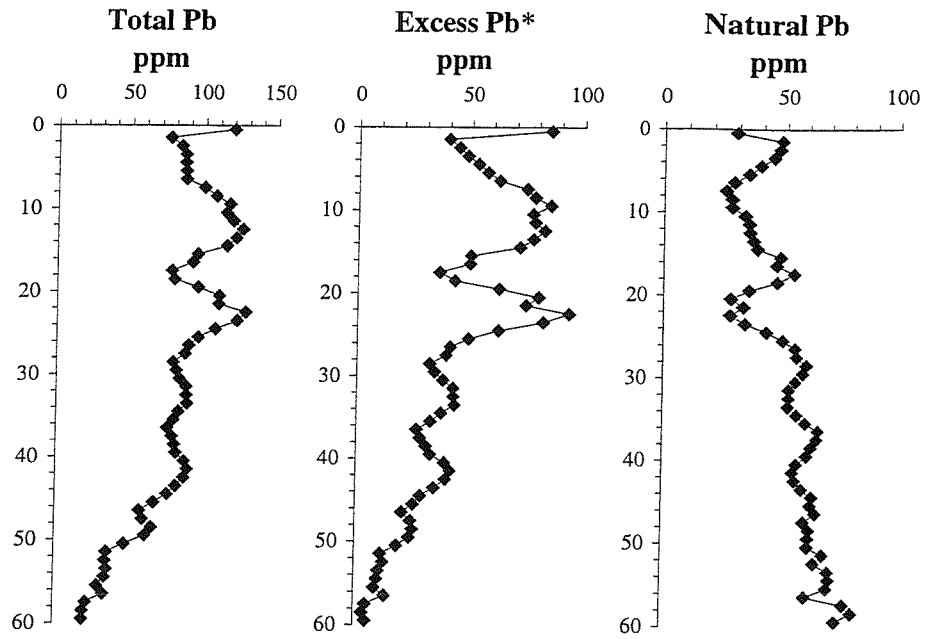

Figure 7.8:
Core HySR5 total, excess and natural (mineral) lead profiles

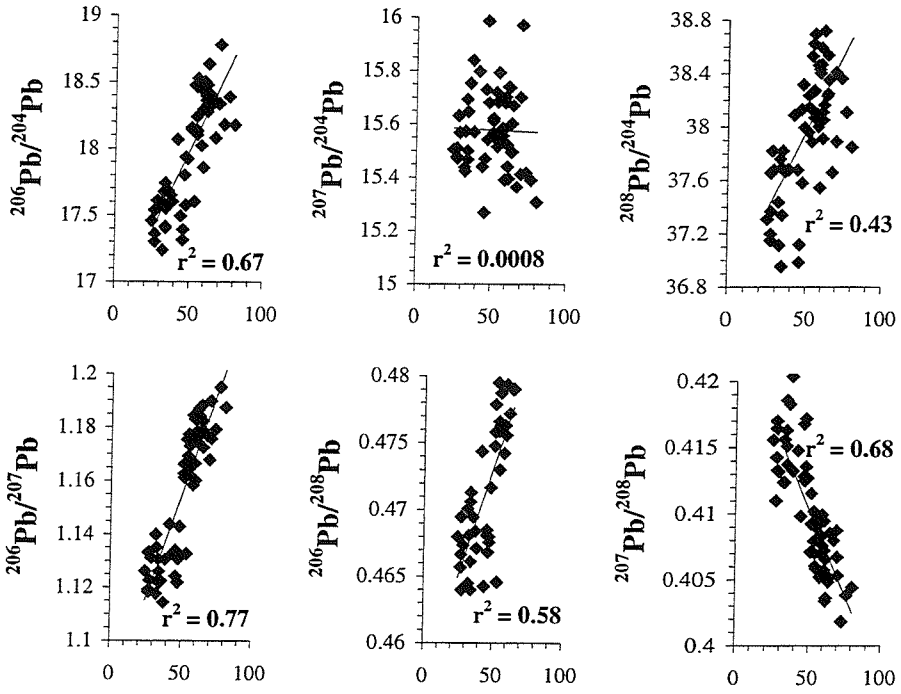

Figure 7.9:
Plots of stable lead isotope ratio vs. % natural lead

7.3.3.3 Anthropogenic lead isotope ratios

Discrimination between the detrital and excess lead components, combined with establishing the isotopic composition of the former, permits calculation of the isotopic composition of the non-detrital lead within the sedimentary load (Equation 7.1; from Ng and Patterson 1982):

$$R_{xs} = [(Pb_{meas} * R_{meas}) - (Pb_{det} * R_{det})] / (Pb_{meas} - Pb_{det}) \quad \textbf{Equation 7.1}$$

where R_{xs} is the isotope ratio of the excess lead fraction,
Pb_{meas} is the total Pb concentration (ppm),
R_{meas} is the overall sediment isotope ratio,
Pb_{det} is the detrital lead concentration (ppm),
and R_{det} is the isotope ratio of the detrital fraction.

The excess lead fraction corresponds to that lead which is not derived from the mineral lattice of sedimentary particles. Most of this lead is likely to be anthropogenic in origin and the isotopic characteristics displayed are of interest to determine the sources of lead ore used for industrial purposes. The perturbation of the natural lead isotopic signature of Hythe Marsh at any given depth is dependent upon the relative proportions of anthropogenic and natural lead present and the isotopic composition of the former source (the latter is assumed to be constant). The various sources of industrial lead ought therefore to be detectable within the anthropogenic fraction of the salt marsh lead load.

The excess isotope ratios calculated from the data are consistent with the anthropogenic use of lead ores with a wide range of isotopic signatures. The values determined for anthropogenically-derived isotope ratios are likely to reflect the pooling of different lead sources within the anthropogenic fraction of the sedimentary lead load and thus might be expected to display ratios characteristic of the mixing of such sources. The plot of $^{206}Pb/^{208}Pb$ vs $^{206}Pb/^{207}Pb$ yields a linear array of data suggesting that the mixing of different anthropogenic lead sources has taken place within the marsh sediments over time as a result of changes in the characteristics of deposited lead (Figure 7.10). The inclusion of known anthropogenic sources on to the chart assists in the demonstration of this mixing trend.

Examination of the vertical distribution of the anthropogenic lead isotope ratios indicates that significant differences exist throughout the length of the core and that this non-detrital portion of the lead load has not been thoroughly mixed during early diagenesis (which would generally serve to remove the anthropogenic isotopic differences between different depth intervals). The deeper samples have an isotopic signature similar to that determined for early-industrial period aerosol materials (Bacon *et al* 1996), the lead of which is sourced mainly from domestic lead ores and local sources of coal (Sugden *et al* 1993). At shallower depths the mean anthropogenic signature becomes heavily influenced by imports of foreign, Precambrian ores, probably from Australia and British Columbia, for use principally as lead alkyl additives in petrol fuels. Most samples, however, fall between these end-member ratios and are representative of a mixture of different sources contributing to the total lead content of the sediment.

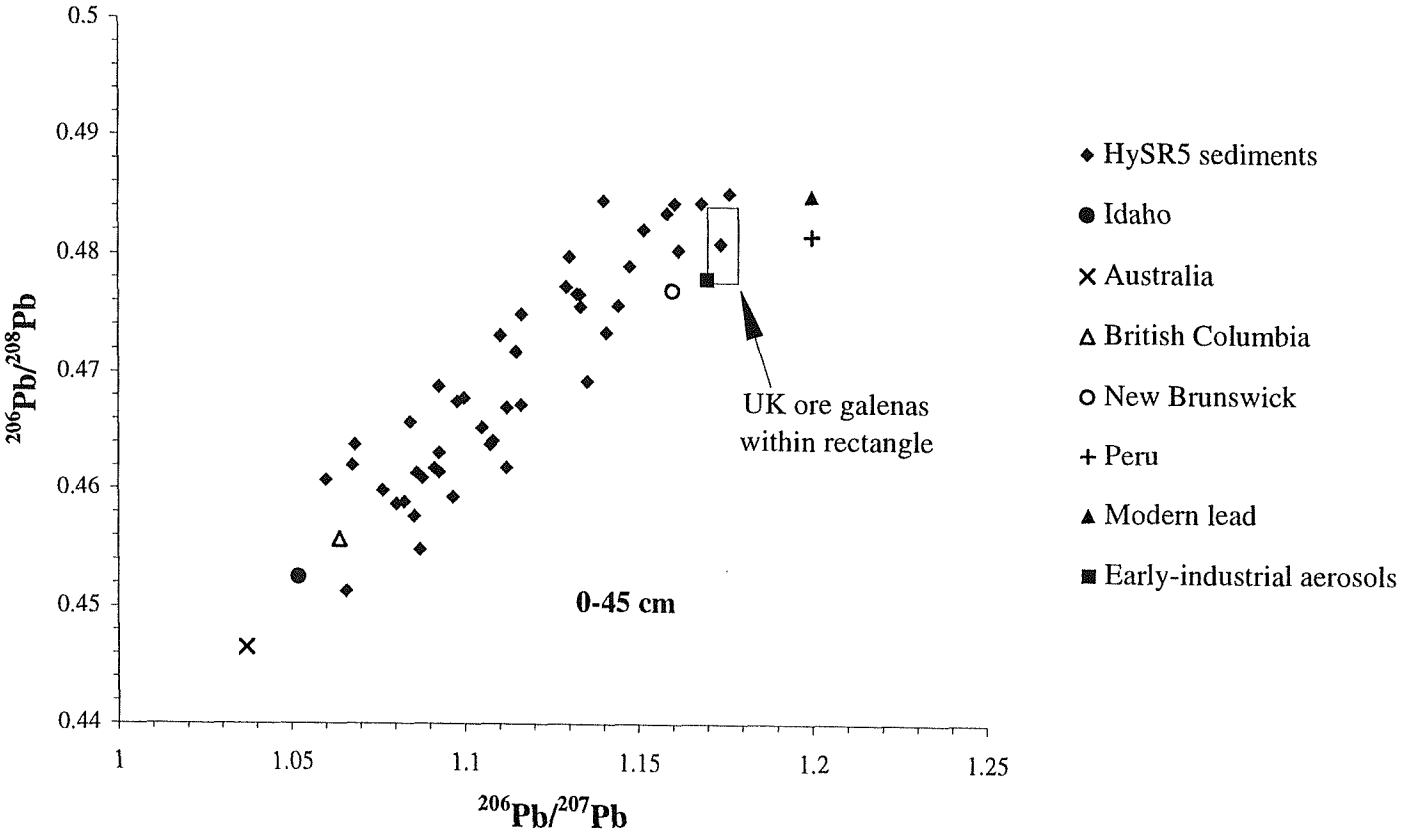

Figure 7.10:
Anthropogenic lead isotope mixing plot determined for core HySR5.

7.3.4 *The timescale of lead deposition*

The determination of sediment accretion rates for core HySR5, through the application of ^{210}Pb- and ^{137}Cs-based techniques, yields mean values of 0.073 and 0.082 g cm^{-2} yr^{-1}, respectively. Use of these figures to calculate a chronology of sediment accumulation at this location on the marsh implies that the core contains a record of sediment which has been accreting since the beginning of the nineteenth century (Figures 4.12 and 4.13). Investigation of the temporal record of isotopic changes within the sediments is reported here in order to obtain as complete a picture as possible of the processes governing lead abundance within the sediment prism. The ^{206}Pb/^{207}Pb profile determined in a second core (HyPb) is compared to that within core HySR5 to assess differences in the accumulation and post-depositional behaviour of lead between two different area of the marsh. The bulk geochemical composition data of these two sediment profiles display considerable differences with respect to organic carbon distribution (Figure 3.4) and this may be of benefit in assessing the importance of the diagenetic processes discussed above involving carbon and lead.

7.3.4.1 HySR5

The oldest sediments within that section of the core profile under consideration here contain the lead isotope signatures characteristic of early-industrial lead for this region. The ^{206}Pb/^{207}Pb ratio ranges from between 1.16 and 1.19 over depths of 26-50 cm, corresponding to sediments deposited during the period 1810-1920 AD (Figure 7.11). Within the sediments deposited during 1915-1925 a sharp decrease in the ^{206}Pb/^{207}Pb ratio is apparent. From 1920 to the present day the sediment isotope ratios are considerably less radiogenic than those deeper in the core on account of mixing with industrial lead derived from more ancient ore bodies. In a high resolution study of the lead isotopic composition of a sediment core from Loch Lomond, Scotland, incorporating ^{137}Cs dating to yield the mean sediment accumulation rate, Farmer *et al* (1996) reported a sharp decline in the ^{206}Pb/^{207}Pb ratio commencing from 1929, soon after the introduction of leaded petrol (Nriagu 1989).

7.3.4.2 HyPb

The sediments of core HyPb consist of uniform pale grey muds, containing a few roots, over 21-37 cm depth. The peaty section of the core is restricted to the surficial 10 cm, although the presence of an organic-rich band is revealed by elevated organic carbon concentrations between 6-14 cm depth. The absence of any major facies change (as revealed by visual logging prior to

core sectioning) throughout the central section of the core highlights the difference between the sedimentary characteristics of cores HySR5 and HyPb.

Interpretation of the ^{210}Pb distribution within core HyPb yields a mean mass accumulation rate of 0.089 g cm^{-2} y^{-1}, which is used to derive the core chronology (Figure 4.12). The temporal variation in the $^{206}Pb/^{207}Pb$ ratio throughout the core profile exhibits a broadly similar trend to that of core HySR5 (Figure 7.11). Between 1820-1900 the $^{206}Pb/^{207}Pb$ ratio present within each core is restricted to the range 1.16-1.18, and then declines sharply during the period 1915-1930 to a value of 1.13-1.14, remaining relatively low throughout the upper section of the core. The initiation of the decline in $^{206}Pb/^{207}Pb$ ratio within core HyPb takes place at an earlier date (~1890) than in core HySR5 which, if representative of the true deposition, may be due to the proximity of the former core to the estuarine water mass. In a study of the isotopic character of lead deposited from the atmosphere at a grassland site in S.E. England, Bacon *et al* (1996) found a similar reduction in the composition of the aerosols to commence during the last decade of the nineteenth century.

Studies of the isotopic composition of lead in the most recent layers of accumulating sediment sequences often report a subsequent rise in the $^{206}Pb/^{207}Pb$ ratio on approaching the sediment surface (e.g. Moor *et al* 1996; Farmer *et al* 1996). This is attributed to the reduction of alkyl-lead additives in petroleum fuels initiated during the late 1960s and enforced more rigorously in 1986 (Associated Octel, *pers. com.*). In the sediment cores from Hythe Marsh there is little clear evidence of such a shift in the overall isotopic composition, although an increase in the anthropogenic $^{206}Pb/^{207}Pb$ ratio (from ~1.080 to ~1.115) is apparent throughout the upper 2 cm of both cores (Figure 7.11). This corresponds to sediment deposited over the last decade and may be due to the reduction of environmental lead contamination from internal combustion engines. However, the sedimentary record of isotopic change within these cores is not considered to be reliable enough to allow quantification of such short-term variation. Strong evidence exists for the involvement of lead in the redox cycle of both iron and manganese within core HyPb (discussion in Chapter 6) and the apparent temporal history of lead isotope deposition is likely to have been affected. The fact that both sediment cores reveal a similar pattern of use of anthropogenic lead, despite the implication of different processes affecting the lead distributions within each core, suggests that historical records may be at least partially preserved (Cundy *et al* 1997; Appendix C).

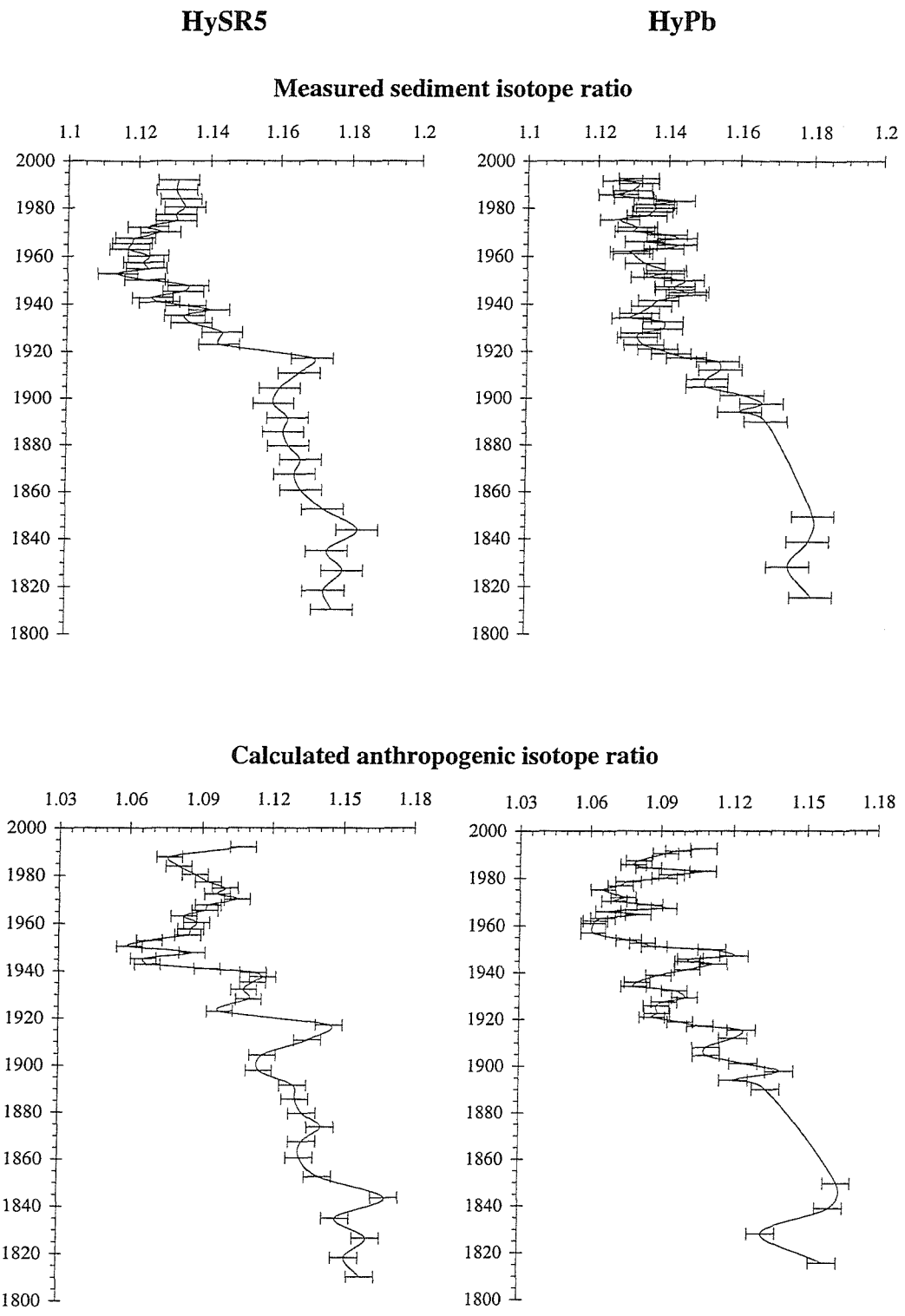

Figure 7.11:

$^{206}Pb/^{207}Pb$ ratios in two separate sediment cores from different areas of the study site, plotted against time of deposition of the sediment (determined from ^{210}Pb chronology). Error bars are drawn at 0.5% (~1 standard deviation) of the measured ratio.

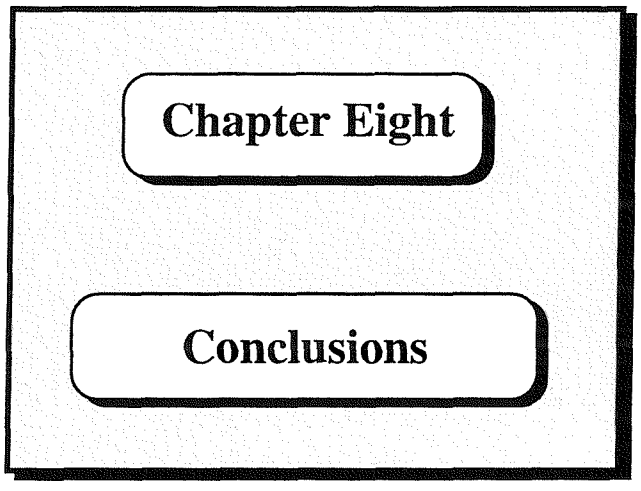
Chapter Eight
Conclusions

Analysis of the geochemistry of sediment cores from Hythe Marsh has yielded high resolution depth-concentration profiles for a number of elements and radionuclides. The main conclusions of this research are summarised below:

- **Geochemistry of major and trace elements**

- Concentration profiles of elements chiefly bound within mineral lattice sites (Si, Al, K, Ti, Cr) are governed by the relative proportions of mineral and organic particles in the sedimentary matrix. Minima observed in the abundance of each of these elements are related to depth horizons rich in organic materials. Following normalisation to aluminium the element profiles reveal a consistent sediment mineralogy both across the marsh and with depth in each core.

- The microbial demand for electron acceptors to oxidise organic carbon affects the distribution of manganese, iron and sulphur within all cores analysed. The inferred reaction zones of each of these elements generally follow the sequence predicted according to thermodynamic calculations. Reduction of manganese oxides commences at shallow depth and results in the extensive recycling of this element within the uppermost few centimetres of the sediments. Iron oxides are present throughout the upper decimetre of three of the cores, beneath which depth reactive ferric iron is depleted, thereby releasing Fe^{2+} into solution. The reactions between this species and a range of likely reduced sulphur species produced at greater depth results in the storage of these two elements as both iron monosulphides and pyrite.

- Concentration profiles of arsenic and phosphorous are heavily influenced by their association with ferric minerals in the surficial sediment layers. These two elements are thus likely to be subjected to considerable recycling along with iron, as the oxide carrier phase is buried and becomes involved in redox cycles driven by organic carbon degradation. The record of the deposition of As and P within the sediment prism is almost completely removed by processes of post-depositional redistribution.

- The behaviour of zinc and nickel within Hythe Marsh cores also discloses the control exerted on some trace metals by the cycling of secondary carrier phases within sediment sequences. The favourable accomodation of metal ions within manganese oxide mineral lattices produces a strong association between these elements within the zone of manganese recycling. A similarly strong affinity for zinc and nickel to adsorb and coprecipitate along

with iron sulphide minerals further results in their redistribution and concentration into distinct depth horizons, dictated by the redox conditions of the sediment prism. The main features of the concentration-depth profiles of Zn and Ni within Hythe Marsh may be attributed to diagenetic processes rather than aspects of their depositional history.

- The abundance of copper at the study site reveals significant anthropogenic contamination of this metal within Southampton Water, sourced mainly from effluents released by the oil refinery at Fawley. Concentration peaks of excess copper, particularly in the more minerogenic lower-marsh sediment cores, can be identified as "pollution spikes" resulting from the expansion of industrial operations along the shoreline of the estuary. Examination of the temporal flux of this metal to the sediment prism, utilising chronologies based on ^{137}Cs and ^{210}Pb dating techniques, suggests that the accreted sediments preserve a reasonable record of the local historical discharge of copper. The high anthropogenic loading relative to natural background levels, combined with a reduced tendency for copper to become involved in early diagenetic processes, is likely to be responsible for this condition.

- Anthropogenic pertubation to the occurrence of lead within Hythe Marsh is revealed by stable isotope analysis. The lead isotopic composition present throughout the sediment profile reflects the mixing of an intrinsic mineral component with lead derived from a range of industrial sources. Furthermore, the deposition of lead having any specific isotopic composition (such as that of Precambrian ore) exhibits considerable vertical variability within the cores. A comparison of two cores retrieved from contrasting areas of the marsh implies a relatively consistent pattern of lead isotopic abundance with depth, and furthermore suggests a major change in the characteristics of lead deposited before and after the period 1900-1920 A.D.. Since post-depositional remobilisation can be inferred from the association of lead with other diagenetic features (manganese oxide, iron oxyhydroxide and iron sulphide enrichments) it must be anticipated that the record of deposition has been at least partially removed. The accuracy of the historical record present at Hythe Marsh therefore requires confirmation, through further investigation into the effects of early diagenesis on lead incorporated into the sediment prism. From the results of the present study (involving analysis of Pb concentration, Pb isotopic composition and ^{210}Pb activity) it seems likely that, although subjected to some diagenetic redistribution, a significant proportion of the overall lead content remains in close proximity to the sediment layer it was buried with.

- The distribution of bromine and iodine is dictated to a large extent by the abundance of organic carbon. Differences in the behaviour of these two elements are apparent, arising from the involvement of iodine in redox reactions. This leads to a decoupling of the relationship between iodine and carbon throughout the sediment profile, particularly in those cores with lower organic contents. Ratios of halogen to organic carbon are at the lower end of those reported for estuarine and nearshore hemipelagic sediments due to the vigorous growth of terrestrial vegetation within the sediment prism.

♦ Radionuclide profiles

Radiometric determinations of the rate of sediment accretion at the study site using ^{137}Cs and ^{210}Pb yield results which are in good agreement with one another. Lead-210 appears to be incorporated into the sediment prism with a constant flux and the sediment accumulation rates appear constant, to a first approximation, over the period of marsh accumulation. The fact that this rate is slightly lower than the estimated mean sea level rise for the region may be the reason for significant marsh erosion over recent decades. Comparison between the depositional flux of both ^{137}Cs (estimated from fallout data) and ^{210}Pb (directly measured in rainfall) with the inventories determined in salt marsh cores produces fairly good agreement and reveals the incorporation of additional, marine-derived activity into salt marsh sediments.

♦ Pore water sampling

Method development of a novel pore water sampler, based on models designed and tested by other workers, appears justified by the profiles of iron and manganese obtained. The ease of preparation and deployment of this probe, in combination with the high sampling resolution provided over a metre of the sediment profile, is highly favourable compared to other devices. Unfortunately, the technique could not be developed sufficiently to allow the determination of trace element concentrations within the duration of this research project, although the ability of the apparatus to retrieve equilibrated pore water samples has been demonstrated. Wider application, involving the analysis of a greater number of solutes, ought to be possible following further refinement of the technique.

References

Algan O., Clayton T., Tranter M. and Collins M.B. (1994). Estuarine mixing of clay minerals in the Solent region, Southern England. *Sed. Geol.* **92**, 241-255.

Allen J.R.L. and Rae J.E. (1986). Time sequence of metal pollution, Severn Estuary, Southwest Britain. *Mar. Poll. Bull.* **17**, 427-431.

Allen J.R.L., Rae J.E. and Zanin P.E. (1990). Metal speciation (Cu, Zn, Pb) and organic matter in an oxic salt marsh, Severn Estuary, Southwest Britain. *Mar. Poll. Bull.* **21**, 574-580.

Anspaugh L.R., Catlin R.J. and Goldman M. (1988). The global impact of the Chernobyl reactor accident. *Science* **242**, 1513-1519.

Appleby P.G. and Oldfield F. (1992). Application of ^{210}Pb to sedimentation studies. In: Ivanovich M. & Harmon R.S. (Eds.), *Uranium series disequilibrium: applications to earth, marine and environmental sciences.* 2nd edn., OUP, Oxford, pp. 731-778.

Armannsson H., Burton J.D., Jones G.B. and Knap A.H. (1985). Trace metals and hydrocarbons from the Southampton Water region, with particular reference to the influence of oil refinery effluent. *Mar. Environ. Res.* **15**, 31-44.

Armentano T.V. and Woodwell G.M. (1975). Sedimentation rates in a Long Island marsh determined by ^{210}Pb dating. *Limnol. Oceanogr.* **20**, 452-456.

Aston S.R. and Duursma E.K. (1973). Concentration effects on ^{137}Cs, ^{65}Zn, ^{60}Co and ^{106}Ru sorption by marine sediments, with geochemical implications. *Neth. J. Sea Res.* **6**, 225-240.

Bacon J.R., Jones K.C., McGrath S.P. and Johnston A.E. (1996). Isotopic character of lead deposited from the atmosphere at a grassland site in the United Kingdom since 1870. *Environ. Sci. Technol.* **30**, 2511-2518.

Belzile N. and Lebel J. (1986). Capture of arsenic by pyrite in nearshore marine sediments. *Chem. Geol.* **54**, 279-281.

Belzile N. and Tessier A. (1990). Interactions between arsenic and iron oxyhydroxides in lacustrine sediments. *Geochim. Cosmochim. Acta* **54**, 103-109.

Bendell-Young L. and Harvey H.H. (1992). The relative importance of manganese and iron oxides and organic matter in the sorption of trace metals by surficial lake sediments. *Geochim. Cosmochim. Acta* **56**, 1175-1186.

Benninger L.K. (1978). ^{210}Pb balance in Long Island Sound. *Geochim. Cosmochim. Acta* **42**, 1165-1174.

Benoit G. and Hemond H.F. (1991). Evidence for diffusive redistribution of ^{210}Pb in lake sediments. *Geochim. Cosmochim. Acta* **55**, 1963-1975.

Berner R.A. (1967). Thermodynamic stability of sedimentary iron sulphides. *Am. J. Sci.* **265**, 773-785.

Berner R.A. (1970). Sedimentary pyrite formation. *Am. J. Sci.* **268**, 1-23.

Berner R.A. (1980). *Early diagenesis: a theoretical approach.* Princeton University Press, Princeton, N.J., 241 pp..

Berner R.A. (1985). Sulphate reduction, organic matter decomposition and pyrite formation. *Phil. Trans. Royal Soc. London, Series A*, **315**, 25-38.

Bertolin A., Rudello D. and Ugo P. (1995). A new device for *in-situ* pore water sampling. *Mar. Chem.* **49**, 233-239.

Boulegue J., Lord C.J. and Church T.M. (1982). Sulphur speciation and associated trace metals in the pore waters of Great Marsh, Delaware. *Geochim. Cosmochim. Acta* **46**, 453-464.

Burton W.M. and Stewart N.G. (1960). Use of long-lived natural radioactivity as an atmospheric tracer. *Nature* **186**, 584-589.

Caçador I., Vale C. and Catarino F. (1996). Accumulation of Zn, Pb, Cu, Cr and Ni in sediments between roots of the Tagus Estuary salt marshes, Portugal. *Est. Coastal Shelf Sci.* **42,** 393-403.

Calmano W. and Förstner U. (Eds.) (1996). *Sediments and toxic substances: environmental effects and ecotoxicity.* Springer-Verlag, Berlin.

Cambray R.S., Cawse P.A., Garland J.A., Gibson J.A.B., Johnson P., Lewis G.N.J., Newton D., Salmon L. and Wade B.O. (1987). Observations on radioactivity from the Chernobyl accident. *Nuc. Energy* **26,** 77-101.

Campbell L.S. and Davies B.E. (1997). Experimental investigation of plant uptake of caesium from soils amended with clinoptilolite and calcium carbonate. *Plant and Soil* **189**, 65-74.

Canfield D.E., Thamdrup B. and Hansen J.W. (1993). The anaerobic degradation of organic matter in Danish coastal sediments: iron reduction, manganese reduction and sulphate reduction. *Geochim. Cosmochim. Acta* **57,** 3867-3883.

Carignan R. and Fleet R.J. (1981). Post-depositional mobility of phosphorous in lake sediments. *Limnol. Oceanogr.* **26**, 361-366.

Carignan R., Rapin F. and Tessier A. (1985). Sediment porewater sampling for metal analysis: a comparison of techniques. *Geochim. Cosmochim. Acta* **49,** 2493-2497.

Carter M.W. and Moghissi A.A. (1977). Three decades of nuclear testing. *Health Phys.* **33**, 55-71.

Chanton J.P., Martens C.S. and Kipphut G.W. (1983). Lead-210 sediment geochronology in a changing coastal environment. *Geochim. Cosmochim. Acta* **47**, 1791-1804.

Chow T.J., Snyder C.B. and Earl J.L. (1975). Isotope ratios of lead as pollutant source indicators. In: *Isotope ratios as pollutant source and behaviour indicators.* IAEA, Vienna, pp. 95-108.

Church T.M., Lord C.J. and Somayajula B.L.K. (1981). Uranium, thorium and lead nuclides in a Delaware salt marsh sediment. *Est. Coastal Shelf Sci.* **13**, 267-275.

Church T.M., Sarin M.M., Fleisher M.Q. and Ferdelman T.G. (1996). Salt marshes: an important coastal sink for dissolved uranium. *Geochim. Cosmochim. Acta* **60**, 3879-3887.

Christian R.R. and Wiebe W.J. (1978). Anaerobic microbial community metabolism in *Spartina alterniflora* soils. *Limnol. Oceanogr.* **23**, 328-336.

Comans R.N.J. and Hockley D.E. (1992). Kinetics of caesium sorption on illite. *Geochim. Cosmochim. Acta* **56**, 1157-1164.

Comans R.N.J., Haller M. and De Preter P. (1991). Sorption of caesium on illite: non-equilibrium behaviour and reversibility. *Geochim. Cosmochim. Acta* **55**, 433-440.

Comans R.N.J., Middleburg J.J., Zonderhuis J., Woittiez J.R.W., De Lange G.J., Das H.A. and Van Der Weijden C.H. (1989). Mobilisation of radiocaesium in pore water of lake sediments. *Nature* **339,** 367-369.

Craft C.B., Seneca E.D. and Broome S.W. (1993). Vertical accretion in microtidal regularly and irregularly flooded estuarine marshes. *Est. Coastal Shelf Sci.* **37**, 371-386.

Croudace I.W. and Cundy A.B. (1995). Heavy metal and hydrocarbon pollution in recent sediments from Southampton Water, Southern England: a geochemical and isotopic study. *Environ. Sci. Technol.* **29**, 1288-1296.

Cundy A.B. (1994). *Radionuclide and geochemical studies of recent sediments from the Solent Estuarine System.* Ph.D. Thesis, Southampton University.

Cundy A.B., Croudace I.W., Thomson J. and Lewis J.T. (1997). Reliability of salt marshes as "geochemical recorders" of pollution input: a case study from contrasting estuaries in Southern England. *Environ. Sci. Technol.* **31**, 1093-1101.

Cutter G.A. and Velinsky D.J. (1988). Temporal variations of sedimentary sulphur in a Delaware salt marsh. *Mar. Chem.* **23,** 311-327.

Davis J.J. (1963). Caesium and its relationships to potassium in ecology. In: Schultz V. and Klement A.W. Jnr. (Eds.), *Radioecology*. Reinhold, New York, pp. 539-556.

Davis R.B., Hess C.T., Norton S.A., Hanson D.W., Hoagland K.D. and Anderson D.S. (1984). ^{137}Cs and ^{210}Pb dating of sediments from soft-water lakes in New England (USA) and Scandinavia, a failure of ^{137}Cs dating. *Chem. Geol.* **44**, 151-185.

Davison W., Grime G.W., Morgan J.A.W. and Clarke K. (1991). Distribution of dissolved iron in sediment pore waters at submillimetre resolution. *Nature* **352**, 323-324.

Davison W., Zhang H. and Grime G.W. (1994). Performance characteristics of gel probes used for measuring the chemistry of pore waters. *Environ. Sci. Technol.* **28**, 1623-1632.

De Lange G.J, Cranston R.E., Hydes D.H. and Boust D. (1992). Extraction of pore water from marine sediments: a review of possible artifacts with pertinent examples from the North Atlantic. *Mar. Geol.* **109**, 53-76.

De Laune R.D., Patrick W.H. Jnr. and Buresh R.J. (1978). Sedimentation rates determined by ^{137}Cs dating in a rapidly accreting salt marsh. *Nature* **275,** 532-533.

Delves H.T. (1988). Biomedical applications of ICP-MS. *Chem. Brit.* **24**, 1009-1012.

Dicks B. and Levell D. (1989). Refinery-effluent discharges into Milford Haven and Southampton Water. In: Dicks B. (Ed.), *Ecological impacts of the oil industry*. Institute of Petroleum, John Wiley and Sons, pp. 287-316.

Di Guilio R.T. and Scanlon P.F. (1985). Heavy metals in aquatic plants, clams and sediments from the Chesapeake Bay, U.S.A.. Implications for waterfowl. *Sci. Tot. Environ.* **41**, 259-274.

Dörr H., Mangini A., Schmitz W., Weber F. and Münnich K.O. (1991). Stable lead and ^{210}Pb in German lake sediments and soils: a tracer for anthropogenic lead emission. In: Vernet J.P. (Ed.), *Heavy metals in the environment*. Elsevier, Amsterdam.

Eakins J.D. and Morrison R.T. (1975). The determination of polonium-210 in urine by coprecipitation with manganese dioxide. AERE - R 7923.

Edmunds W.M. (1996). Bromine geochemistry of British groundwaters. *Min. Mag.* **60**, 275-284.

Evans D.W., Alberts J.J. and Clark R.A. III (1983). Reversible ion-exchange fixation of caesium-137 leading to mobilization from reservoir sediments. *Geochim. Cosmochim. Acta* **47**, 1041-1049.

Farmer J.G. and Lovell M.A. (1986). Natural enrichment of arsenic in Loch Lomond sediments. *Geochim. Cosmochim. Acta* **50**, 2059-2067.

Farmer J.G., Eades L.J., MacKenzie A.B., Kirika A. and Bailey-Watts T.E. (1996). Stable lead isotope record of lead pollution in Loch Lomond sediments since 1630 A.D.. *Environ. Sci. Technol.* **30**, 3080-3083.

Faure G. (1977). *Principles of isotope geology*. John Wiley and Sons, New York.

Fenchel T. and Finlay B.J. (1995). Ecology and evolution in anoxic worlds. OUP, Oxford, 276 pp.

Ferdelman T.G., Church T.M. and Luther G.W. III (1991). Sulphur enrichment of humic substances in a Delaware salt marsh sediment core. *Geochim. Cosmochim. Acta* **55**, 979-988.

Flury M. and Papritz A. (1993). Bromine in the natural environment: occurrence and toxicity. *J. Environ. Qual.* **22**, 747-758.

Flynn W.W. (1968). The determination of low levels of polonium-210 in environmental materials. *Anal. Chim. Acta* **43**, 221-227.

Francis C.W., Chester G. and Haskin L.A. (1970). Determination of lead-210 mean residence times in the atmosphere. *Environ. Sci. Technol.* **4**, 586-589.

Francis C.W. and Brinkley F.S. (1976). Preferential adsorption of ^{137}Cs to micaceous minerals in contaminated freshwater sediment. *Nature* **260**, 511-513.

François R. (1987). The influence of humic substances on the geochemistry of iodine in nearshore and hemipelagic marine sediments. *Geochim. Cosmochim. Acta* **51**, 2417-2427.

French P.W., Allen J.R.L. and Appleby P.G. (1994). Lead-210 dating of a modern period salt marsh deposit from the Severn Estuary (Southwest Britain) and its implications. *Mar. Geol.* **118**, 327-334.

Froelich P.N., Klinkhammer G.P., Bender M.L., Luedtke N.A., Heath G.R., Cullen D., Dauphin P., Hammond D., Hartman B. and Maynard V. (1979). Early oxidation of organic matter in pelagic sediments of the eastern equatorial Atlantic: suboxic diagenesis. *Geochim. Cosmochim. Acta* **43**, 1075-1090.

Gardner W.D., Wolaver T.G. and Mitchell M. (1988). Spatial variations in the sulphur chemistry of salt marsh sediments at North Inlet, South Carolina. *J. Mar. Res.* **46**, 815-836.

Giblin A.E. and Howarth R.W. (1984). Pore water evidence for a dynamic sedimentary iron cycle in salt marshes. *Limnol. Oceanogr.* **29**, 311-327.

Gilkes R.J. (1968). Clay mineral provinces in the Tertiary sediments of the Hampshire Basin. *Clay Minerals* **7**, 351-361.

Gleason M.L. and Zieman J.C. (1981). Influence of tidal inundation on internal oxygen supply of Spartina alterniflora and Spartina patens. *Est. Coastal Shelf Sci.* **13**, 47-57.

Goldberg E.D. (1963). Geochronology with ^{210}Pb. *Symposium on radioactive dating*, I.A.E.A., Vienna, pp. 121-130.

Goldberg E.D., Gamble E., Griffin J.J. and Koide M. (1977). Pollution history of Naragansett Bay as recorded in its sediments. *Est. Coastal Mar. Sci.* **5**, 549-561.

Goldberg E.D. (1976). Pollution history of estuarine sediments. *Oceanus* **19**, 18-26.

Goldhaber M.B. and Kaplan I.R. (1974). The sulphur cycle. In: Goldberg E.D. (Ed.), *The sea (vol. 5, Marine Chemistry)*, John Wiley and Sons, pp. 569-655.

Goreau T.J. (1977). Quantitative effects of sediment mixing on stratigraphy and biogeochemistry: a signal theory approach. *Nature* **265**, 525-526.

Grousset F.E., Quétel C.R., Thomas B., Buat-Ménard P., Donard O.F.X. and Bucher A. (1994). Transient lead isotopic signatures in the Western European Atmosphere. *Environ. Sci. Technol.* **28**, 1605-1608.

Guerzoni S., Frignani M., Giordani P. and Frascari F. (1984). Heavy metals in sediments from different environments of a northern Adriatic Sea area, Italy. *Environ. Geol. Water Sci.* **6**, 111-119.

Hamelin B., Grousset F. and Sholkovitz E.R. (1990). Lead isotopes in surficial pelagic sediments from the North Atlantic. *Geochim. Cosmochim. Acta* **54**, 37-47.

Harvey G.R. (1980). A study of the chemistry of iodine and bromine in marine sediments. *Mar. Chem.* **8**, 327-332.

Hem J.D. (1978). Redox processes at surfaces of manganese oxide and their effects on aqueous metal ions. *Chem.Geol.* **21**, 199-218.

Hesslein R.H. (1976). An in situ sampler for close interval pore water studies. *Limnol. Oceanogr.* **21**, 912-914.

Hines M.E., Knollmeyer S.L. and Tugel J.B. (1989). Sulphate reduction and other sedimentary biogeochemistry in a northern New England salt marsh. *Limnol. Oceaogr.* **24**, 578-590.

Hooke J. and Riley R. (1987). Historical changes on the Hampshire coast 1870-1965. Portsmouth Polytechnic publication.

Howarth R.W. (1979). Pyrite: its rapid formation in a salt marsh and its importance in ecosystem metabolism. *Science* 203, 49-51.

Howarth R.W. and Teal J.M. (1979). Sulphate reduction in a New England salt marsh. *Limnol. Oceanogr.* **24**, 999-1013.

Hubbard J.C.E. (1965). Spartina marshes in Southern England, VI: pattern of invasion in Poole Harbour. *J. Ecol.* **53**, 799-813.

Huerta-Diaz M.A. and Morse J.W. (1992). Pyritization of trace metals in anoxic marine sediments. *Geochim. Cosmochim. Acta* **56**, 2681-2702.

Hurst R (1996). The lead fingerprints of gasoline contamination. *Environ. Sci. Technol.* **30,** 304A.

Ivanovich M. and Harmon R.S. (Eds.) (1992). *Uranium series disequilibrium: applications to earth, marine and environmental sciences.* 2nd edn., OUP, Oxford.

Jahnke R.A. (1988). A simple and reliable pore water sampler. *Limnol. Oceanogr.* **33,** 483-487.

Jean G.E. and Bancroft G.M. (1986). Heavy metal adsorption by sulphide mineral surfaces. *Geochim. Cosmochim. Acta* **50**, 1455-1463.

Johnson C.A. (1986). The regulation of trace element concentrations in river and estuarine waters contaminated with acid mine drainage: The adsorption of Cu and Zn on amorphous Fe oxyhydroxides. *Geochim. Cosmochim. Acta* **50**, 2433-2438.

Kerfoot W.C., Lauster G. and Robbins J.A. (1994). Palaeolimnological study of copper mining around Lake Superior: artificial varves from Portage Lake provide a high resolution record. *Limnol. Oceaogr.* **39**, 649-669.

Kersten M., Förstner U., Krause P., Kriews M., Dannecker W., Garbe-Schönberg C-D., Höck M., Terzenbach U. and Graßl H. (1992). Pollution source reconnaissance using stable lead isotope ratios ($^{206}Pb/^{207}Pb$). In: Vernet J.P. (Ed.), *Impact of heavy metals on the environment.* Elsevier, Amsterdam, pp. 311-325.

Koide M., Soutar A. and Goldberg E.D. (1972). Marine geochronology with Pb-210. *Earth Planet. Sci. Lett.* **14,** 442-446.

Koide M., Bruland K.W. and Goldberg E.D. (1973). Th-228/Th-232 and Pb-210 geochronologies in marine and lake sediments. *Geochim. Cosmochim. Acta* **37**, 1171-1187.

Korkisch J. (1989). *Handbook of ion exchange resins: their application to inorganic analytical chemistry (vol. VI).* CRC Press, Florida, 342 pp..

Kostka J.E. and Luther G.W. III (1994). Partitioning and speciation of solid phase iron in saltmarsh sediments. *Geochim. Cosmochim. Acta* **58,** 1701-1710.

Krishnaswamy S., Lal D., Martin J.M. and Meybeck M. (1971). Geochronology of lake sediments. *Earth Planet. Sci. Lett.* **11,** 407-414.

Krom M.D., Davison P., Zhang H. and Davison W. (1994). High resolution pore-water sampling with a gel sampler. *Limnol. Oceanogr.* **39**, 1967-1972.

Krumbein W.E. (1983). *Microbial geochemistry.* Blackwell Scientific, Oxford, 330 pp..

Lee G.F. (1975). Role of hydrous metal oxides in the transport of heavy metals in the environment. In: Krenkel P.A. (Ed.), *Heavy metals in the aquatic environment.* Pergamon Press, pp 137-147.

Lepland A. and Stevens R.L. (1996). Authigenic manganese mineralogy in the Landsort Deep, West-Central Baltic Sea. *GFF* **118,** 118-119.

Li Y.H. and Gregory S.C. (1974). Diffusion of ions in sea water and deep sea sediments. *Geochim. Cosmochim. Acta* **38**, 703-714.

Livingstone H.D., Bowen V.T and Kupferman S.L. (1982). Radionuclides from Windscale discharges, I: Non-equilibrium tracer experiments in high latitude oceanography. *J. Mar. Res.* **40**, 253-272. Radionuclides from Windscale discharges, II: Their dispersion in Scottish and Norwegian coastal circulation. *J. Mar. Res.* **40**, 1227-1258.

Lomenick T.F. and Tamura T. (1965). Naturally occurring fixation of ^{137}Cs on sediments of lacustrine origin. *Soil Sci. Soc. Am. Proc.* **29**, 383-386.

Longmore M.E., Torgersen T., O'Leary B.M. and Luly J.G. (1986). Caesium-137 redistribution in the sediments of the playa, Lake Tyrrell, northwestern Victoria, I. Stratigraphy and caesium-137 mobility in the upper sediments. *Palaeogeo. Palaeoclim. Palaeoecol.* **54**, 181-195.

Lord C.J. and Church T.M. (1983). The geochemistry of salt marshes: sedimentary ion diffusion, sulphate reduction and pyritisation. *Geochim. Cosmochim. Acta* **47**, 1381-1391.

Loring D.H. (1991). Normalization of heavy-metal data from estuarine and coastal sediments. *J. Mar. Sci.* **48**, 101-115.

Luther G.W. III, Meyerson A.L., Krajewski J.J. and Hines R. (1980). Metal sulphides in estuarine sediments. *J. Sed. Pet.* **50**, 1117-1120.

Luther G.W. III, Giblin A., Howarth R.W. and Ryans R.A. (1982). Pyrite and oxidised iron mineral phases formed from pyrite oxidation in salt marsh and estuarine sediments. *Geochim. Cosmochim. Acta* **46**, 2665-2669.

Luther G.W. III, Giblin A.E. and Varsolona R. (1985). Polarographic analysis of sulphur species in marine pore waters. *Limnol. Oceanogr.* **30**, 727-736.

Luther G.W. III and Church T.M. (1988). Seasonal cycling of sulphur and iron in pore waters of a Delaware salt marsh. *Mar. Chem.* **23**, 295-309.

Luther G.W. III, Kostka J.E., Church T.M., Sulzberger B. and Stumm W. (1992). Seasonal iron cycling in a salt marsh sedimentary environment: the importance of ligand complexes with Fe(II) and Fe(III) in the dissolution of Fe(III) minerals and pyrite, respectively. *Mar. Chem.* **40**, 81-103.

Luther G.W., Shellenbarger P.A. and Brendell P.J. (1996). Dissolved organic Fe(III) and Fe(II) complexes in salt marsh pore waters. *Geochim. Cosmochim. Acta* **60**, 951-960.

Lyle M. (1983). The brown-green colour transition in marine sediments: a marker of the Fe(II), Fe(III) redox boundary. *Limnol. Oceanogr.* **28**, 1026-1033.

MacKenzie A.B., Scott R.D. and Williams T.M. (1987). Mechanisms for northward dispersal of Sellafield waste. *Nature* **329**, 42-45.

MacMillan D.H.T. (1952). The approach channels to Southampton. *J. Inst. Navigation* **5**, 178-194.

Maher W.A. (1985). Mode of occurrence and speciation of arsenic in some pelagic and estuarine sediments. *Chem. Geol.* **47**, 333-345.

Malcolm S.J. and Price N.B. (1984). The behaviour of iodine and bromine in estuarine sediments. *Mar. Chem.* **15**, 263-271.

Manners J.G. (1975). Die-back of Spartina in the Solent. In: Stranack F. and Coughlan J. (Eds.), *Spartina in the Solent.* de Rothschild symposium, Exbury, Hampshire, pp 7-10.

Mantoura R.F.C., Dickson A. and Riley J.P. (1978). The complexation of metals with humic materials in natural waters. *Est. Coastal Mar. Sci.* **6**, 387-408.

Mayer L.M., Macko S.A., Mook W.H. and Murray S. (1981). The distribution of bromine in recent sediments and its use as a source indicator for organic matter. *Org. Geochem.* **3**, 37-42.

McCaffrey R.J. and Thomson J. (1980). A record of the accumulation of sediment and trace metals in a Connecticut salt marsh. *Adv. Geophys.* **22**, 165-236.

McHenry J.R., Ritchie J.C. and Gill A.C. (1973). Accumulation of fallout caesium-137 in soils and sediments in selected water sheds. *Water Resource Res.* **9**, 676-686.

McLaren J.W., Mykytiuk A.P., Willie S.N. and Berman S.S. (1985). Determination of trace metals in sea water by inductively coupled plasma mass spectrometry with preconcentration on silica-immobilised 8-hydroxyquinoline. *Anal. Chem.* **57**, 2907-2911.

Milan C.S., Swenson E.M., Turner R.E. and Lee J.M. (1995). Assessment of the ^{137}Cs method for estimating sediment accumulation rates: Louisiana salt marshes. *J. Coastal Res.* **11**, 296-307.

Monna F., Lancelot J., Croudace I.W., Cundy A.B. and Lewis J.T. (1997). Pb isotopic composition of airborne particulate material from France and the southern United Kingdom: implications for Pb pollution sources in urban areas. *Environ. Sci. Technol.* **31**, 2277-2286.

Moor H.C., Schaller T. and Sturm M. (1996). Recent changes in stable lead isotope ratios in sediments of Lake Zug, Switzerland. *Environ. Sci. Technol.* **30**, 2928-2933.

Moorbath S. (1962). Lead isotope abundance studies on mineral occurrences in the British Isles and their geological significance. *Phil. Trans. Royal Soc. London* **254**, 295-360.

Moore J.N., Ficklin W.H. and Johns C. (1988). Partitioning of arsenic and metals in reducing sulphidic sediments. *Environ. Sci. Technol.* **22**, 432-437.

Morse J.W. (1994). Interaction of trace metals with authigenic sulphide minerals: implications for their bioavailability. *Mar. Chem.* **46**, 1-6.

Nedwell D.B. and Abraham J.W. (1978). Bacterial sulphate reduction in relation to sulphur geochemistry in two contrasting areas of salt marsh sediments. *Est. Coastal Mar. Sci.* **6**, 341-351.

Ng A. and Patterson C.C. (1982). Changes of lead and barium with time in California offshore basin sediments. *Geochim. Cosmochim. Acta* **46**, 2307-2321.

Nriagu J.O. (1989). A global assessment of natural sources of atmospheric trace metals. *Nature* **338**, 47-49.

Patel B., Patel S. and Pawar S. (1978). Desorption of radioactivity from nearshore sediments. *Est. Coastal Mar. Sci.* **7**, 49-58.

Patterson C.C. (1971). Lead. In: Houd D.W. (Ed.), *Impingement of man on the oceans*. John Wiley and Sons, New York, pp. 245-258.

Pederson T.F. and Price N.B. (1980). The geochemistry of iodine and bromine in the sediments of the Panama Basin. *J. Mar. Res.* **38**, 397-411.

Peirson D.H., Cambray R.S. and Spicer G.S. (1966). Lead-210 and polonium-210 in the atmosphere. *Tellus* **18,** 427-433.

Pellenbarg R.E. (1978). *Spartina alterniflora* litter and the aqueous surface microlayer in the salt marsh. *Est. Coastal Mar. Sci.* **6**, 187-195.

Pellenbarg R.E. (1984). On *Spartina alterniflora* litter and trace metal biogeochemistry of a salt marsh. *Est. Coastal Shelf Sci.* **18**, 331-346.

Pellenbarg R.E. and Church T.M. (1979). The estuarine surface microlayer and trace metal cycling in a salt marsh. *Science* **203**, 1010-1012.

Peterson M.L. and Carpenter R. (1986). Arsenic distributions in porewaters and sediments of Puget Sound, Lake Washington, the Washington Coast and Saanich Inlet, B.C.. *Geochim. Cosmochim. Acta* **50,** 353-369.

Pethick J.S. (1992). Salt marsh geomorphology. In: Allen J.R.L. and Pye K. (Eds.), *Salt marshes: morphodynamics, conservation and engineering significance*. University Press, Cambridge, pp. 41-62.

Picard G.L. and Felbeck G.T. Jnr. (1976). The complexation of iron by marine humic acid. *Geochim. Cosmochim. Acta* **40**, 1347-1350.

Playford K., Lewis G.N.J. and Carpenter R.C. (1992). *Radioactive fallout in air and rain: results to the end of 1990.* AEA-EE-0362, HMSO.

Poet S.E., Moore H.E. and Martell E.A. (1972). Lead-210, Bismuth-210 and Polonium-210 in the atmosphere: Accurate ratio measurement and application to aerosol residence times. *J. Geophys. Res.* 77, 6515-6527.

Prandle D. and Beechley J. (1991). Marine dispersion of caesium-137 released from Sellafield and Chernobyl. *Geophys. Res. Lett.* **18**, 1723-1726.

Price N.B., Calvert S.E. and Jones P.G.W. (1970). The distribution of iodine and bromine in the sediments of the south western Barents Sea. *J. Mar. Res.* **28**, 22-34.

Price N.B. and Calvert S.E. (1977). The contrasting geochemical behaviour of iodine and bromine in recent sediments from the Namibian Shelf. *Geochim. Cosmochim. Acta* **41**, 1769-1775.

Rashid M.A. and King L.H. (1969). Molecular weight distribution measurements on humic and fulvic acid fractions from marine clays on the Scotian Shelf. *Geochim. Cosmochim. Acta* **33**, 147-151.

Rashid M.A. and Leonard J.D. (1973). Modifications in the solubility and precipitation behaviour of various metals as a result of their interaction with sedimentary humic acid. *Chem. Geol.* **11**, 89-97.

Rashid M.A. (1985). *Geochemistry of marine humic compounds.* Springer-Verlag, New York, 300 pp..

Ravichandran M., Baskaran M., Santschi P.H. and Bianchi T.S. (1995). History of trace metal pollution in Sabine-Neches estuary, Beaumont, Texas. *Environ. Sci. Technol.* **29**, 1495-1503.

Rickard D.T. (1975). Kinetics and mechanism of pyrite formation at low temperatures. *Am. J. Sci.* **275**, 636-652.

Ridgeway I.M. and Price N.B. (1987). Geochemical associations and post-depositional mobility of heavy metals in coastal sediments: Loch Etive, Scotland. *Mar. Chem.* **21**, 229-248.

Ritchie J.C. and McHenry J.R. (1990). Application of radioactive fallout caesium-137 for measuring soil erosion and sediment accumulation rates and patterns: a review. *J. Environ. Qual.* **19,** 215-233.

Robbins J.A. and Edgington R.R. (1975). Determination of recent sedimentation rates in Lake Michigan using Pb-210 and Cs-137. *Geochim. Cosmochim. Acta* **39,** 285-304.

Robbins J.A. (1978). Geochemical and geophysical applications of radioactive lead. In: Nriagu J.O. (Ed.), *Biogeochemistry of lead in the environment.* Elsevier Scientific, Amsterdam, pp. 285-393.

Rogowski A.S. and Tamura T. (1970). Environmental mobility of caesium-137. *Radiation Botany* **10**, 35-45.

Salomans W. and Förstner U. (1984). *Metals in the hydrocycle.* Springer-Verlag, Berlin, 349 pp..

Sanders J.G. (1980). Arsenic cycling in marine systems. *Mar. Env. Res.* **3**, 257-266.

Santschi P., Höhener P., Benoit G. and Buchholtz-ten Brink M. (1990). Chemical processes at the sediment-water interface. *Mar. Chem.* **30,** 269-315.

Schaffner L.C., Diaz R.J., Olsen C.R. and Larsen I.L. (1987). Faunal characteristics and sediment accumulation processes in the James River Estuary, Virginia. *Est. Coastal Shelf Sci.* **25**, 211-226.

Sharifi A.R., Croudace I.W. and Austin R.L. (1991). Benthic foraminiferids as pollution indicators in Southampton Water, southern England, U.K.. *J. Micropalaeontol.* **10**, 109-113.

Shaw T.J., Gieskes J.M. and Jahnke R.A. (1990). Early diagenesis in differing depositional environments: the response of transition metals in pore water. *Geochim. Cosmochim. Acta* **54,** 1233-1246.

Shennan I. (1983). Holocene crustal movements and sea level changes in Great Britain. *J. Quat. Sci.* **4,** 77-89.

Shimmield G.B. and Pedersen T.F. (1990). Geochemistry of reactive trace metals and halogens in hemipelagic continental margin sediments. *Rev. Aquat. Sci.* **3**, 255-279.

Shirahata M.J., Elias R.V., Patterson C.C. and Koide M. (1980). Chronological variations in concentrations and isotopic composition of anthropogenic atmospheric lead in sediments of a remote subalpine pond. *Geochim. Cosmochim. Acta* **44**, 149-169.

Shotyk W., Nesbitt H.W. and Fyfe W.S. (1990). The behaviour of major and trace elements in complete vertical peat profiles from three *Sphagnum* bogs. *Int. J. Coal Geol.* **15,** 163-190.

Skei J.M., Loring D.H. and Rantala R.T.T. (1988). Partitioning and enrichment of trace metals in a sediment core from Framvaren, South Norway. *Mar. Chem.* **23**, 269-281.

Smith J.T. and Comans R.N.J. (1996). Modelling the diffusive transport and remobilisation of ^{137}Cs in sediments: the effects of sorption kinetics and reversibility. *Geochim. Cosmochim. Acta* **60,** 995-1004.

Smith J.T., Appleby P.G., Hilton J. and Richardson N. (in press). Inventories and fluxes of ^{210}Pb, ^{137}Cs and ^{241}Am determined from the soils of three small catchments in Cumbria, U.K.. *J. Environ. Rad.* (accepted).

Stumpf R.P. (1983). The process of sedimentation on the surface of a salt marsh. *Est. Coastal Shelf Sci.* 17; 495-508.

Suess E. (1979). Mineral phases formed in anoxic sediments by microbial decomposition of organic matter. *Geochim. Cosmochim. Acta* **43**, 339-352.

Sugden C.L., Farmer J.G. and MacKenzie A.B. (1993). Isotopic ratios of lead in contemporary environmental materials from Scotland. *Environ. Geochem. Health* **15,** 59-65.

Swanson V.E., Frost I.C., Rader L.F. and Haffman C. (1966). Metal sorption by north west Florida humate. U.S. Geological Survey, Professional Paper **550-C**, 174-177.

Taylor I. (1991). *Novel chelating silicas for the preconcentration of ultra trace0 metals in natural waters*. Ph.D. Thesis, Southampton University.

Ten Haven H.L., De Leeuw J.W., Schenck P.A. and Klaver G.T. (1988). Geochemistry of Mediterranean sediments. Bromine/organic carbon and uranium/organic carbon as indicators of input and post-depositional oxidation, respectively. *Org. Geochem.* **13**, 255-261.

Tessier A., Rapin F. and Carignan R. (1985). Trace metals in oxic lake sediments: possible adsorption on to iron oxyhydroxides. *Geochim. Cosmochim. Acta* **49**, 183-194.

Tessier A., Fortin D., Belzile N., DeVitre R.R. and Leppard G.G. (1996). Metal sorption to diagenetic iron and manganese oxyhydroxides and associated organic matter: narrowing the gap between field and laboratory measurements. *Geochim. Cosmochim. Acta* **60**, 387-404.

Thamdrup B., Finster K., Fossing H., Hansen J.W. and Jørgensen B.B. (1994). Thiosulphate and sulphite distributions in pore water of marine sediments related to manganese, iron and sulphur geochemistry. *Geochim. Cosmochim. Acta* **58,** 67-73.

Thomson J., Higgs N.C., Croudace I.W., Colley S. and Hydes D.J. (1993). Redox zonation of elements at an oxic/post-oxic boundary in deep-sea sediments. *Geochim. Cosmochim. Acta* **57**, 579-595.

Thomson J., Higgs N.C., Wilson T.R.S., Croudace I.W., De Lange G.J. and Van Santvoort P.J.M. (1995). Redistribution and geochemical behaviour of redox-sensitive elements around S1, the most recent eastern Mediterranean sapropel. *Geochim. Cosmochim. Acta* **59,** 3487-3501.

Tipping E. (1981). The adsorption of aquatic humic substances by iron oxides. *Geochim. Cosmochim. Acta* **45**, 191-199.

Tubbs C.R. (1980). Processes and impacts in the Solent. In: *The Solent Estuarine System - an assessment of present knowledge*. N.E.R.C. Series C, No.**22**, pp. 1-5.

Turekian K.K and Wedepohl K.H. (1961). Distribution of the elements in some major units of the Earth's crust. *Geol. Soc. Am. Bull.* **72,** 175-192.

Turekian K.K., Nozaki Y. and Benninger L.K. (1977). Geochemistry of atmospheric radon and radon products. *Annual Rev. Earth Planet. Sci.* **5**, 227-255.

Ullman W.J. and Aller R.C. (1985). The geochemistry of iodine in nearshore carbonate sediments. *Geochim. Cosmochim. Acta* **49**, 967-978.

Upstill-Goddard R.C. and Elderfield H. (1988). The role of diagenesis in the estuarine budgets of iodine and bromine. *Cont. Shelf. Res.* **8**, 405-430.

Urban N.R., Eisenreich S.J., Grigal D.F. and Schurr K.T. (1990). Mobility and diagenesis of Pb and ^{210}Pb in peat. *Geochim. Cosmochim. Acta* **54,** 3329-3346.

Valette-Silva N.J. (1993). The use of sediment cores to reconstruct historical trends in contamination of estuarine and coastal sediments. *Estuaries* **16,** 577-588.

Van Cappellen P. and Wang Y.F. (1996). Cycling of iron and manganese in surface sediments: a general theory for the coupled transport and reaction of carbon, oxygen, nitrogen, sulphur, iron and manganese. *Am. J. Sci.* **296**, 197-243.

Van der Weijden C.H. (1992). Early diagenesis and marine pore water. In: Wolf K.H. and Chilingarian G.V. (Eds.), *Diagenesis, vol. III.* Elsevier, Amsterdam, pp. 13-134.

Wallmann K., Peterson W., Reiners C. and Gramm H. (1996). Trace element diagenesis in polluted sediments of the River Elbe estuary. In: Calmano W. and Förstner U. (Eds.), *Sediments and toxic substances: environmental effects and ecotoxicity.* Springer-Verlag, Berlin, pp. 197-213.

Watson P.G. and Frickers T.E. (1990). A multilevel *in situ* pore water sampler for use in intertidal sediments and laboratory microcosms. *Limnol. Oceanogr.* **35**, 1381-1389.

Widerlund A. and Ingri J. (1995). Early diagenesis of arsenic in sediments of the Kalix River Estuary, northern Sweden. *Chem. Geol.* **125**, 185-196.

Williams T.M. (1992). Diagenetic metal profiles in recent sediments of a Scottish freshwater loch. *Environ. Geol. Water Sci.* **20**, 117-123.

Williams T.M. (1993). Particulate metal speciation in surficial sediments from Loch Dee, southwest Scotland, U.K.. *Environ. Geol.* **21**, 62-69.

Williams T.P., Bubb J.M. and Lester J.N. (1994). Metal accumulation within salt marsh environments: a review. *Mar. Poll. Bull.* **28**, 277-290.

Wise S.M. (1980). Caesium-137 and lead-210: a review of the techniques and some applications in geomorphology. In: Cullingford R.A., Davidson D.A. and Lewin J. (Eds.), *Timescales in geomorphology.* John Wiley and Sons, New York, pp. 109-127.

Woodworth P.L. (1987). Trends in UK mean sea level. *Mar. Geodesy* **11**, 57-87.

Zuo Z. (1992). *Dynamic behaviour of ^{210}Pb, ^{210}Po and ^{137}Cs in coastal and shelf environments.* Thesis Rijksuniversiteit Utrecht, Geologica Ultraiectina No. **87**.

Zwolsman J.J.G., Berger G.W. and Van Eck G.T.M. (1993). Sediment accumulation rates, historical input, postdepositional mobility and retention of major elements and trace metals in salt marsh sediments of the Scheldt estuary, SW Netherlands. *Mar. Chem.* **44**, 73-94.

Appendix A

Methods of pore water retrieval

The association of any particular element with the solid phase in aquatic environments is often a reversible process (e.g. Santschi *et al* 1990). Diagenetic cycling of elements within sediment sequences may take place *via* reaction of metastable phases releasing dissolved species into the pore waters. These ions and complexes are able to migrate along concentration gradients away from the site of reaction and may either be reincorporated into the solid phase at other depth horizons or alternatively escape from the sediments altogether. A complete understanding of the behaviour and fate of elements in a sedimentary system therefore demands assessment of this dissolved pool through pore water analysis. The collection of interstitial waters from sediments may be effected through a variety of procedures each with certain advantages and disadvantages of practicality and applicability. The most important of these consist of extraction- and equilibration-based techniques.

The collection of pore water samples must be done with great care if artifacts arising from the sampling procedure are to be minimised (de Lange *et al* 1992). Water samples retrieved from the anoxic environments found beneath sediment-water interfaces are easily susceptible to oxidation once removed from their *in-situ* location. The principal factors which may result in sample interference include contamination by oxygen, pressure changes leading to solid-solution interactions and the conditions (e.g. temperature) of sample storage prior to and during extraction (Carignan *et al* 1985). Of the various techniques available some are more likely than others to generate certain of the potential artifacts, but in all cases it is important to use sufficiently clean apparatus and observe stringent experimental procedures in order to minimise inaccuracies. For the purposes of most trace metal analyses the pore water samples may be acidified following collection to stabilise the dissolved species, but must be handled with extreme care prior to this because of the potential for contamination.

A 1 Extraction methods:

A 1.1 *Squeezing*

The squeezing of individual sediment samples to express the aqueous phase through a filter and into a collection vessel is one of the more common methods of pore water collection. Samples are typically obtained via the retrieval of a sediment core followed by sectioning, under an anoxic atmosphere (usually a nitrogen-filled glove-box), into slices suitable for compression. Certain authors report that the pressure at which squeezing is carried out is able to affect the chemical composition of the pore waters through dissolution and precipitation reactions, although this artifact is believed to be relatively insignificant below pressures of ~1 kbar (de

Lange *et al* 1992). The pore size of the filters used during extraction should be sufficient to remove colloidal materials from the waters and permit the passage of dissolved species only. Filtration may be carried out in either one stage (e.g. squeezing though 0.45 μm membrane filters; Froelich *et al* 1979) or two stages (e.g. squeezing through paper followed by refiltration through 0.45 μm membranes; Thomson *et al* 1993). The sample sizes used in this technique are typically 1-2 cm thick slices of sedimentary material, although published results rarely involve the analysis of more than a few tens of samples, irrespective of the length of core being analysed, due to the labour-intensive nature of the procedure. A relatively new application of the squeezing technique is that of whole-core squeezing, whereby pore water samples at a much finer resolution of ~ 1 mm may be obtained. This involves the compression of complete sediment cores or sections thereof, under an anoxic atmosphere, on to a grooved surface, which segregates the waters expressed from different depth intervals, or the squeezing of pore fluids through filters and tubes placed over ports along the sediment core, such as the apparatus described by Jahnke (1988). Despite improving the resolution of the technique, as well as decreasing the time needed to collect multiple samples, whole-core squeezing still retains problematic operational requirements. Chief amongst these is the need to prevent any atmospheric input due to the potential for oxygen contamination, which would severely upset the speciation of redox sensitive components within the samples.

A 1.2 *Centrifugation and filtration*

As an alternative to the squeezing of sediments to separate their solid and aqueous components, centrifugation is effective in providing supernatant liquids which may be drawn through a membrane filter. Sample preparation is similar to that employed during squeezing, since an anoxic atmosphere must still be provided during sectioning of the sediment core, centrifugation and filtration. Typical durations and speeds of centrifugation applied to samples during this procedure are 10-30 minutes at 5000 - 12000 rpm (e.g. de Lange *et al* 1992; Peterson and Carpenter 1986; Luther III *et al* 1985). Carignan *et al* (1985) report that at speeds of 5000 rpm their centrifugation procedure gave higher and more variable concentrations for Cu, Zn and organic carbon as compared to a dialysis method conducted in parallel. When the speed was increased to 11000 rpm the results of the two methods were more comparable for these dissolved species. The incomplete separation of particulate Cu, Zn and C_{org} from the aqueous phase during centrifugation was suggested to be responsible for this effect (Carignan *et al* 1985). As with the squeezing of sediment samples, the demanding procedure of centrifugation and filtration often results in projects processing no more than a few tens of samples in total. However, these two techniques together, due to their ability to deliver reproducible and reliable

results, comprise the basis for the methods of most reported studies into the chemical composition of sediment interstitial waters.

A 1.3 *Syringe extraction*

A less time consuming method for removing the water from a sediment core involves the use of a syringe, with an in-line filter, to extract pore fluids by suction (e.g. Williams 1992). This process may be facilitated through prior preparation of the coring device to allow the insertion of the syringe tip directly into the sediment through, for example, membrane-sealed pre-drilled holes spaced regularly along the length of the coring tube (e.g. Farmer and Lovell 1986). As with the methods discussed so far the introduction of oxygen into any part of the apparatus must be strictly avoided when dealing with anoxic sediments, and the syringe extraction may therefore be best performed in an oxygen-free environment, such as a nitrogen- or helium-filled tent or glove-bag, rather than immediate sampling in the field. The potential for pore waters to move over considerable vertical distances during extraction and the difficulties inherent in determining the extent of this effect may yield inaccurate concentration profiles. The technique is otherwise favourable due to its relative simplicity and low cost of operation.

A 1.4 *Sipping*

The three methods considered above all involve the initial retrieval of sediment cores from which the interstitial waters are later separated, the inherent difficulties of which have already been discussed. To make pore water extraction less liable to these experimental artifacts a considerable amount of effort has been devoted to the design and construction of *in-situ* collection devices (e.g. Watson and Frickers 1990; Bertolin *et al* 1995). These methods cannot themselves be considered free of experimental problems but are able to minimise many of the obstacles associated with the sediment coring techniques. The sipping of interstitial fluids from depth within a sediment prism into a suitable collection vessel must be carried out without exposure to oxygen and other contaminants. This is usually effected through the application of a vacuum to the sampling device, thereby removing the resident atmosphere, before extracting the aqueous samples. The apparatus required to effect this withdrawal typically forms a vertical array of chambers held by a plastic probe and connected to the surface with narrow suction tubes. The samples may then be dispensed into individual containers within an evacuated jar.

Sipping equipment is relatively costly to construct and may not be suitable under conditions when the sediment surface is difficult to access directly by hand. Further limitation of the use of

these samplers derives from the increased complexity of the apparatus reducing the possible sampling resolution as well as restricting the depth over which samples may readily be retrieved. However, the added ability to remove samples at different times, with the device remaining *in-situ* throughout, increases the benefit of this technique as compared to other methods.

A 2 Equilibration methods

A 2.1 *Dialysis*

As an alternative to the direct extraction of interstitial water it is also possible to bring about the equilibration of sediment pore waters with an aqueous phase artificially introduced into the sedimentary system (Hesslein 1976). The collection vessels with which sampling is effected may be in the form of isolated packets of deioinised water, such as porous-membrane bags buried individually at different depths within the sediment, or a single device able to sample several depths simultaneously, such as the chambered perspex apparatus of Carignan *et al* (1985). The collection containers (usually with a volume of a few millilitres) are separated from the pore water with a diffusive membrane which allows the free passage of dissolved species whilst excluding colloidal and particulate materials. After a suitable period of time, typically days to weeks depending on the diffusive characteristics of the equipment, the waters held within the device equilibrate with the waters of the sediment intersticies and may be carefully removed to obtain the sample material. Obviously, this time dependent nature of this process makes it unsuitable for systems where the pore water composition undergoes rapid change. The technique may also be subject to artifacts arising from the incomplete equilibration of the aqueous phases, membrane breakdown and contamination (Carignan *et al* 1985). The comparative study carried out by Carignan *et al* (1985) of dialysis and centrifugation techniques led to the conclusion that, because of its simplicity and apparent reliability, *in-situ* dialysis is well suited to the study of trace constituents in sediment pore waters.

A 2.2 *DET: a new form of dialysis*

In more recent years considerable research has been devoted to the development of a new kind of equilibration system, employing a hydrated gel as the aqueous carrier phase rather than utilising packets of deionised water (Davison *et al* 1991; Davison *et al* 1994). The gel is considerably easier to handle both in the laboratory and in the field, and also facilitates the construction of the holding device. Depending on the application sought for the sampler, gel

layers may be fabricated with a thickness of < 1 mm, thereby allowing rapid (< 1 hr) equilibration with the pore water (Davison *et al* 1991). A continuous strip of polyacrylamide gel, held between plastic plates and fronted by a 0.45 μm membrane filter, may be inserted into the sediment prism (following deoxygenation of the apparatus) and easily removed once sufficient time has passed for equilibrium to be achieved. The initial applications of this method to the study of dissolved iron and manganese distributions immersed the apparatus into a solution of 1 mmol l^{-1} NaOH after retrieval from the sediment body. Under these high pH conditions the oxidative precipitation of iron is almost instantaneous within the gel layer which may then be sectioned prior to analysis. Once "fixed" in this fashion the samples form a stable medium immune to many artifacts associated with the techniques discussed above and, furthermore, may be cut into thin strips allowing a high resolution of sampling interval. In order for the application of the technique to the study of species not readily precipitated by the alkaline immersion stage the gel must instead be rapidly sliced before diffusion within the gel layer smears the equilibrated concentration profiles. This method has been employed successfully to obtain data on the distribution of nitrate and sulphate within lake sediment pore waters, and the results were found to agree well with those obtained from conventional pore water extraction methods (Krom *et al* 1994).

A 3 Method appraisal

In order to analyse the pore waters of Hythe Marsh the following parameters need to be considered before deciding on which method is most suitable for sample retrieval: the desired sampling resolution, the volume of sample obtained and the analytes of interest, the cost efficiency and the ease of deployment of the apparatus. An alternative procedure to that of core removal and sectioning followed by either centrifugation or squeezing is desirable due to the time consuming nature of these methods creating limitations on the number of samples which may be readily processed.

A respectable sampling resolution for the purposes of this study would be provided by contiguous samples spaced at one centimetre intervals over a depth of up to a metre. Laboratory trials undertaken on the sipper designed by Watson and Frickers (1990), kindly loaned for demonstration and testing purposes, concluded that an extension of this 10 cm sampling device to a metre or so in length, whilst retaining the same 1 cm interval sampling resolution, would be technically difficult to construct and also require considerable financial investment. The prototype suction device proposed by Bertolin *et al* (1995) consisted of 9 extraction ports spaced at 10 cm intervals along its length of 90 cm. An apparatus with many tens of sampling

orifices, along with associated connection tubes and collection vessels, was ruled out from use during this study due to the problematic nature of its construction.

The determination of concentrations of particular analytes within pore waters is intrinsically related to the sample volume obtainable since this must provide enough material to allow measurement of the required species. Restrictions on these two considerations are not common to many of the sampling techniques, although they are especially important when contemplating the application of the polyacrylamide gel equilibration. The uses of DET reported in the literature may not be suitable for the analysis of trace components on account of the thin film of gel only providing a small volume of aqueous material. However, this technique is of interest due to its novelty and relatively limited application to date and was therefore pursued as an avenue of research, with modifications being made along the way in an attempt to tailor the apparatus to the requirements of the project. The employment of gel samplers is inexpensive and can be effected with relative ease in most laboratories. When the NaOH fixing stage is omitted in favour of a rapid dissemination of the gel pieces the method can also be applied to the analysis of a wide range of dissolved species provided that they exhibit normal diffusive behaviour within the matrix and do not interact chemically with the polymer structure. The sampling resolution obtainable with this approach is additionally superior to the other methods. The gel sampler utilised in this study forms a modification of the previous versions in terms of both the depth sampled and the mechanism by which those samples are obtained.

Appendix B

Raw Data

HySR1 Data

Sample:		1	2	3	4	5	6	7	8	9	10	11	12	13	14	15
Depth	cm	0.5	1.5	2.5	3.5	4.5	5.5	6.5	7.5	8.5	9.5	10.5	11.5	12.5	13.5	14.5
dry density	g cm^{-3}	0.56	0.49	0.63	0.59	0.52	0.45	0.50	0.54	0.53	0.51	0.39	0.55	0.44	0.41	0.43
LOI	wt.%	20.1	17.6	17.2	16.1	15.5	16.6	15.4	16.1	14.8	14.9	15.7	15.0	15.1	17.0	18.1
C_{org}	wt.%	7.3	5.4	4.7	4.0	4.2		4.0	4.4	3.9	3.9		3.7			
Si	wt.%	23.93	24.47	24.74	25.16	25.52	24.93	25.23	24.98	25.68	25.28	24.59	25.12	25.05	24.04	23.70
Al	wt.%	7.78	8.06	8.30	8.35	8.31	8.31	8.60	8.58	8.54	8.69	8.63	8.76	8.73	8.43	8.38
K	wt.%	2.22	2.30	2.31	2.32	2.36	2.38	2.42	2.40	2.42	2.44	2.45	2.50	2.52	2.41	2.42
Ti	wt.%	0.47	0.47	0.49	0.50	0.50	0.49	0.50	0.50	0.50	0.50	0.50	0.50	0.50	0.49	0.49
Cr	ppm	95	101	104	105	102	105	107	109	106	105	106	104	106	104	102
Na	wt.%	1.73	1.73	1.65	1.57	1.76	1.70	1.65	1.67	1.64	1.69	1.78	1.73	1.79	1.91	1.99
Cl	wt.%	3.08	2.72	2.42	2.16	2.28	2.43	2.30	2.44	2.37	2.45	2.72	2.34	3.26	3.00	2.88
Mg	wt.%	0.96	0.96	0.94	0.94	0.95	0.91	0.99	0.99	1.00	1.02	1.06	1.06	1.09	1.06	1.08
Ca	wt.%	0.26	0.16	0.14	0.13	0.14	0.14	0.15	0.16	0.16	0.19	0.20	0.21	0.22	0.21	0.23
Fe	wt.%	3.61	3.98	3.94	3.97	3.89	4.13	3.83	3.60	3.58	3.57	3.55	3.58	3.67	3.79	4.10
Mn	wt.%	0.011	0.011	0.012	0.013	0.013	0.013	0.013	0.014	0.014	0.015	0.015	0.016	0.016	0.016	0.017
S	wt.%	0.70	0.66	1.46	1.75	1.52	1.29	1.41	1.41	1.29	1.35	1.37	1.39	1.45	1.80	2.23
As	ppm	29	31	32	36	29	28	30	31	27	25	27	24	27	28	32
P	wt.%	0.08	0.08	0.07	0.06	0.06	0.08	0.07	0.07	0.07	0.06	0.07	0.06	0.06	0.06	0.06
Pb	ppm	75	40	148	146	101	84	105	115	119	117	117	124	132	131	115
Zn	ppm	85	86	127	206	168	141	200	190	194	201	197	172	160	159	188
Ni	ppm	26	27	38	44	37	34	38	39	37	39	38	36	34	34	37
Cu	ppm	53	40	57	43	43	39	48	47	49	45	38	35	33	31	29
Br	ppm	319	312	247	210	218	258	246	266	259	258	287	280	282	305	316
I	ppm	85	91	92	71	73	86	79	83	84	79	91	89	88	94	93
^{137}Cs	Bq kg^{-1}	9	4	3	2	0	1	0								
% error		8	19	26	35		58									
$^{210}Pb_{xs}$	Bq kg^{-1}	n. d.														
% error		n. d.														
$^{206}Pb/^{204}Pb$		n. d.														
$^{207}Pb/^{204}Pb$		n. d.														
$^{208}Pb/^{204}Pb$		n. d.														

Table B 1(a): Sediment geochemical data.

HySR1 Data

Sample:		16	17	18	19	20	21	22	23	24	25	26	27	28	29	30
Depth	cm	15.5	16.5	17.5	18.5	19.5	20.5	21.5	22.5	23.5	24.5	25.5	26.5	27.5	28.5	29.5
dry density	g cm^{-3}	0.34	0.47	0.41	0.33	0.42	0.50	0.39	0.53	0.43	0.40	0.35	0.35	0.47	0.41	0.37
LOI	wt.%	19.3	18.4	18.1	17.8	17.6	18.8	20.0	19.9	19.7	19.9	19.7	19.5	18.1	18.1	17.7
C_{org}	wt.%		4.8													
Si	wt.%	23.06	23.66	23.71	23.78	23.52	23.52	22.86	22.98	23.19	23.00	23.09	23.85	24.88	24.52	24.71
Al	wt.%	8.19	8.44	8.39	8.43	8.30	8.23	8.01	8.10	8.08	7.83	7.82	7.95	8.08	8.32	8.41
K	wt.%	2.42	2.35	2.47	2.50	2.44	2.41	2.36	2.37	2.39	2.33	2.33	2.41	2.48	2.50	2.54
Ti	wt.%	0.47	0.48	0.48	0.49	0.49	0.48	0.46		0.47	0.47	0.47	0.48	0.50	0.50	0.50
Cr	ppm	99	94	100	103	102	99	96		96	94	97	98	101	104	100
Na	wt.%	2.05	1.99	2.04	2.04	2.03	2.04	2.01	2.08	2.00	2.17	2.26	2.19	2.07	1.93	1.96
Cl	wt.%	3.38	3.01	3.10	3.10	3.13	3.14	3.15		3.12	3.56	3.88	3.58	3.44	3.23	3.39
Mg	wt.%	1.07	1.09	1.10	1.11	1.09	1.08	1.07	1.07	1.06	1.05	1.07	1.07	1.04	1.08	1.11
Ca	wt.%	0.24	0.26	0.26	0.26	0.28	0.29	0.27	0.27	0.27	0.26	0.26	0.26	0.26	0.26	0.26
Fe	wt.%	4.14	4.13	4.15	4.01	4.12	4.23	4.62	4.50	4.27	4.21	4.07	4.02	4.08	3.82	3.84
Mn	wt.%	0.018	0.018	0.019	0.020	0.020	0.019	0.019		0.019	0.021	0.021	0.021	0.019	0.018	0.018
S	wt.%	2.31	2.22	2.21	2.00	2.22	2.66	3.09		2.52	2.51	2.34	2.22	2.00	2.00	2.05
As	ppm	41	37	35	33	33	35	37		32	32	31	37	33	29	31
P	wt.%	0.06	0.06	0.06	0.06	0.05	0.06	0.06	0.06	0.06	0.05	0.05	0.06	0.06	0.06	0.06
Pb	ppm	105	97	96	98	92	91	89		93	96	90	88	91	91	91
Zn	ppm	180	159	151	148	143	140	137		131	136	148	163	144	138	139
Ni	ppm	39	41	41	40	38	37	37		35	33	34	34	34	35	35
Cu	ppm	28	26	26	26	25	26	26		27	30	32	31	30	26	25
Br	ppm	329	315	299	293	276	272	268		273	299	312	291	269	250	254
I	ppm	85	82	73	67	67	72	77		71	67	71	70	75	69	67
^{137}Cs	Bq kg^{-1}															
% error																
$^{210}Pb_{xs}$	Bq kg^{-1}															
% error																
$^{206}Pb/^{204}Pb$																
$^{207}Pb/^{204}Pb$																
$^{208}Pb/^{204}Pb$																

Table B 1(b): Sediment geochemical data.

HySR1 Data

Sample:		31	32	33	34	35	36	37	38	39	40	41	42	43	44	45
Depth	cm	30.5	31.5	32.5	33.5	34.5	35.5	36.5	37.5	38.5	39.5	40.5	41.5	42.5	43.5	44.5
dry density	g cm^{-3}	0.50	0.41	0.47	0.51	0.49	0.44	0.41	0.44	0.40	0.48	0.44	0.48	0.49	0.49	0.56
LOI	wt.%	16.9	17.1	16.5	16.2	16.1	17.2	17.6	17.9	17.6	17.0	16.4	15.8	15.2	15.3	15.1
C_{org}	wt.%	3.9		3.9	3.8	3.8	4.1									
Si	wt.%	25.08	25.21	25.17	25.06	25.00	24.27	24.19	24.43	24.59	24.89	25.23	25.63	26.04	25.65	25.60
Al	wt.%	8.36	8.29	8.44	8.56	8.66	8.35	8.24	8.21	8.15	7.81	7.77	7.94	8.11	7.95	7.90
K	wt.%	2.51	2.50	2.50	2.57	2.66	2.52	2.41	2.52	2.39	2.30	2.32	2.35	2.37	2.37	2.37
Ti	wt.%	0.51	0.51	0.51	0.50	0.51	0.49	0.49	0.49	0.49	0.49	0.50	0.51	0.52	0.52	0.51
Cr	ppm	98	101	100	105	106	102	101	99	98	96	98	100	103	96	98
Na	wt.%	1.93	1.91	1.85	1.78	1.71	1.86	1.94	1.83	1.87	2.00	1.87	1.82	1.78	1.78	1.78
Cl	wt.%	3.08	3.18	2.88	2.79	2.74	2.94	3.05	2.79	3.14	2.82	2.91	2.91	2.58	2.86	2.49
Mg	wt.%	1.10	1.10	1.11	1.11	1.10	1.10	1.08	1.05	1.03	1.05	1.05	1.07	1.10	1.09	1.10
Ca	wt.%	0.26	0.26	0.26	0.26	0.26	0.26	0.25	0.26	0.25	0.26	0.27	0.29	0.32	0.34	0.36
Fe	wt.%	3.68	3.71	3.72	3.93	3.85	3.93	3.97	4.39	4.37	4.36	4.17	4.16	4.16	4.04	4.19
Mn	wt.%	0.018	0.018	0.018	0.019	0.019	0.018	0.018	0.018	0.018	0.017	0.018	0.020	0.020	0.020	0.021
S	wt.%	1.93	2.07	1.92	2.02	1.99	2.19	2.52	2.95	2.87	3.10	2.65	2.34	2.05	1.97	2.10
As	ppm	25	25	22	24	23	24	23	28	24	28	33	27	25	23	23
P	wt.%	0.06	0.06	0.06	0.05	0.05	0.05	0.05	0.05	0.05	0.06	0.06	0.06	0.06	0.06	0.06
Pb	ppm	92	90	88	89	88	85	81	83	86	76	72	71	71	71	73
Zn	ppm	137	144	141	139	137	136	137	134	119	117	120	112	112	113	111
Ni	ppm	35	34	35	36	36	36	36	36	35	34	34	33	32	33	34
Cu	ppm	26	28	27	26	26	23	24	24	22	21	23	20	21	23	22
Br	ppm	245	237	232	225	221	229	235	218	216	234	218	202	187	179	170
I	ppm	70	69	69	67	62	63	62	64	63	74	77	72	68	62	62
^{137}Cs	Bq kg^{-1}															
% error																
$^{210}Pb_{xs}$	Bq kg^{-1}															
% error																
$^{206}Pb/^{204}Pb$																
$^{207}Pb/^{204}Pb$																
$^{208}Pb/^{204}Pb$																

Table B 1(c): Sediment geochemical data.

HySR1 Data

Sample:		46	47	48	49	50	51	52	53	54	55	56	57	58	59	60
Depth	cm	45.5	46.5	47.5	48.5	49.5	50.5	51.5	52.5	53.5	54.5	55.5	56.5	57.5	58.5	59.5
dry density	g cm^{-3}	0.52	0.61	0.44	0.49	0.45	0.49	0.50	0.52	0.48	0.43	0.43	0.41	0.45	0.44	0.46
LOI	wt.%	15.7	15.7	16.0	16.0	15.5	15.6	15.9	16.5	17.3	17.5	17.9	18.4	19.1	19.2	18.7
C_{org}	wt.%															
Si	wt.%	25.20	25.37	25.30	25.49	25.53	25.60	25.50	25.08	24.80	24.47	24.68	24.40	24.15	23.82	24.35
Al	wt.%	7.80	7.81	7.81	8.00	8.13	8.15	8.16	8.06	7.88	7.72	7.64	7.53	7.35	7.26	7.43
K	wt.%	2.32	2.34	2.33	2.36	2.35	2.42	2.42	2.38	2.33	2.30	2.30	2.26	2.24	2.26	2.26
Ti	wt.%	0.51	0.52	0.52	0.51	0.51	0.51	0.50	0.50	0.50	0.49	0.49	0.48	0.48	0.48	0.49
Cr	ppm	99	101	102	99	97	103	101	98	103	97	96	93	95	89	98
Na	wt.%	1.79	1.72	1.77	1.78	1.73	1.85	1.86	1.89	2.00	2.02	2.08	2.09	2.17	2.19	2.12
Cl	wt.%	2.62	2.50	2.54	2.57	2.56	2.55	2.87	2.79	2.92	3.07	3.04	2.59	3.50	3.69	3.42
Mg	wt.%	1.10	1.10	1.11	1.12	1.12	1.13	1.12	1.11	1.09	1.08	1.07	1.03	1.06	1.05	1.05
Ca	wt.%	0.37	0.38	0.39	0.39	0.38	0.37	0.36	0.35	0.33	0.30	0.29	0.28	0.27	0.28	0.28
Fe	wt.%	4.71	4.60	4.47	4.16	3.82	3.76	3.94	4.05	4.23	4.32	4.28	4.18	4.17	4.54	4.33
Mn	wt.%	0.022	0.023	0.023	0.024	0.024	0.023	0.024	0.023	0.023	0.023	0.022	0.023	0.022	0.021	0.021
S	wt.%	2.48	2.35	2.19	2.06	1.80	1.79	1.85	2.08	2.49	2.68	2.89	2.16	2.71	3.05	2.80
As	ppm	28	24	20	24	21	25	22	24	25	20	26	19	26	36	30
P	wt.%	0.06	0.06	0.06	0.06	0.06	0.06	0.06	0.06	0.06	0.06	0.05	0.05	0.05	0.05	0.06
Pb	ppm	73	74	74	75	75	77	78	82	81	82	87	82	82	80	78
Zn	ppm	112	114	123	114	112	114	114	123	110	112	113	108	111	116	120
Ni	ppm	34	34	34	34	34	33	33	34	31	32	33	31	31	32	34
Cu	ppm	23	23	23	23	23	22	25	22	23	23	23	23	23	23	22
Br	ppm	164	160	162	156	154	156	164	173	183	193	202	203	232	219	203
I	ppm	57	57	57	49	51	53	53	57	55	59	61	57	72	68	65
^{137}Cs	Bq kg^{-1}															
% error																
$^{210}Pb_{xs}$	Bq kg^{-1}															
% error																
$^{206}Pb/^{204}Pb$																
$^{207}Pb/^{204}Pb$																
$^{208}Pb/^{204}Pb$																

Table B 1(d): Sediment geochemical data.

HySR1 Data

Sample:		61	62	63	64	65	66	67	68	69	70	71	72	73	74	75
Depth	cm	60.5	61.5	62.5	63.5	64.5	65.5	66.5	67.5	68.5	69.5	70.5	71.5	72.5	73.5	74.5
dry density	g cm^{-3}	0.42	0.46	0.46	0.41	0.36	0.36	0.40	0.39	0.39	0.43	0.43	0.49	0.48	0.63	0.48
LOI	wt.%	18.4	19.3	18.9	19.1	21.1	22.5	22.3	21.1	22.4	19.2	18.1	17.1	17.7	17.0	16.3
C_{org}	wt.%															
Si	wt.%	24.29	23.74	23.86	23.18	22.43	21.73	22.34	22.77	21.73	23.43	23.75	24.15	23.80	24.06	24.64
Al	wt.%	7.48	7.40	7.74	7.93	7.72	7.49	7.58	7.65	7.28	7.81	7.87	7.99	7.88	7.95	8.19
K	wt.%	2.28	2.25	2.32	2.34	2.27	2.21	2.23	2.26	2.13	2.29	2.24	2.31	2.29	2.35	2.40
Ti	wt.%	0.49	0.48	0.47	0.47	0.44	0.43	0.44	0.45	0.44	0.47	0.47	0.47	0.46	0.47	0.48
Cr	ppm	98	93	97	101	94	91	88	95	88	92	94	95	95	94	95
Na	wt.%	2.07	2.11	2.15	2.10	2.30	2.41	2.46	2.29	2.32	2.07	1.89	1.78	1.84	1.84	1.83
Cl	wt.%	3.47	3.52	3.41	3.10	3.96	4.21	4.28	3.94	4.19	3.22	2.89	2.49	2.52	2.56	2.48
Mg	wt.%	1.05	1.04	1.07	1.10	1.11	1.10	1.17	1.17	1.13	1.15	1.13	1.12	1.12	1.14	1.15
Ca	wt.%	0.28	0.27	0.28	0.28	0.31	0.33	0.39	0.42	0.45	0.71	1.14	1.25	1.21	0.88	0.74
Fe	wt.%	4.38	4.39	4.38	4.69	4.65	4.70	4.25	4.16	4.07	4.12	3.93	4.10	4.25	4.26	4.15
Mn	wt.%	0.022	0.023	0.023	0.023	0.027	0.029	0.029	0.030	0.033	0.032	0.031	0.029	0.026	0.026	0.025
S	wt.%	2.84	3.07	3.00	3.27	3.72	3.77	3.18	3.18	3.36	2.71	2.55	2.43	2.73	2.84	2.55
As	ppm	25	26	21	24	24	26	25	27	30	25	21	19	18	17	17
P	wt.%	0.06	0.06	0.06	0.06	0.06	0.06	0.06	0.06	0.06	0.06	0.06	0.06	0.05	0.05	0.06
Pb	ppm	75	73	81	76	77	69	66	60	56	54	53	52	50	49	49
Zn	ppm	113	116	112	120	116	108	104	97	97	95	95	94	96	96	98
Ni	ppm	32	32	33	34	33	32	32	32	33	33	33	33	32	34	35
Cu	ppm	23	23	24	22	21	19	21	19	18	17	17	17	19	17	17
Br	ppm	195	201	204	201	231	248	251	227	236	200	188	176	184	172	163
I	ppm	66	68	58	53	56	59	58	53	50	46	40	43	42	40	37
^{137}Cs	Bq kg^{-1}															
% error																
$^{210}Pb_{xs}$	Bq kg^{-1}															
% error																
$^{206}Pb/^{204}Pb$																
$^{207}Pb/^{204}Pb$																
$^{208}Pb/^{204}Pb$																

Table B 1(e): Sediment geochemical data.

HySR1 Data

Sample:		76	77	78	79	80
Depth	cm	75.5	76.5	77.5	78.5	79.5
dry density	g cm^{-3}	0.43	0.49	0.48	0.63	0.48
LOI	wt.%	15.9	15.6	15.6	16.7	17.4
C_{org}	wt.%					
Si	wt.%	24.57	24.66	24.76	23.95	23.52
Al	wt.%	8.24	8.18	8.14	7.98	7.85
K	wt.%	2.39	2.37	2.38	2.27	2.23
Ti	wt.%	0.49	0.48	0.48	0.46	0.45
Cr	ppm	101	102	97	95	92
Na	wt.%	1.74	1.65	1.66	1.68	1.63
Cl	wt.%	2.19	2.23	2.18	2.17	2.08
Mg	wt.%	1.13	1.12	1.11	1.11	1.10
Ca	wt.%	0.78	0.85	0.81	1.67	2.11
Fe	wt.%	4.22	4.27	4.40	4.41	4.46
Mn	wt.%	0.026	0.027	0.027	0.026	0.028
S	wt.%	2.50	2.61	2.65	2.74	2.79
As	ppm	18	21	24	16	14
P	wt.%	0.05	0.05	0.05	0.05	0.05
Pb	ppm	45	42	41	41	38
Zn	ppm	95	95	93	92	91
Ni	ppm	34	35	34	34	33
Cu	ppm	18	18	16	15	14
Br	ppm	156	152	149	165	166
I	ppm	38	38	39	39	41
^{137}Cs	Bq kg^{-1}					
% error						
$^{210}Pb_{xs}$	Bq kg^{-1}					
% error						
$^{206}Pb/^{204}Pb$						
$^{207}Pb/^{204}Pb$						
$^{208}Pb/^{204}Pb$						

Table B 1(f): Sediment geochemical data.

HyPb Data

Sample:		1	2	3	4	5	6	7	8	9	10	11	12	13	14	15
Depth	cm	0.25	0.75	1.25	1.75	2.25	2.75	3.25	3.75	4.25	4.75	5.25	5.75	6.25	6.75	7.25
dry density	g cm^{-3}	0.19	0.17	0.17	0.21	0.30	0.32	0.26	0.22	0.27	0.25	0.27	0.28	0.32	0.29	0.29
LOI	wt.%	30.4	31.5	30.6	32.1	32.8	30.7	34.0	31.9	31.4	30.4	29.0	28.0	27.5	29.8	31.3
C_{org}	wt.%	n. d.														
Si	wt.%	19.85	19.70	20.08	19.71	19.49	20.23	19.16	19.78	19.98	20.19	20.65	21.17	21.36	20.36	19.93
Al	wt.%	6.37	6.36	6.48	6.40	6.31	6.48	6.13	6.30	6.44	6.61	6.97	7.21	7.32	7.01	6.92
K	wt.%	1.90	1.89	1.79	1.94	1.92	1.95	1.93	1.90	1.75	1.93	2.02	2.02	2.06	2.03	2.02
Ti	wt.%	0.40	0.38	0.39	0.37	0.36	0.38	0.35	0.36	0.37	0.37	0.39	0.41	0.41	0.39	0.38
Cr	ppm	82	79	80	81	81	86	85	83	91	91	95	96	98	96	94
Na	wt.%	2.09	1.98	2.05	2.02	2.00	1.89	1.82	1.96	1.81	1.75	1.67	1.69	1.73	1.80	1.92
Cl	wt.%	4.74	4.45	4.19	3.85	3.79	3.43	3.21	3.15	3.19	2.99	2.87	2.88	2.79	3.03	3.35
Mg	wt.%	1.02	0.99	1.00	0.98	0.96	0.97	0.91	0.92	0.93	0.95	0.97	1.00	1.00	0.98	1.00
Ca	wt.%	1.03	0.84	0.71	0.59	0.43	0.40	0.38	0.40	0.35	0.34	0.32	0.32	0.29	0.31	0.31
Fe	wt.%	3.99	3.81	3.83	3.53	3.66	3.89	3.81	3.98	4.17	4.21	4.07	3.66	3.54	3.78	3.41
Mn	wt.%	0.021	0.017	0.016	0.014	0.013	0.013	0.012	0.012	0.012	0.012	0.012	0.012	0.012	0.011	0.010
S	wt.%	0.91	0.82	0.82	0.78	0.74	0.68	0.67	0.66	0.66	0.62	0.60	0.58	0.57	0.61	0.69
As	ppm	34	34	35	34	40	39	38	43	43	43	43	38	36	43	42
P	wt.%	0.18	0.17	0.17	0.17	0.19	0.19	0.20	0.21	0.20	0.19	0.17	0.14	0.13	0.15	0.13
Pb	ppm	163	130	119	92	87	85	85	86	91	90	89	81	82	84	86
Zn	ppm	148	144	144	139	135	136	129	130	129	125	120	115	110	114	107
Ni	ppm	28	29	29	29	29	30	29	30	29	29	30	30	31	31	30
Cu	ppm	113	110	113	114	113	110	110	115	123	129	137	143	150	165	178
Br	ppm	543	573	586	627	678	711	702	726	732	706	697	686	650	678	714
I	ppm	90	83	79	87	101	109	102	103	115	112	119	104	100	107	104
^{137}Cs	Bq kg^{-1}	n. d.														
% error		n. d.														
$^{210}Pb_{xs}$	Bq kg^{-1}	53	69	79	74	74	80	80	73	75	61	64	60	53	59	63
% error		3	4	4	4	3	3	3	3	3	3	4	4	4	4	4
$^{206}Pb/^{204}Pb$			17.752	17.816	17.754		17.942	17.783	17.764	17.873	17.975	17.973	18.101	17.963	17.829	
$^{207}Pb/^{204}Pb$			15.690	15.811	15.689		15.883	15.798	15.720	15.652	15.826	15.815	15.943	15.843	15.832	
$^{208}Pb/^{204}Pb$			37.914	37.856	37.728		38.333	37.788	37.799	37.435	38.120	37.977	37.924	37.969	37.911	

Table B 2(a): Sediment geochemical data.

HyPb Data

Sample:		16	17	18	19	20	21	22	23	24	25	26	27	28	29	30
Depth	cm	7.75	8.25	8.75	9.25	9.75	10.25	10.75	11.25	11.75	12.25	12.75	13.25	13.75	14.25	14.75
dry density	g cm^{-3}	0.25	0.33	0.21	0.32	0.15	0.31	0.25	0.18	0.15	0.18	0.31	0.31	0.29	0.18	0.28
LOI	wt.%	32.1	32.9	34.4	35.2	37.1	34.8	33.0	33.9	33.8	30.9		27.2		26.1	
C_{org}	wt.%															
Si	wt.%	19.85	19.63	19.20	18.94	18.30	19.14	19.70	19.39	19.36	20.28		21.53		21.68	
Al	wt.%	6.94	6.95	6.77	6.71	6.51	6.70	6.81	6.71	6.66	7.01		7.43		7.45	
K	wt.%	1.93	2.04	1.97	1.90	1.94	1.95	2.05	2.03	2.01	2.13		2.22		2.23	
Ti	wt.%	0.38	0.39	0.38	0.37		0.37	0.38	0.38	0.38	0.39	0.41	0.42	0.41	0.42	0.40
Cr	ppm	93	91	91	89		88	85	88	87	90	91	92	92	93	88
Na	wt.%	2.01	2.05	2.19	2.27	2.27	2.29	2.50	2.47	2.65	2.56		2.44		2.60	
Cl	wt.%	3.63	3.57	3.89	4.04	3.99	4.09	4.09	4.68	5.13	4.67		4.26		4.98	
Mg	wt.%	1.02	1.02	1.02	1.04	1.00	1.03	1.04	1.03	1.04	1.04		1.06		1.08	
Ca	wt.%	0.31	0.30	0.31	0.31	0.31	0.30	0.28	0.29	0.29	0.30		0.28		0.28	
Fe	wt.%	2.91	2.64	2.41	2.26	2.21	2.22	2.25	2.27	2.24	2.39		2.58		2.91	
Mn	wt.%	0.010	0.010	0.010	0.009		0.009	0.009	0.010	0.009	0.010	0.010	0.010	0.011	0.010	0.010
S	wt.%	0.75	0.75	0.79	0.85	0.85	0.89	0.82	0.87	0.94	0.82		0.79		0.78	
As	ppm	38	37	35	34		33	30	30	30	29	27	27	27	32	32
P	wt.%	0.11	0.09	0.09	0.08	0.07	0.07	0.07	0.07	0.06	0.07		0.07		0.09	
Pb	ppm	83	81	76	76		69	68	75	73	79	79	78	79	78	83
Zn	ppm	107	106	106	101		95	95	99	96	102	97	101	99	98	94
Ni	ppm	29	30	29	29		29	29	29	29	29	29	30	30	30	28
Cu	ppm	194	205	221	261		278	289	278	254	265	244	197	210	160	200
Br	ppm	691	677	702	675		602	554	564	575	550	538	537	561	586	631
I	ppm	89	87	74	84		77	73	58	59	68	93	101	103	83	118
^{137}Cs	Bq kg^{-1}															
% error																
$^{210}Pb_{xs}$	Bq kg^{-1}	50	49	42	39	32	31	25	29	24	26		23		20	23
% error		2	3	2	2	2	2	2	5	2	2		2		2	4
$^{206}Pb/^{204}Pb$		18.030	17.933	18.413	18.322	18.138	18.382	18.204	17.942	18.088			17.940		17.718	17.611
$^{207}Pb/^{204}Pb$		15.939	15.864	16.156	16.034	16.003	16.088	15.986	15.891	16.007			15.826		15.547	15.463
$^{208}Pb/^{204}Pb$		37.948	37.871	38.990	38.567	38.268	38.566	38.117	37.768	38.407			37.981		37.467	37.316

Table B 2(b): Sediment geochemical data.

HyPb Data

Sample:		31	32	33	34	35	36	37	38	39	40	41	42	43	44	45
Depth	cm	15.25	15.75	16.25	16.75	17.25	17.75	18.25	18.75	19.25	19.75	20.25	20.75	21.25	21.75	22.25
dry density	g cm^{-3}	0.23	0.24	0.23	0.24	0.20	0.20	0.22	0.19	0.20	0.23	0.22	0.26	0.35	0.30	0.27
LOI	wt.%	24.6		25.0		25.0		25.4		24.9		23.7		22.4		22.0
C_{org}	wt.%															
Si	wt.%	21.52		20.93		21.08		21.23		21.29		22.06		22.46		22.87
Al	wt.%	7.42		7.22		7.33		7.42		7.50		7.77		8.06		8.10
K	wt.%	2.22		2.10		2.20		2.23		2.30		2.27		2.50		2.39
Ti	wt.%	0.40	0.39	0.39	0.40	0.41	0.41	0.42	0.42	0.42	0.44	0.43	0.45	0.44	0.44	0.45
Cr	ppm	87	81	85	85	87	84	88	89	92	93	93	94	96	95	98
Na	wt.%	2.67		2.77		2.97		3.04		3.10		2.92		2.79		2.61
Cl	wt.%	5.50		5.79		5.34		5.70		5.49		5.33		4.95		4.59
Mg	wt.%	1.09		1.09		1.12		1.14		1.14		1.15		1.21		1.15
Ca	wt.%	0.31		0.34		0.33		0.32		0.32		0.30		0.28		0.27
Fe	wt.%	4.08		4.78		4.15		3.47		3.53		3.14		2.92		2.91
Mn	wt.%	0.011	0.011	0.010	0.011	0.011	0.011	0.011	0.010	0.011	0.011	0.011	0.011	0.011	0.011	0.011
S	wt.%	0.77		0.76		0.67		0.69		0.69		0.65		0.63		0.59
As	ppm	43	49	61	59	55	45	44	41	49	36	37	31	31	29	31
P	wt.%	0.13		0.19		0.16		0.13		0.13		0.10		0.08		0.07
Pb	ppm	93	104	123	138	95	86	103	92	108	94	99	91	100	103	104
Zn	ppm	94	97	98	101	99	97	99	108	104	105	103	103	108	116	120
Ni	ppm	28	28	27	28	28	27	28	28	28	28	28	29	29	29	30
Cu	ppm	152	114	115	102	92	93	85	81	81	69	69	61	64	61	49
Br	ppm	648	672	696	689	700	728	715	703	712	638	642	609	617	611	599
I	ppm	117	123	125	126	112	107	105	96	99	92	95	88	106	105	105
^{137}Cs	Bq kg^{-1}															
% error																
$^{210}Pb_{xs}$	Bq kg^{-1}	32	30	34	34	27	19	22		27		21		16	13	15
% error		5	4	5	4	4	2	4		5		5		5	2	5
$^{206}Pb/^{204}Pb$		17.950	17.936		17.858	17.752	17.677	17.404		17.527		17.621		17.742	17.776	17.528
$^{207}Pb/^{204}Pb$		15.812	15.670		15.637	15.542	15.425	15.196		15.410		15.519		15.672	15.734	15.391
$^{208}Pb/^{204}Pb$		38.068	37.794		37.975	37.649	37.324	36.883		37.394		37.245		37.696	37.635	36.979

Table B 2(c): Sediment geochemical data.

HyPb Data

Sample:		46	47	48	49	50	51	52	53	54	55	56	57	58	59	60
Depth	cm	22.75	23.25	23.75	24.25	24.75	25.25	25.75	26.25	26.75	27.25	27.75	28.25	28.75	29.25	29.75
dry density	g cm^{-3}	0.24	0.32	0.35	0.28	0.27	0.30	0.33	0.35	0.30	0.31	0.30	0.35	0.34	0.35	0.28
LOI	wt.%		21.8		21.5		21.3		21.1		20.5		20.3		20.1	
C_{org}	wt.%															
Si	wt.%		22.89		23.04		23.09		23.18		23.31		23.39		23.45	
Al	wt.%		8.19		8.30		8.27		8.27		8.27		8.28		8.25	
K	wt.%		2.42		2.36		2.47		2.31		2.43		2.43		2.43	
Ti	wt.%	0.46	0.45	0.45	0.45	0.45	0.45	0.46	0.47	0.46	0.46	0.47	0.46		0.45	
Cr	ppm	100	94	101	96	99	95	100	101	96	100	99	101		100	
Na	wt.%		2.57		2.52		2.46		2.53		2.69		2.66		2.75	
Cl	wt.%		5.11		4.62		5.05		4.49		4.82		5.11		5.50	
Mg	wt.%		1.14		1.15		1.16		1.17		1.17		1.17		1.18	
Ca	wt.%		0.26		0.26		0.26		0.26		0.26		0.26		0.27	
Fe	wt.%		2.87		2.85		2.92		2.95		2.94		2.96		2.96	
Mn	wt.%	0.011	0.011	0.011	0.011	0.011	0.011	0.012	0.012	0.011	0.012	0.012	0.012		0.012	
S	wt.%		0.67		0.61		0.67		0.62		0.63		0.64		0.74	
As	ppm	28	31	32	30	32	33	32	32	32	30	28	30		26	
P	wt.%		0.07		0.07		0.06		0.06		0.06		0.06		0.06	
Pb	ppm	111	113	116	115	110	113	106	104	105	105	100	98		93	
Zn	ppm	127	129	127	125	121	135	125	116	112	113	106	107		106	
Ni	ppm	31	31	31	31	31	32	31	32	33	33	32	32		32	
Cu	ppm	38	49	43	34	33	38	29	29	31	29	28	28		30	
Br	ppm	568	610	591	585	600	582	560	567	576	538	532	553		544	
I	ppm	100	110	115	105	107	119	117	99	118	118	124	129		138	
^{137}Cs	Bq kg^{-1}															
% error																
$^{210}Pb_{xs}$	Bq kg^{-1}	14	16	14	15	14	13	12	12	13	13		10		11	
% error		2	5	5	5	5	6	5	5	5	5		5		5	
$^{206}Pb/^{204}Pb$			17.545	17.361	17.377	17.250		17.705	17.622	17.638	17.932		17.923		17.891	
$^{207}Pb/^{204}Pb$			15.409	15.330	15.357	15.219		15.568	15.442	15.398	15.536		15.518		15.538	
$^{208}Pb/^{204}Pb$			37.302	37.027	37.035	36.785		37.556	37.431	37.086	37.859		37.860		37.898	

Table B 2(d): Sediment geochemical data.

HyPb Data

Sample:		61	62	63	64	65	66	67	68	69	70	71	72	73	74	75
Depth	cm	30.25	30.75	31.25	31.75	32.25	32.75	33.25	33.75	34.25	34.75	35.25	35.75	36.25	36.75	37.25
dry density	g cm^{-3}	0.30	0.32	0.32	0.29	0.35	0.31	0.32	0.35	0.38	0.37	0.37	0.35	0.33	0.41	0.38
LOI	wt.%	20.3		20.3		21.5		20.2		17.9		18.0		19.7		19.2
C_{org}	wt.%															
Si	wt.%	23.39		23.42		22.96		23.38		24.31		24.19		23.42		23.40
Al	wt.%	8.22		8.23		8.05		8.23		8.46		8.43		8.20		8.22
K	wt.%	2.40		2.41		2.38		2.45		2.47		2.44		2.41		2.36
Ti	wt.%	0.46	0.44	0.46	0.46	0.45	0.46	0.46	0.48	0.47	0.48	0.47	0.44	0.45	0.43	0.45
Cr	ppm	99	94	98	96	96	96	96	99	96	103	100	93	96	92	94
Na	wt.%	2.74		2.71		2.86		2.76		2.46		2.45		2.58		2.46
Cl	wt.%	5.06		4.94		5.29		4.93		4.49		4.39		4.50		4.15
Mg	wt.%	1.18		1.19		1.18		1.19		1.18		1.18		1.17		1.17
Ca	wt.%	0.27		0.27		0.28		0.27		0.25		0.25		0.25		0.27
Fe	wt.%	2.97		2.95		2.92		3.03		3.19		3.36		3.58		4.08
Mn	wt.%	0.012	0.011	0.012	0.012	0.011	0.011	0.012	0.012	0.012	0.012	0.012	0.011	0.011	0.011	0.012
S	wt.%	0.71		0.79		0.93		1.01		1.18		1.46		1.88		2.48
As	ppm	27	30	27	30	32	32	34	28	29	30	34	38	38	41	39
P	wt.%	0.06		0.06		0.05		0.05		0.05		0.05		0.05		0.05
Pb	ppm	93	96	87	88	89	82	84	81	83	86	87	83	80	83	89
Zn	ppm	103	104	103	107	109	105	107	113	125	136	136	134	127	135	159
Ni	ppm	32	31	31	31	31	31	31	32	33	35	35	34	34	34	37
Cu	ppm	29	30	27	30	30	28	27	24	25	23	22	23	21	23	24
Br	ppm	548	584	554	557	571	545	522	472	433	417	432	455	436	438	401
I	ppm	138	137	128	125	135	126	118	102	110	119	129	135	122	137	132
^{137}Cs	Bq kg^{-1}															
% error																
$^{210}Pb_{xs}$	Bq kg^{-1}	9		8		7		5		4		4		2		2
% error		5		5		5		5		6		5		5		5
$^{206}Pb/^{204}Pb$		18.010		17.768		18.046		18.032		18.123						
$^{207}Pb/^{204}Pb$		15.643		15.305		15.474		15.541		15.526						
$^{208}Pb/^{204}Pb$		38.273		37.118		37.835		37.746		37.821						

Table B 2(e): Sediment geochemical data.

HyPb Data

Sample:		76	77	78	79	80	81	82	83	84	85	86	87	88	89	90
Depth	cm	37.75	38.25	38.75	39.25	39.75	40.25	40.75	41.25	41.75	42.25	42.75	43.25	43.75	44.25	44.75
dry density	g cm^{-3}	0.39	0.41	0.43	0.41	0.40	0.39	0.43	0.39	0.43	0.46	0.43	0.45	0.48	0.51	0.44
LOI	wt.%		23.1		20.8		19.7		19.7		19.8		18.2		18.4	
C_{org}	wt.%															
Si	wt.%		22.38		22.76		23.17		23.23		23.17		23.78		23.86	
Al	wt.%		7.84		7.96		7.99		7.84		7.84		7.96		7.96	
K	wt.%		1.83		2.20		2.35		2.31		2.31		2.34		2.30	
Ti	wt.%	0.46	0.40	0.40	0.40	0.44	0.43	0.39	0.43	0.40	0.43	0.40	0.42	0.45	0.45	0.45
Cr	ppm	97	85	85	82	91	91	80	88	83	91	86	86	92	94	88
Na	wt.%		2.18		2.30		2.17		2.12		2.07		2.01		1.95	
Cl	wt.%		4.36		4.10		3.35		3.26		3.37		3.45		3.20	
Mg	wt.%		1.09		1.11		1.11		1.09		1.09		1.09		1.08	
Ca	wt.%		0.26		0.28		0.28		0.29		0.30		0.33		0.29	
Fe	wt.%		4.15		4.64		4.68		4.91		4.92		4.97		4.87	
Mn	wt.%	0.012	0.011	0.011	0.011	0.012	0.013	0.012	0.013	0.012	0.013	0.013	0.014	0.015	0.015	0.015
S	wt.%		4.41		5.25		4.11		4.23		4.06		4.43		3.65	
As	ppm	42	53	47	48	43	34	49	40	39	36	38	35	30	29	31
P	wt.%		0.05		0.05		0.06		0.06		0.06		0.06		0.06	
Pb	ppm	91	89	88	89	88	84	82	78	73	73	73	73	73	73	71
Zn	ppm	154	154	155	147	133	128	134	126	121	112	111	110	113	120	122
Ni	ppm	38	37	36	34	36	35	35	36	33	33	32	33	34	35	34
Cu	ppm	24	24	25	25	24	21	22	21	19	21	21	22	21	20	21
Br	ppm	377	410	389	406	383	376	364	364	379	380	366	336	334	335	317
I	ppm	108	122	122	132	125	111	120	113	113	117	116	111	98	101	92
^{137}Cs	Bq kg^{-1}															
% error																
$^{210}Pb_{xs}$	Bq kg^{-1}		3		3		2		1		2		0		1	
% error			5		6		6		6		5		6		6	
$^{206}Pb/^{204}Pb$													18.126			
$^{207}Pb/^{204}Pb$													15.355			
$^{208}Pb/^{204}Pb$													37.555			

Table B 2(f): Sediment geochemical data.

HyPb Data

Sample:		91	92	93	94	95	96	97	98	99	100
Depth	cm	45.25	45.75	46.25	46.75	47.25	47.75	48.25	48.75	49.25	49.75
dry density	g cm^{-3}	0.51	0.46	0.41	0.51	0.50	0.47	0.45	0.43	0.42	0.46
LOI	wt.%	17.3		16.5		16.8		16.2		16.0	
C_{org}	wt.%										
Si	wt.%	24.24		24.52		24.30		24.48		24.63	
Al	wt.%	8.09		8.21		8.18		8.25		8.18	
K	wt.%	2.35		2.43		2.43		2.41		2.45	
Ti	wt.%	0.45	0.46	0.46	0.43	0.46	0.45	0.46	0.46	0.48	0.46
Cr	ppm	90	93	93	89	94	97	90	96	100	95
Na	wt.%	1.95		2.06		2.13		2.20		2.04	
Cl	wt.%	3.22		3.20		3.32		3.71		3.18	
Mg	wt.%	1.11		1.13		1.12		1.12		1.13	
Ca	wt.%	0.30		0.29		0.30		0.31		0.33	
Fe	wt.%	4.82		4.61		4.71		4.73		4.77	
Mn	wt.%	0.015	0.015	0.015	0.015	0.015	0.015	0.016	0.016	0.016	0.017
S	wt.%	3.66		3.52		3.66		3.75		2.86	
As	ppm	27	27	22	27	24	24	26	24	20	26
P	wt.%	0.06		0.05		0.06		0.06		0.05	
Pb	ppm	74	73	70	68	67	68	70	67	69	73
Zn	ppm	116	106	103	110	106	108	107	107	105	109
Ni	ppm	34	32	32	31	32	32	31	31	32	33
Cu	ppm	21	21	21	20	20	21	20	21	22	22
Br	ppm	300	313	313	317	319	302	302	292	282	279
I	ppm	88	92	85	89	83	88	88	82	75	77
^{137}Cs	Bq kg^{-1}										
% error											
$^{210}Pb_{xs}$	Bq kg^{-1}	0		0		0		0		0	
% error		6		5		6		6		6	
$^{206}Pb/^{204}Pb$		18.175				18.145				18.201	
$^{207}Pb/^{204}Pb$		15.415				15.459				15.424	
$^{208}Pb/^{204}Pb$		37.598				37.601				37.571	

Table B 2(g): Sediment geochemical data.

HySR2 Data

Sample:		1	2	3	4	5	6	7	8	9	10	11	12	13	14	15
Depth	cm	0.5	1.5	2.5	3.5	4.5	5.5	6.5	7.5	8.5	9.5	10.5	11.5	12.5	13.5	14.5
dry density	g cm^{-3}	0.46	0.46	0.46	0.44	0.45	0.43	0.40	0.43	0.42	0.40	0.38	0.38	0.38	0.38	0.34
LOI	wt.%	22.6	24.7	22.0	23.6	21.9	21.0	22.8	23.2	20.6	19.9	23.5	25.7	21.8	21.1	20.7
C_{org}	wt.%	n. d.														
Si	wt.%	22.19	22.21	22.88	22.12	22.90	23.74	22.87	22.20	24.21	24.23	22.99	21.91	23.40	24.14	24.36
Al	wt.%	7.05	7.30	7.46	7.39	7.62	7.81	7.61	7.33	8.27	8.34	8.02	7.82	8.30	8.24	8.38
K	wt.%	2.00	2.15	2.16	2.11	2.18	2.27	2.20	2.10	2.35	2.37	2.31	2.14	2.36	2.30	2.36
Ti	wt.%	0.44	0.42	0.43	0.42	0.43	0.45	0.43	0.41	0.47	0.49	0.46	0.44	0.47	0.46	0.48
Cr	ppm	91	94	96	97	96	106	102	102	115	115	107	104	108	106	106
Na	wt.%	1.37	1.66	1.56	1.60	1.56	1.51	1.62	1.68	1.55	1.46	1.58	1.71	1.94	1.75	1.71
Cl	wt.%	2.53	2.85	2.55	2.66	2.56	2.50	2.77	2.88	2.55	2.19	2.56	3.08	2.75	2.74	2.71
Mg	wt.%	1.01	1.06	1.05	1.02	1.01	1.00	0.99	0.98	1.06	1.05	1.07	1.06	1.10	1.08	1.08
Ca	wt.%	2.09	0.62	0.51	0.52	0.38	0.32	0.33	0.35	0.29	0.27	0.28	0.30	0.28	0.28	0.28
Fe	wt.%	4.37	4.12	4.80	4.41	5.28	4.17	4.21	5.29	3.17	2.84	2.74	2.50	2.68	2.74	2.76
Mn	wt.%	0.029	0.019	0.018	0.017	0.017	0.014	0.014	0.013	0.013	0.013	0.012	0.011	0.012	0.012	0.013
S	wt.%	1.26	0.83	0.61	0.62	0.60	0.51	0.53	0.55	0.47	0.47	0.57	0.63	0.53	0.54	0.53
As	ppm	28	32	36	34	35	31	36	50	32	24	27	30	27	31	25
P	wt.%	0.14	0.15	0.17	0.17	0.18	0.13	0.14	0.21	0.11	0.08	0.07	0.07	0.08	0.08	0.08
Pb	ppm	102	78	79	86	87	75	75	83	86	82	79	88	100	92	98
Zn	ppm	155	160	157	149	151	125	120	116	112	125	140	138	132	131	126
Ni	ppm	31	32	33	33	33	32	30	30	31	33	33	33	34	34	33
Cu	ppm	136	134	120	121	129	145	147	153	185	229	280	332	322	374	262
Br	ppm	252	372	408	432	396	372	420	408	324	276	276	372	372	384	396
I	ppm	98	96	115	115	120	95	115	128	88	73	58	74	92	86	84
^{137}Cs	Bq kg^{-1}	8	13	19	20	18	17	19	19	24	26	37	42	55	60	36
% error		13	8	7	8	9	13	8	10	7	7	6	4	5	4	6
$^{210}Pb_{xs}$	Bq kg^{-1}	41	55	52	49	38	35	36	34	36	32	36	41	37	27	21
% error		3	3	3	3	4	2	3	3	3	3	3	3	3	3	3
$^{206}Pb/^{204}Pb$		n. d.														
$^{207}Pb/^{204}Pb$		n. d.														
$^{208}Pb/^{204}Pb$		n. d.														

Table B 3(a): Sediment geochemical data.

HySR2 Data

Sample:		16	17	18	19	20	21	22	23	24	25	26	27	28	29	30
Depth	cm	15.5	16.5	17.5	18.5	19.5	20.5	21.5	22.5	23.5	24.5	25.5	26.5	27.5	28.5	29.5
dry density	g cm^{-3}	0.30	0.27	0.37	0.36	0.31	0.35	0.32	0.45	0.44	0.40	0.48	0.56	0.50	0.52	0.56
LOI	wt.%	20.5	21.7	21.0	20.3	19.6	19.2	18.7	17.5	17.3	17.2	17.3	17.2	17.5	17.3	18.2
C_{org}	wt.%															
Si	wt.%	24.18	24.11	24.05	24.30	24.73	24.72	25.09	25.12	25.12	25.29	25.20	24.83	24.74	24.56	24.34
Al	wt.%	8.21	8.12	8.06	8.18	8.30	8.32	8.51	8.50	8.50	8.51	8.51	8.40	8.37	8.40	8.35
K	wt.%	2.32	2.31	2.29	2.34	2.38	2.37	2.44	2.45	2.46	2.43	2.42	2.41	2.42	2.43	2.43
Ti	wt.%	0.48	0.47	0.48	0.48	0.49	0.49	0.49	0.50	0.49	0.50	0.49	0.49	0.49	0.49	0.48
Cr	ppm	104	103	103	105	103	107	105	103	106	108	103	106	105	102	100
Na	wt.%	1.59	1.69	1.69	1.71	1.67	1.65	1.69	1.64	1.59	1.59	1.55	1.58	1.59	1.59	1.72
Cl	wt.%	2.58	3.01	2.92	2.79	2.65	2.65	2.67	2.47	2.55	2.56	2.40	2.39	2.23	2.23	2.39
Mg	wt.%	1.05	1.04	1.03	1.06	1.05	1.04	1.07	1.06	1.07	1.08	1.06	1.05	1.06	1.07	1.08
Ca	wt.%	0.25	0.26	0.25	0.25	0.25	0.25	0.25	0.25	0.25	0.24	0.25	0.25	0.25	0.24	0.24
Fe	wt.%	2.67	2.70	2.67	2.80	2.85	2.82	2.87	2.97	3.01	3.05	3.34	3.72	4.12	4.31	4.53
Mn	wt.%	0.013	0.012	0.012	0.013	0.013	0.013	0.013	0.013	0.013	0.013	0.013	0.013	0.013	0.014	0.013
S	wt.%	0.56	0.53	0.52	0.51	0.48	0.47	0.48	0.55	0.60	0.76	1.13	1.56	1.93	2.04	2.33
As	ppm	26	28	27	27	22	23	23	26	30	28	36	35	34	32	34
P	wt.%	0.08	0.07	0.08	0.08	0.08	0.07	0.07	0.08	0.08	0.07	0.07	0.07	0.07	0.07	0.06
Pb	ppm	100	103	101	106	105	101	98	101	93	96	106	110	110	118	118
Zn	ppm	137	149	147	136	127	124	134	162	158	168	192	183	160	144	137
Ni	ppm	33	33	33	33	32	31	32	36	35	37	41	43	39	38	37
Cu	ppm	211	151	124	99	87	75	72	64	56	51	47	44	39	35	31
Br	ppm	420	432	420	456	456	444	432	396	396	360	312	276	288	300	336
I	ppm	89	92	94	107	105	101	99	88	95	89	83	81	83	86	96
^{137}Cs	Bq kg^{-1}	25	27	20	17	14	10	7	5	5	3	2	2	0	0	0
% error		8	6	7	8	10	7	16	14	25	26	53	34			
$^{210}Pb_{xs}$	Bq kg^{-1}	20	20	23	24	25	23	17	17	12	11	13	11	9	8	7
% error		4	4	4	4	4	4	4	4	8	5	4	4	2	2	2
$^{206}Pb/^{204}Pb$																
$^{207}Pb/^{204}Pb$																
$^{208}Pb/^{204}Pb$																

Table B 3(b): Sediment geochemical data.

HySR2 Data

Sample:		31	32	33	34	35	36	37	38	39	40	41	42	43	44	45
Depth	cm	30.5	31.5	32.5	33.5	34.5	35.5	36.5	37.5	38.5	39.5	40.5	41.5	42.5	43.5	44.5
dry density	g cm^{-3}	0.57	0.49	0.45	0.41	0.39	0.38	0.41	0.43	0.41	0.42	0.42	0.38	0.42	0.50	0.48
LOI	wt.%	17.3	16.9	17.1	17.2	17.1	17.8	17.6	17.7	17.1	17.4	18.0	17.4	17.1	16.7	17.1
C_{org}	wt.%															
Si	wt.%	24.05	24.62	24.58	24.80	25.02	24.38	24.50	24.62	24.66	24.45	24.35	24.43	24.73	24.77	24.58
Al	wt.%	8.50	8.48	8.54	8.56	8.56	8.33	8.43	8.38	8.37	8.31	8.27	8.25	8.29	8.35	8.23
K	wt.%	2.44	2.38	2.45	2.41	2.48	2.41	2.42	2.41	2.41	2.41	2.35	2.41	2.42	2.42	2.38
Ti	wt.%	0.49	0.49	0.49	0.49	0.49	0.49	0.49	0.49	0.49	0.49	0.49	0.49	0.49	0.49	0.49
Cr	ppm	102	102	106	104	102	102	103	103	103	102	103	102	101	102	103
Na	wt.%	1.76	1.72	1.80	1.88	1.94	1.93	1.93	1.92	1.93	1.89	1.91	1.84	1.78	1.78	1.76
Cl	wt.%	2.54	2.55	2.76	2.93	2.98	3.02	2.99	3.00	3.12	3.07	3.11	2.95	2.80	2.69	2.68
Mg	wt.%	1.10	1.09	1.09	1.11	1.12	1.09	1.10	1.10	1.08	1.08	1.10	1.08	1.08	1.09	1.07
Ca	wt.%	0.25	0.25	0.25	0.25	0.25	0.25	0.25	0.25	0.25	0.25	0.25	0.25	0.25	0.25	0.26
Fe	wt.%	4.43	4.12	4.10	4.00	3.93	3.90	3.89	3.92	4.02	4.16	4.21	4.23	4.44	4.67	4.84
Mn	wt.%	0.013	0.013	0.013	0.013	0.012	0.013	0.013	0.013	0.013	0.014	0.014	0.014	0.014	0.015	0.016
S	wt.%	2.10	2.00	2.03	2.07	2.06	2.20	2.17	2.25	2.23	2.41	2.46	2.46	2.62	2.70	2.79
As	ppm	35	37	37	35	37	36	33	29	29	27	32	34	35	36	36
P	wt.%	0.06	0.06	0.06	0.06	0.06	0.06	0.06	0.06	0.06	0.06	0.06	0.06	0.06	0.06	0.06
Pb	ppm	104	102	99	95	95	96	97	90	89	89	89	89	86	83	84
Zn	ppm	132	131	132	133	130	139	136	134	142	148	150	155	151	139	133
Ni	ppm	38	36	36	36	36	36	37	37	34	35	36	39	45	43	40
Cu	ppm	29	29	28	28	28	30	32	32	32	33	32	33	30	26	26
Br	ppm	348	372	396	396	396	408	384	372	336	324	312	276	264	252	264
I	ppm	105	118	118	112	114	108	106	97	94	90	89	80	78	78	89
^{137}Cs	Bq kg^{-1}															
% error																
$^{210}Pb_{xs}$	Bq kg^{-1}	7	7	7	7	5	6	5	4	5	4	4	3	3	2	2
% error		4	4	4	4	2	2	2	2	2	2	2	4	4	2	4
$^{206}Pb/^{204}Pb$																
$^{207}Pb/^{204}Pb$																
$^{208}Pb/^{204}Pb$																

Table B 3(c): Sediment geochemical data.

HySR3 Data

Sample:		1	2	3	4	5	6	7	8	9	10	11	12	13	14	15
Depth	cm	0.5	1.5	2.5	3.5	4.5	5.5	6.5	7.5	8.5	9.5	10.5	11.5	12.5	13.5	14.5
dry density	g cm^{-3}	0.27	0.23	0.22	0.20	0.15	0.19	0.17	0.22	0.23	0.18	0.22	0.19	0.18	0.18	0.21
LOI	wt.%	41.3	41.5	38.1	43.0	52.3	52.7	57.1	52.5	47.9	42.9	36.9	34.4	35.2	36.2	36.6
C_{org}	wt.%	15.8		13.1		22.8								12.3	14.0	
Si	wt.%	17.27	17.51	18.54	16.65	13.55	13.40	12.02	13.34	15.18	16.72	18.64	19.48	19.43	18.98	18.68
Al	wt.%	5.81	5.85	6.39	5.91	4.97	4.99	4.55	4.74	5.38	5.90	6.54	6.76	6.77	6.59	6.39
K	wt.%	1.66	1.67	1.76	1.74	1.43	1.43	1.34	1.34	1.53	1.64	1.83	1.78	1.79	1.76	1.79
Ti	wt.%	0.35	0.34	0.37	0.30	0.28	0.26	0.25	0.28	0.31	0.34	0.38	0.39	0.39	0.39	0.38
Cr	ppm	72	80	87	75	72	67	61	66	73	81	87	84	90	87	86
Na	wt.%	1.47	1.86	1.91	1.92	2.15	2.08	1.99	2.60	2.33	2.28	2.26	2.23	2.23	2.40	2.69
Cl	wt.%	2.86	3.03	3.06	4.36	4.73	4.81	4.95	4.52	4.14	4.01	3.65	3.81	3.89	3.98	4.20
Mg	wt.%	0.83	0.81	0.87	0.86	0.83	0.84	0.79	0.83	0.81	0.83	0.86	0.92	0.90	0.90	0.88
Ca	wt.%	0.43	0.31	0.29	0.34	0.38	0.38	0.39	0.39	0.31	0.29	0.27	0.25	0.24	0.26	0.27
Fe	wt.%	2.46	1.80	1.78	2.00	1.48	1.47	1.29	1.52	1.29	1.72	1.97	2.10	1.60	1.66	1.97
Mn	wt.%	0.018	0.012	0.012	0.010	0.009	0.009	0.008	0.008	0.010	0.011	0.012	0.013	0.012	0.012	0.012
S	wt.%	0.76	0.75	0.62	0.84	0.90	0.99	1.09	1.02	0.90	0.84	0.73	0.72	0.72	0.76	0.78
As	ppm	34	52	41	45	50	50	50	46	36	38	31	29	29	31	34
P	wt.%	0.19	0.14	0.12	0.11	0.12	0.11	0.10	0.13	0.14	0.15	0.14	0.13	0.12	0.12	0.13
Pb	ppm	151	85	65	76	96	94	106	106	110	104	94	84	75	70	69
Zn	ppm	133	97	80	73	75	78	88	100	108	113	108	105	123	108	89
Ni	ppm	27	27	26	25	25	25	27	28	29	29	29	29	29	29	28
Cu	ppm	97	114	125	151	166	185	233	258	223	177	142	130	120	114	112
Br	ppm	450	1032	963	1052	1112	1077	1209	1015	838	774	634	611	606	612	600
I	ppm	73	65	47	50	49	43	40	46	51	55	61	62	63	66	71
^{137}Cs	Bq kg^{-1}	13	37	24	22	26	26	37	47	70	104	127	95	98	79	67
% error		23	16	20	23	25	19	17	23	19	8	6	10	9	11	9
$^{210}Pb_{xs}$	Bq kg^{-1}	110	115	67	73	86	78	85	65	67	60	50	40	33	30	25
% error		3	3	3	2	2	2	3	2	2	2	2	2	3	3	2
$^{206}Pb/^{204}Pb$		n. d.														
$^{207}Pb/^{204}Pb$		n. d.														
$^{208}Pb/^{204}Pb$		n. d.														

Table B 4(a): Sediment geochemical data.

HySR3 Data

Sample:		16	17	18	19	20	21	22	23	24	25	26	27	28	29	30
Depth	cm	15.5	16.5	17.5	18.5	19.5	20.5	21.5	22.5	23.5	24.5	25.5	26.5	27.5	28.5	29.5
dry density	g cm^{-3}	0.18	0.16	0.16	0.16	0.15	0.22	0.25	0.32	0.37	0.37	0.40	0.32	0.35	0.39	0.39
LOI	wt.%	37.9	42.9	39.9	39.3	40.5	38.6	30.9	27.2	23.0	23.8	25.3	24.5	24.2	23.6	24.2
C_{org}	wt.%	15.7			15.0				8.3	6.9	6.7	6.9	6.4	6.1	6.2	
Si	wt.%	18.01	16.51	17.32	17.53	17.20	17.80	20.20	21.60	22.87	22.65	22.14	22.30	22.43	22.56	22.51
Al	wt.%	6.17	5.66	5.96	6.04	5.94	6.20	7.11	7.58	8.01	7.96	7.85	7.81	7.77	7.86	7.70
K	wt.%	1.74	1.50	1.61	1.62	1.61	1.67	1.90	2.07	2.18	2.17	2.12	2.14	2.16	2.14	2.13
Ti	wt.%	0.37	0.34	0.36	0.37	0.36	0.36	0.41	0.44	0.46	0.46	0.46	0.46	0.46	0.46	0.46
Cr	ppm	80	76	81	79	80	78	90	97	99	101	98	98	98	95	97
Na	wt.%	2.85	3.20	3.35	3.29	3.35	3.20	2.76	2.46	2.32	2.26	2.28	2.49	2.51	2.65	2.53
Cl	wt.%	5.14	6.01	6.11	6.25	6.02	5.58	4.48	3.51	3.38	3.22	3.22	3.58	3.46	3.55	3.72
Mg	wt.%	0.89	0.92	0.95	0.96	0.96	0.97	1.02	1.01	1.05	1.03	1.02	1.06	1.04	1.03	1.03
Ca	wt.%	0.29	0.29	0.29	0.29	0.29	0.27	0.26	0.24	0.24	0.23	0.22	0.23	0.24	0.23	0.23
Fe	wt.%	2.20	1.48	1.61	1.64	1.28	1.58	2.32	2.23	2.69	2.62	2.57	2.64	2.57	2.72	2.63
Mn	wt.%	0.011	0.010	0.011	0.011	0.012	0.011	0.013	0.014	0.015	0.015	0.015	0.014	0.014	0.014	0.014
S	wt.%	0.89	0.99	0.95	0.94	0.96	0.90	0.70	0.59	0.54	0.53	0.56	0.63	0.66	0.70	0.74
As	ppm	30	41	42	39	40	36	30	28	24	27	25	26	27	31	29
P	wt.%	0.13	0.10	0.11	0.10	0.10	0.09	0.10	0.11	0.11	0.11	0.10	0.10	0.10	0.10	0.07
Pb	ppm	69	71	69	71	79	89	95	106	112	110	108	93	92	90	77
Zn	ppm	88	83	84	91	94	105	108	108	105	107	108	100	93	90	98
Ni	ppm	27	24	25	24	24	24	27	29	30	31	30	31	30	29	30
Cu	ppm	118	121	100	92	90	74	54	43	37	33	30	27	26	26	27
Br	ppm	616	651	636	623	632	566	512	469	451	483	495	482	483	472	464
I	ppm	59	55	53	54	52	66	70	76	75	85	87	91	91	90	80
^{137}Cs	Bq kg^{-1}	62	42	36	22	16	0	19	23	13	28	9	8	0	0	0
% error		17	26	27	34	38		20	31	41	37	37	45			
$^{210}Pb_{xs}$	Bq kg^{-1}	21	21	20	17	16	16	15	16	15	18	19	7	9	4	9
% error		3	3	3	3	4	4	3	3	3	3	10	3	3	3	3
$^{206}Pb/^{204}Pb$																
$^{207}Pb/^{204}Pb$																
$^{208}Pb/^{204}Pb$																

Table B 4(b): Sediment geochemical data.

HySR3 Data

Sample:		31	32	33	34	35	36	37	38	39	40	41	42	43	44	45
Depth	cm	30.5	31.5	32.5	33.5	34.5	35.5	36.5	37.5	38.5	39.5	40.5	41.5	42.5	43.5	44.5
dry density	g cm^{-3}	0.33	0.31	0.35	0.34	0.42	0.41	0.40	0.51	0.42	0.43	0.46	0.53	0.49	0.49	0.63
LOI	wt.%	25.3	29.1	28.8	24.3	21.3	21.5	22.7	23.1	22.0	21.9	21.9	22.1	21.6	20.9	19.8
C_{org}	wt.%	7.4	9.1	8.7	6.0	5.5	5.3	5.6	5.2	5.3	5.0	5.2	5.2	4.5	4.0	4.1
Si	wt.%	21.90	20.67	20.78	22.54	23.49	23.39	22.89	22.28	22.27	22.25	21.90	21.80	22.12	22.54	23.16
Al	wt.%	7.51	7.09	7.19	7.76	7.98	7.97	7.68	7.59	7.67	7.66	7.52	7.32	7.42	7.47	7.58
K	wt.%	2.03	1.95	1.95	2.17	2.26	2.22	2.17	2.13	2.17	2.17	2.13	2.03	2.07	2.09	2.05
Ti	wt.%	0.45	0.42	0.42	0.46	0.48	0.48	0.47	0.45	0.45	0.45	0.44	0.44	0.45	0.46	0.47
Cr	ppm	95	87	91	96	101	98	97	96	96	95	96	94	95	95	95
Na	wt.%	2.69	3.01	2.85	2.49	2.43	2.32	2.44	2.37	2.39	2.24	2.36	2.17	2.15	2.06	1.91
Cl	wt.%	4.04	4.59	4.45	3.50	3.08	3.35	3.36	3.20	3.07	2.87	2.91	3.04	3.02	2.79	2.52
Mg	wt.%	1.04	1.03	1.02	1.04	1.07	1.06	1.04	1.03	1.04	1.01	1.02	1.01	1.00	1.01	1.04
Ca	wt.%	0.22	0.24	0.24	0.22	0.21	0.21	0.21	0.21	0.22	0.22	0.23	0.24	0.25	0.28	0.35
Fe	wt.%	3.20	2.54	2.68	2.51	2.85	2.93	3.10	4.01	4.49	4.81	5.43	6.15	5.80	5.60	5.57
Mn	wt.%	0.014	0.013	0.013	0.015	0.015	0.015	0.015	0.016	0.016	0.017	0.017	0.018	0.020	0.022	0.025
S	wt.%	0.88	1.04	0.97	0.78	0.81	0.93	1.43	2.23	2.51	2.67	3.14	3.49	3.13	2.80	2.69
As	ppm	42	45	44	33	22	26	47	55	44	29	33	35	32	26	27
P	wt.%	0.07	0.06	0.06	0.06	0.06	0.06	0.06	0.06	0.07	0.06	0.06	0.06	0.06	0.06	0.07
Pb	ppm	77	79	88	71	68	77	89	102	93	84	81	80	77	72	70
Zn	ppm	101	87	87	91	89	99	150	212	207	137	124	121	119	112	111
Ni	ppm	30	28	27	28	29	30	36	43	39	34	33	32	32	32	32
Cu	ppm	28	28	29	26	24	24	23	24	25	23	23	23	23	21	21
Br	ppm	490	518	505	420	370	357	375	365	335	305	312	328	324	316	290
I	ppm	75	78	80	80	74	67	74	71	72	75	74	89	88	73	64
^{137}Cs	Bq kg^{-1}															
% error																
$^{210}Pb_{xs}$	Bq kg^{-1}	3	5	6	1	-1	0	2	4	2	2	0	1	0	0	0
% error		3	3	3	3	3	3	3	3	3	3	3	3	4	5	4
$^{206}Pb/^{204}Pb$																
$^{207}Pb/^{204}Pb$																
$^{208}Pb/^{204}Pb$																

Table B 4(c): Sediment geochemical data.

HySR5 Data

Sample:		1	2	3	4	5	6	7	8	9	10	11	12	13	14	15
Depth	cm	0.5	1.5	2.5	3.5	4.5	5.5	6.5	7.5	8.5	9.5	10.5	11.5	12.5	13.5	14.5
dry density	g cm^{-3}	0.31	0.30	0.25	0.26	0.19	0.19	0.16	0.17	0.17	0.15	0.20	0.20	0.19	0.16	0.17
LOI	wt.%	36.2	35.2	31.6	33.9	41.3	47.5	55.9	54.7	48.0	44.7	37.2	31.8	28.5	28.3	28.6
C_{org}	wt.%	14.8			13.6			26.0			19.4			10.4		
Si	wt.%	18.35	18.45	19.29	18.66	15.85	13.83	11.27	11.45	13.81	15.14	17.90	19.66	20.95	21.12	21.14
Al	wt.%	5.88	6.19	6.67	6.55	5.71	5.03	4.15	4.22	4.99	5.46	6.39	6.99	7.42	7.48	7.43
K	wt.%	1.81	1.91	2.00	1.96	1.69	1.56	1.29	1.28	1.50	1.63	1.93	2.05	2.19	2.22	2.21
Ti	wt.%	0.40	0.37	0.40	0.38	0.35	0.30	0.25	0.26	0.31	0.34	0.39	0.44	0.46	0.46	0.46
Cr	ppm	95	103	109	110	97	89	76	81	92	95	108	115	121	121	120
Na	wt.%	1.95	2.13	2.04	2.18	2.37	2.58	2.37	2.41	2.39	2.43	2.35	2.18	2.08	2.02	2.08
Cl	wt.%	4.17	4.08	3.49	4.08	4.64	5.59	6.12	6.14	5.44	5.07	4.63	3.88	3.64	3.43	3.42
Mg	wt.%	0.93	0.97	1.00	1.02	0.99	1.02	0.96	0.98	1.02	1.04	1.06	1.06	1.05	1.04	1.05
Ca	wt.%	0.68	0.40	0.36	0.39	0.43	0.48	0.51	0.51	0.48	0.44	0.37	0.30	0.28	0.27	0.27
Fe	wt.%	2.81	2.98	3.76	3.50	3.16	2.62	2.24	2.29	2.40	2.24	2.27	2.31	2.38	2.34	2.27
Mn	wt.%	0.017	0.012	0.013	0.012	0.011	0.010	0.009	0.009	0.010	0.010	0.012	0.014	0.014	0.014	0.015
S	wt.%	0.76	0.70	0.60	0.67	0.78	0.97	1.13	1.17	1.07	1.01	0.97	0.84	0.80	0.77	0.81
As	ppm	29	42	42	40	46	50	55	56	54	48	38	31	25	25	26
P	wt.%	0.16	0.20	0.24	0.25	0.28	0.27	0.25	0.28	0.28	0.27	0.19	0.13	0.11	0.10	0.09
Pb	ppm	120	76	83	86	86	87	87	100	108	117	115	120	126	122	115
Zn	ppm	121	97	98	98	97	96	96	99	106	113	122	127	136	135	124
Ni	ppm	28	29	30	31	29	29	27	29	30	30	32	32	33	32	32
Cu	ppm	91	111	121	134	141	156	176	197	189	169	149	126	109	100	99
Br	ppm	530	852	790	872	1032	1194	1345	1388	1260	1149	965	788	669	654	647
I	ppm	82	87	107	111	112	97	102	105	104	99	99	90	91	95	100
^{137}Cs	Bq kg^{-1}	12	39	27	28	28	25	31	43	54	64	72	80	77	66	49
% error		10	6	6	8	20	9	7	7	4	6	3	4	4	6	8
$^{210}Pb_{xs}$	Bq kg^{-1}	100	93	85	76	66	58	47	45	46	40	36	38	40	34	32
% error		3	3	3	3	3	3	3	3	3	3	3	3	3	3	3
$^{206}Pb/^{204}Pb$		17.608	17.572	17.800	17.491	17.600	17.740	17.548	17.459	17.358	17.300	17.237	17.404	17.548	17.681	17.649
$^{207}Pb/^{204}Pb$		15.567	15.541	15.728	15.440	15.570	15.692	15.631	15.504	15.510	15.470	15.424	15.499	15.646	15.753	15.839
$^{208}Pb/^{204}Pb$		37.677	37.581	38.130	37.678	37.680	37.695	37.821	37.308	37.197	37.150	37.112	37.339	37.820	37.663	37.680

Table B5(a): Sediment geochemical data.

HySR5 Data

Sample:		16	17	18	19	20	21	22	23	24	25	26	27	28	29	30
Depth	cm	15.5	16.5	17.5	18.5	19.5	20.5	21.5	22.5	23.5	24.5	25.5	26.5	27.5	28.5	29.5
dry density	g cm^{-3}	0.21	0.16	0.20	0.15	0.13	0.12	0.14	0.20	0.25	0.35	0.39	0.46	0.47	0.46	0.51
LOI	wt.%	25.7	29.9	30.2	37.7	43.8	47.3	40.3	42.3	32.8	25.5	21.8	18.3	18.9	19.1	19.6
C_{org}	wt.%	9.5			15.4			17.5			9.6			6.1		
Si	wt.%	22.00	20.68	20.46	17.91	16.14	14.76	17.30	16.97	19.64	22.37	23.60	24.54	24.47	24.04	24.13
Al	wt.%	7.75	7.22	7.13	6.27	5.60	5.11	6.03	5.92	6.88	7.71	8.02	8.35	8.24	8.05	8.07
K	wt.%	2.25	2.15	2.12	1.91	1.80	1.64	1.79	1.79	2.03	2.22	2.28	2.42	2.40	2.35	2.32
Ti	wt.%	0.47	0.46	0.44	0.39	0.34	0.32	0.37	0.35	0.42	0.47	0.49	0.52	0.51	0.51	0.50
Cr	ppm	117	113	115	103	92	90	98	97	106	118	124	130	124	128	122
Na	wt.%	1.99	2.14	2.19	2.39	2.45	2.36	2.39	2.29	2.11	1.90	1.74	1.56	1.65	1.63	1.69
Cl	wt.%	3.11	3.55	3.53	4.28	4.95	5.00	4.24	3.96	3.40	2.83	2.39	2.00	2.00	2.13	2.25
Mg	wt.%	1.05	1.02	1.02	0.96	0.93	0.89	0.96	0.94	0.99	1.05	1.05	1.06	1.06	1.05	1.07
Ca	wt.%	0.26	0.27	0.26	0.28	0.30	0.29	0.28	0.31	0.28	0.26	0.22	0.21	0.21	0.21	0.24
Fe	wt.%	2.36	2.20	2.18	1.83	1.46	1.17	1.73	1.70	2.06	2.39	2.66	2.95	3.16	3.24	3.58
Mn	wt.%	0.015	0.015	0.014	0.012	0.012	0.011	0.012	0.012	0.015	0.013	0.013	0.014	0.014	0.014	0.015
S	wt.%	0.77	0.91	0.99	1.19	1.36	1.36	1.08	1.17	0.92	0.78	0.82	0.97	1.39	1.61	2.00
As	ppm	25	26	25	28	35	37	38	38	30	26	24	25	30	25	24
P	wt.%	0.08	0.08	0.07	0.07	0.06	0.06	0.06	0.06	0.06	0.06	0.05	0.04	0.04	0.04	0.05
Pb	ppm	95	92	78	80	96	110	110	128	123	108	96	90	88	79	82
Zn	ppm	118	117	110	114	127	139	129	129	124	117	115	139	136	123	124
Ni	ppm	33	31	30	27	26	24	26	25	28	30	31	35	36	34	35
Cu	ppm	83	90	86	97	119	119	83	56	38	29	27	25	26	27	25
Br	ppm	596	646	613	663	703	715	731	719	658	544	420	334	318	304	298
I	ppm	103	117	115	111	103	91	91	95	102	114	95	80	80	75	79
^{137}Cs	Bq kg^{-1}	45	34	25	19	16	15	14	8	7	5	3	2	2	0	0
% error		6	9	8	11	10	14	11	19	14	25	17	48	37		
$^{210}Pb_{xs}$	Bq kg^{-1}	21	21	16	14	18	24	23	26	22	17	11	8	5	4	3
% error		3	3	4	3	3	3	3	3	3	3	3	3	3	3	3
$^{206}Pb/^{204}Pb$		17.933	17.313	17.602	17.389	17.415	17.542	17.597	17.536	17.675	18.067	17.921	18.140	18.103	17.855	18.021
$^{207}Pb/^{204}Pb$		15.985	15.268	15.542	15.469	15.466	15.478	15.437	15.476	15.572	15.797	15.680	15.515	15.532	15.390	15.556
$^{208}Pb/^{204}Pb$		38.318	36.984	37.889	37.118	36.952	37.364	37.434	37.656	37.760	38.087	37.994	38.120	38.273	37.545	38.000

Table B 5(b): Sediment geochemical data.

HySR5 Data

Sample:		31	32	33	34	35	36	37	38	39	40	41	42	43	44	45
Depth	cm	30.5	31.5	32.5	33.5	34.5	35.5	36.5	37.5	38.5	39.5	40.5	41.5	42.5	43.5	44.5
dry density	g cm^{-3}	0.39	0.48	0.41	0.45	0.46	0.54	0.65	0.63	0.67	0.55	0.66	0.52	0.57	0.62	0.63
LOI	wt.%	20.8	20.7	20.0	20.1	19.7	18.2	16.1	15.3	16.2	16.7	17.1	16.5	15.9	15.4	15.1
C_{org}	wt.%	7.0			6.3			4.3			4.8					
Si	wt.%	23.43	23.59	23.77	23.61	23.55	24.28	25.04	25.58	24.98	24.84	24.75	25.09	25.25	25.20	25.04
Al	wt.%	7.82	7.79	7.82	7.84	7.87	8.07	8.40	8.66	8.52	8.36	8.27	8.22	8.15	8.09	8.14
K	wt.%	2.26	2.30	2.27	2.30	2.32	2.36	2.43	2.46	2.46	2.42	2.41	2.21	2.37	2.37	2.38
Ti	wt.%	0.50	0.49	0.49	0.46	0.46	0.47	0.49	0.50	0.49	0.49	0.47	0.47	0.47	0.48	0.48
Cr	ppm	123	124	120	106	108	112	117	121	118	116	112	110	108	116	111
Na	wt.%	1.75	1.78	1.76	1.74	1.70	1.58	1.40	1.40	1.41	1.51	1.56	1.52	1.53	1.52	1.41
Cl	wt.%	2.43	2.44	2.38	2.35	2.36	2.03	1.62	1.59	1.74	1.81	2.19	2.05	2.10	1.87	1.73
Mg	wt.%	1.06	1.08	1.06	1.08	1.08	1.08	1.10	1.11	1.10	1.10	1.09	1.10	1.12	1.13	1.13
Ca	wt.%	0.25	0.26	0.25	0.25	0.25	0.25	0.24	0.25	0.29	0.25	0.25	0.27	0.35	0.42	0.55
Fe	wt.%	3.72	3.75	3.68	3.80	3.81	3.99	4.01	3.85	3.62	3.52	3.68	3.80	4.01	4.24	4.50
Mn	wt.%	0.016	0.016	0.016	0.015	0.015	0.016	0.017	0.016	0.016	0.015	0.015	0.016	0.017	0.018	0.020
S	wt.%	2.09	2.24	2.12	2.10	2.15	2.13	1.90	1.62	1.50	1.48	2.04	2.00	2.25	2.23	2.50
As	ppm	24	20	21	26	22	24	32	20	23	23	23	27	27	29	24
P	wt.%	0.05	0.05	0.05	0.05	0.05	0.05	0.05	0.05	0.05	0.05	0.05	0.05	0.05	0.05	0.05
Pb	ppm	84	88	89	89	83	80	76	79	81	82	87	90	87	82	76
Zn	ppm	119	124	127	123	120	117	112	113	108	110	114	112	111	110	110
Ni	ppm	34	34	33	34	34	35	36	37	37	36	38	37	37	37	37
Cu	ppm	25	25	26	26	25	23	22	25	25	24	22	20	21	21	22
Br	ppm	303	307	303	301	292	260	209	204	224	222	222	211	210	196	167
I	ppm	80	83	80	81	84	74	67	62	69	70	73	75	77	77	64
^{137}Cs	Bq kg^{-1}															
% error																
$^{210}Pb_{xs}$	Bq kg^{-1}	4	4	4	4	2	2	0	1	0	0	0	0			
% error		3	3	3	4	4	4	4	4	4	4	4	4			
$^{206}Pb/^{204}Pb$		18.236	18.139	18.151	18.153	18.131	18.292	18.371	18.321	18.476	18.500	18.524	18.476	18.462	18.457	18.633
$^{207}Pb/^{204}Pb$		15.687	15.621	15.611	15.566	15.568	15.682	15.669	15.496	15.740	15.701	15.793	15.718	15.682	15.584	15.738
$^{208}Pb/^{204}Pb$		38.264	37.958	38.147	38.236	38.067	38.405	38.353	38.249	38.719	38.595	38.695	38.532	38.623	38.462	38.993

Table B 5(c): Sediment geochemical data.

HySR5 Data

Sample:		46	47	48	49	50	51	52	53	54	55	56	57	58	59	60
Depth	cm	45.5	46.5	47.5	48.5	49.5	50.5	51.5	52.5	53.5	54.5	55.5	56.5	57.5	58.5	59.5
dry density	g cm^{-3}	0.69	0.82	0.90	0.79	0.84	0.93	1.12	1.16	1.00	1.26	1.06	1.09	1.32	1.55	1.32
LOI	wt.%	14.5	12.4	13.2	13.4	12.5	10.5	9.3	8.8	9.4	8.9	7.3	7.2	5.1	5.2	5.5
C_{org}	wt.%															
Si	wt.%	27.03	29.57	29.34	28.18	29.46	32.53	34.76	35.56	34.41	34.58	36.80	36.12	38.72	38.68	39.01
Al	wt.%	7.10	6.30	6.02	6.90	6.41	4.96	4.11	3.80	4.30	4.15	3.52	3.46	2.87	2.75	2.49
K	wt.%	2.12	1.94	1.88	2.06	1.92	1.55	1.39	1.28	1.41	1.42	1.24	1.21	1.11	1.07	0.96
Ti	wt.%	0.46	0.45	0.44	0.46	0.45	0.41	0.40	0.41	0.42	0.43	0.45	0.42	0.44	0.46	0.40
Cr	ppm	108	108	102	107	115	108	95	100	102	93	106	99	86	93	96
Na	wt.%	1.41	1.12	1.23	1.30	1.21	0.96	0.87	0.81	0.83	0.95	0.78	0.70	0.56	0.57	0.56
Cl	wt.%	1.82	1.52	1.78	1.78	1.66	1.65	1.42	1.36	1.35	1.46	1.38	1.17	0.86	0.98	1.11
Mg	wt.%	1.00	0.87	0.84	0.95	0.87	0.67	0.54	0.51	0.57	0.56	0.45	0.42	0.31	0.30	0.29
Ca	wt.%	0.48	0.31	0.28	0.30	0.25	0.19	0.17	0.16	0.19	0.21	0.18	0.16	0.13	0.14	0.14
Fe	wt.%	4.30	3.54	3.71	3.85	3.48	2.77	2.29	2.05	2.29	2.35	2.10	2.15	1.83	1.74	1.71
Mn	wt.%	0.018	0.017	0.016	0.017	0.016	0.013	0.012	0.012	0.013	0.014	0.014	0.013	0.012	0.012	0.012
S	wt.%	3.02	2.46	3.00	2.58	2.54	2.35	2.33	2.24	2.18	2.33	2.40	2.21	1.93	2.07	2.18
As	ppm	26	18	23	19	16	12	8	10	8	10	8	5	5	5	8
P	wt.%	0.05	0.04	0.04	0.05	0.04	0.03	0.03	0.03	0.03	0.03	0.02	0.02	0.02	0.02	0.02
Pb	ppm	67	58	60	66	62	48	36	35	36	35	30	34	22	20	20
Zn	ppm	99	84	86	95	88	66	51	53	60	55	45	42	37	33	36
Ni	ppm	33	29	30	32	31	25	21	21	23	22	17	17	13	14	15
Cu	ppm	20	17	18	19	17	12	10	9	10	10	8	6	6	4	4
Br	ppm	160	154	156	142	136	116	95	90	97	93	73	64	44	44	53
I	ppm	65	59	59	54	46	34	25	23	28	24	17	18	7	8	13
^{137}Cs	Bq kg^{-1}															
% error																
$^{210}Pb_{xs}$	Bq kg^{-1}															
% error																
$^{206}Pb/^{204}Pb$		18.275	18.394	18.431	18.321	18.360	18.394	18.080	18.407	18.336	18.776	18.334	18.440	18.388	18.176	18.177
$^{207}Pb/^{204}Pb$		15.395	15.601	15.579	15.440	15.520	15.523	15.364	15.495	15.410	15.970	15.699	15.680	15.389	15.307	15.415
$^{208}Pb/^{204}Pb$		38.164	38.537	38.434	38.054	38.112	37.912	37.659	38.233	37.892	39.402	38.409	38.471	38.109	37.850	38.365

Table B 5(d): Sediment geochemical data.

Sample ID	Collection period		Rainfall cm d^{-1}	^{210}Pb activity mBq dm^{-3}	+/-	^{210}Pb flux µBq cm^{-2} d^{-1}	+/-
Rf 1	23-Mar-93	01-Apr-93	0.55	50.5	2.0	27.6	1.1
Rf 2	01-Apr-93	16-Apr-93	0.36	68.6	9.7	24.6	3.5
Rf 3	16-Apr-93	29-Apr-93	0.21	112.0	13.0	23.4	2.7
Rf 4	29-Apr-93	21-May-93	0.13	153.2	17.5	20.1	2.3
Rf 5	21-May-93	03-Jun-93	0.32	179.1	39.1	57.3	12.5
Rf 6	03-Jun-93	21-Jun-93	0.32	104.0	12.0	33.2	3.8
Rf 7	21-Jun-93	16-Jul-93	0.14	38.5	6.8	5.3	0.9
Rf 8	16-Jul-93	14-Aug-93	0.13	71.2	9.8	9.3	1.3
Rf 9	14-Aug-93	13-Sep-93	0.33	104.0	13.2	34.5	4.4
Rf 10	13-Sep-93	05-Oct-93	0.14	91.9	12.4	12.8	1.7
Rf 11	05-Oct-93	09-Oct-93	1.96	39.4	8.2	77.3	16.2
Rf 12	09-Oct-93	20-Oct-93	0.42	20.6	3.6	8.7	1.5
Rf 13	20-Oct-93	16-Nov-93	0.19	31.2	3.3	5.9	0.6
Rf 14	16-Nov-93	07-Dec-93	0.27	109.3	9.2	29.1	2.4
Rf 15	07-Dec-93	22-Dec-93	0.67	27.4	3.6	18.3	2.4
Rf 16	22-Dec-93	05-Jan-94	0.63	27.7	3.3	17.5	2.1
Rf 17	05-Jan-94	19-Jan-94	0.47	49.7	5.3	23.6	2.5
Rf 18	19-Jan-94	09-Feb-94	0.28	35.2	4.0	9.8	1.1
Rf 19	09-Feb-94	03-Mar-94	0.21	141.5	12.4	29.3	2.6
Rf 20	03-Mar-94	31-Mar-94	0.10	82.1	10.1	8.5	1.0
Rf 21	31-Mar-94	29-Apr-94	0.29	68.9	8.3	19.7	2.4
Rf 22	29-Apr-94	27-May-94	0.33	113.9	12.8	37.2	4.2
Rf 23	27-May-94	07-Jul-94	0.05	108.7	18.1	5.7	1.0
Rf 24	07-Jul-94	02-Aug-94	0.03	18.7	5.2	0.6	0.2
Rf 25	02-Aug-94	26-Aug-94	0.17	85.2	10.4	14.9	1.8
Rf 26	26-Aug-94	12-Sep-94	0.31	68.6	10.2	21.1	3.2
Rf 27	12-Sep-94	05-Oct-94	0.27	59.5	8.9	16.0	2.4
Rf 28	05-Oct-94	20-Oct-94	0.09	100.0	10.9	9.3	1.0
Rf 29	20-Oct-94	07-Nov-94	0.44	45.9	7.2	20.3	3.2
Rf 30	07-Nov-94	14-Nov-94	0.65	105.8	17.4	69.2	11.4
Rf 31	14-Nov-94	28-Nov-94	0.10	26.9	6.4	2.6	0.6

Table B 6(a):

Rainfall data used to calculate annual $^{210}Pb_{xs}$ fluxes.

Sample ID	Collection period		Rainfall cm d^{-1}	^{210}Pb activity mBq dm^{-3}	+/-	^{210}Pb flux µBq cm^{-2} d^{-1}	+/-
Rf 32	28-Nov-94	08-Dec-94	0.74	48.9	10.4	35.9	7.7
Rf 33	08-Dec-94	23-Dec-94	0.06	85.5	9.2	5.4	0.6
Rf 34	23-Dec-94	04-Jan-95	0.49	74.2	10.9	36.6	5.4
Rf 35	04-Jan-95	17-Jan-95	0.15	143.7	16.2	22.3	2.5
Rf 36	17-Jan-95	20-Jan-95	1.42	56.4	8.6	79.9	12.2
Rf 37	20-Jan-95	24-Jan-95	0.69	26.3	5.3	18.0	3.6
Rf 38	24-Jan-95	30-Jan-95	0.87	40.7	11.1	35.3	9.7
Rf 39	30-Jan-95	06-Feb-95	0.45	86.1	16.9	38.5	7.5
Rf 40	06-Feb-95	13-Feb-95	0.88	55.4	13.3	49.0	11.7
Rf 41	13-Feb-95	21-Feb-95	0.86	48.2	13.8	41.2	11.8
Rf 42	21-Feb-95	24-Feb-95	0.64	47.8	10.2	30.5	6.5
Rf 43	24-Feb-95	03-Mar-95	0.26	70.7	6.8	18.0	1.7
Rf 44	03-Mar-95	13-Mar-95	0.19	38.1	4.1	7.4	0.8
Rf 45	13-Mar-95	19-Mar-95	0.20	19.7	1.3	3.9	0.3
Rf 46	19-Mar-95	13-Apr-95	0.03	42.0	3.0	1.1	0.1
Rf 47	13-Apr-95	25-Apr-95	0.12	52.2	3.8	6.3	0.5
Rf 48	25-Apr-95	24-May-95	0.06	44.3	6.1	2.5	0.3
Rf 49	24-May-95	19-Jun-95	0.10	18.5	2.3	1.8	0.2
Rf 50	19-Jun-95	26-Jun-95	0.27	73.6	8.4	19.8	2.3
Rf 51	26-Jun-95	06-Sep-95	0.02	83.8	10.0	1.9	0.2
Rf 52	06-Sep-95	13-Sep-95	0.76	20.2	1.9	15.4	1.5
Rf 53	13-Sep-95	27-Sep-95	0.57	15.9	1.6	9.1	0.9
Rf 54	27-Sep-95	23-Oct-95	0.14	60.7	4.6	8.2	0.6
Rf 55	23-Oct-95	06-Nov-95	0.18	35.1	2.7	6.2	0.5
Rf 56	06-Nov-95	28-Nov-95	0.36	74.4	6.2	26.9	2.2
Rf 57	28-Nov-95	21-Dec-95	0.23	108.9	7.8	25.3	1.8
Rf 58	21-Dec-95	04-Jan-96	0.36	34.6	3.2	12.6	1.2
Rf 59	04-Jan-96	22-Jan-96	0.35	39.7	3.6	14.0	1.3
Rf 60	22-Jan-96	12-Feb-96	0.31	77.8	8.5	23.8	2.6
Rf 61	12-Feb-96	28-Feb-96	0.25	66.2	5.6	16.7	1.4
Rf 62	28-Feb-96	22-Mar-96	0.15	165.2	11.5	25.1	1.8
Rf 63	22-Mar-96	09-Apr-96	0.05	124.9	9.9	6.2	0.5

Table B 6(b):

Rainfall data used to calculate annual $^{210}Pb_{xs}$ fluxes.

Probe #1 Sample	Fe^{2+} ppm	Mn^{2+} ppm	Depth cm	Probe #1 Sample	Fe^{2+} ppm	Mn^{2+} ppm	Depth cm
1	4.0	0.08	0.5	**39**	3.5	0.04	39.5
2	5.0	0.13	1.5	**40**	4.9	0.02	40.5
3	7.0	0.22	2.5	**41**	4.0	0.01	41.5
4	20.1	0.25	3.5	**42**	3.5	0.05	42.5
5	54.4	0.30	4.5	**43**	3.1	0.04	43.5
6	83.8	0.35	5.5	**44**	2.2	0.05	44.5
7	90.3	0.32	6.5	**45**	1.8	0.00	45.5
8	86.1	0.28	7.5	**46**	2.2	0.04	46.5
9	75.1	0.22	8.5	**47**	2.6	0.04	47.5
10	84.3	0.25	9.5	**48**	2.2	0.01	48.5
11	104.8	0.24	10.5	**49**	2.4	0.01	49.5
12	107.6	0.24	11.5	**50**	2.3	0.05	50.5
13	100.8	0.23	12.5	**51**	2.7	0.01	51.5
14	76.9	0.19	13.5	**52**	3.2	0.06	52.5
15	71.1	0.21	14.5	**53**	2.4	0.05	53.5
16	46.5	0.21	15.5	**54**	2.8	0.02	54.5
17	36.3	0.20	16.5	**55**	3.5	0.04	55.5
18	32.3	0.21	17.5	**56**	3.5	0.05	56.5
19	30.7	0.22	18.5	**57**	3.0	0.04	57.5
20	29.7	0.23	19.5	**58**	3.5	0.02	58.5
21	30.5	0.22	20.5	**59**	2.5	0.04	59.5
22	24.1	0.24	21.5	**60**	3.9	0.07	60.5
23	24.1	0.20	22.5	**61**	2.5	0.04	61.5
24	23.8	0.20	23.5	**62**	3.1	0.03	62.5
25	24.2	0.17	24.5	**63**	5.1	0.06	63.5
26	26.0	0.20	25.5	**64**	2.5	0.02	64.5
27	23.2	0.19	26.5	**65**	3.6	0.05	65.5
28	22.1	0.17	27.5	**66**	3.2	0.04	66.5
29	23.3	0.16	28.5	**67**	2.5	0.04	67.5
30	15.7	0.12	30.5	**68**	3.5	0.05	68.5
31	12.4	0.13	31.5	**69**	5.6	0.06	69.5
32	12.9	0.11	32.5	**70**	10.8	0.08	70.5
33	8.4	0.09	33.5	**71**	12.6	0.07	71.5
34	8.1	0.11	34.5	**72**	16.6	0.10	72.5
35	9.6	0.08	35.5	**73**	19.3	0.08	73.5
36	5.7	0.08	36.5	**74**	22.6	0.09	74.5
37	5.8	0.05	37.5	**75**	20.5	0.08	75.5
38	6.2	0.04	38.5	**76**	16.8	0.13	77.5

Table B 7(a):
ICP-AES data from the first deployment of the chambered gel pore water sampler.

#2 Sample	Fe^{2+} ppm	Mn^{2+} ppm	Depth cm	#2 Sample	Fe^{2+} ppm	Mn^{2+} ppm	Depth cm	#2 Sample	Fe^{2+} ppm	Mn^{2+} ppm	Depth cm
1	31.7	0.013	0.5	**33**	25.6	0.016	32.5	**65**	2.4	0.012	64.5
2	43.7	0.020	1.5	**34**	20.9	0.016	33.5	**66**	3.0	0.011	65.5
3	31.9	0.012	2.5	**35**	20.0	0.020	34.5	**67**	2.3	0.011	66.5
4	20.3	0.007	3.5	**36**	16.6	0.015	35.5	**68**	2.4	0.012	67.5
5	39.2	0.017	4.5	**37**	20.9	0.018	36.5	**69**	2.5	0.012	68.5
6	38.8	0.017	5.5	**38**	17.5	0.018	37.5	**70**	1.5	0.012	69.5
7	41.5	0.017	6.5	**39**	17.5	0.016	38.5	**71**	1.5	0.013	70.5
8	29.4	0.014	7.5	**40**	17.1	0.016	39.5	**72**	1.7	0.017	71.5
9	46.7	0.017	8.5	**41**	15.8	0.018	40.5	**73**	1.5	0.013	72.5
10	47.7	0.018	9.5	**42**	12.8	0.018	41.5	**74**	2.3	0.014	73.5
11	48.2	0.019	10.5	**43**	10.9	0.015	42.5	**75**	2.4	0.013	74.5
12	33.4	0.014	11.5	**44**	10.3	0.019	43.5	**76**	1.6	0.014	75.5
13	39.0	0.018	12.5	**45**	9.6	0.019	44.5	**77**	1.6	0.016	76.5
14	33.4	0.018	13.5	**46**	8.4	0.023	45.5	**78**	0.9	0.012	77.5
15	31.9	0.020	14.5	**47**	8.0	0.021	46.5	**79**	1.2	0.014	78.5
16	24.2	0.011	15.5	**48**	6.2	0.022	47.5	**80**	0.7	0.014	79.5
17	25.8	0.012	16.5	**49**	5.9	0.022	48.5	**81**	0.0	0.010	80.5
18	29.9	0.013	17.5	**50**	4.8	0.026	49.5	**82**	0.2	0.013	81.5
19	45.7	0.020	18.5	**51**	4.9	0.023	50.5	**83**	0.3	0.011	82.5
20	37.2	0.014	19.5	**52**	4.4	0.022	51.5	**84**	0.0	0.009	83.5
21	45.7	0.017	20.5	**53**	4.9	0.022	52.5	**85**	0.7	0.009	84.5
22	29.2	0.010	21.5	**54**	4.1	0.020	53.5	**86**	0.3	0.008	85.5
23	44.5	0.015	22.5	**55**	3.4	0.021	54.5	**87**	0.3	0.012	86.5
24	45.3	0.014	23.5	**56**	3.6	0.018	55.5	**88**	0.4	0.017	87.5
25	48.6	0.017	24.5	**57**	3.8	0.018	56.5	**89**	0.6	0.023	88.5
26	49.9	0.017	25.5	**58**	5.1	0.018	57.5	**90**	5.6	0.028	89.5
27	47.4	0.021	26.5	**59**	6.7	0.018	58.5	**91**	11.4	0.031	90.5
28	44.8	0.019	27.5	**60**	3.1	0.016	59.5	**92**	9.9	0.029	91.5
29	36.5	0.018	28.5	**61**	2.4	0.014	60.5	**93**	1.5	0.026	92.5
30	31.4	0.017	29.5	**62**	2.4	0.013	61.5	**94**	2.3	0.022	93.5
31	28.0	0.016	30.5	**63**	2.7	0.014	62.5				
32	27.7	0.017	31.5	**64**	2.1	0.011	63.5				

Table B 7(b):
ICP-AES data from the second deployment of the chambered gel pore water sampler.

DET sample	Fe^{2+} ppm	Depth cm	DET sample	Fe^{2+} ppm	Depth cm
1	38.24	1.5	39	76.72	39.5
3	31.55	3.5	41	71.31	41.5
5	25.74	5.5	43	65.12	43.5
6	16.35	6.5	45	65.07	45.5
7	13.92	7.5	46	56.37	46.5
9	9.45	9.5	47	63.21	47.5
11	5.89	11.5	49	48.89	49.5
13	6.31	13.5	51	42.79	51.5
15	5.67	15.5	53	36.66	53.5
16	3.22	16.5	55	35.44	55.5
17	4.44	17.5	56	31.59	56.5
19	1.75	19.5	57	37.93	57.5
21	1.44	21.5	59	31.75	59.5
23	28.52	23.5	61	14.61	61.5
25	62.41	25.5	63	10.64	63.5
26	89.24	26.5	65	7.88	65.5
27	83.08	27.5	66	8.12	66.5
29	86.52	29.5	67	9.53	67.5
31	80.17	31.5	69	11.46	69.5
33	88.91	33.5	71	11.89	71.5
35	76.37	35.5	73	15.51	73.5
36	84.67	36.5	75	12.42	75.5
37	88.83	37.5			

Table B 7(c):
ICP-AES data from the second deployment of the thin-film (DET) gel pore water sampler.

Appendix C

Publications

Environ. Sci. Technol. 1997, 31, 1093–1101

Reliability of Salt Marshes as "Geochemical Recorders" of Pollution Input: A Case Study from Contrasting Estuaries in Southern England

ANDREW B. CUNDY,*,[1]
IAN W. CROUDACE,[‡]
JOHN THOMSON,[‡] AND JAMES T. LEWIS[‡]

Department of Geography and Earth Sciences, Brunel University, Borough Road, Isleworth, London TW7 5DU, U.K., and Southampton Oceanography Centre, European Way, Southampton, SO14 3ZH, U.K.

Temperate, mesotidal salt marshes are usually good "geochemical recorders" of pollutant input. Dated salt marsh cores from the Hamble, Itchen (Southampton Water), and Beaulieu estuaries (southern U.K.) are assessed. Sediments show clear labeling from effluents, which varies depending on their proximity to major urban or industrial areas. For elements where input is dominantly from a single source and periods of peak discharge are known (i.e., Cu, ^{137}Cs, and ^{60}Co), historical records of pollutant input can be reconstructed, provided redistribution through sediment mixing or early diagenetic processes is minimal. Where the pollutant has a range of sources (i.e., Pb) or where physical mixing in-estuary produces a time-integrated signal, it can prove extremely difficult to relate concentration depth profiles to discharge histories. Using concentration and stable Pb isotope data, the observed temporal input of Pb to these marshes is shown to reflect a complex, mixed marine/atmospheric input from regional (automobile emission) and local (urban/industrial) sources. While general trends in pollutant loading may still be observed, it is extremely difficult to reconstruct accurately temporal trends in Pb input and sources of Pb in these estuaries using salt marsh records due to the importance of local, poorly-defined Pb sources and in-estuary mixing processes.

Introduction

Following the development of radiometric dating using isotopes with half-lives suitable for the study of recent anthropogenic processes (^{210}Pb, ^{137}Cs, ^{241}Am), vertical cores of estuarine and coastal sediments have been increasingly used to reconstruct the history of coastal pollution (e.g., 1–7). Salt marsh sediments in particular have been used in numerous studies as due to their clay-rich nature and consequently large adsorption capacity they represent a major repository for contaminants (*8*). Their stabilized, vegetated nature and dense root system also make them less susceptible to post-depositional disturbance than adjacent mudflat areas. For sediments to provide a useful history of anthropogenic input to the coastal environment, cored material must be dominantly fine-grained and clay-rich (adsorptive), dateable, have reasonably high rates of sediment accumulation (>0.3 cm yr^{-1}), be relatively undisturbed, and there should not have been significant redistribution of elements through mixing/early diagenetic processes. Where these conditions have been met, salt marsh sediments have been successfully used to reconstruct contaminant chronologies at various coastal sites (see review by Valette-Silver; *8*). In the U.K., contaminant chronologies have been derived from salt marsh deposits in a number of areas, e.g., the Severn estuary (e.g., refs 6 and 9), Cornwall (*10*), and Cumbria (*11*). In many cases, pollutant profiles retained by sediments have shown good correlation with local industrial activity/urbanisation, allowing their use as a dating tool (e.g., refs 9 and 11–13). Despite the success of these studies, in the dynamic estuarine environment, sediment mixing and redistribution prior to deposition presents a major problem to sediment-based historical reconstructions, where varying time lags between input of the pollutant and its deposition on the marsh surface may produce a time-integrated discharge record. MacKenzie et al. (*14*) examined the vertical distribution of discharge products from the Sellafield nuclear reprocessing plant in salt marsh sediments from SW Scotland and found that the dominant transport mechanism of Sellafield waste to the marsh sites involved redistribution of contaminated silt. The marsh sediments thus retained a record of the time-integrated Sellafield discharges rather than of temporal variations in individual releases. Early diagenetic remobilization of radionuclides and heavy metals may also perturb contaminant chronologies, with a number of studies finding evidence of metal mobility following deposition (see review by Farmer; *15*).

The present study examines the suitability of salt marsh sediments from the Solent estuarine system, southern U.K. as historical recorders of anthropogenic input. Sites have been chosen to represent contrasting estuaries, a comparatively undeveloped estuary (Beaulieu) and a heavily industrialized and urbanized estuary (Hythe and Hamble, Southampton Water). Elemental analysis focuses on Cu and Pb due to the widespread release of both elements into the local marine environment. Cu has a relatively well-defined historical input from industrial processes on the west side of Southampton Water, and although sources of Pb are less well-defined, source discrimination is often possible through measurement of its stable isotopic composition (discussed later).

Study Area. The sites studied are located in the Solent region of southern England (Figure 1). The Beaulieu estuary is situated within the New Forest, a tourist and conservation area. Large sections of the land surrounding the estuary are privately owned, and the area has comparatively little industrial/residential development. In contrast, the Southampton Water area (Itchen estuary) has experienced significant industrial, residential, and leisure development during this century. The Hamble Estuary (situated on the eastern side of Southampton Water) has undergone significant development for recreational purposes (construction of four marinas), while the Hythe area is intensively developed, with the large Esso oil refinery at Fawley and related industries that use the feedstock from the refinery (Figure 1).

Methods

Cores (0.4 m × 10 cm diameter) were taken using a hand-driven PVC tube from salt marsh sites at Beaulieu, Hythe, and Hamble in spring 1992. The marshes in this area have been shown to exhibit slight variation in geochemical conditions, pollutant fluxes, and sediment accumulation rate

* Corresponding author telephone: +44 181 891 8235; fax: +44 181 891 8237; e-mail: andrew.cundy@brunel.ac.uk.
[1] Brunel University.
[‡] Southampton Oceanography Centre.

S0013 936X(96)00622-0 CCC: $14.00

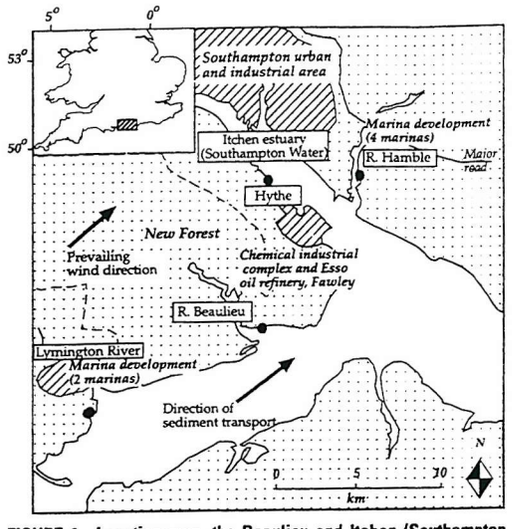

FIGURE 1. Location map, the Beaulieu and Itchen (Southampton Water) estuaries, southern England. Salt marsh sites studied are shown by the filled circles. Major industrial, residential, and leisure developments and prevailing wind and current directions are also shown.

in relation to proximity to the marsh edge (*16*). All cores collected for this study were taken at a standard distance (2 m) from the edge of the main creek channel on each marsh to minimize this effect and allow comparison between marshes. Sediment compaction caused by the coring method was measured on-site and found to be minimal (<5% in all cases). On return to the laboratory, the cores were sliced in half, X-radiographed, photographed, and described before being sampled at 2 or 1 cm increments for geochemical analysis.

Samples were pelletized for trace element determinations and fused for major element determinations on a Philips PW1400 sequential X-ray fluorescence spectrometer system. The precision of this technique is very good for elements present at levels well above detection limit (typically 1–5 ppm for a 100 s count time) and is nominally 1% RSD for major elements and 5% RSD for trace elements. Lead isotopic abundances were determined using a VG Elemental PQ2+ inductively-coupled plasma mass spectrometer (ICP-MS). Lead was extracted from the sediments for this analysis using a double leach with aqua regia, and the leachate was preconcentrated on Dowex 1X8 200–400# columns using 0.5 M HBr (*17*). The Pb isotopic standard NIST 981 was used to assess accuracy and precision, and sample blanks were run to determine possible contamination from reagents and sample handling. The 1 σ precision of each $^{206}Pb/^{207}Pb$ ratio was better than ±0.5% and better than ±0.8% for each $^{206}Pb/^{204}Pb$ ratio.

Sediment accumulation rates were assessed using the ^{137}Cs, ^{60}Co, and ^{210}Pb dating methods. ^{60}Co and ^{137}Cs activities were determined by γ-spectrometry with a Canberra 30% P-type HPGe detector. Errors were typically in the order of 4% (1 σ), detection limits were 0.5 Bq/kg. ^{210}Pb activity was determined by a proxy method through α-spectrometric measurement of its granddaughter nuclide ^{210}Po. The method employed was based on Flynn (*18*), using double acid leaching of the sediment with ^{209}Po as an isotopic tracer and autodeposition of the Po isotopes in the leachate onto silver disks. Detection limits were 1 Bq/kg. The unsupported ^{210}Pb activity was estimated by subtraction of the value of constant ^{210}Pb activity at depth (approximately 12 Bq/kg).

TABLE 1. Net Sediment Accumulation Rates at Each Site, Derived Using ^{137}Cs, ^{60}Co, and ^{210}Pb Data

	sediment accumulation rate (mm y^{-1}) derived from		
site	^{210}Pb dating	^{137}Cs dating	^{60}Co dating
Beaulieu	3	2–5	< 3
Hythe	5	6	8–9
Hamble	5	2–3	possible remobilization

Results

Sediment Accumulation Rates. Sediment accumulation rates of ca. 3 mm yr^{-1} at Beaulieu, 5–8 mm yr^{-1} at Hythe, and 2–5 mm yr^{-1} at Hamble are estimated from the ^{210}Pb, ^{60}Co, and ^{137}Cs data (Table 1). ^{210}Pb-derived sediment accumulation rates are calculated according to the Constant Initial Concentration (CIC) model (*19*). ^{137}Cs-derived values ascribe the subsurface maximum in ^{137}Cs activity to the 1963 peak fallout from atmospheric weapons testing and are quoted as a range because of the smoothed shape of the ^{137}Cs activity/depth profile (Figure 2). A Chernobyl-derived activity maximum is generally ill-defined or absent at a 2 cm sampling resolution (*13*). ^{60}Co is present in the study area following its release from the AEE Winfrith reactor site (60 km to the west of the study area in Dorset). Maximum discharge of ^{60}Co occurred in 1980/1981, providing a peak in activity in local salt marsh deposits that may be used to derive rates of sediment accumulation in a similar manner to ^{137}Cs (*13*). The vertical distribution of ^{137}Cs and ^{60}Co in relation to preservation of discharge histories is discussed below.

The agreement between the ^{210}Pb, ^{137}Cs, and ^{60}Co dating estimates is satisfactory at the Beaulieu site. At the Hamble and Hythe sites, however, agreement between the dating methods is relatively poor, due to possible early diagenetic remobilization of ^{60}Co at the Hamble site and the first-order nature of the ^{60}Co dating technique (discussed in Cundy and Croudace; *13*). Consequently, the ^{137}Cs and ^{210}Pb estimates are preferred for the Hamble and Hythe sites (time-axis in Figure 2).

Intercore Variation. The detrital minerals deposited in the Solent estuaries are largely derived from the weathering of Tertiary strata (mostly sands and clays) in the Hampshire Basin and to a first approximation the composition is likely to be constant at each site. With this assumption, variations in chemical composition between sites may be examined using an "isocon" plot [Figure 3, data from a core from the Pennington marshes, Lymington (Figure 1), are shown for comparison]. Isocon plots allow a simple visual comparison of the average composition of the sediments, and the similarity between averaged Beaulieu and Lymington data on the one hand and averaged Hamble and Hythe data on the other is immediately evident. Elements that plot on or near the isocon lines in all cases include the major elements Al, K, Ti, and Si and indicate little intersite variation in sediment composition. Enriched elements that plot above the isocon lines when Hamble and Hythe data are compared with Beaulieu or Lymington data are trace elements that may have local anthropogenic inputs. Specifically these are the elements Cu, Pb, Zn, Br, and As, which are derived from local industry such as the oil refinery at Fawley on Southampton Water, from associated petrochemical industries near Hythe, and from wastewater outfalls to Southampton Water. Concentrations of these elements at the sites examined are thus likely to reflect the scale of pollutant or anthropogenic inputs rather than inherent compositional variations.

Source Discrimination and Reconstruction of "Pollution Histories". The salt marshes cored potentially provide historical records of pollutant input to these estuaries, as

(a) Sediment accumulation rates have been established through simultaneous use of a number of radiometric dating techniques.

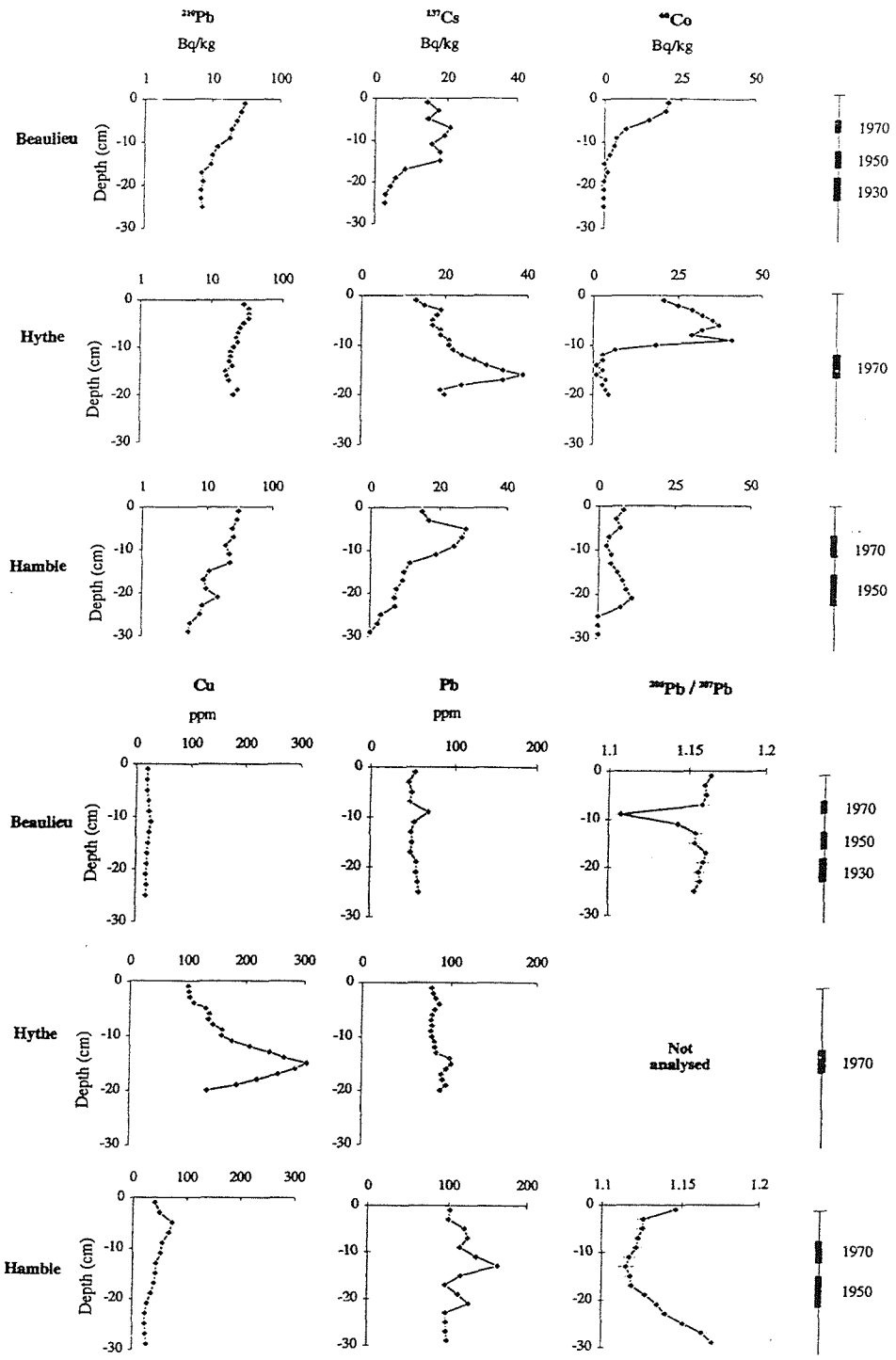

FIGURE 2. ^{210}Pb, ^{137}Cs, ^{60}Co, Cu, Pb, and ^{206}Pb/^{207}Pb vs depth for Beaulieu, Hythe, and Hamble salt marsh cores. Unless otherwise indicated, error bars are smaller than the diamond marker symbol. A chronology derived from ^{137}Cs, ^{60}Co, and ^{210}Pb dating is also shown.

(b) A variety of elements are present at enriched concentrations, reflecting the scale of anthropogenic input from industrial/urban effluents.

(c) Sedimentation rate at these sites is relatively rapid, and there is no evidence of sediment removal through erosion.

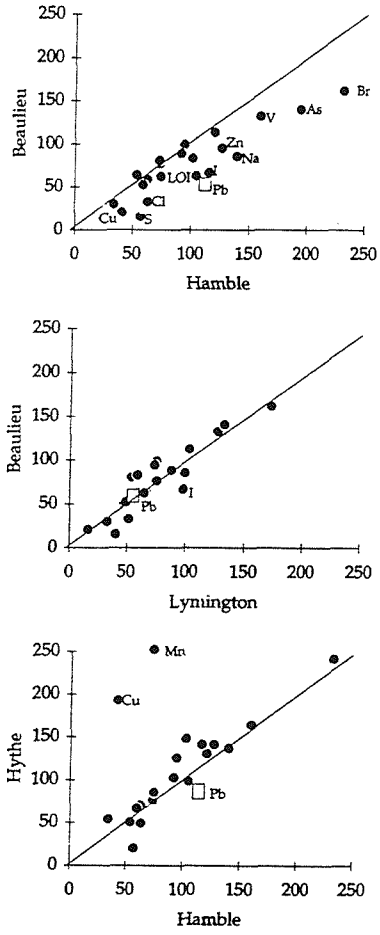

FIGURE 3. Isocon diagrams (after Grant; *44*) for Beaulieu, Lymington, Hamble, and Hythe salt marshes. Individual points represent average concentration of element in cores from each site multiplied by the following factors to ensure all elements plot on the same scale: Major elements (wt %): SiO_2, 1; TiO_2, 100; Al_2O_3, 5; Fe_2O_3, 20; MnO, 5000; MgO, 50; CaO, 100; Na_2O, 50; K_2O, 50; P_2O_5, 500; S, 50; Cl, 50 (LOI, 5); trace elements (ppm): Br, 0.5; I, 1; Pb, 1; Zn, 1; Ni, 2; Cr, 1; V, 1; As, 5; Cu, 1. For legibility, only those elements that plot significantly off the line of equal concentration are labeled.

(d) Similar salt marsh deposits have been used elsewhere in the reconstruction of pollution histories (i.e., Valette-Silver; *8*).

None of the sites studied is cored deeply enough to allow analysis of changes in pollutant loading over the entire industrial period in this area. They do, however, provide a record of the period of rapid industrial expansion following the Second World War. Pre-industrial values are estimated from pre-industrial sediments analyzed by Croudace and Cundy (*7*).

The preservation of historical records in these marshes may be assessed by comparing the vertical distribution of those elements that have known input terms with those with multiple or poorly-constrained sources.

Elements with Known Input Terms: Cu, ^{60}Co and ^{137}Cs. These are components with a single major source and a relatively well-constrained input history.

The main contributor of Cu into Southampton Water is the Esso oil refinery at Fawley (*20*), and while the discharge pattern of Cu is not known in detail, significant discharges of Cu into Southampton Water occurred following the development and expansion of the refinery from the 1950s with a program of effluent quality improvements being implemented in 1971. Despite the likely pulsed nature of the refinery discharges (it is probable that Cu is continuously output with an occasional spike, see ref 21), the Hamble and Hythe sites in this study exhibit a broad subsurface maximum in Cu concentration (Figure 2). Both sites show increasing Cu concentrations after ca. 1950, reaching a maximum in the late 1960s/early 1970s and subsequently decreasing; the decrease corresponding to the post-1971 effluent quality improvements at Fawley. Although the subsurface Cu maximum is far better defined at the Hythe site, both Hythe and Hamble sites retain a smoothed, time-averaged record of effluent discharges from the Esso refinery, supplied by input of Cu-labeled sediments from the Fawley area. Excess Cu (Cu_{xs}) fluxes at each site were calculated by subtracting a value for local background Cu (assumed the same as in mineralogically similar pre-industrial deposits from Southampton Water, ca. 15 ppm) from the measured concentration. The excess Cu flux is apparently dependent on proximity to the refinery outfall at Fawley, with the maximum Cu_{xs} flux at Hythe (69 μg cm^{-2} yr^{-1}) much higher than at Hamble (10 μg cm^{-2} yr^{-1}) (Table 2). Even higher Cu fluxes of up to 1500 μg cm^{-2} yr^{-1} have been observed in a subtidal core taken from the area around the refinery outfall (*7*). Locally, Cu fluxes vary slightly according to coring site. Cu_{xs} values ranging from 11 to 24 μg cm^{-2} yr^{-1} were observed in a cross-marsh coring transect carried out in the Hamble estuary (Table 2; *16*), the lower fluxes occurring in back-marsh areas. Despite local variability, accreting salt marsh sites in that study retained a broad subsurface maximum in Cu flux corresponding to the refinery discharge record, as observed here.

^{60}Co present in Solent estuaries is derived from the AEE Winfrith site in Dorset. Discharge histories for ^{60}Co are published in annual reports (e.g., ref 22), which show that low-level discharges began in 1970 and continued until closure of the reactor in 1990. Peak discharges occurred in 1975 and 1980/1981. Discharges have continued since 1990 but are a small fraction of what they were during the reactor life. Measured vertical distributions of ^{60}Co in accumulating sediments show a maximum in activity corresponding to the 1980/1981 peak discharge event (based on ^{210}Pb and ^{137}Cs dating and modeling of discharge data; *13*). Measurement of the vertical distribution of ^{60}Co may thus be used as a first-order dating technique, provided that a thorough examination of trace element geochemistry is carried out to check for possible early diagenetic movement. A full interpretation of the ^{60}Co activity-depth profiles observed in sediments from the Solent region is given in ref 13. The Beaulieu and Hamble sites show a surface maximum and exponential decline in activity, characteristic of marsh sites with lower rates of sediment accumulation (<4–5 mm yr^{-1}), although significant downcore migration due to early diagenesis is apparent in the Hamble core (shown by the lower, broad maximum at 21 cm depth) (Figure 2). The Hythe site shows two subsurface activity maxima, the lower corresponding to the 1980/1981 peak discharges from AEE Winfrith. As for Cu, the observed profile of ^{60}Co is a time-integrated discharge signal but maintains a subsurface maximum that can be used as a first-order dating tool (Table 1).

Vertically cored salt marshes in the Solent area typically show two subsurface maxima in ^{137}Cs activity, a lower (main) maximum interpreted as corresponding to 1963 (fallout maximum from weapons testing) with a weak maximum corresponding to 1986 (Chernobyl incident) (*13*). This Chernobyl maximum is often not identifiable at a 2 cm sampling resolution. As the Beaulieu profile illustrates (Figure 2), however, interpretation of vertical profiles is often problematic due to post-depositional migration of ^{137}Cs (e.g.,

TABLE 2. Cu_{xs}, Pb, and $^{210}Pb_{excess}$ Fluxes and Inventories for Salt Marsh Sites from Southampton Water and Surrounding Areas (Locations Shown in Figure 1)[a]

site	max Cu_{xs} flux ($\mu g\ cm^{-2}\ yr^{-1}$)	Pb flux ($\mu g\ cm^{-2}\ yr^{-1}$)	$^{210}Pb_{excess}$ flux ($Bq\ cm^{-2}\ yr^{-1}$)	Pb flux/$^{210}Pb_{excess}$ flux
Beaulieu	3	12	0.0094	1287
Hythe	69	21	0.0097	2144
Hamble	10	19	0.0075	2600
Hamble salt marsh transect[b]				
core 1	11	20	0.0075	2706
core 2	24	40	0.0117	3401
core 3	19	37	0.0140	2607
core 5	20	31	0.0107	2869
core 7	19	34	0.0113	3017
lake sediments (Loch Lomond)[c]		3		
Ombrotrophic peats (Scotland)[d]		4 (maximum)	0.009	422
Narragansett Bay sediments (upper bay)[e]		19–33 (mean = 28.5)	0.003–0.019 (mean = 0.011)	1477–9433 (mean = 4206)
rainfall (western Europe)[f]			0.01	

[a] Values from other areas are included for comparison. Total Pb flux rather than excess Pb (or anthropogenic Pb) values are used to allow comparison with previously published data. [b] Cundy and Croudace (*16*). [c] Sugden et al (*36*). [d] Sugden et al (*45*). [e] Bricker (*5*). [f] Appleby and Oldfield (*46*).

ref 23) and deposition lag (the time difference between peak ^{137}Cs fallout and the deposition of this fallout in the sedimentary column). Reworking of labeled sediment and incorporation of sediments from eroded areas will time-integrate the ^{137}Cs input to the marsh, often producing a broad, smoothed subsurface maximum in the sediment column rather than the discrete pulses of activity seen in the atmospheric fallout record. The time-averaged profile of the 1963 subsurface maximum reduces the accuracy of ^{137}Cs dating, hence sediment accumulation rates derived from this method are given as ranges (Table 1). An alternative argument would be that these signatures could be due to discharges from the nuclear reprocessing plants at Sellafield (Cumbria, NW England) or Cap de la Hague (northern France). Transport of discharges from the Cap de la Hague site is predominantly eastward, along the French coastline toward Kent and the North Sea (*24*) consequently, this site is unlikely to be a significant source of activity to the areas sampled. ^{137}Cs discharged from Sellafield shows relatively conservative behavior in seawater and is generally transported northward around the coast of Scotland and into the North Sea (*25, 26*). The wide dispersal of ^{137}Cs from the Sellafield site gives rise to the possibility that sediments analyzed in this study are labeled with Sellafield-derived rather than fallout-derived radionuclides. $^{134}Cs/^{137}Cs$ and $^{238}Pu/^{239,240}Pu$ ratios in samples from the coastline of southern England, published in annual reports by the U.K. Ministry of Agriculture Fisheries and Food (MAFF) (*27*), indicate the presence of nuclear power station discharge products, although it has been proposed that these may be derived from the Atomic Energy Establishment at Winfrith in Dorset and have a relatively localized influence (*13*). Maximum ^{137}Cs discharges from Sellafield occurred over the period 1974–1977 (Figure 4). Due to the sampling increment used and time-averaged nature of the ^{137}Cs profile in these cores, it would be difficult to categorically state that the observed ^{137}Cs maximum does not correspond to Sellafield discharges. Recently acquired high-resolution ^{210}Pb data from front-marsh deposits at Hythe (analyzed at 1 cm depth increments to 50 cm depth), however, justify the conclusion that the lower main ^{137}Cs peak is derived from atmospheric fallout from weapons testing (Figure 4; *28*), clearly dating the ^{137}Cs maximum to 1963.

Elements with Multiple or Poorly-Constrained Sources: Pb (and Stable Pb Isotopes). In each of the above cases, a known discharge signal can be related to a time-integrated concentration or activity profile in the sediment column and used to provide estimates of both sediment accumulation rate and changes in pollutant loading. Such studies are far more problematic where inputs of the pollutant elements are not well-constrained or where the element may have multiple sources, for example, Pb. Lead is an important heavy metal because of its known toxicity and its release from various industrial /technological activities. The increase in coal combustion and metal smelting associated with the Industrial Revolution increased the release of Pb to the environment (*29*), and the use of alkyllead fuel additives after 1923 caused a dramatic increase in atmospheric Pb emissions (*30*). By 1965 the amount of Pb that had been combusted in gasoline was estimated at over 2.6 million t (*31*), and in 1968 combustion of gasoline contributed over 98% to the total Pb emitted to the atmosphere. Since 1986, however, Pb emissions have decreased due to regulatory restrictions on the use of alkyl-leaded fuel. Recent measurements using airborne particulates indicate that, while gasoline is still the main source of Pb in urban areas, other contributory sources can now be identified following the reduction in vehicular Pb emissions (*32*).

Temporal trends in Pb deposition have been analyzed by coring a number of different sedimentary environments and are even evident in ice cores at remote high latitude locations (*33*). The estuarine environment also provides a sink for anthropogenic Pb, and recent estuarine sediments have been shown to preserve temporal variations in lead input (e.g. refs 5 and 10) and Pb isotopic ratios (*34, 35*; discussed below). In the U.K., as elsewhere, Pb isotope ratios indicate an increasing input of industrially-derived lead since ca. 1850 (*2, 36*).

Pb concentrations at the Hamble site range from 100 to 160 ppm, with concentration maxima occurring at 13 and 21 cm depth (Figure 2). At the Hythe site, Pb concentrations show less variability with depth, ranging from 80 to 100ppm with a broad concentration maximum at 15 cm depth. Pb concentrations at the Beaulieu site average 50 ppm with a maximum in concentration (68 ppm) at 9 cm depth. Mineralogically similar pre-industrial or early industrial sediments from a subtidal core taken from Southampton Water exhibit Pb concentrations of 24 ± 4 ppm (*7*). Each core therefore exhibits above-background concentrations of Pb to maximum depths sampled, indicating the presence of both local detrital mineral Pb and an anthropogenic Pb component throughout the sampled sections (1900–present at Beaulieu, 1960–

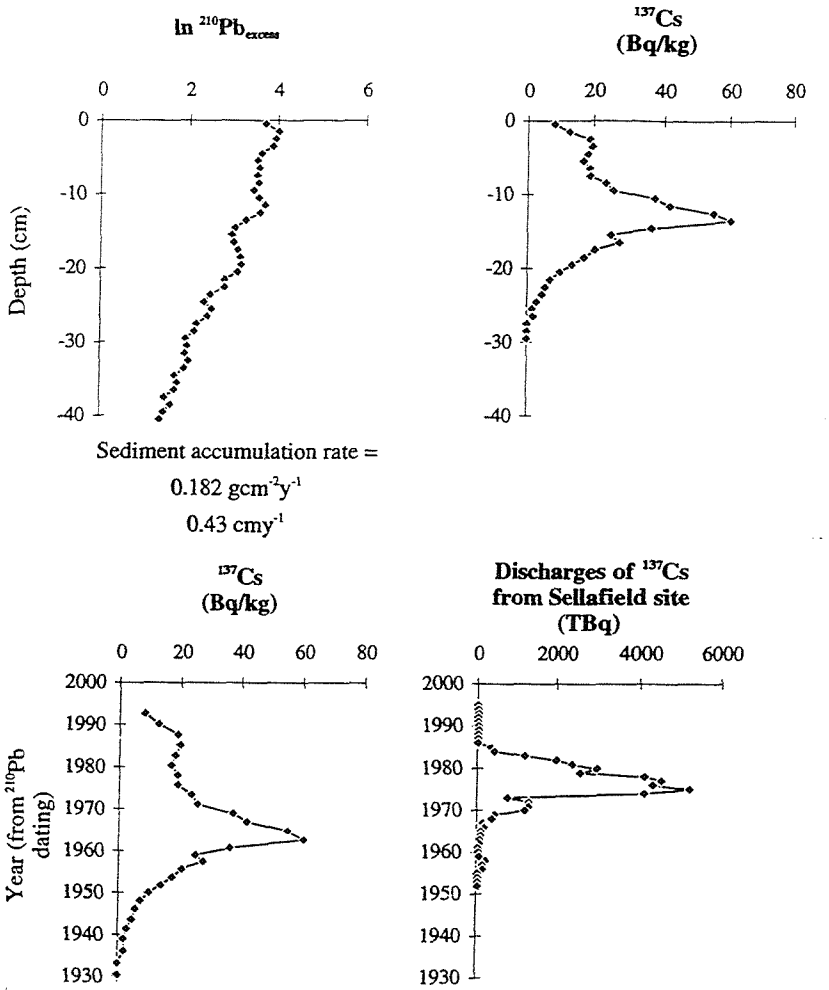

FIGURE 4. $^{210}Pb_{excess}$ and ^{137}Cs vs depth for front marsh deposits at Hythe (data from ref 28). ^{137}Cs vs year (year axis derived using ^{210}Pb data) is also shown to enable comparison with the record of Sellafield discharges (from ref 47).

present at Hythe and 1930–present at Hamble).

Pb flux data (Table 2) shows a considerably higher Pb input to the Hythe and Hamble marshes than at Beaulieu (ca. 20 μg cm^{-2} yr^{-1} at Hythe and Hamble, 12 μg cm^{-2} yr^{-1} at Beaulieu). These fluxes reflect proximity to industrial and urban sources of Pb around Southampton Water. To account

TABLE 3. Lead Isotope Ratios in Major Ore Deposits and Contemporary Environmental Materials[a]

ore producer	major district(s)	host rock age	$^{206}Pb/^{207}Pb$
Australia	Mt. Isa and Broken Hill	Precambrian	1.037
Canada	British Columbia	Precambrian	1.064
Canada	New Brunswick	Ordovician	1.160
USA	Missouri	Pennsylvanian	1.385
USA	Idaho	Precambrian	1.052
Former Yugoslavia	Trepca	Tertiary	1.195

environmental material	source	$^{206}Pb/^{207}Pb$
coal	domestic users, Edinburgh and Inverness	1.185
gasoline	Edinburgh	1.082
gasoline	Southampton (1988)	1.065
gasoline	Southampton (1995)	1.059–1.079
refuse incinerator fly ashes	Germany, France, Japan	1.14–1.16
pre/early industrial sediment	Southampton Water	1.18

[a] Data from refs 7, 32, 39, 41, 42, and 48.

for potential differences in flux arising from either loss or focusing of sediment, Pb flux was normalized to the $^{210}Pb_{excess}$ flux (^{210}Pb has a dominantly natural source, and so flux variations are a result of sedimentary processes rather than anthropogenic input. It thus provides an independent flux against which to "normalize" the Pb flux). The same trends are observed following this normalization procedure, Pb flux is much higher at Hythe and Hamble than at Beaulieu. Normalized fluxes observed in Southampton Water are comparable to those found in Narragansett Bay, MA (5; Table 2) where Pb fluxes to estuarine marshes were observed to vary considerably with distance from Pb source areas. While Pb fluxes and Pb enrichments are useful determinants of pollutant input, such data alone are insufficient to differentiate between sources of Pb enrichment. Pb isotope ratios provide an additional means of Pb source discrimination and have been applied in a range of sedimentary settings (*2, 7, 29, 33, 37*). The isotopic composition of Pb in an ore is determined by the age and genesis of the deposit (*38*). The $^{206}Pb/^{207}Pb$ ratio, where the isotopes are derived through radioactive decay of ^{238}U and ^{235}U respectively, is characteristic of each ore body and shows the greatest range as compared with other Pb isotope ratios. Typical isotopic compositions from different Pb deposits (Table 3) illustrate that more ancient ores are less radiogenic, i.e., have lower $^{206}Pb/^{207}Pb$ ratios than younger ores. The isotopic composition of industrial Pb will therefore depend on the source of the ore used, may be blended from different sources at any given time, and will also vary with time as supply sources change.

Thus in any given environment the measured Pb isotopic composition is a mixture of the inherent local value (e.g., the sediment) and anthropogenic Pb derived from one (or several) exotic ore bodies. In favorable cases, investigations of Pb isotopic composition can be used to infer the contribution of anthropogenic Pb to a particular environment, if the anthropogenic inputs have a distinctive and known Pb isotopic composition. For example, Associated Octel, the dominant U.K. manufacturer of alkyllead gasoline additives, mostly use a mixture of Australian ($^{206}Pb/^{207}Pb = 1.04$) and Canadian ($^{206}Pb/^{207}Pb = 1.16$) Precambrian ores, with varying amounts of U.S. Mississippi Valley Pb ores ($^{206}Pb/^{207}Pb = 1.38$). The sources used are generally dictated by the market price of Pb and in the U.K. have mostly involved the use of Precambrian ores. The rapidly expanding gasoline consumption by U.K. vehicles caused an increasing contribution of these less radiogenic (ancient) ores to total atmospheric Pb input, although recent legislation has significantly reduced the addition of alkyllead since 1986 (Figure 5). Unfortunately, while it is known that the Pb added to gasoline was derived from the above ore bodies, there are no data on the exact isotopic composition of the alkyllead additive over the period of increasing car usage (Associated Octel, personal communication). Analysis of pump gasoline, however, indicates that Australian and Canadian ores are currently dominant. Delves (personal communication) analyzed motor vehicle emissions in Southampton in 1988 and obtained a $^{206}Pb/^{207}Pb$ ratio of 1.065 ± 0.003. In 1995, analysis of premium pump gasoline from the Southampton area gave $^{206}Pb/^{207}Pb$ ratios between 1.059 and 1.079 (*32*).

The isotopic signatures of Pb used for other industrial purposes have not been investigated as extensively as those for gasoline additives, but it seems likely that to a first approximation Pb for other purposes would also be sourced according to market supply and demand economics. Coal burning has also added Pb to the environment, but its identification by isotopic methods can be difficult, especially when the isotopic composition of typical coals is very similar to that of the local rock type from which sediment is derived. This is the case around the Solent, where the typical $^{206}Pb/^{207}Pb$ value for pre-industrial sediments in the area is 1.18 (*7*), compared with a value for U.K. coal of 1.185 (*39*).

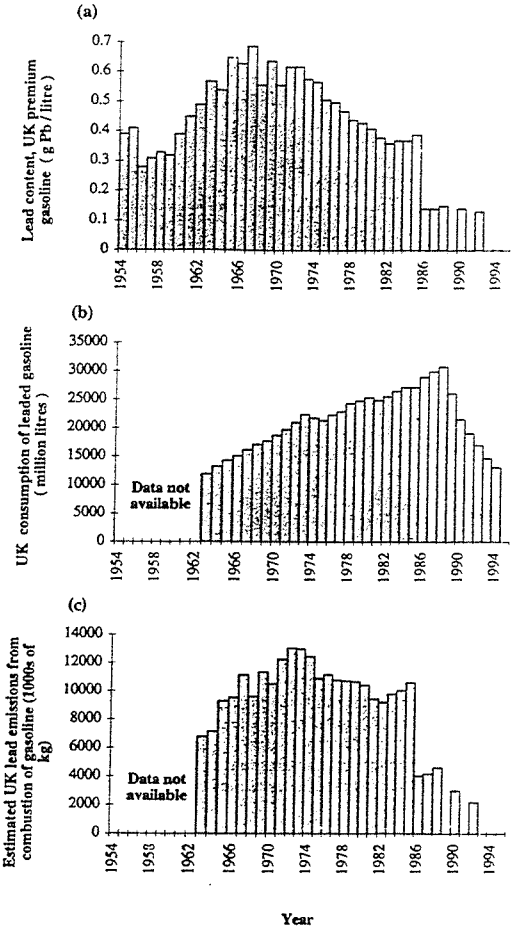

FIGURE 5. Trends in Pb emissions from gasoline consumption in the U.K. (a) Average lead content of U.K. premium gasoline since 1954. The data have been provided by the Fuels Technology Group, Associated Octel Company Ltd. Data are not available prior to 1954 and for 1989 and 1991. Associated Octel is the main U.K. manufacturer of alkyllead additives. (b) U.K. consumption of leaded gasoline since 1963, data from Department of Transport, U.K. Data are not available before 1963. (c) Estimated U.K. lead emissions from combustion of gasoline, calculated by multiplying the above data sets.

Pb Isotopic Distribution at Hamble and Beaulieu. The $^{206}Pb/^{207}Pb$ ratios in the Hamble core show a C-shaped pattern with depth, with high $^{206}Pb/^{207}Pb$ values (ca. 1.17) at the base of the core, gradually decreasing to 1.12 at intermediate and shallow depths with a slight increase to 1.14 near the surface (Figure 2). A two end-member mixing model indicates a gradual mixing of Pb sources with time, where less radiogenic or ancient Pb (shown by the U.K. gasoline and Australian Precambrian ore end-members) is input into the estuary and is mixed with more radiogenic Pb or young Pb (as shown by U.K. coal and inherent detrital Pb end-members) by estuarine processes prior to deposition at the marsh surface (Figure 6). Subsurface maxima in Pb shown by the Pb concentration-depth profile (Figure 2) do not cause major fluctuations in Pb isotopic ratio. This indicates that the Pb maxima may be caused by input of mixed, labeled estuarine sediments from Southampton Water in a pulse of inorganic accumulation, which would typically have the same Pb isotopic ratio as the sediment already at the marsh surface. It should also be noted that early diagenetic remobilization of Pb and ^{210}Pb,

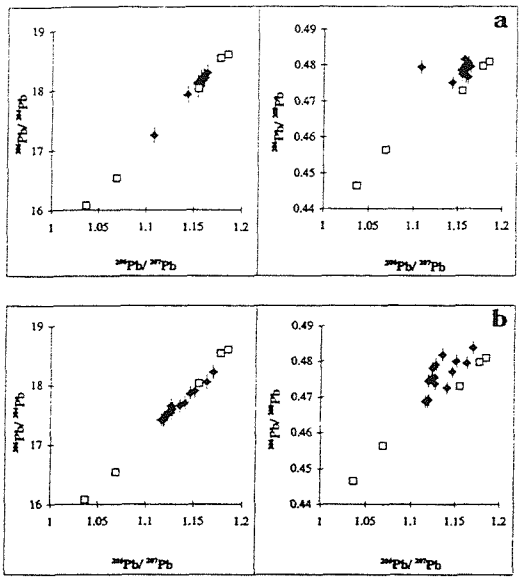

FIGURE 6. $^{206}Pb/^{204}Pb$ vs $^{206}Pb/^{207}Pb$ and $^{206}Pb/^{208}Pb$ vs $^{206}Pb/^{207}Pb$ for the Beaulieu (a) and Hamble (b) salt marsh sites. Values for environmental materials are shown by open square symbols, and from bottom left to top right represent Australian (Broken Hill) Precambrian ore, Southampton gasoline, refuse incinerator fly ashes (France), inherent detrital lead, and coal. Precambrian ore values from Chow et al. (45), gasoline and refuse incinerator fly ash values from Monna et al. (32), and coal ratio after Sugden et al. (39). The value for inherent lead is taken as approximate to that of pre-industrial deposits from Fawley, Southampton Water (7).

as proposed in Cundy and Croudace (*16*), may have affected the preservation of the Pb input history. The vertical distribution of Pb in this marsh is atypical of other marshes in the Hamble estuary, which do not show large subsurface Pb maxima (*16*). Hence lateral variability and inhomogeneity of sedimentary processes in these marshes renders the determination of Pb input trends on the basis of concentration data alone extremely difficult.

The $^{206}Pb/^{207}Pb$ value of 1.17 at the base of the core indicates that in ca. 1930 Pb input was dominantly from a mixed early industrial (a pre-automobile, mainly coal-burning) and inherent Pb source. As discussed previously, these are practically indistinguishable using Pb isotope ratios (Table 3). A decrease in $^{206}Pb/^{207}Pb$ ratios to 1.12 occurred progressively between the base of the core (ca. 1930) and 13 cm depth (ca. 1960) (Figure 2). Kersten et al. (*35*), Sugden et al. (*36*), and Farmer et al. (*40*) attribute such decreases in $^{206}Pb/^{207}Pb$ to the increase in Pb from automobile emissions. The progressive decrease in $^{206}Pb/^{207}Pb$ indicates that a similar effect may be occurring at the Hamble site, where an increase in car exhaust emissions since the 1930s has caused a gradual increase in the anthropogenic (less radiogenic) Pb load. After 1960, the data for the Hamble core show a slight increase in ratio from 1.12 to 1.13, indicating a relative decrease in importance of less radiogenic Pb. This, however, is not consistent with automobile emission data (Figure 5). Estimated national Pb emissions from the combustion of gasoline steadily increased over the period 1963–1973, remaining relatively constant between 1974 and 1985, with a significant decrease after 1985. Instead the increase in $^{206}Pb/^{207}Pb$ may represent a change in the ore used to manufacture alkyllead gasoline additives (i.e., an increasing proportion of the Pb used may be derived from Mississippi Valley ores, $^{206}Pb/^{207}Pb$ = 1.38). This is not, however, consistent with the Pb isotopic composition in recent gasoline (in 1988 and 1995, $^{206}Pb/^{207}Pb$ = 1.06–1.08; Delves, personal communication; *32*). More likely, this increase in ratio may represent input of Pb via effluents from expanding industrial and urban sources around Southampton Water. The multiplicity of potential Pb sources around Southampton makes ascribing a characteristic industrial Pb isotope ratio extremely difficult. Various authors (*32, 41, 42*) have however proposed that refuse incinerator fly ashes could constitute a representative indicator of a general industrial Pb source. Pb-containing products are mixed and homogenized during incineration, and the Pb isotopic signature averaged to provide a characteristic industrial value, typically in the range 1.14–1.16 (*41, 42*). These industrial Pb ratios have been found to be similar in Germany, France, and Japan. Consequently, a ratio of 1.14–1.16 is likely to be a good first approximation for industrially-derived Pb in the Southampton region. Subsequent in-estuary mixing of this higher ratio industrial Pb with Pb from automobile emissions could cause the post-1960 increase in $^{206}Pb/^{207}Pb$ ratio. The observed increase in the $^{206}Pb/^{207}Pb$ ratio to 1.145 at the sediment surface may result from increasing usage of unleaded gasoline since 1986 (Figures 2 and 5). The Pb isotopic ratios observed at the Hamble site are thus likely to be the result of mixed atmospheric/marine inputs and represent a time-integrated Pb input history.

$^{206}Pb/^{207}Pb$ ratios in the Beaulieu salt marsh are not consistent with those observed in the Hamble core, indicating considerable interestuary variation and highlighting the importance of local Pb sources in these estuaries. Stable Pb isotope ratios at Beaulieu are relatively constant between 0–7 and 11–25 cm depth, the observed value of 1.16 indicating a dominantly inherent/coal burning source (Figure 2). In contrast to the Hamble site, there is little evidence for variation in Pb sources or for input of automobile-derived Pb between 1970 and the present or between 1900 and 1950. This may be due to the fact that the area of the Beaulieu estuary sampled (the mouth of the river at Exbury) is a sparsely populated area with little industry and only a minor road network (limiting atmospheric and marine input of Pb). Sediment transport paths in this area are dominantly eastward (*43*), inhibiting input of labeled sediment from the Southampton Water area. In contrast to the constant ratios observed in the rest of the core, a large decrease in the $^{206}Pb/^{207}Pb$ ratio to 1.11 occurs at 7–11 cm depth, which indicates a significant, transient input of less radiogenic Pb in the early 1960s. Assuming two end-member mixing, ratios for the Beaulieu core show a sharp transient shift toward the ancient Pb end-member rather than the progressive mixing observed at the Hamble site (Figure 6). The source of this transient Pb spike is difficult to ascertain without detailed local discharge records. The lack of Pb-producing heavy industry in the immediate area and the transient (unmixed) nature of the spike indicate that the source of the Pb may be a localized, small-scale event.

The observed time input of Pb in these salt marshes does not reflect atmospheric pollutant input but instead reflects a more complex, mixed marine/atmospheric input. In-estuary mixing processes and the importance of local, poorly-defined sources mean that it is extremely difficult to relate concentration-depth profiles and Pb isotopic data to pollutant input histories. In such cases, source discrimination through Pb isotopic studies or determining accurate rates of sediment accretion through pollutant profiles have limited application, although general trends in pollutant loading may still be observed.

Acknowledgments

This research was funded by the University of Southampton Advanced Studies Committee. The authors thank Prof. Bob Nesbitt for the use of the VG PQ2+ ICP-MS (funded through EEC Brite EURAM II BRE-CT92-0299). We are indebted to

Dr. Tak Hirata and Dr. Andy Milton for their technical expertise and valuable assistance. The authors are also grateful to Dr. Nakhwa of the Fuels Technology Group, Associated Octel Limited, and the Department of Transport, U.K. for providing alkyllead concentration and gasoline consumption data for U.K. gasolines and to G. Benoit and N. Urban for providing helpful comments on an earlier version of this paper.

Literature Cited

(1) Chow, T. J.; Bruland, K. W.; Bertine, K. K.; Soutar, A.; Koide, M.; Goldberg, E. D. *Science* **1973**, *181*, 551–552.
(2) Clifton, R. J.; Hamilton, E. I. *Estuarine Coastal Mar. Sci.* **1979**, *8*, 259–269.
(3) McCaffrey, R. J.; Thomson, J. *Adv. Geophys.* **1980**, *22*, 165–236.
(4) Bopp, R. F.; Simpson, H. J.; Olsen, C. R.; Trier, R. M.; Kostyk, N. *Environ. Sci. Technol.* **1982**, *16*, 666–676.
(5) Bricker, S. B. *Estuaries* **1993**, *16*, 589–607.
(6) French, P. W.; Allen, J. R. L.; Appleby, P. G. *Mar. Geol.* **1994**, *118*, 327–334.
(7) Croudace, I. W.; Cundy, A. B. *Environ. Sci. Technol.* **1995**, *29*, 1288–1296.
(8) Valette-Silver, N. J. *Estuaries* **1993**, *16*, 577–588.
(9) Allen, J. R. L.; Rae, J. E. *Mar. Pollut. Bull.* **1986**, *17*, 427–431.
(10) Yim, W. W-S. *Mar. Pollut. Bull.* **1976**, *7*, 147–150.
(11) Hamilton, E. I.; Clarke, K. R. *Sci. Total Environ.* **1984**, *35*, 325–386.
(12) Allen, J. R. L. *Sediment. Geol.* **1988**, *58*, 1–21.
(13) Cundy, A. B.; Croudace, I. W. *Estuarine Coastal Shelf Sci.* **1996**, *43*, 449–467.
(14) MacKenzie, A. B.; Scott, R. D.; Allan, R. L.; Ben Shaban, Y. A.; Cook, G. T.; Pulford, I. D. *J. Environ. Radioact.* **1994**, *23*, 39–69.
(15) Farmer, J. G. *Environ. Geochem. Health* **1991**, *13*, 76–83.
(16) Cundy, A. B.; Croudace, I. W. *Mar. Chem.* **1995**, *51*, 115–132.
(17) Korkisch, J.; Sorio, A. *Talanta* **1975**, *22*, 273.
(18) Flynn, W. W. *Anal. Chim. Acta* **1968**, *43*, 221–227.
(19) Krishnaswami, S.; Lal, D.; Martin, J. M.; Maybeck, M. *Earth Planet. Sci. Lett.* **1971**, *11*, 407–414.
(20) Dicks, B.; Levell, D. Refinery-effluent discharges into Milford Haven and Southampton Water. *Ecological impacts of the oil industry*; Dicks, B. Ed.; Wiley: New York, 1989; pp 287–316.
(21) Sharifi, A. R. Heavy metal pollution and its effects on recent foraminiferids from Southampton Water, southern England. Ph.D. Dissertation, University of Southampton, 1994.
(22) AEE Winfrith. *Annual report on radioactive discharges from Winfrith and monitoring the environment 1992*; AEA Technology Report WER-8-1992; AEA: July 1993.
(23) Zwolsman, J. J. G.; Berger, G. W.; Van Eck, G. T. M. *Mar. Chem.* **1993**, *44*, 73–94.
(24) Salomon, J. C.; Guegueniat, P.; Breton, M. Mathematical model of ^{125}Sb transport and dispersion in the Channel. *Radionuclides in the Study of Marine Processes*; Kershaw, P. J., Woodhead, D. S., Eds.; Elsevier: New York, 1991; pp 74–84.
(25) Jefferies, D. F.; Preston, A.; Steele, A. K. *Mar. Pollut. Bull.* **1973**, *4*, 118–122.
(26) Livingston, H. D.; Bowen, V. T. *Nature* **1977**, *269*, 586–588.
(27) Hunt, G. J. *Aquatic Environment Monitoring Reports*; Published Annually, Directorate of Fisheries Research, Lowestoft.
(28) Lewis, J. T. The record of deposition and the migration of elements in salt marshes. Ph.D. Dissertation, University of Southampton, 1997.
(29) Shirahata, M. J.; Elias, R. V.; Patterson, C. C.; Koide, M. *Geochim. Cosmochim. Acta* **1980**, *44*, 149–169.
(30) Erel, Y.; Patterson, C. C. *Geochim. Cosmochim. Acta* 1994, *58*, 3289–3296.
(31) Faure, G. *Principles of isotope geology*, 2nd ed.; Wiley: New York, 1986.
(32) Monna, F.; Lancelot, J.; Croudace, I. W.; Cundy, A. B.; Lewis, J. T. *Environ. Sci. Technol.* Submitted.
(33) Rosman, K. J. R.; Chisholm, W.; Boutron, C. F.; Candelone, J. P.; Hong, S. *Geochim. Cosmochim. Acta* **1994**, *58*, 3265–3270.
(34) Elbaz-Poulichet, F.; Holliger, P.; Martin, J. M.; Petit, D. *Sci. Total Environ.* **1986**, *54*, 61–76.
(35) Kersten, M.; Förstner, U.; Krause, P.; Kriews, M.; Dannecker, W.; Garbe-Schönberg, C.-D.; Höck, M., Terzenbach, U., Grassl, H. Pollution source reconnaissance using stable lead isotope ratios ($^{206}/^{207}Pb$). In *Trace metals in the environment, Vol. II, Impact of heavy metals in the environment*; Vernet, J.-P., Ed.; Elsevier: Amsterdam, 1992; pp 311–325.
(36) Sugden, C. L.; Farmer, J. G.; MacKenzie, A. B. Isotopic characterisation of lead inputs and behaviour in recent Scottish freshwater loch sediments. In *Proceedings of the Eighth International Conference on Heavy Metals in the Environment, Vol. 1*; CEP: Edinburgh, 1991; pp 511–514.
(37) Hamelin, B.; Grousset, F.; Sholkovitz, E. R. *Geochim. Cosmochim. Acta* **1990**, *54*, 37–47.
(38) Doe, B. R.; Stacey, J. S. *Econ. Geol.* **1974**, *69*, 757–776.
(39) Sugden, C. L.; Farmer, J. G.; MacKenzie, A. B. *Environ. Geochem. Health* **1993**, *15*, 59–65.
(40) Farmer, J. G.; Eades, L. J.; MacKenzie, A. B.; Kirika, A.; Bailey-Watts, T. E. *Environ. Sci. Technol.* **1996**, *30*, 3080–3083.
(41) Mukai, H.; Furuta, N.; Fujii, T.; Ambe, Y.; Sakamoto, K.; Hashimoto, Y. *Environ. Sci. Technol.* **1993**, *27*, 1347–1356.
(42) Hamester, M.; Stechmann, H.; Steiger, M.; Dannecker, M. *Sci. Total Environ.* **1994**, *146/147*, 321–323.
(43) Dyer, K. R. Sedimentation and sediment transport. In *The Solent estuarine system—an assessment of present knowledge*; NERC Public Series C No. 22; NERC: 1980; pp 20–24.
(44) Grant, J. A. *Econ. Geol.* **1986**, *81*, 1976–1982.
(45) Sugden, C. L.; Farmer, J. G.; MacKenzie, A. B. Lead and $^{206}Pb/^{207}Pb$ profiles in ^{210}Pb-dated ombrotrophic peat cores from Scotland. In *Proceedings of the Eighth International Conference on Heavy Metals in the Environment, Vol. 1*; CEP: Edinburgh, 1991; pp 90–93.
(46) Appleby, P. G.; Oldfield, F. Application of ^{210}Pb to sedimentation studies. In *Uranium-series disequilibrium. Applications to earth, marine and environmental sciences*, 2nd ed.; Ivanovich, M., Harmon, R. S., Eds.; Oxford Science: Oxford, 1992; pp 731–778.
(47) Gray, J.; Jones, S. R.; Smith, A. D. *J. Radiol. Prot.* **1995**, *15*, 99–131.
(48) Chow, T. J.; Snyder, C. B.; Earl, J. L. Isotope ratios of lead as pollutant source indicators. In *Isotope ratios as pollutant source and behaviour indicators*; IAEA: Vienna, 1975; pp 95–108.

Received for review July 16, 1996. Revised manuscript received November 13, 1996. Accepted November 18, 1996.[®]

ES960622D

[®] Abstract published in *Advance ACS Abstracts*, February 1, 1997.

Environ. Sci. Technol. 1997, 31, 2277–2286

Pb Isotopic Composition of Airborne Particulate Material from France and the Southern United Kingdom: Implications for Pb Pollution Sources in Urban Areas

FABRICE MONNA,*,†,‡ JOEL LANCELOT,† IAN W. CROUDACE,§ ANDREW B. CUNDY,∥ AND JAMES T. LEWIS§

Laboratoire de Géochimie Isotopique, URA-CNRS 1763, Université de Montpellier II, Place E. Bataillon, Case courrier 066, 34095 Montpellier Cedex 05, France, Department of Geology, Southampton Oceanography Centre, Southampton, SO14 3ZH, U.K., and Department of Geography & Earth Sciences, Brunel University, Borough Road, London TW7 5DU, U.K.

Pb isotopic studies of airborne particulate matter, incinerator ash, and gasoline have been carried out to determine sources of Pb pollution in urban areas from France and the southern United Kingdom. $^{206}Pb/^{207}Pb$ ratios in gasoline range from 1.061 to 1.094 (average values are 1.084 for France and 1.067 for the U.K.) while for industrially-derived Pb, $^{206}Pb/^{207}Pb$ ratios vary from 1.143 to 1.155. Natural Pb is more radiogenic and literature values for pre-industrial sediments give $^{206}Pb/^{207}Pb$ ratios of 1.19–1.20 in France and 1.17–1.19 in the U.K. The measured Pb isotopic signature of airborne particulate matter reflects the relative importance of each of these sources, and samples taken from urban areas close to traffic in France and the U.K. show $^{206}Pb/^{207}Pb$ ratios that vary widely from 1.085 to 1.158. While alkyl-lead additives in gasoline are typically still the dominant source of Pb in urban particulate matter, the relative importance of gasoline-derived Pb has decreased, and as a result other sources (industrial and natural) can be identified using isotopic studies. This is a consequence of recent EU environmental legislation that significantly limits concentrations of Pb in gasoline and the increased market penetration of unleaded gasoline. In addition, at a given location, the Pb isotopic composition of particulate matter can vary considerably due to temporal variations in sources (i.e., variations in traffic density) and with wind direction.

Introduction

Investigative studies of lead isotope compositions are well-established in geochemistry and geochronology and are increasingly used in environmental science (see the Clair C. Patterson Special Issue, *Geochim. Cosmochim. Acta* **1994**, *58*). While Pb concentration measurements may provide useful information about potential enrichments of this element, the sources of this Pb will often be ambiguous. To resolve this uncertainty, Pb isotope ratios are studied. Pb has four stable isotopes: ^{204}Pb, ^{206}Pb, ^{207}Pb, and ^{208}Pb. The last three are radiogenic isotopes and are produced by the radioactive decay of ^{238}U, ^{235}U, and ^{232}Th respectively (^{204}Pb is non-radiogenic). Each lead ore deposit has its own characteristic Pb isotopic composition, depending on its age (strictly the time that the lead separated from its source rocks) and on its conditions of genesis (*1*). The isotopic composition of Pb in environmental materials is thus dependent on the ore bodies from which it was derived. In the environment, Pb isotopic ratios reflect the mixing of local/natural Pb with anthropogenic inputs, and mixing processes can be quantified if each source of lead has a distinctive isotopic composition. This principle has been used in a variety of media to determine anthropogenic Pb sources, for example, in freshwater (*2–5*), in sediments (*6–11*), and in aerosols (*12–19*). In France and the U.K., and in western Europe as a whole, the Pb currently used in anthropogenic processes is derived from foreign sources (ore bodies) that commonly have distinctly different isotopic compositions from the local/natural Pb present in rocks and soils. The isotopic signature of this anthropogenic lead is subject to economic factors (commodity, prices) and consequently may change with time according to the origin of the Pb ores used. It is thus essential to make frequent isotopic measurements to maintain a reliable database of anthropogenic Pb for a particular cultural region. Where investigations of environmental fluxes of Pb over a long period are made (i.e., in sedimentary or ice cores), it is clear that a good knowledge of the isotopic character of anthropogenic Pb is required if reliable historical pollution reconstructions are to be carried out. Studies of Pb in the United States are well established and varied, and the subject has a long history (*8, 20–23*). However, the European perspective is not so well established, and fewer data are available.

In this study, recently acquired isotopic data for pollution sources in France and the U.K. are presented, with measurements of airborne particulate matter collected from urban areas. The data provide a better understanding of local variability in Pb sources and show the relative importance of natural and anthropogenic Pb sources in urban air at a number of differing sites. The changing contributions of gasoline-derived Pb to the overall anthropogenic input of lead, due to changes in the use of unleaded petrol over the last 20 years, is also discussed.

Methodology

Sampling. Airborne particulate matter was sampled in 12 French cities and two cities in the U.K. Where possible, sampling was carried out using a PPA60 (France) or TEOM (U.K.) instrument (Amiens, Caen, Le Havre, Lille, Paris, Montpellier, Strasbourg, Toulouse, and London). These devices have a multidirectional head that removes airborne particulate matter above 10 μm and aspirates the ambient air at a fixed-flow rate of 25 L mn^{-1} (PPA60) or 13 L mn^{-1} (TEOM). Samples were collected over 24 h on cellulose–nitrate membrane filters (porosity, 0.8; total diameter, 47 mm; exposed diameter, 33 mm). For other cities, where this equipment was not available, particulate matter was sampled using FILTROMAT equipment over a 24-h period at a fixed-flow rate of 100 L h^{-1} (Bar-le-Duc, Clermont Ferrand, Nantes, and Nice) or using precleaned 0.2-μm PTFE membrane filters attached to a diaphragm pump (Southampton sites). Samples from Southampton were collected over periods ranging from 7 to 10 days and so represent a time-integrated measurement. In addition, five ash samples were removed from electrostatic filters from a French urban incinerator, and 16 leaded gasoline samples were collected in both countries into precleaned glass vials directly from the pump.

* Corresponding author e-mail: monna@sc2a.unige.ch.
† Université de Montpellier II.
‡ Present address: Institut FA Forel, 10 Route de Suisse, CH 1290 Versoix, Switzerland.
§ Southampton Oceanography of Centre.
∥ Brunel University.

S0013-936X(96)00870-X CCC: $14.00

Chemical and Isotopic Analysis. (A) TIMS Analysis. Analyses of French and United Kingdom (London) samples were performed using TIMS at Montpellier. Sample preparation was carried out under Class 100 laminar air flow clean benches in a clean room. Almost all the particulate matter was removed from the filters by ultrasonic agitation in 5 mL of deionized water with the help of a PTFE spatula. Filters were agitated for 2 min only to avoid partial decomposition of the filter, which may introduce a significant blank contribution. Acid digestion of the matrix was avoided for the same reason. The 100% removal of particulate material from the filter is not essential (as the above method of removal is unlikely to be particle size selective), and so the Pb isotopic composition of the material extracted is likely to be representative of the entire sample (Pb isotopic composition is independent of the amount of Pb extracted). After the removal of the filter, the water mixture containing the collected particulate matter was evaporated to dryness, and the residue was digested in 2 mL of high-purity aqua regia at 90 °C for 24 h. For the incinerator ashes, a few milligrams was digested in a PTFE beaker with a mixture of distilled HF, HNO_3, and HCl heated at 90 °C for 1 week. For gasoline, 5 μL was slowly evaporated at 20 °C, and the residue was digested following the same procedure. The solutions were then evaporated, and 200 μL of 0.5 N HBr was added.

Pb separation was achieved using Bio-Rad AG1-X4 anion exchange resin following the conventional technique (*5, 24*): loading of the sample in 0.5 N HBr, washing twice with 1 mL of 0.5 N HBr, and a final elution of Pb with 0.5 mL of 6 N HCl. This operation was repeated to purify the sample and to ensure a stable thermal emission during measurements. Pb was loaded on a single Re filament using the silica gel/phosphoric acid method (*25*). Measurements of Pb isotopic ratios were carried out by thermal ionization mass spectrometry (TIMS) on a VG SECTOR mass spectrometer equipped with five Faraday cups using simultaneous multicollection in static mode. Regular measurements of the Pb standard, NIST 981, allowed the correction of the data for mass fractionation (1.35 ± 0.05 ‰ per amu). Analytical precision was found to be better than 1‰ for $^{206}Pb/^{204}Pb$, $^{207}Pb/^{204}Pb$, and $^{208}Pb/^{204}Pb$ ratios and better than 0.2‰ for $^{206}Pb/^{207}Pb$ and $^{208}Pb/^{206}Pb$ ratios. Blank measurements, determined using a ^{207}Pb spike, show that Pb added during the analytical procedure by the operator is less than 0.25% of the Pb concentration in the samples and thus does not require correction. Duplicates of three aerosol samples (Le Havre, Lille, and Paris) show good reproducibility and confirm the significance of the analytical data.

(B) ICP–MS Measurements. Isotopic analyses of Southampton airborne particulate samples and of U.K. gasoline were performed at Southampton using a VG PlasmaQuad 2+ ICP–MS. This instrument has a very high sensitivity and produces a count rate of approximately 5.10^5 cps/ppb for Pb. Pb was preconcentrated in a similar manner to that described above, and the details are given in ref 11. MilliQ+ water and PRIMAR acids (Fisher) were used during all chemical manipulations. NIST 981 was used to monitor accuracy and to correct for mass fractionation, and procedural blanks were run to determine possible contamination from reagents and general handling. The only notable interference in ICP–MS measurements is the ^{204}Hg isobaric overlap on ^{204}Pb that is readily corrected for by monitoring ^{200}Hg. Analytical precision was generally better than 1% for $^{206}Pb/^{204}Pb$, $^{207}Pb/^{204}Pb$, and $^{208}Pb/^{204}Pb$ ratios and better than 8‰ for $^{206}Pb/^{207}Pb$ and $^{208}Pb/^{206}Pb$ ratios.

Results

Geochemists prefer conventionally to use Pb isotopic ratios incorporating ^{204}Pb due to the mathematical simplification of using a non-radiogenic isotope. However, environmental scientists tend to use $^{206}Pb/^{204}Pb$ vs $^{206}Pb/^{207}Pb$ or $^{206}Pb/^{207}Pb$ vs $^{208}Pb/^{206}Pb$ because of their better analytical precision. Here we use $^{206}Pb/^{207}Pb$ vs $^{208}Pb/^{206}Pb$ for comparability with recent studies obtained using ICP–MS and also present conventional $^{206}Pb/^{204}Pb$ vs $^{208}Pb/^{204}Pb$ diagrams.

The environmental materials analyzed in the present study have distinct lead isotopic signatures (Tables 1 and 2). Gasolines possess the least radiogenic isotopic signatures, and Pb isotopic ratios show little regional variation. In France, $^{206}Pb/^{207}Pb$ ratios range from 1.069 to 1.094 (average: 1.084 ± 0.009 at 1σ) whereas in the U.K. slightly lower values are found: $^{206}Pb/^{207}Pb$ ratios ranging between 1.059 and 1.079 (average: 1.067 ± 0.007). Ashes from the French urban incinerator gave much higher (more radiogenic) $^{206}Pb/^{207}Pb$ ratios ranging from 1.143 to 1.154 (average: 1.149 ± 0.005), similar to values for liquid urban wastes from Southern France (*5*) (average $^{206}Pb/^{207}Pb$ = 1.157 ± 0.007, 1σ). The greatest variations in isotopic composition occurred in urban airborne particulate matter (sampled in nine French cities and two U.K. cities during the period November 1994–January 1996) that had $^{206}Pb/^{207}Pb$ ratios between 1.085 and 1.158. Both regional and temporal variations in the Pb isotopic composition of urban airborne particulate matter were obvious. At a national scale, $^{206}Pb/^{207}Pb$ ratios varied between 1.100 at Nantes and 1.145 at Toulouse, while locally two different sites in the same city, examined during the same day, show very distinct isotopic signatures: 1.104 (Toulouse station 6) and 1.145 (Toulouse station 12) (Table 1). In addition, substantial temporal variations were observed at west London (Teddington), where the Pb isotopic composition of airborne particles was monitored daily over two periods of approximately 1 week each in November 1995 and in January 1996. Here, the $^{206}Pb/^{207}Pb$ ratios varied between 1.114 and 1.127 during the November 1995 sampling period and between 1.124 and 1.158 during the January 1996 sampling period (Table 2). For each period, the more radiogenic values are observed during the weekend or when the wind is from a SE direction (authors preliminary unpublished data). If the integrated sampling time is longer, as at Southampton (3–7 days), these variations are less clear. The regional and temporal variability in Pb isotopic composition reflects local variations in the relative importance of gasoline, industrial, and natural Pb sources and is discussed in the following sections.

Discussion

Isotopic Characterization of Pb Sources. (A) Pb from Gasoline. Despite direct pump sampling of several different gasoline suppliers (Esso, Total, Agip, etc.), the range of measured $^{206}Pb/^{207}Pb$ ratios is rather small for each country and so represents a relatively homogeneous source. The values are the lowest ever reported for French and U.K. gasoline: the average $^{206}Pb/^{207}Pb$ ratio for French samples is 1.084 ± 0.009 (1σ), while the average for U.K. samples is 1.067 ± 0.007. In France and the U.K., the Octel Co. (Associated Octel in the U.K.) is the main producer of tetraethyl and tetramethyl lead (TEL–TML) added to fuels as an antiknock compound. This company supplies nearly 80% of the Pb alkyls used in the refineries of both countries. Production of TEL–TMLs from U.S. companies has totally ceased due to national legislative requirements. Most of the Pb currently used in TEL–TML production is derived from the Precambrian Pb–Zn ore deposits of Australia and Canada, with minor contributions from Morocco and other sources [Octel Co., France (1995) and Associated Octel, U.K., personal communication, (1996)]. Pb from Australian and Canadian ores are characterized by low radiogenic signatures; the 1600–1700 Ma Broken Hill (New South Wales) and Mount Isa (Queensland) Pb ores show $^{206}Pb/^{207}Pb$ ratios in the range 1.03–1.04 (*1*). The Mesozoic Pb–Zn province from Morocco shows a much more radiogenic $^{206}Pb/^{207}Pb$ ratio of approximately 1.16–1.17. A mixing of 80% Australian Pb with

TABLE 1. Pb Isotopic Composition of Airborne Particulate Matter, Gasoline, and Incinerator Ashes in France

location/(station)	organization	date	characteristics	$^{206}Pb/^{204}Pb$	$^{207}Pb/^{204}Pb$	$^{208}Pb/^{204}Pb$	$^{206}Pb/^{207}Pb$	$^{208}Pb/^{206}Pb$
				Airborne Particulate Matter				
Amiens	ASQAP	Sep 1, 1995	urban	17.276 ± 0.006	15.552 ± 0.006	37.10 ± 0.02	1.1108 ± 0.0001	2.1476 ± 0.0003
Bar-le-duc	AIRLOR	Sep 1, 1995		17.543 ± 0.005	15.563 ± 0.005	37.38 ± 0.01	1.1279 ± 0.0001	2.1309 ± 0.0003
Caen	ESPAC	Sep 7, 1995		17.329 ± 0.011	15.535 ± 0.010	37.15 ± 0.03	1.1155 ± 0.0001	2.1440 ± 0.0003
		Sep 8, 1995		17.350 ± 0.008	15.548 ± 0.008	37.19 ± 0.02	1.1158 ± 0.0001	2.1438 ± 0.0003
Clermont-Ferrand	AMPAC	Sep 1, 1995		17.448 ± 0.011	15.553 ± 0.011	37.28 ± 0.03	1.1219 ± 0.0001	2.1366 ± 0.0003
Le Havre	AIR NORMAND	Aug 14, 1995		17.236 ± 0.004	15.536 ± 0.005	37.09 ± 0.01	1.1094 ± 0.0001	2.1517 ± 0.0003
duplicate				17.248 ± 0.005	15.552 ± 0.005	37.09 ± 0.02	1.1091 ± 0.0001	2.1508 ± 0.0003
Lille	AREMA LRT	Sep 1, 1995		17.288 ± 0.009	15.544 ± 0.009	37.16 ± 0.02	1.1123 ± 0.0001	2.1492 ± 0.0003
duplicate				17.285 ± 0.005	15.540 ± 0.006	37.11 ± 0.02	1.1124 ± 0.0001	2.1469 ± 0.0003
Paris	Préfecture de Police	Sep 13, 1995		17.425 ± 0.005	15.542 ± 0.005	37.26 ± 0.02	1.1212 ± 0.0002	2.1386 ± 0.0004
duplicate				17.448 ± 0.011	15.553 ± 0.011	37.28 ± 0.03	1.1219 ± 0.0001	2.1366 ± 0.0003
Montpellier								
station 1	AMPADI	Jan 27, 1995		17.453 ± 0.007	15.567 ± 0.007	37.28 ± 0.02	1.1211 ± 0.0001	2.1361 ± 0.0003
station 4		Jan 29, 1995		17.382 ± 0.004	15.577 ± 0.005	37.23 ± 0.01	1.1159 ± 0.0001	2.1421 ± 0.0003
station 1		Jan 29, 1995		17.401 ± 0.007	15.564 ± 0.007	37.24 ± 0.02	1.1181 ± 0.0001	2.1402 ± 0.0003
station 1		Sep 7, 1995		17.202 ± 0.005	15.543 ± 0.005	37.05 ± 0.02	1.1068 ± 0.0001	2.1539 ± 0.0003
Nantes	LOIRESTU'AIR	Sep 7, 1995		17.084 ± 0.005	15.519 ± 0.005	36.91 ± 0.01	1.1008 ± 0.0001	2.1603 ± 0.0003
Nice	QUALIT'AIR06	Sep 21, 1995		17.445 ± 0.005	15.547 ± 0.005	37.27 ± 0.02	1.1221 ± 0.0001	2.1363 ± 0.0003
Strasbourg	ASPA	Sep 1, 1995		17.566 ± 0.018	15.490 ± 0.016	37.31 ± 0.04	1.1342 ± 0.0002	2.1236 ± 0.0004
		Sep 4, 1995		17.611 ± 0.006	15.558 ± 0.006	37.42 ± 0.02	1.1319 ± 0.0001	2.1250 ± 0.0003
Toulouse								
station 6	ORAMIP	Sep 7, 1995		17.139 ± 0.013	15.522 ± 0.013	36.96 ± 0.03	1.1042 ± 0.0001	2.1563 ± 0.0004
station 12		Sep 7, 1995	urban/smelter	17.892 ± 0.004	15.622 ± 0.004	37.90 ± 0.01	1.1453 ± 0.0001	2.1184 ± 0.0004
				Gasolines				
ELF	Leaded gasoline	Oct 1995	pump	16.564 ± 0.005	15.490 ± 0.005	36.41 ± 0.02	1.0693 ± 0.0001	2.1980 ± 0.0004
Leclerc Supermarket				16.759 ± 0.004	15.510 ± 0.005	36.59 ± 0.02	1.0806 ± 0.0001	2.1832 ± 0.0004
Monoprix Supermarket				17.014 ± 0.003	15.549 ± 0.004	36.95 ± 0.01	1.0942 ± 0.0001	2.1719 ± 0.0004
total		Nov 1995		16.996 ± 0.007	15.534 ± 0.007	36.89 ± 0.02	1.0942 ± 0.0001	2.1705 ± 0.0003
Esso		Dec 1995		16.679 ± 0.005	15.511 ± 0.005	36.53 ± 0.01	1.0753 ± 0.0001	2.1904 ± 0.0003
AGIP				16.897 ± 0.006	15.534 ± 0.006	36.80 ± 0.02	1.0878 ± 0.0001	2.1777 ± 0.0003
BP				16.641 ± 0.007	15.499 ± 0.008	36.47 ± 0.02	1.0736 ± 0.0001	2.1914 ± 0.0004
Shell				16.837 ± 0.006	15.510 ± 0.006	36.70 ± 0.02	1.0856 ± 0.0001	2.1796 ± 0.0003
Carrefour Supermarket				17.068 ± 0.004	15.597 ± 0.005	37.09 ± 0.02	1.0943 ± 0.0001	2.1728 ± 0.0004
				Industrial Pb				
urban incinerator	CIVOM Sete	Sep 30, 1993	ashes	17.894 ± 0.004	15.661 ± 0.005	38.00 ± 0.01	1.1427 ± 0.0001	2.1236 ± 0.0003
		Oct 29, 1993		18.057 ± 0.007	15.698 ± 0.007	38.25 ± 0.02	1.1501 ± 0.0002	2.1183 ± 0.0007
		Dec 03, 1993		17.987 ± 0.003	15.634 ± 0.004	38.03 ± 0.01	1.1504 ± 0.0001	2.1143 ± 0.0003
		Jan 06, 1994		18.009 ± 0.003	15.595 ± 0.010	37.95 ± 0.01	1.1547 ± 0.0001	2.1070 ± 0.0002

TABLE 2. Pb Isotopic Composition of Airborne Particulate Matter and Gasoline in the U.K.

location	date	characteristics	$^{206}Pb/^{204}Pb$	$^{207}Pb/^{204}Pb$	$^{208}Pb/^{204}Pb$	$^{206}Pb/^{207}Pb$	$^{208}Pb/^{206}Pb$
			Airborne Particulate Matter				
Portswood (Southampton)	Nov 10, 1994	city suburb	17.05 ± 0.05		36.92 ± 0.05	1.105 ± 0.002	2.165 ± 0.003
	Jan 8, 1995		17.05 ± 0.05		36.92 ± 0.05	1.102 ± 0.002	2.165 ± 0.003
	Nov 28, 1994		17.20 ± 0.05		37.08 ± 0.05	1.111 ± 0.002	2.155 ± 0.003
Southampton	Oct 21, 1994	city center	16.91 ± 0.05		36.76 ± 0.05	1.089 ± 0.003	2.175 ± 0.003
	Oct 20, 1994		16.92 ± 0.05		36.79 ± 0.05	1.096 ± 0.003	2.174 ± 0.003
	Oct 28, 1994		17.02 ± 0.05		36.89 ± 0.05	1.098 ± 0.003	2.167 ± 0.003
	Nov 18, 1994		16.92 ± 0.05		36.74 ± 0.05	1.098 ± 0.003	2.172 ± 0.003
	Nov 5, 1994		17.09 ± 0.05		36.99 ± 0.05	1.098 ± 0.003	2.165 ± 0.003
	Nov 25, 1994		17.02 ± 0.05		36.86 ± 0.05	1.101 ± 0.003	2.166 ± 0.003
	Dec 10, 1994		17.10 ± 0.05		36.96 ± 0.05	1.101 ± 0.003	2.161 ± 0.003
	Dec 17, 1994		17.00 ± 0.05		36.86 ± 0.05	1.101 ± 0.003	2.168 ± 0.003
	Dec 3, 1994		17.05 ± 0.05		36.82 ± 0.05	1.102 ± 0.003	2.160 ± 0.003
	Dec 27, 1994		16.97 ± 0.05		36.80 ± 0.05	1.103 ± 0.003	2.169 ± 0.003
	Dec 23, 1994		17.01 ± 0.05		36.83 ± 0.05	1.104 ± 0.003	2.165 ± 0.003
	Dec 30, 1994		17.10 ± 0.05		36.89 ± 0.05	1.106 ± 0.003	2.157 ± 0.003
London (Teddington)	Sat Nov 4, 1995	urban	17.564 ± 0.004	15.602 ± 0.005	37.66 ± 0.01	1.1257 ± 0.0001	2.1440 ± 0.0003
	Sun Nov 5, 1995		17.573 ± 0.003	15.588 ± 0.003	37.64 ± 0.01	1.1273 ± 0.0001	2.1418 ± 0.0003
	Mon Nov 6, 1995		17.341 ± 0.003	15.563 ± 0.003	37.31 ± 0.01	1.1143 ± 0.0001	2.1513 ± 0.0003
	Wed Nov 8, 1995		17.347 ± 0.003	15.546 ± 0.004	37.21 ± 0.01	1.1159 ± 0.0001	2.1449 ± 0.0003
	Thu Nov 9, 1995		17.351 ± 0.007	15.537 ± 0.007	37.15 ± 0.02	1.1168 ± 0.0001	2.1409 ± 0.0003
	Fri Nov 10, 1995		17.379 ± 0.007	15.568 ± 0.007	37.27 ± 0.02	1.1163 ± 0.0001	2.1444 ± 0.0003
	Thu Jan 18, 1996		17.513 ± 0.006	15.575 ± 0.006	37.39 ± 0.02	1.1244 ± 0.0001	2.1347 ± 0.0003
	Fri Jan 19, 1996		17.522 ± 0.010	15.588 ± 0.010	37.43 ± 0.03	1.1241 ± 0.0002	2.1360 ± 0.0004
	Sat Jan 20, 1996		17.790 ± 0.003	15.602 ± 0.003	37.69 ± 0.01	1.1403 ± 0.0001	2.1187 ± 0.0003
	Sun Jan 21, 1996		18.074 ± 0.007	15.606 ± 0.007	37.95 ± 0.02	1.1582 ± 0.0001	2.0993 ± 0.0003
	Mon Jan 22, 1996		18.032 ± 0.007	15.602 ± 0.007	37.86 ± 0.02	1.1557 ± 0.0001	2.0997 ± 0.0003
			Gasolines				
Texaco (Southampton)	Nov–Dec 1994	leaded 4* gasoline	16.61 ± 0.05		36.49 ± 0.05	1.059 ± 0.003	2.197 ± 0.003
Tesco Supermarket (S'ton)			16.62 ± 0.05		36.44 ± 0.05	1.061 ± 0.003	2.196 ± 0.003
BP (Southampton)			16.60 ± 0.05		36.39 ± 0.05	1.062 ± 0.003	2.197 ± 0.003
total (Southampton)			16.69 ± 0.05		36.43 ± 0.05	1.066 ± 0.003	2.195 ± 0.003
Esso (Southampton)			16.64 ± 0.05		36.39 ± 0.05	1.068 ± 0.003	2.191 ± 0.003
ELF (Southampton)			16.70 ± 0.05		36.59 ± 0.05	1.076 ± 0.003	1.189 ± 0.003
Shell (Southampton)			16.72 ± 0.05		36.65 ± 0.05	1.079 ± 0.003	2.186 ± 0.003

20% of Moroccan Pb gives a ratio of 1.06. This calculated value is comparable with the mean of $^{206}Pb/^{207}Pb$ ratio measured today in French gasoline (1.084 ± 0.009; 1σ). In the U.K. in the late 1980s, Associated Octel used a mixture of Australian and Canadian ores in the approximate proportion 70:30 giving a $^{206}Pb/^{207}Pb$ ratio of 1.076 (*26*) similar to the mean currently measured. The virtual monopoly for alkyl-lead additives held by the Octel Co., in both France and the U.K., implies a signature that is relatively homogeneous regardless of gasoline supplier. However, it should be noted that U.K. additives may not be exactly identical to those recipes used in France since the Octel Co. operates independently in both countries and may therefore purchase Pb from different sources.

(B) Pb from Industrial Emissions. It is difficult to precisely define the isotopic signature of an overall industrial Pb source because of the multiplicity of existing emissions. In addition, the Pb used by U.K. and French industry is dominantly imported since all indigenous Pb–Zn mineral deposits have been worked out in both countries. In the case of gasoline, it is possible to characterize a general Pb isotopic signature due to the effective market monopoly of the Octel Co., but it is obviously not possible to follow the same approach for industrial emissions. While it is likely that industrial emissions have a widely varying Pb isotopic composition (as shown by several workers), Mukai et al. (*16*) and Hamester et al. (*19*) have shown that the Pb isotopic composition of fly ashes from refuse incinerators can be used as a useful indicator of industrial Pb sources. All Pb-containing products are burned and mixed, and the lead isotope ratios are averaged to provide a representative "industrial Pb" signature. Data for the urban incinerator at Sète give $^{206}Pb/^{207}Pb$ ratios varying from 1.143 to 1.155 (Table 1). The range may be due to slight variation in the nature of burned products. Identical ratios have been recently found for the same kind of samples from Germany ~1.142–1.159 (*19*) and in Japan 1.15 (*16*). These values are comparable to those previously found in liquid urban waste (~1.147–1.160) in southern France (*5*) and are much more radiogenic than those from gasoline. The application of the Student's *t*-test indicates that the differences between Pb from gasoline and industrial Pb are significant at greater than the 99.9% level. The imports thus are likely to include younger Pb ores (which are more radiogenic) than those from Australia. It is interesting to note that this range also corresponds to the world average of the main Pb ore deposits.

(C) Natural Pb Derived from Rocks and Soils. In France, $^{206}Pb/^{207}Pb$ ratios ranging from 1.193 to 1.200 were measured in pre-industrial sediments sampled in the Thau basin (southern France) and dated at more than 200 yr BP (*27*). Almost the same values were observed (1.197–1.210) in the pre-industrial sediments of the Seine, Loire, Gironde, and Rhône Rivers (*3*). This ratio is likely to be typical throughout France because most of the natural Pb is derived from Variscan continental crust (granite and metamorphic rocks) and from Mezosoic and Cenozoic sediments. This Pb has a $^{206}Pb/^{207}Pb$ ratio ranging from 1.18 to 1.20 (*28*). A remote contribution due to dust transport from North Africa and the Sahara may also occur, although the isotopic composition of these aerosols does not differ significantly from the local/natural Pb. Aerosols from Senegal and a sample from the Matmata loess (southern Tunisia) exhibit $^{206}Pb/^{207}Pb$ ratios of 1.193 and 1.198, respectively (*18, 29*). Due to the lack of isotopic variation between these natural Pb sources, they will simply be considered as French natural lead.

In the U.K., the situation is very similar, however, with slightly less radiogenic ratios as shown by the studies of Hamilton and Clifton (*7*), Croudace and Cundy (*11*), and Sugden et al. (*15*). Pre-industrial sediments from Swansea Bay, Southampton Water, and central Scotland analyzed in these studies gave $^{206}Pb/^{207}Pb$ ratios between 1.17 and 1.19.

Origin of Pb in Airborne Particulate Matter from Urban Areas. In many previous studies, the Pb isotopic composition of urban particulate material, sampled in zones exposed to heavy vehicle traffic, has been considered to be dominated by automotive exhaust emissions. However, since the Pb isotopic composition of airborne particles in both countries shows a wide range of $^{206}Pb/^{207}Pb$ ratios (1.085–1.158), they cannot be due entirely to automotive emissions because measured gasolines range from 1.059 to 1.094. Plotted on $^{206}Pb/^{207}Pb$ vs $^{208}Pb/^{206}Pb$ and $^{206}Pb/^{204}Pb$ vs $^{208}Pb/^{204}Pb$ diagrams, the points fall between the gasoline and the industrial domains (Figure 1). It is clear that the Pb from gasoline is an indisputable source since the Pb isotopic compositions of the urban aerosols cannot be explained by simple binary mixing between natural Pb and industrial Pb alone. In addition, the contribution of natural Pb cannot be excluded because the observed signatures can be reconstructed by three end member as well as two end member mixing. For these reasons, it is impossible to calculate the contribution of each component precisely. To do this, an examination of local influences such as the proximity of industries, traffic density, wind direction, and long-term monitoring of Pb isotopes would be required. Such calculations, though possible, are of limited use because they require generalizations to describe the behavior of the Pb at a given site based on only a few samples. Estimations of the gasoline component that avoid the problem of a ternary mixing solution can be made by initially considering binary mixing of gasoline and industrial Pb using the following conventional mixing equation:

$$X_1 = \frac{(^{206}Pb/^{204}Pb)_{SAMP} - (^{206}Pb/^{204}Pb)_{IND}}{(^{206}Pb/^{204}Pb)_{G} - (^{206}Pb/^{204}Pb)_{IND}} \quad (1)$$

where X_1 is the percentage contribution of gasoline; $(^{206}Pb/^{204}Pb)_G$, $(^{206}Pb/^{204}Pb)_{IND}$, and $(^{206}Pb/^{204}Pb)_{SAMP}$ are the isotopic signatures of the gasoline and industrial end-members and of the airborne particulate sample, respectively. This equation uses the $^{206}Pb/^{204}Pb$ ratio, but similar equations can be developed for the other isotope ratios.

Furthermore, binary mixing between gasoline and the more radiogenic natural Pb component gives the following equation:

$$X_2 = \frac{(^{206}Pb/^{204}Pb)_{SAMP} - (^{206}Pb/^{204}Pb)_{NAT}}{(^{206}Pb/^{204}Pb)_{G} - (^{206}Pb/^{204}Pb)_{NAT}} \quad (2)$$

where X_2 represents the contribution of gasoline in this mixing model and $(^{206}Pb/^{204}Pb)_{NAT}$ is the isotopic composition of pre-industrial sediments. The average isotopic compositions of each end member used for the mixing models are shown in Table 3. Although the isotopic composition of the industrial end member has not yet been empirically defined for the southern U.K., a French signature is assumed to be reasonable.

Some differences occur between the $^{206}Pb/^{207}Pb$–$^{208}Pb/^{206}Pb$ and $^{206}Pb/^{204}Pb$–$^{208}Pb/^{204}Pb$ graphs (Figure 1): particularly for gasoline values near the lower part of the $^{206}Pb/^{207}Pb$–$^{208}Pb/^{206}Pb$ couple and for U.K. particulate material. This is explained by the fact that samples having different $^{206}Pb/^{204}Pb$ and $^{207}Pb/^{204}Pb$ ratios can have a similar $^{206}Pb/^{207}Pb$ ratio, which is also true for all other ratios that do not include the ^{204}Pb isotope. To reduce this effect, X_1 and X_2 are calculated by averaging the results obtained with each ratio. The range between X_1 and X_2 is a measure of the uncertainty on the estimate of the percentage contribution of gasoline-derived Pb when considering mixing between gasoline, industrial, and natural Pb.

As described below, the isotopic composition of gasoline-derived Pb has shown significant changes over the last 30 years. The models used here assume that resuspension of

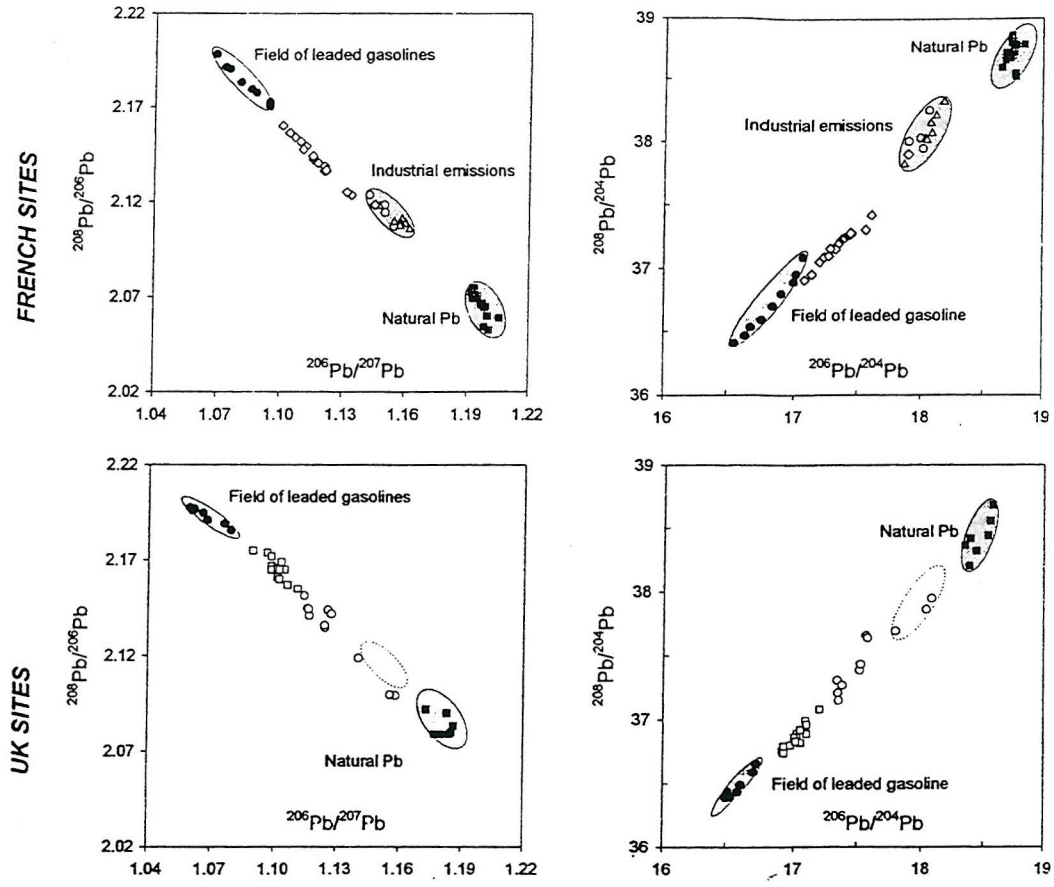

FIGURE 1. $^{208}Pb/^{206}Pb$ vs $^{206}Pb/^{207}Pb$ and $^{208}Pb/^{204}Pb$ vs $^{206}Pb/^{204}Pb$ in environmental samples from France and the U.K. (●) leaded gasoline, (gray circles) ashes from urban incinerator, (△) liquid urban waste (*5*), (■) pre-industrial sediment (*3, 5, 7, 26*), (◇) airborne particulate matter from French urban areas, (○) airborne particulate matter from London, (□) airborne particulate matter from Southampton.

TABLE 3. Average Isotopic Composition of Gasoline-Derived, Industrial, and Local/Natural Pb in France and the U.K.[a]

	n	$^{206}Pb/^{204}Pb$	$^{208}Pb/^{204}Pb$	$^{206}Pb/^{207}Pb$	$^{208}Pb/^{206}Pb$
		End Members in France			
gasoline	9	16.83	36.71	1.084	2.182
industrial emissions	13	18.03	38.07	1.155	2.112
pre-/early industrial sediments	16	18.73	38.72	1.197	2.066
		End Members in U.K.			
gasoline	7	16.60	36.48	1.067	2.193
industrial emissions	*b*	18.03	38.07	1.155	2.112
pre-/early industrial sediments	7	18.45	38.41	1.184	2.082

[a] *n*, number of samples. [b] Isotopic composition of the 'industrial' end member in the U.K. is assumed to be the same as in France.

"old" gasoline-derived Pb into the urban atmosphere has an insignificant impact on the gasoline end member. Several studies have shown that contaminants introduced into urban areas (i.e., ^{137}Cs) have relatively low residence time in urban dusts, with half-lives usually less than 1 year (*30, 31*). That part of the Pb emitted in the 1960s and 1970s that has not been removed from urban areas by rainfall is likely to be present in a form not readily amenable to resuspension (e.g., in soils). Consequently, in the vicinity of dense automotive traffic, the contribution of old gasoline-derived Pb is likely to be relatively small.

Origin of Pb in French Airborne Particulate Matter. It is apparent that if the isotopic signature of airborne particulate matter is similar to that of gasoline, the uncertainty (range between X_1 and X_2) is slight, i.e., for Nantes (Figure 2). By contrast, if the isotopic signature approaches industrial values, as found for station 12 of Toulouse, the contribution from gasoline is poorly constrained. In spite of this sometimes poor discrimination, samples can be divided into three groups. For Nantes, Toulouse station 6, Montpellier, and Le Havre, measurements show that 70−80% of Pb is derived from gasoline combustion, decreasing to 40−70% for Clermont-Ferrand, Paris, Amiens, Strasbourg, Lille, Caen, and Bar-le-Duc. Finally, a gasoline Pb contribution ranging from 10 to 40% is calculated for airborne particulate matter collected from Toulouse station 12. Figure 3 shows the change in

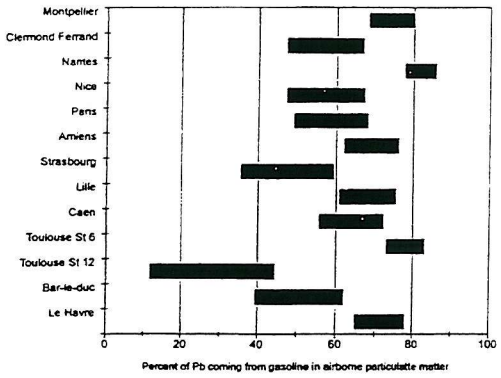

FIGURE 2. Calculated percentage contribution of gasoline-derived Pb to total airborne particulate Pb in urban areas from France.

airborne Pb concentration over time at the various French sites used in this study, since 1984. At most sites examined, the airborne Pb concentration has greatly decreased due to EU (European Union) legislation that has imposed reductions on the amount of Pb added to gasoline (0.15 g/L at present, compared with 0.65 g/L in the period 1965–1975, Associated Octel, personal communication) and on permitted Pb emissions and also the increasing use of unleaded gasoline. Pb concentrations shown in Figure 3 are generally much lower than the upper limit fixed by the EU of 2 $\mu g/m^3$ Pb as an annual average. Only Toulouse station 12 has not seen a general Pb decrease. This station, located in the center of the city, is close to a lead smelter used for battery recycling. This factory is a significant Pb polluter with an average emission rate of 0.2 kg day^{-1} (1993 value). The influence of an industrial input is evident at station 12, and only ~10% of the total Pb at this site is derived from gasoline combustion based on calculations using eq 1; the natural component is relatively insignificant. The other sampling site at Toulouse (station 6), located 4 km from station 12, is exposed to very dense vehicle traffic and shows a relatively high airborne Pb concentration when compared to the other French cities. Here, the $^{206}Pb/^{207}Pb$ ratio (1.104) indicates that, on the day sampled, the contribution from industrial activities was negligible, highlighting the dominantly local impact of the smelter. At Strasbourg, a rather radiogenic signature has also been found. This cannot be explained by a more radiogenic contribution from German gasolines because these have approximately the same Pb isotopic composition as French gasoline (*19*). Moreover, it is notable that in recent years more than 90% of German gasoline used is unleaded as compared with 50% and 40% for the U.K. and France, respectively (Associated Octel, personal communication). A more likely explanation is that sampling of material at Strasbourg was carried out in a zone that is now traffic-free, which explains why the Pb content and the gasoline contribution are so low.

Origin of Pb in U.K. Airborne Particulate Matter. (A) Teddington, West London. Airborne particulate samples collected from the Teddington area of west London show a large range in Pb isotopic ratios (Figure 4). This short-term variability is likely to be a result of varying wind direction and traffic densities. The major road in this area is to the west of the sampling site, and the least radiogenic values are found when the wind is from the west. Under SE winds, which cross areas of low traffic density, the most radiogenic data are found. The data confirm that Pb isotopic composition is also a function of traffic density since more radiogenic values are measured at the weekends. During weekend periods, traffic density is substantially lower than on weekdays when considerable congestion occurs due to commuter traffic. Even during days with higher traffic density, the contribution of Pb derived from gasoline does not exceed ~ 60% (Figure 4).

(B) Southampton. Samples in Southampton were collected using a low-volume air sampler over several days, and therefore the data represent generalized values and cannot be used to evaluate short-term effects. Air particles were

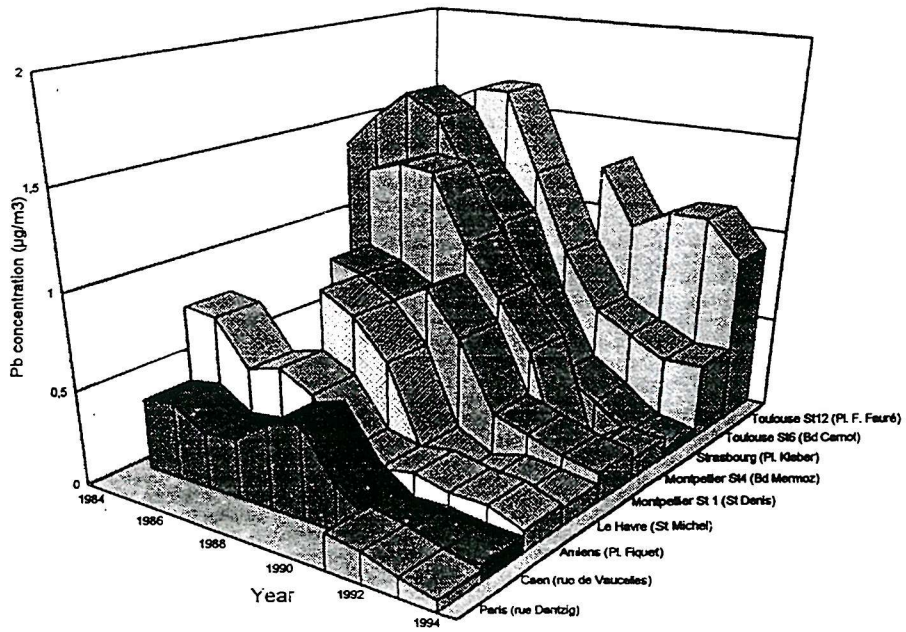

FIGURE 3. Temporal change in Pb concentration in urban air at various French sites (data from ORAMIP, ASPA, AMPADI, AIRNORMAND, ASQAP, ADEME, and LCPP, personal communication, 1995).

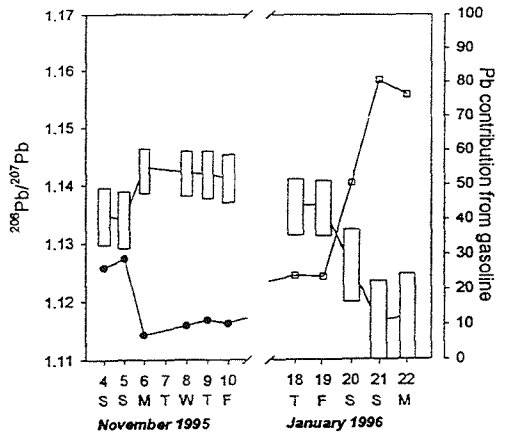

FIGURE 4. Evolution of $^{206}Pb/^{207}Pb$ ratios in airborne particulate matter collected at London (Teddington) in November 1995 (●) and January 1996 (□). The boxes represent the calculated contribution of Pb from gasoline (from eqs 1 and 2).

collected from a busy city center site and also from a suburb of the city (Portswood) that is also exposed to appreciable traffic. The former sampling site was by the main road while the latter was a garden site. The results show that gasoline-derived Pb makes a major contribution to particulate Pb in both areas: 61–84% of Pb is derived from gasoline combustion at the city center site and 56–74% at the Portswood suburban site.

These results confirm that gasoline is the main source of Pb in most French and in southern U.K. urban areas. However, following environmental legislation restricting concentrations of Pb in gasoline and the increased market penetration of unleaded gasoline, other sources of Pb can now be identified using isotopic studies and are likely to become increasingly evident.

Evolution of Pb Isotopic Signatures in Environmental Materials. The results from this study can be used to extend the existing database that describes the changing isotopic composition of anthropogenic Pb with time (Figure 5). This type of information is indispensable in historical reconstruction of Pb pollution sources in sediment and ice-core records or other environments (*32–35*). Table 4 summarizes the published data since 1965. In France, Chow et al. (*22*) measured a $^{206}Pb/^{207}Pb$ ratio of 1.162–1.163 in gasoline directly whereas many other workers have obtained data indirectly through the sampling of aerosols. These later workers considered that their results were more or less representative of automotive emissions. In 1975, grass sampled in the vicinity of a Parisian highway gave a ratio of 1.128 while in 1981 filtered aerosols taken in a car park near Paris were measured at 1.101 (*2, 3*). During the same period, Flament (*36*) found a similar ratio of 1.093 for aerosols collected along a highway in northern France. Monna et al. (*5*) reported slightly higher values of 1.109–1.111 for airborne particulate matter sampled in 1987, a few meters from heavy traffic in Montpellier. Finally, in 1988 Grousset et al. (*29*) collected aerosols from Lyon that had $^{206}Pb/^{207}Pb$ ratios of 1.096. In the U.K., the available data are more limited. Hamilton and Clifton (*7*) reported $^{206}Pb/^{207}Pb$ ratios of 1.126 and 1.105 in 1968 and 1971, respectively, measured in airborne particles from London and 1.134 in airborne particulate matter from Cardiff in 1968. More recently, Sugden et al. (*15*) found $^{206}Pb/^{207}Pb$ ratios ranging from 1.056 to 1.093 in Edinburgh over the period 1989–1991. The trends in the U.K. and France show a significant decrease in the $^{206}Pb/^{207}Pb$ ratio during

TABLE 4. Previously Published Pb Isotopic Compositions of Environmental Samples from France and the U.K.

	ref	method	year	sampling	$^{208}Pb/^{204}Pb$	$^{207}Pb/^{204}Pb$	$^{206}Pb/^{204}Pb$	$^{206}Pb/^{207}Pb$	$^{208}Pb/^{206}Pb$
				France					
Paris	22	TIMS	1966	gasoline	18.25			1.162	2.113
Paris	22	TIMS	1968	gasoline	18.24			1.163	2.113
Paris	2	TIMS	1975	grass sample				1.128	
Paris	2, 3	TIMS	Dec 1981	aerosols car park	17.25 ± 0.05	15.56 ± 0.05	37.49 ± 0.13	1.101 ± 0.001	
Gravelines	3	TIMS	1984	aerosol/highway	16.99	15.54	36.87	1.093	2.170
Montpellier	5	TIMS	Sep 1987	urban air/filter	17.385 ± 0.044	15.663 ± 0.039	37.471 ± 0.101	1.1093 ± 0.0004	
Montpellier	5	TIMS	Sep 1987	urban air/filter	17.270 ± 0.003	15.556 ± 0.004	37.172 ± 0.011	1.1102 ± 0.0001	
Montpellier	5	TIMS	Sep 1987	urban air/filter	17.332 ± 0.029	15.603 ± 0.027	37.306 ± 0.064	1.1108 ± 0.0003	
Lyon	29	ICP–MS	1988	car parking	16.749 ± 0.111	15.280 ± 0.086	35.274 ± 0.331	1.096 ± 0.003	2.102
				U.K.					
Cardiff	7	TIMS	1968	air particles	17.86			1.134	2.165
London	7	TIMS	1968	air particles	17.45			1.126	2.141
London	7	TIMS	1971	air particles	17.32			1.105	
Edinburgh	15	ICP–MS	1989–1991	urban air/filter				1.056–1.093	

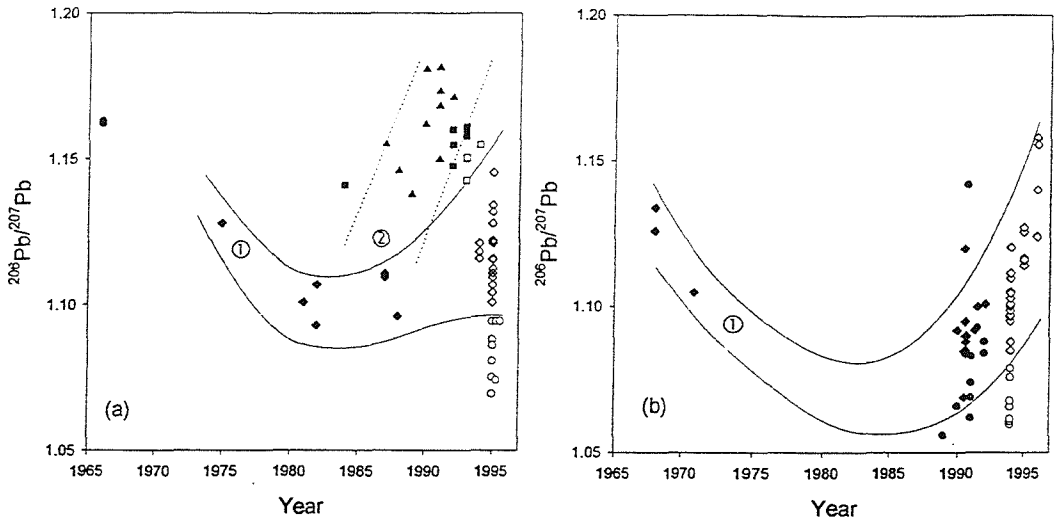

FIGURE 5. Change in $^{206}Pb/^{207}Pb$ ratio since 1965 for potential sources of Pb and airborne particulate matter in France (a) and the U.K. (b). Closed symbols, data from literature (see Table 4 for references); open symbols, this study: (○) gasoline, (□) industrial emissions. Field 1 represents the isotopic evolution of samples collected in urban areas (◇), and field 2 represents the isotopic evolution of aerosols collected in French mountains (△) (*18*).

1965–1980, which could be interpreted as a growing use of Australian lead. However, as mentioned above for both countries, modern urban aerosols have an isotopic signature that is always more radiogenic than those of gasoline, and so it is uncertain that the Pb isotopic ratios obtained in the past for aerosols perfectly reflect those in gasoline. Consequently, all results obtained using indirect sampling can only be considered as the upper limit of the gasoline component since other contributions cannot be excluded.

Concerning industrial Pb, there are few direct measurements available. In 1984, Petit measured $^{206}Pb/^{207}Pb$ ratios close to 1.141 in the atmosphere at various industrial sites of northern France (*3*), and $^{206}Pb/^{207}Pb$ ratios between 1.147 and 1.161 have been measured in liquid urban waste (*5*). This kind of sampling allows a general assessment of the isotopic composition of industrially derived Pb, although values obtained may be slightly low due to mixing with gasoline-derived Pb. However, such values are in agreement with the range found from ashes from urban incinerators: 1.143–1.155. Although the database is preliminary, the isotopic signature seems to have remained rather constant over the last decade, but there are insufficient data available prior to the 1980s.

Grousset et al. (*18*) have shown a decrease of Pb content and a corresponding increase in $^{206}Pb/^{207}Pb$ ratios in French mountain aerosols since 1985 (see Figure 5), which was attributed to the decreasing input of Pb from automobile emissions. In urban areas, the same phenomenon is often noted, but to a lesser extent due to proximity to the sources of Pb pollution. In the urban environment, Pb derived from other sources (industrial and natural) has increased in relative terms and can no longer be neglected when assigning a characteristic anthropogenic Pb signature. Hence, even where Pb isotopes can be successfully applied in environmental studies, great care must be taken to define the isotopic character of all individual sources of Pb with representative sampling programs. Additionally, it is desirable that such isotopic monitoring is carried out frequently to provide a better database showing variations with time so that evolutionary changes in the Pb pollution record can be understood.

Acknowledgments

We wish to express special thanks to M. Ducate and B. Vuillot, AMPADI, R. Stroebel, ADEME; M. Geraud, QUALITAIR 06; J. P. de la Massa, ORAMIP; A. Target, ASPA; J. P. Goguet, ESPAC; M. Luittre, ASQAP; J. F. Laquerriere, AIR NORMAND; O. Soudier, AIRLOR; J. Attia, LCPP; S. Pellier, AMPAC; L. Levaudel, AIRMARAIX; and S. Gottard, AREMA for their help during sampling and also N. Clauer and F. Grousset for their precious experience and their helpful comments. The Southampton group thank Prof. Bob Nesbitt for the use of the Fisons Elemental PQ2+ ICP–MS and Dr. Nakhwa of Associated Octel for his generous assistance with supplying data. John Coates of the London Borough of Richmond upon Thames is thanked for providing air filters and traffic flow and weather data.

Literature Cited

(1) Doe, B. R.; Stacey, J. S. *Econ. Geol.* **1974**, *69*, 757.
(2) Elbaz-Poulichet, F.; Holliger, P.; Huang, W.; Martin, J.-M. *Nature* **1984**, *308*, 409.
(3) Elbaz-Poulichet, F.; Holliger, P.; Martin J-M.; Petit, D. *Sci. Total Environ.* **1986**, *54*, 61.
(4) Erel, Y.; Patterson, C. *Geochim. Cosmochim. Acta* **1994**, *58*, 3289.
(5) Monna, F.; Ben Othman, D.; Luck, J.-M. *Sci. Total Environ.* **1995**, *166*, 19.
(6) Petit, D. *Earth Planet. Sci. Lett.* **1974**, *23*, 199.
(7) Hamilton, E. I.; Clifton, R. J. *Estuarine Coastal Mar. Sci.* **1979**, *8*, 271.
(8) Shirahata, H.; Elias, R. W.; Patterson, C. C. *Geochim. Cosmochim. Acta* **1980**, *44*, 149.
(9) Petit, D.; Mennessier, J. P.; Lamberts, L. *Atmos. Environ.* **1984**, *18* (6), 1189.
(10) Hirao, J.; Mabuchi, H.; Fukuda, E.; Tanaka, H.; Imamura, T.; Todoroki, H.; Kimura K.; Matsumoto, E. *Geochem. J.* **1986**, *20*, 1.
(11) Croudace, I. W.; Cundy, A. B. *Environ. Sci. Technol.* **1995**, *29* (5), 1288.
(12) Maring, H.; Settle, D. M.; Buat-Ménard, P.; Dulac, F.; Patterson, C. C. *Nature* **1987**, *300*, 154.
(13) Hamelin, B.; Grousset, F. E.; Biscaye, P. E.; Zindler, A.; Prospero, J. M. *J. Geophys. Res.* **1989**, *94* (C11), 16243.
(14) Hopper, J. F.; Ross, H. B.; Sturges, W. T.; Barrie, L. A. *Tellus* **1991**, *43B*, 45.
(15) Sugden, C. L.; Farmer, J. G.; Mackenzie, A. B. *Environ. Geochem. Health* **1993**, *15*, 50.

(16) Mukai, H.; Furuta, N.; Fujii, T.; Ambe, Y.; Sakamoto, K.; Hashimoto, Y. *Environ. Sci. Technol.* **1993**, *27* (7), 1347.
(17) Mukai, H.; Tanaka, A.; Fudjii, T.; Nakao, M. *J. Geophys. Res.* **1994**, *99* (D2), 3717.
(18) Grousset, F. E.; Quétel, C. R.; Thomas, B.; Buat-Ménard, P.; Donard O. F. X.; Buchet, A. *Environ. Sci. Technol.* **1994**, *28*, 1605.
(19) Hamester, M.; Stechmann, H.; Steiger, M.; Dannecker, M. *Sci. Total Environ.* **1994**, *146/147*, 321.
(20) Rabinowitz, M. B.; Wetherill, G. W. *Environ. Sci. Technol.* **1972**, *6* (8), 705.
(21) Chow, T. J.; Earl, J. L. *Nature* **1973**, *176*, 510.
(22) Chow, T. J.; Snyder, C.; Earl, J. L. In *Isotope ratios as pollutant source and behaviour indicators*; IAEA: Vienna, 1975; p 95.
(23) Sturges, W. T.; Barrie, L. A. *Nature* **1987**, *329*, 144.
(24) Strelow, F. W. E. *Anal. Chem.* **1978**, *50* (9), 1359.
(25) Cameron, A. E.; Smith D. H.; Walker, R. L. *Anal. Chem.* **1969**, *41* (3), 525.
(26) Delves, H. T. *Chem. Brit.* **1988**, *24*, 1009.
(27) Lancelot, J.; Monna, F.; Mercadier, H. Presented at the EUG VIII conference, Strasbourg, France, 1995.
(28) Michard-Vitrac, A.; Albarede, F.; Allegre, C. J. *Nature* **1981**, *291*, 460.
(29) Grousset, F. E.; Quetel, C. R.; Thomas, B.; Donard, B. F. X.; Lambert, C. E.; Guillard, F.; Monaco, A. *Mar. Chem.* **1995**, *48*, 291.
(30) Dominik, J.; Burrus, D.; Vernet, J.-P. *Earth Planet. Sci. Lett.* **1987**, *84*, 165.
(31) Allott, R. W.; Kelly, M.; Hewitt, C. N. *Environ. Sci. Technol.* **1992**, *26*, 2142.
(32) Rosman, K. J. R.; Chisholm, W.; Boutron, C. F.; Candelone, J. P.; Hong, S. *Geochim. Cosmochim. Acta* **1994**, *58* (15), 3265.
(33) Rosman, K. J. R.; Chisholm, W.; Boutron, C. F.; Candelone, J. P.; Görlach, U. *Nature* **1993**, *362*, 333.
(34) Farmer, J. G.; Eades, L. J.; MacKenzie, A. B.; Kirika, A.; Bailey-Watts, T. E. *Environ. Sci. Technol.* **1996**, *30*, 3080.
(35) Bacon, J. R.; Jones, K. C.; McGrath, S. P.; Jonhston, A. E. *Environ. Sci. Technol.* **1996**, *30*, 2511.
(36) Flament, P. Ph.D. Dissertation, University of Lille, France, 1985.

Received for review October 9, 1996. Revised manuscript received February 19, 1997. Accepted February 25, 1997.[⊗]

ES960870+

[⊗] Abstract published in *Advance ACS Abstracts,* May 1, 1997.